

## CANADIAN THESES ON MICROFICHE

## THÈSES CANADIENNES SUR MICROFICHE



National Library of Canada  
Collections Development Branch

Canadian Theses on  
Microfiche Service

Ottawa, Canada  
K1A 0N4

Bibliothèque nationale du Canada  
Direction du développement des collections

Service des thèses canadiennes  
sur microfiche

### NOTICE

The quality of this microfiche is heavily dependent upon the quality of the original thesis submitted for microfilming. Every effort has been made to ensure the highest quality of reproduction possible.

If pages are missing, contact the university which granted the degree.

Some pages may have indistinct print especially if the original pages were typed with a poor typewriter ribbon or if the university sent us an inferior photocopy.

Previously copyrighted materials (journal articles, published tests, etc.) are not filmed.

Reproduction in full or in part of this film is governed by the Canadian Copyright Act, R.S.C. 1970, c. C-30. Please read the authorization forms which accompany this thesis.

### AVIS

La qualité de cette microfiche dépend grandement de la qualité de la thèse soumise au microfilmage. Nous avons tout fait pour assurer une qualité supérieure de reproduction.

S'il manque des pages, veuillez communiquer avec l'université qui a conféré le grade.

La qualité d'impression de certaines pages peut laisser à désirer, surtout si les pages originales ont été dactylographiées à l'aide d'un ruban usé ou si l'université nous a fait parvenir une photocopie de qualité inférieure.

Les documents qui font déjà l'objet d'un droit d'auteur (articles de revue, examens publiés, etc.) ne sont pas microfilmés.

La reproduction, même partielle, de ce microfilm est soumise à la Loi canadienne sur le droit d'auteur, SRC 1970, c. C-30. Veuillez prendre connaissance des formules d'autorisation qui accompagnent cette thèse.

THIS DISSERTATION  
HAS BEEN MICROFILMED  
EXACTLY AS RECEIVED

LA THÈSE A ÉTÉ  
MICROFILMÉE TELLE QUE  
NOUS L'AVONS REÇUE

Canada

Analysis and Design of Optimal Three-Phase PWM Rectifiers  
and Rectifier-Inverter Frequency Changers

Young-Goo Kang

A Thesis  
in  
The Department  
of  
Electrical Engineering

Presented in Partial Fulfillment of the Requirements  
for the Degree of Doctor of Philosophy at  
Concordia University  
Montréal, Québec, Canada

June 1985



Young-Goo Kang, 1985

ABSTRACT

Analysis and Design of Optimum Three-Phase PWM Rectifiers  
and Rectifier-Inverter Frequency Changers

Young-Goo Kang, Ph.D.  
Concordia University, 1985

Steadily decreasing prices and improving performance of semiconductor devices are beginning to have a considerable influence on the design of conventional static power converter circuits. This influence is in the form of either new converter topologies or innovative control methods for traditional topologies, the objectives being: cost reduction, weight and size reduction, better efficiency and increased reliability in both cases. In view of this, this thesis focuses on the optimum design of three-phase PWM rectifiers and Rectifier - Inverter (voltage source) Frequency Changers (RIFC's) for high performance applications by means of the minimization of reactive elements, such as ac/dc filter components, input power-factor correction capacitors, etc..


In order to achieve this optimum design, some advanced PWM control techniques, which include the typical sinusoidal PWM (SPWM), the modified SPWM, and the optimized PWM, are applied to both rectifiers and inverters. These PWM control techniques yield minimum possible harmonic distortion of the input/output waveforms and maximum possible input voltage utilization at practical switching frequencies. Moreover;

to facilitate the analysis of the aforementioned converters, a suitable computer-aided analysis method, which is based on the switching function concept, is introduced.

Algorithms for designing the associated ac/dc filters are proposed, with special emphasis on the optimum input filter design, since no comprehensive information on this topic is available. By applying properly selected PWM control techniques to three-phase rectifiers it is shown that the size of input/output filters can be reduced significantly and the input power factor can be improved considerably. Also, results show that the optimum RIFC system, which consists of a PWM rectifier and a PWM inverter employing the advanced PWM control techniques, requires considerably smaller sized reactive elements.

While predicting frame (motor) mounted static power converters, this thesis introduces and thoroughly analyzes two new RIFC topologies. The main feature of these topologies is that they do not require any dc link reactive component.

Finally, in order to establish the feasibility of the proposed new topologies and control techniques, and to evaluate the effectiveness of the employed analytical techniques, predicted key results are verified experimentally.



# ACKNOWLEDGEMENTS

I wish to express my gratitude to Dr. P.D. Ziogas and Dr. V.R. Stefanovic, my research advisors, for their guidance, support, and encouragement during all the stages of this thesis.

My indebtedness to Mr. E.P. Wiechmann, with whom I had useful discussions in the early stages of this research is acknowledged.

Help given by Mr. Danny Juras, technician of the University's Power Electronics Laboratory, is very much appreciated.

My deepest appreciation is reserved for my wife, Kyung-Sook, without whose patience this thesis could not have been accomplished.

I would also like to express my thanks to my children, Ji-Eun and Byung-Woo, who were not receiving the full services of a father.

TABLE OF CONTENTS

ABSTRACT	iii
ACKNOWLEDGEMENTS	v
LIST OF TABLES	ix
LIST OF FIGURES	xi
LIST OF ABBREVIATIONS AND PRINCIPAL SYMBOLS	xvi
CHAPTER 1 INTRODUCTION	1
1.1 General	1
1.2 Review of Previous Work	10
1.2.1 Three-phase forced commutated rectifiers	10
1.2.2 Three-phase rectifier-inverter frequency changers	13
1.3 Scope of the Thesis	14
CHAPTER 2 SWITCHING FUNCTIONS	16
2.1 Introduction	16
2.2 Sinusoidal PWM (SPWM) Switching Functions	20
2.3 Modified SPWM (MSPWM) Switching Functions	29
2.4 Optimized PWM (OPWM) Switching Functions	39
2.5 Conventional Single-Pulse Switching Function	41
2.6 Discussion	45
2.7 Conclusion	46
CHAPTER 3 ANALYSIS AND DESIGN OF OPTIMUM THREE-PHASE PWM RECTIFIERS	47
3.1 Introduction	47
3.2 System Description and Principles of Operation	48

3.3	Input Stage Analysis and Input Filter Design	58
3.3.1	Input stage analysis	58
3.3.2	Total harmonic distortion of the input line current	60
3.3.3	Total harmonic distortion of the input voltage	67
3.3.4	Total KVA rating of the input filter	70
3.3.5	Displacement power factor angle	71
3.3.6	Design of an optimum input filter	73
3.3.7	Evaluation of the optimum input filter	75
3.4	Output Stage Analysis and Output Filter Design	81
3.4.1	Output stage analysis	81
3.4.2	Ripple factor of the load voltage	86
3.4.3	Ripple factor of the rectifier output current	91
3.4.4	Selection of the output filter component values	92
3.4.5	Evaluation of the output filter	96
3.5	Discussion	101
3.6	Design Example and Experimental Results	102
3.7	Conclusion	107
CHAPTER 4	OPTIMUM SYSTEM DESIGN OF A THREE-PHASE RECTIFIER-INVERTER FREQUENCY CHANGER (RIFC)	108
4.1	Introduction	108
4.2	Generalized Transfer Function of a Three-Phase AC to AC Converter	110
4.3	System Description and Principles of Operation	116
4.4	RIFC Input Stage Analysis and Input Filter Design	119
4.5	DC Link Analysis and DC Link Filter Design	123

4.6	Evaluation of the RIFC Structures	129
4.7	Simulated Results	135
4.8	Conclusion	138
CHAPTER 5	RECTIFIER-INVERTER FREQUENCY CHANGERS WITH SUPPRESSED DC LINK COMPONENTS (SRIFC)	139
5.1	Introduction	139
5.2	System Description and Principles of Operation	140
5.3	Output Stage Analysis	145
5.3.1	Output stage analysis with SRIFC Structure #1	150
5.3.2	Output stage analysis with SRIFC Structure #2	156
5.4	Input Stage Analysis and Input Filter Design	163
5.4.1	Input stage analysis and input filter design with SRIFC Structure #1	169
5.4.2	Input stage analysis and input filter design with SRIFC Structure #2	175
5.5	Discussion	180
5.6	Experimental Results	181
5.7	Conclusion	182
CHAPTER 6	CONCLUSION	187
6.1	Conclusions	187
6.2	Suggestions for Future Work	190
REFERENCES		191
APPENDIX A	Third-Harmonic-Injection SPWM Switching Function	200
APPENDIX B	Computer-Aided Analysis and Design Programs	204

# LIST OF TABLES

Table 1.1	Applications of static power converters	2
Table 2.1	Maximum fundamental amplitudes of four kinds of switching functions	45
Table 3.1	Optimum rectifier input filter data	77
Table 3.2	Rectifier output filter data	95
Table 4.1	RIFC input filter design data	120
Table 4.2	Rectifier switch ratings of RIFC structures	121
Table 4.3	RIFC dc link filter design data	130
Table 4.4	Inverter switch ratings of RIFC structures	131
Table 4.5	Performance characteristics of RIFC structures	133
Table 4.6	Selected design data of RIFC structures	134
Table 5.1	Frequency spectra of rectifier output voltages with SRIFC Structures #1 and #2	151
Table 5.2	Ratio-changing method for SRIFC Structure #1	155
Table 5.3	Frequency spectra of inverter output voltage and current with SRIFC Structure #1 ( $f_o=100$ Hz)	158
Table 5.4	Frequency spectra of inverter output voltage and current with SRIFC Structure #1 ( $f_o=42$ Hz)	159
Table 5.5	Ratio-changing method for SRIFC Structure #2	162
Table 5.6	Frequency spectra of inverter output voltage and current with SRIFC Structure #2 ( $f_o=60$ Hz)	165
Table 5.7	Frequency spectra of inverter output voltage and current with SRIFC Structure #2 ( $f_o=42$ Hz)	166
Table 5.8	Frequency spectra of SRIFC rectifier switching functions	171
Table 5.9	Input line current frequency spectra with SRIFC Structure #1 ( $f_o=100$ Hz)	174

Table 5.10 SRIFC input filter data

176

Table 5.11 Input line current frequency spectra with SRIFC  
Structure #2 ( $f_0=60$  Hz)

179

# LIST OF FIGURES

Fig. 1.1	Simplified block diagram of a static power converter	3
Fig. 1.2	Simplified block diagram of three-phase ac/ac converters	7
Fig. 2.1	Typical three-phase phase-controlled bridge rectifier	18
Fig. 2.2	The SPWM switching function	22
Fig. 2.3	Examples of SPWM gating signals for voltage-source and current-source converters with $N_h = 15$ and $M = 0.8$ (a) For voltage-source converters (b) For current-source converters	24 25
Fig. 2.4	Examples of the frequency spectra of SPWM switching functions with $N_h = 15$ and 21 at $M = 1$	27
Fig. 2.5	Variation of dominant harmonic components, $d_1$ and $d_h$ , of a SPWM switching function as a function of the modulation index, $M$	28
Fig. 2.6	$DF_s$ -vs- $N_h$ plot with SPWM switching functions at $M = 1$	30
Fig. 2.7	The MSPWM switching function	31
Fig. 2.8	Examples of MSPWM gating signals for voltage-source and current-source converters with $N_h = 12$ and $M = 0.6$ (a) For voltage-source converters (b) For current-source converters	33 34
Fig. 2.9	Examples of the frequency spectra of MSPWM switching functions with $N_h = 8$ and 12 at $M = 1$	36
Fig. 2.10	Variation of dominant harmonic components, $d_1$ and $d_h$ , of an MSPWM switching function as a function of the modulation index, $M$	37
Fig. 2.11	$DF_s$ -vs- $N_h$ plot with MSPWM switching functions at $M = 1$	38
Fig. 2.12	The OPWM switching function	40
Fig. 2.13	Examples of the frequency spectra of OPWM switching function with $N_h = 7$ and 9	42

Fig. 2.14	$DF_s$ -vs- $N_h$ plot with OPWM switching functions	43
Fig. 2.15	Frequency spectrum of the conventional single-pulse switching function	44
Fig. 3.1	Simplified circuit diagram of a three-phase rectifier studied	49
Fig. 3.2	Rectifier voltage control by means of SPWM scheme	50
Fig. 3.3	Rectifier voltage control by means of MSPWM scheme	51
Fig. 3.4	Rectifier voltage control by means of OPWM scheme	52
Fig. 3.5	Rectifier voltage control by means of the conventional method	53
Fig. 3.6	Gating signals for the $S_3$ (wt) type of switching function with $N_h = 9$	56
Fig. 3.7	Implementation of the $S_3$ (wt) type of switching function	57
Fig. 3.8	Distortion factors of rectifier input line current versus the normalized output voltage	59
Fig. 3.9	TIPF -vs- $V_{dcN}$ plots without input filters	61
Fig. 3.10	Analytical model of a lossless input filter	62
Fig. 3.11	$THD_i$ -vs- $X_{Ci}$ plots for various $X_{Li}$ values with the OPWM switching function	66
Fig. 3.12	$THD_v$ -vs- $X_{Ci}$ plots corresponding to the $THD_i$ plots	69
Fig. 3.13	TKVA -vs- $X_{Ci}$ plots corresponding to the $THD_i$ and $THD_v$ plots	72
Fig. 3.14	Displacement power-factor angle corresponding to the $THD_i$ and $THD_v$ plots	74
Fig. 3.15	Flow chart of the CAD program for designing optimum input filter	76
Fig. 3.16	$THD_i$ values versus $V_{dcN}$ with the specified input filters in Table 3.1	78
Fig. 3.17	$THD_v$ values versus $V_{dcN}$ with the specified input filters in Table 3.1	79

Fig. 3.18	TIPF values versus $V_{dcN}$ with the specified input filters in Table 3.1	80
Fig. 3.19	Distortion factors of rectifier output voltages, versus $V_{dcN}$	87
Fig. 3.20	Analytical model of a lossless output filter	88
Fig. 3.21	Ripple factors of the load voltage versus $X_{L_0}$ for various $X_{L_0}$ values with the OPWM switching function	93
Fig. 3.22	Ripple factors of the rectifier output current corresponding to the Fig. 3.21	94
Fig. 3.23	Ripple factors of the load voltages versus $V_{dcN}$ with the specified output filters in Table 3.2	97
Fig. 3.24	Ripple factors of the rectifier output currents versus $V_{dcN}$ with the specified output filters in Table 3.2	98
Fig. 3.25	$RF_V$ (eqn. (3.39)) -vs- $V_{dcN}$ plots with the output filters in Table 3.2	99
Fig. 3.26	$RF_I$ (eqn. (3.40)) -vs- $V_{dcN}$ plots with the output filters in Table 3.2	100
Fig. 3.27	Experimental input line current of the rectifier, $I_a$ , and its frequency spectrum	104
Fig. 3.28	Experimental ac source line current, $I_s$ , and its frequency spectrum	104
Fig. 3.29	Experimental input voltage, $V_a$ , and its frequency spectrum	104
Fig. 3.30	Experimental rectifier output voltage, $V_r$ , and its frequency spectrum	105
Fig. 3.31	Experimental load voltage, $V_f$ , and its frequency spectrum	105
Fig. 3.32	Experimental rectifier output current, $I_r$ , and its frequency spectrum	105
Fig. 4.1	Simplified circuit diagram of a three-phase rectifier-inverter frequency changer	109
Fig. 4.2	Simplified block diagram of a generalized three-phase to three-phase frequency changer	111

Fig. 4.3	Simplified block diagram of an indirect frequency changer	111
Fig. 4.4	Analytical model of the RIFC dc link	124
Fig. 4.5	RMS ripple current of the MSPWM inverter input current versus the modulation index, M, for various load power factors	126
Fig. 4.6	RMS ripple current of the SPWM inverter input current versus the modulation index, M, for various load power factors	128
Fig. 4.7	Simulated input line current waveform of the RIFC Structure #3-2 with ripple-free dc link current and its frequency spectrum	136
Fig. 4.8	Simulated filtered ac source current waveform of the RIFC Structure #3-2 and its frequency spectrum	136
Fig. 4.9	Simulated input line-to-neutral voltage waveform of the RIFC Structure #3-2 and its frequency spectrum	136
Fig. 4.10	Simulated rectifier output voltage waveform of the RIFC Structure #3-2 and its frequency spectrum	137
Fig. 4.11	Simulated dc link current waveform of the RIFC Structure #3-2 and its frequency spectrum	137
Fig. 4.12	Simulated inverter input voltage waveform of the RIFC Structure #3-2 and its frequency spectrum	137
Fig. 5.1	Simplified circuit diagram of the SRIFC system	141
Fig. 5.2	Simplified circuit diagram of the proposed SRIFC Structure #1	142
Fig. 5.3	Simplified circuit diagram of the proposed SRIFC Structure #2	144
Fig. 5.4	Frequency spectra of the unwanted components of the rectifier output voltage and the inverter switching function, with SRIFC Structure #1	152
Fig. 5.5	Characteristics of the ratio-changing method applicable to the inverter of the SRIFC Structure #1	154
Fig. 5.6	Simulated waveforms related to the output of the SRIFC Structure #1 ( $f_o=100$ Hz)	157

Fig. 5.7	Frequency spectra of the unwanted components of the rectifier output voltage and the inverter switching function, with the SRIFC Structure #2	160
Fig. 5.8	Characteristics of the ratio-changing method applicable to the inverter of the SRIFC Structure #2	161
Fig. 5.9	Simulated waveforms related to the output of the SRIFC Structure #2 ( $f_o=60$ Hz)	164
Fig. 5.10	Frequency spectra of the unwanted components of the inverter input current and the rectifier switching function, with the SRIFC Structure #1	170
Fig. 5.11	RMS value of the dominant harmonic component, $d_1$ and $d_h$ , of the inverter input current versus the modulation index, $M$ , for various load power factors	172
Fig. 5.12	Simulated waveforms related to the input line current, with the SRIFC Structure #1 ( $f_o=100$ Hz)	173
Fig. 5.13	Frequency spectra of the unwanted components of the inverter input current and the rectifier switching function, with the SRIFC Structure #2	177
Fig. 5.14	Simulated waveforms related to the input line current, with the SRIFC Structure #2 ( $f_o=60$ Hz)	178
Fig. 5.15	Experimental waveforms with the SRIFC Structure #1	183
Fig. 5.16	Experimental waveforms with the SRIFC Structure #2	184
Fig. A.1	The THI-SPWM switching function	202
Fig. A.2	Frequency spectra of the SPWM and the THI-SPWM switching function with $N_h=15$ and $M=1$	203

LIST OF ABBREVIATIONS AND PRINCIPAL SYMBOLS

$A_c$	Amplitude of a carrier signal
$A_k$	Amplitude of the k-th harmonic component of a (rectifier) switching function
$A_r$	Amplitude of a reference signal
$B_k$	Amplitude of the k-th harmonic component of a inverter switching function
C	Capacitor
$C_1$	Input filter capacitor of a converter
CKVA	kVA rating of the $C_1$
$C_o$	Output (dc) filter capacitor
$DF_s$	Distortion factor of a switching function
$DF_{v_r}$	Distortion factor of a rectifier output voltage
$d_l$	Order of the lower dominant harmonic component
$d_h$	Order of the higher dominant harmonic component
$f_c$	Carrier frequency
$f_i$	Input frequency of a converter
$f_{ih,n;n=1,2,3}$	Unwanted frequency component in the input line current of an SRIFC
$f_o$	Output frequency of a converter
$f_{oh,n;n=1,2,3}$	Unwanted frequency components in the output line voltage of an SRIFC
$f_r$	Reference frequency
$f_s$	Switching frequency of a converter switch
$f_{sc}$	Switching frequency of a current-source converter switch
$f_{si}$	Switching frequency of an inverter switch
$f_{sv}$	Switching frequency of a voltage-source converter switch

Page XVII omitted

$I_{x,k}; x=a,b,c$	Amplitude of the k-th component in the $I_x(\omega t)$
$I'_{x,k}; x=a,b,c$	Amplitude of the k-th component in the $I'_x(\omega t)$
$K_I$	Value of the $THD_I$ limit in %
$K_V$	Value of the $THD_V$ limit in %
$L_i$	Input filter inductor
LKVA	kVA rating of the $L_i$
$L_o$	Output filter inductor
M	Modulation index
MSPWM	Modified SPWM
$N_h$	Number of pulses per half-cycle in a switching function
OPWM	Optimized PWM
PWM	Pulse-width modulation (or modulated)
$RF_{I_r}$	Ripple factor of a rectifier output current
$RF_{I'_r}$	Ripple factor of a rectifier output current in terms of the maximum dc current
$RF_{v_f}$	Ripple factor of the load voltage of a rectifier
$RF_{v'_f}$	Ripple factor of the load voltage of a rectifier in terms of the maximum dc voltage
RIFC	Rectifier-inverter frequency changer
$R_L$	Resistance of a rectifier load
$[S_I(\omega t)]$	Matrix of a 3- $\phi$ inverter switching function
$S_{nx}(\omega t)$	General symbol for switching functions where $n=1,2,3,4$ and $x=a,b,c$
SPWM	Sinusoidal PWM
SRIFC	RIFC with suppressed dc link
$[S_R(\omega t)]$	Matrix of a 3- $\phi$ rectifier switching function
$S_1(\omega t)$	SPWM switching function

$S_2(\omega t)$	MSPWM switching function
$S_3(\omega t)$	Optimized PWM switching function
$S_3'(\omega t)$	Version of the $S_3(\omega t)$ function
$S_4(\omega t)$	Conventional single-pulse switching function
SW	General symbol for converter switches
$S_I$	Inverter switch
$S_R$	Rectifier switch
THD <sub>i</sub>	Total harmonic distortion of the input line current of a rectifier
THD <sub>v</sub>	Total harmonic distortion of the input voltage of a rectifier
THI-SPWM	Third-harmonic-injection SPWM
TIPF	Total input power factor of a converter
TKVA	Total kVA rating of an ac (input) filter
$V_{an}, V_{bn}, V_{cn}$	Three-phase line to neutral voltages
$V_a(\omega t)$	Rectifier input (phase a) voltage with input filter
$V_{a,k}$	Amplitude of the k-th component in the $V_a(\omega t)$
$V_a'(\omega t)$	AC mains (phase a) voltage with input filter
$V_{ab}, V_{bc}, V_{ca}$	Three-phase line to line voltages
$V_{dc}$	DC component of a rectifier output voltage
$V_{dcN}$	Normalized $V_{dc}$
$V_f(\omega t)$	Load voltage of a rectifier
$V_{f,n}$	Amplitude of the n-th component in the $V_f(\omega t)$
$V_f$	RMS value of the $V_f(\omega t)$
$V_1$	Amplitude of the ac mains voltage
$[V_I(t)]$	Matrix of three-phase input voltages of a converter
$[V_O(t)]$	Matrix of three-phase inverter output voltages
$V_{oab}(\omega t)$	RIFC (or SRIFC) output line to line voltage

$[V_{oh}(t)]$	Matrix of the unwanted components in the output voltages of an SRIFC
$V_{oh,a}(t)$	Unwanted components of the $[V_{oh}(t)]$ for phase a
$V_r(\omega t)$	Rectifier output voltage
$V_{r,n}$	Amplitude of the n-th component in the $V_r(\omega t)$
$x$	Phase a, b, or c in a three-phase converter
$X_{C_1}$	Impedance of the $C_1$ at fundamental input frequency
$X_{C_0}$	Impedance of the $C_0$ at fundamental input frequency
$X_{L_1}$	Impedance of the $L_1$ at fundamental input frequency
$X_{L_0}$	Impedance of the $L_0$ at fundamental input frequency
$Z_{o,n}$	Equivalent output impedance of a rectifier at the n-th frequency
$\alpha$	General symbol for a phase delay angle
$\alpha_k$	The k-th commutation point in a switching function
$\phi$	General symbol for phase
$\phi_n$	Phase displacement of the n-th harmonic component
$\eta_I$	Voltage utilization factor of an inverter
$\eta_R$	Voltage utilization factor of a rectifier
$\eta_T$	Total voltage utilization factor of an RIFC
$\rho$	Ratio between the price of inductor and that of capacitor for same kVA rating
$\theta_1$	Phase displacement between voltage and current at fundamental frequency
$\theta_n$	Phase displacement of the n-th harmonic component
$\omega$	General symbol for angular frequencies
$\omega_1$	Angular frequency of an ac mains
$\omega_0$	Angular frequency of an inverter output frequency

## CHAPTER 1

### INTRODUCTION

#### 1.1 General

Continuing improvements in semiconductor technology and in power converter circuits have led to widespread use of static power converters. They come in many forms for many applications such as shown in Table 1.1. Fig. 1.1 shows the simplified block diagram of a static power converter. The input and output can be either ac form or dc form, the conversion scheme belonging to one of the four main categories which include ac/dc, dc/ac, dc/dc, and ac/ac conversion. Since the output voltage (or current) and the input current (or voltage) are defined by the switching operations of the converter switches, there always exist some unwanted harmonic components in the input and output waveforms. Therefore, the input and output filters are generally introduced to reduce the generated harmonic components to certain acceptable levels.

Among the four conversion processes, the ac/dc process is of considerable practical importance, because the original source of energy is generally in ac form. Consequently, the ac/dc converter is an indispensable part of any application requiring dc power and of those requiring ac power. The main fields of application of the ac/dc converter are [1], [2], [3], [4];

TABLE 1.1: APPLICATIONS OF STATIC POWER CONVERTERS.

<p><b>AEROSPACE AND DEFENSE</b></p> <ul style="list-style-type: none"> <li>Aircraft Power Supplies</li> <li>Laser Power Supplies</li> <li>Radar/Sonar Power Supplies</li> <li>Solid State Relays</li> <li>Sonobuoy Flashers</li> <li>Space Power Supplies</li> <li>VLF Transmitters</li> </ul> <p><b>CONSUMER</b></p> <ul style="list-style-type: none"> <li>Audio Amplifiers</li> <li>Electric Door Openers</li> <li>Heat Controls <ul style="list-style-type: none"> <li>Electric Blankets</li> <li>Electric Dryer</li> <li>Food Warmer Tray</li> <li>Furnace</li> <li>Oven</li> <li>Range Surface Unit</li> </ul> </li> <li>High Frequency Lighting</li> <li>Light Dimmers</li> <li>Light Flashers</li> <li>Motor Controls <ul style="list-style-type: none"> <li>Air Conditioning</li> <li>Blender</li> <li>Electric Fan</li> <li>Food Mixer</li> <li>Garage Door Opener</li> <li>Hand Power Tool</li> <li>Model Train</li> <li>Movie Projector</li> <li>Sewing Machine</li> <li>Slot Car</li> </ul> </li> <li>RF Amplifiers</li> <li>Security Systems</li> <li>TV Deflection</li> </ul>	<p><b>INDUSTRIAL</b></p> <ul style="list-style-type: none"> <li>Mercury-Arc Lamp Ballasts</li> <li>Motor Drives <ul style="list-style-type: none"> <li>Cement Kiln</li> <li>Conveyor</li> <li>Crane and Hoist</li> <li>Machine Tool</li> <li>Mining</li> <li>Oil Well Drilling</li> <li>Paper Mill</li> <li>Printing Press</li> <li>Pump and Compressor</li> <li>Steel Mill</li> <li>Synthetic Fiber</li> </ul> </li> <li>Power Supplies <ul style="list-style-type: none"> <li>Aluminum Reduction</li> <li>Battery Charger</li> <li>Computer</li> <li>Electrochemical</li> <li>Electroplating</li> <li>Electrostatic Precipitator</li> <li>Induction Heating</li> <li>Laboratory</li> <li>Mining</li> <li>Particle Accelerator</li> <li>Welding</li> </ul> </li> <li>Static Relays and Circuit Breakers</li> <li>Ultrasonic Generators</li> </ul> <p><b>POWER SYSTEMS</b></p> <ul style="list-style-type: none"> <li>Gas Turbine Starting</li> <li>Generator Exciters</li> <li>HVDC</li> <li>Nuclear Reactor Control Rod Drives</li> <li>Solar Power Supplies</li> <li>Synchronous Machine Starting</li> <li>Uninterruptible Power Supplies</li> <li>VAR Compensation</li> <li>Wind Generator Converters</li> </ul> <p><b>TRANSPORTATION</b></p> <ul style="list-style-type: none"> <li>Electronic Ignition</li> <li>Linear Induction Motor Control</li> <li>Motor Drives <ul style="list-style-type: none"> <li>Electric Vehicle</li> <li>Elevator</li> <li>Fork Lift Truck</li> <li>Locomotive</li> <li>Mass Transit</li> <li>People Movers</li> </ul> </li> </ul>
--	---

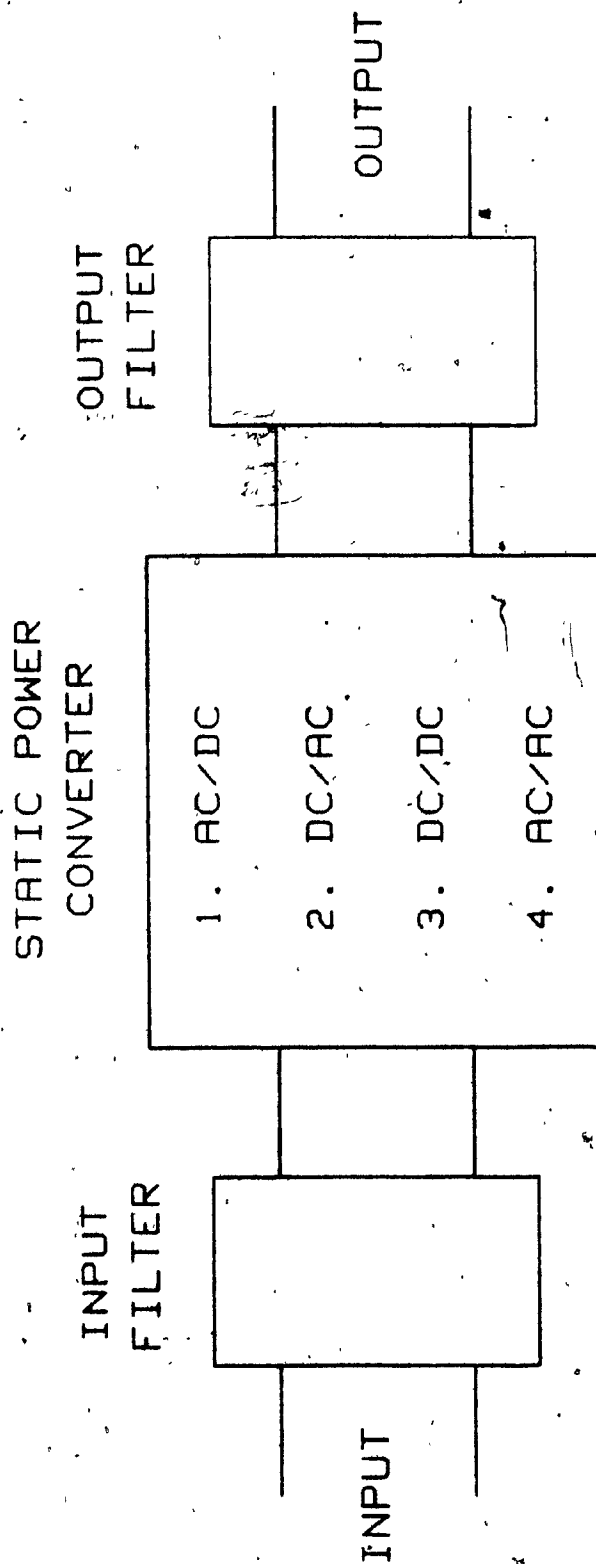


Fig. 1.1: Simplified block diagram of a static power converter.

- (i) as the controllable dc supply for the field and armature windings of dc motor drives,
- (ii) as the current-source for high inductance excitation coils of the field winding on ac and dc machines and magnet supplies,
- (iii) for the dc link between the ac mains and an inverter or a chopper,
- (iv) as the dc supply in battery chargers, electromechanical installations, dc arc furnaces, and dc welders,
- (v) in the induction motor drive with a slip recovery scheme, and
- (vi) as the HVDC transmission terminals.

For static power conversion from a three-phase mains, the thyristor phase-controlled rectifier is most widely used in both industrial and commercial applications. It is attractive because its inherent ruggedness and control signals are easily generated by simple circuitry. However, it has some undesirable properties, which include a poor input power factor and low-order harmonic components in ac line currents. The former property is mainly due to phase displacement which is an unavoidable inherent property of phase-controlled rectifier. Economics as well as system voltage-regulation requirements make it desirable to improve the overall system power factor. This power-factor improvement is typically accomplished by using shunt power-factor correction capacitors [5], [6], [7], [8], [9], [10]. However, if not applied correctly, these capacitors can produce other problems such as parallel resonance between the capacitor bank and the system inductive reactance, resonance with a generated harmonic, capacitor fuse-blowing,

and increased noise on the power system. There are also several methods for power-factor improvement of rectifiers without using the shunt capacitors [11], [12], [13], [14]. Without loss of generality, the best way of improving power factor is through the use of forced commutation, if applications permit. The latter property creates a number of problems for the power distribution network and for other electrical systems in the vicinity of the rectifier [15], [16], [17], [18], [19], [20], [21]. In other words, harmonic currents, which the power system is required to provide, cause an increase in heating. Sometimes, in the peak current levels in the power distribution systems, the impedance of the distribution system will cause these harmonics to distort the supply voltage, causing increased losses and electromagnetic interference (EMI) to other loads (such as computers, numerically controlled machines, appliances, power line carrier-communication systems, relaying equipment, and other sophisticated electronic equipment which are very sensitive to power line pollution) elsewhere on the power lines. It is therefore necessary to introduce filters on the input side of the rectifier to reduce the total harmonic distortion (THD) of the line current to a certain acceptable level. The output voltage of a rectifier is not pure dc, but contains substantial ripple components. Since the magnitude of this ripple becomes worse as the delay (i.e. control) angle increases, a dc side filter must generally be included to reduce the effect of this ripple on the loads.

Speed control of ac machines has become practical, by controlling the frequency of the applied voltages, and there are many aspects of

variable-frequency drive systems which are of current interest [22], [23], [24], [25]. For example, numerous types of speed and acceleration control systems are being investigated and designed to meet specific system requirements. Typical applications of variable-frequency drive systems include :

- Textile manufacturing
- Chemical processing
- Glass manufacturing
- Machine tools
- Polymer forming
- Food processing
- Material handling and packaging
- Printing and paper making
- Grinders
- Pumps

Depending on how the conversion is achieved, all frequency changer designs can be grouped into two families: direct and indirect conversions (Fig. 1.2). Frequency conversion is performed directly, when a properly operated set of switches connects the input lines directly with output lines [26]. It is performed indirectly when the input energy is first transferred into an intermediate storage link (DC or HF), and then from the intermediate link to the output. The intermediate storage decouples the input port from the output port, thus preventing the increase of output subharmonics and the disturbance

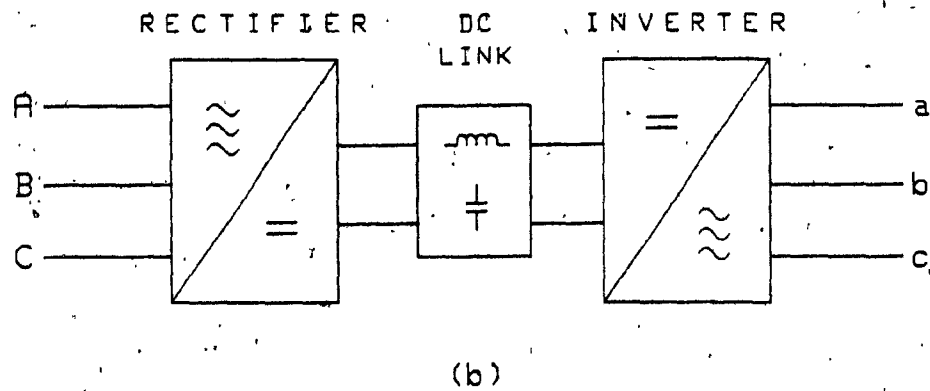
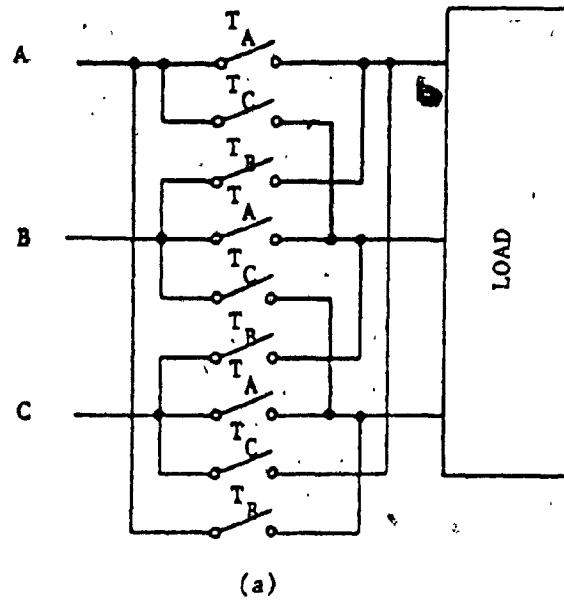


Fig. 1.2: Simplified block diagram of three-phase ac/ac frequency changers.

- a) Direct conversion.
- b) Indirect conversion.

of the input port. On the other hand, output subharmonics, in turn, tend to affect direct converters. Since their output waveform synthesis is usually not very accurate, some of the input line modulation is present in the converter output.

The 'beating' between input and output frequencies is the most common source of output subharmonics, highly undesirable on inductive loads. For this reason, the most widely used converters are indirect, with a dc link. In addition, ac/dc and dc/ac converter technologies are relatively well established, so that a Rectifier-Inverter Frequency Changer (RIFC) usually consists of well known circuit block.

A typical RIFC system employs two stages of power conversion. In the first stage, a fixed frequency ac supply voltage is rectified to produce the required dc bus by using a diode (uncontrolled) or a thyristor (phase-controlled) rectifier. In the second stage, the dc bus voltage is inverted to ac form at a required output frequency by using a PWM inverter. In most cases, this arrangement results in power converter structures with bulky components which are difficult to package, mainly due to the presence of large reactive elements such as ac/dc filter components. For example, with typical modern RIFC structures the largest part of the cabinet space (and hence floor space) is occupied by the ac/dc inductors and capacitors. Also, these reactive components frequently account for most of the cabinet content and weight, and hence determine the type of structure and the price of the cabinet itself. Therefore, a need for novel, effective, and

economical techniques of reactive element minimization exists. In fact, recent trends in static power converter design are towards minimizing the volume to output kVA ratio, resulting in cost reduction through advanced packaging concepts, and hence one can soon expect to see power electronics located on the machine frame of small ac motors [22], [24].

These trends have mainly been supported by the recent advances in power semiconductor technology which have produced fast gate turn-off switching devices (such as MOSFET's, bipolar transistors, GTO's etc.) [27], [28] at competitive prices. Consequently, the thyristor switches in rectifiers and inverters are gradually being replaced by the more recent gate turn-off switching devices in low to medium power applications. Therefore, for the first time, it is now becoming feasible to apply advanced PWM harmonic control techniques to both rectifiers and inverters, reducing the low-order harmonics and hence the filter and overall converter sizes. Moreover, with the advent of very large scale integration (VLSI) technology, the availability of low cost and powerful microprocessors makes it feasible to implement complex converter control strategies that previously could not be considered. The microcomputer-based control system provides not only substantial hardware simplification and improvement of reliability, but also performance optimization, impossible with the use of dedicated hardware control. Another important trend setting factor is the strict harmonic standards adopted by many utility companies around the world [29] (it is also expected that there will be new strict harmonic standards in North America soon).

Because of these trends in the evolution of static power converter structures, this thesis focuses on 'optimum converter system' design through the minimization of reactive elements such as ac/dc filter components, power-factor correction capacitors, and commutation inductors and capacitors. In the context of this thesis, 'optimum system' is the system that satisfies a given set of operating specifications with minimum sized reactive components at practical switching frequencies. Another motivation for focusing on this topic is that there is no comprehensive information about the ac input filter design of a rectifier, and no one has dealt with rectifier and inverter as a one RIFC system in order to design an optimum converter system. In this thesis, three-phase PWM rectifier structures for dc loads, and RIFC structures with dc link components, along with suppressed dc link components for ac loads are investigated.

## 1.2 Review of Previous Work

In this section, previous work related to three-phase forced commutated rectifiers and RIFC's is reviewed.

### 1.2.1 Three-phase forced commutated rectifiers

Forced commutated rectifiers are chosen in order to eliminate the drawbacks of the traditional line commutated rectifier. Hence, the application of PWM control techniques to rectifiers is of great interest. However, and mainly because of the ruggedness of line

commutated rectifier, they have attracted relatively little attention in comparison to PWM inverters. Proliferation of static converters, however, is forcing utility power companies to introduce stricter input current harmonic standards. Therefore, it is anticipated that continuing converter proliferation over the next several years will make harmonic distortion the most important single problem in static power conversion [14].

Lienau et al. investigated self-commutated converters for ac or dc traction applications [30]. They have employed multi-step switching operations and pulse operations using thyristors to improve input power factor and line current waveform, but these methods of controlling output voltage have not been efficient.

Kataoka et al. investigated a three-phase pulse-width controlled rectifier to improve input power factor and line current waveform using thyristors with auxiliary commutation circuits [31]. They used multi-pulse having equal pulse-widths for three-phase applications to reduce the harmonic components. Compared to the typical sinusoidal PWM scheme [32], this type of pulse-width modulation (PWM) is inefficient and moreover, no data in designing the input and output filters have been made available.

Another approach aimed at improving the input power factor and the line current waveform has been proposed by Marino et al. [33], and by Divan and Barton [29]. In this case, two cascaded convertors are used: first is a simple ac/dc diode rectifier; the second, which is supplied

by the first through a suitable dc filter, is a controlled dc/dc converter. The resulting harmonic components of the supply currents depend on the mode of operation of the chopper; the line-currents can contain subharmonic components and/or form an unbalanced set of three-phase input currents.

Zäch investigated a so-called pulse-time control, a special type of PWM, to improve the input power factor as well as the line current harmonic distortion of rectifiers [34]. This method of controlling the output voltage results in poor input voltage utilization, and the corresponding switching frequencies are considerably higher than those required with the control methods proposed in this thesis.

In addition, a reactive power and unity power-factor control scheme utilizing transistor switches has been proposed by Busse and Holtz [35]. It requires a multi-loop implementation and employs a rather inefficient and complex PWM technique. Moreover, the work presented in [35] does not include any data on actual line current distortion, nor values of the input/output filter components.

Finally, Doradla et al. have recently investigated a sinusoidal PWM three-phase ac/dc converter for dc motor drive applications [36]. In this system, the SPWM gating signals are applied only to the upper group switches, and only 120 degree single-pulse gating signals to lower group switches, thus working like a semi-SPWM-controlled rectifier. Consequently, the input line currents do not exhibit half-wave symmetry, and this results in inefficient suppression of unwanted voltage and current components.

### 1.2.2 Three-phase rectifier-inverter frequency changers

The analysis and design of RIFC systems have so far been focused on the inverting stage, and are therefore limited to the optimization of the interaction between inverter and ac load. Areas of concern such as ac mains-rectifier interaction and rectifier-inverter interaction have, in most cases, been ignored or dealt separately from each other. Consequently, the analysis and optimum design of critical system components such as ac (input) and dc (link) filters have been ignored or performed outside the proper context.

There has been some previous work on rectifier-inverter (voltage source) systems for induction motor drives [37], [38], [39] [40]. In particular, Krause and Woloszyk dealt with prediction of the performance of a rectifier-inverter induction motor drive system in [37]; Lipo and Krause investigated stability analysis of the drive system in [38], [39]; and Lipo et al. studied harmonic torque and speed pulsations in the drive system described in [40]. However, these works focused only on the performance of ac machine.

### 1.3 Scope of the Thesis

This thesis is divided into five chapters, and a brief outline of its contents is in order.

As indicated by the title of this thesis, the steady state characteristics of three-phase rectifier systems are investigated first. Then, the investigation is further extended to RIFC (voltage source) systems with and without dc link filter (in this context the 'system' includes the required ac/dc side filters). The main objective of this thesis is the 'optimum' design of such systems by the means of the minimization of reactive components, and by the introduction of the analytical techniques required to achieve this objective. To achieve this primary goal, some advanced PWM harmonic control techniques are employed to both rectifiers and inverters, and the techniques to design optimum ac/dc side filters are developed by using a switching function concept, with suitable computer-aided analysis and design methods.

In Chapter 2, some advanced PWM switching functions, as well as the conventional one (for comparison purposes), are described and discussed in detail.

In Chapter 3, three-phase PWM rectifier systems are thoroughly analyzed and evaluated. The techniques to design optimum ac/dc filters are developed, and some comparisons related to filter components are made. Finally, a design example is provided and the predicted key results are experimentally verified by a 1 KW laboratory set-up.

In Chapter 4, three kinds of three-phase RIFC (voltage source) structures with dc link components are investigated. The optimum ac/dc filters for each structure are designed by using the techniques developed in Chapter 3, and some salient data are compared to each other. Also, the performance evaluation of the overall system for each structure is presented so that the optimum RIFC system may be chosen. Finally, the predicted key results are verified by simulation on a HP9836-DATA6000 system.

In Chapter 5, two kinds of three-phase RIFC structures without dc link components (which are novel structures) are thoroughly analyzed and discussed. Some of the theoretical key results are experimentally verified by a prototype laboratory set-up.

## CHAPTER 2

### SWITCHING FUNCTIONS

#### 2.1 Introduction

Consider a general static power converter shown in Fig. 1.1. Assuming that the input voltage(s)  $[V_I(t)]$  and output voltage(s)  $[V_O(t)]$  of the converter are defined, then the transfer function of the converter  $[H(t)]$  can be defined by:

$$[H(t)] = [V_O(t)]/[V_I(t)] \quad (2.1)$$

The realization of the transfer function  $[H(t)]$  can be achieved only by means of a set of switches which operate according to some predetermined switching patterns. The mathematical expression describing the switching pattern of a switch is called an 'existence function' [41]. The existence function for a single switch assumes unit value whenever the switch is closed, and is zero whenever the switch is open. In a converter, each switch is closed and opened according to some repetitive pattern; hence, its existence function will take the form of a train of pulses with unit amplitudes. However, since the dependent output (or input) waveforms of a converter are determined by the switching operations of the switches, some means of formally and quantitatively describing the switching pattern of a phase (not a switch) is needed to simplify the analysis and design of a converter. The mathematical expression used for that purpose is herein

termed as a 'switching function', and it is defined as the function describing the switching pattern of a phase, having three-level amplitudes 1, 0, and -1.

To clarify, consider the typical three-phase phase-controlled bridge rectifier shown in Fig. 2.1. The six gating signals with zero phase shift are shown in Fig. 2.1b to Fig. 2.1g. Since the output current  $I_r$  is reflected into the input line currents by the switching operations of the six switches, any one of the three input line currents of the rectifier can be expressed by:

$$I_x(\omega t) = I_r \cdot S_{nx}(\omega t), \quad \begin{matrix} n=1,2,3,\dots \\ x=a,b,c \end{matrix} \quad (2.2)$$

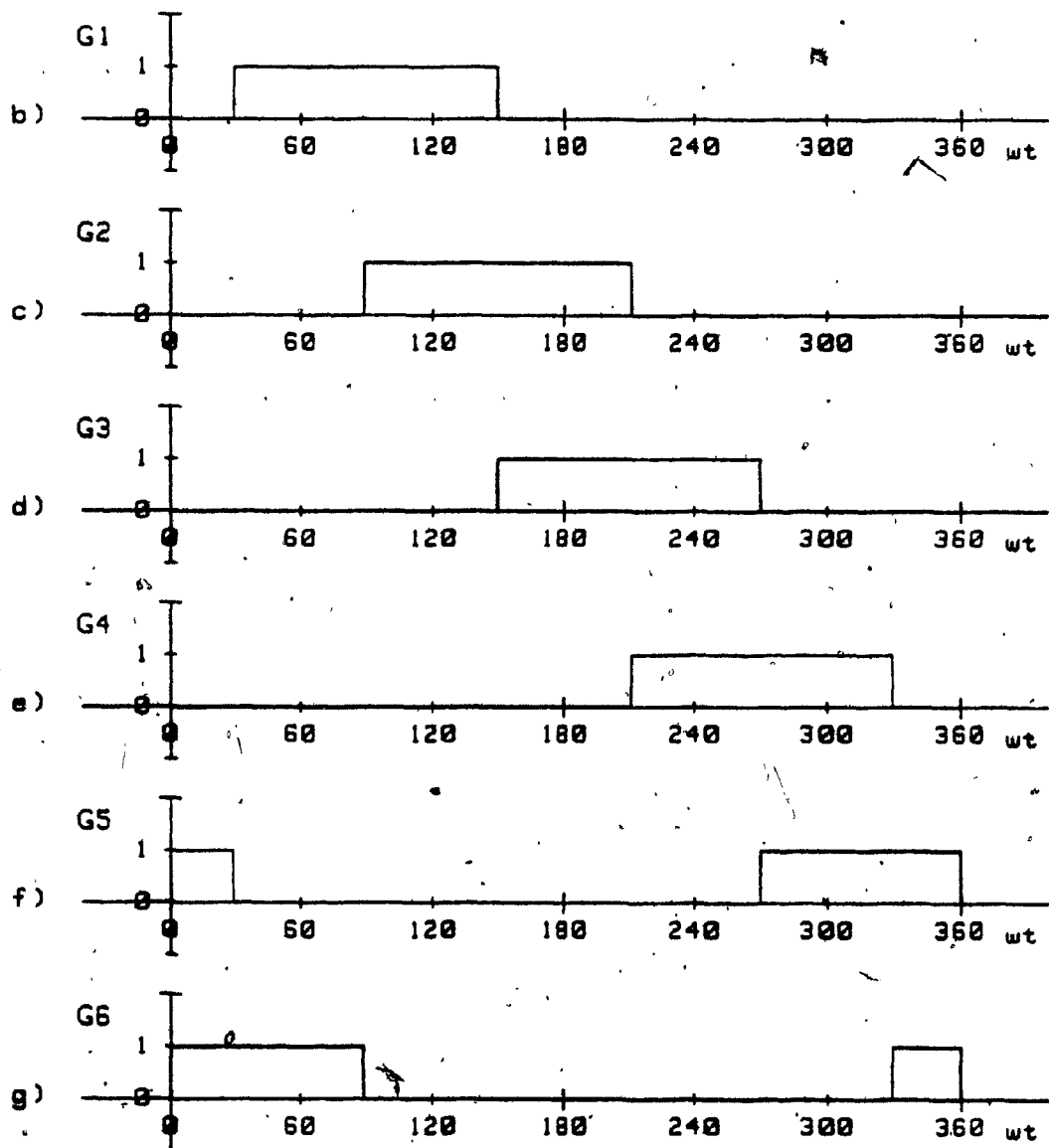
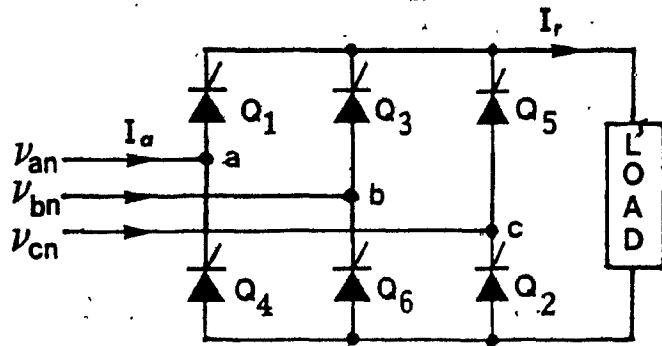
where

$I_x^*(\omega t)$  = input line current corresponding to phase x  
 $S_{nx}(\omega t)$  = switching function corresponding to phase x  
 n = type of switching function (will be used in the following sections).

As apparent in Fig. 2.1h, the  $I_x(\omega t)$  is a three-level waveform having the amplitudes  $I_r$ , 0, and  $-I_r$  when the output current  $I_r$  is assumed to be ripple-free. Thus, in this particular case, the switching function  $S_{nx}(\omega t)$  is defined as the function having exactly the same waveform as  $I_x(\omega t)$  but with the amplitudes 1, 0, and -1 (Fig. 2.1i). Moreover, since a switching function  $S_{nx}(\omega t)$  contains an infinite number of harmonic components, it can be expressed in terms of the Fourier series given by:

---

\* For convenience, w is often used for  $\omega$  (Ex:  $\omega t = wt$ ).



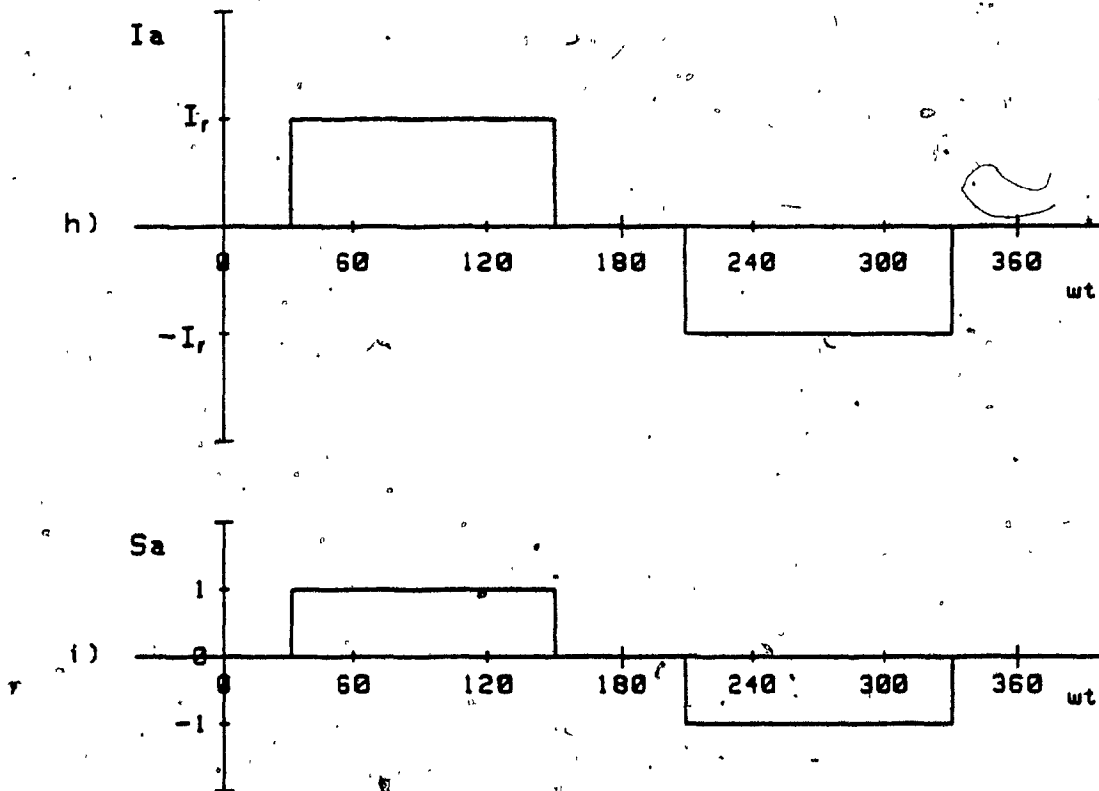


Fig. 2.1: Typical three-phase phase-controlled bridge rectifier.

- a) The simplified circuit diagram.
- b-g) Gating signals with delay angle  $\alpha=0$ .
- h) Input line current of the rectifier.
- i) Switching function of the rectifier.

$$S_{na}(\omega t) = \sum_{k=1}^{\infty} A_k \sin k\omega t \quad (2.3)$$

where

$A_k$  = amplitude of the  $k$ -th frequency component in the  $S_{nx}(\omega t)$ .

Also, the output voltage of the rectifier  $V_r(\omega t)$  can be determined in terms of the switching function  $S_{nx}(\omega t)$  as follows:

$$V_r(\omega t) = V_{an}(\omega t) \cdot S_{na}(\omega t) + V_{bn}(\omega t) \cdot S_{nb}(\omega t) + V_{cn}(\omega t) \cdot S_{nc}(\omega t) \quad (2.4)$$

where

$V_{xn}(\omega t)$  = line-to-neutral (or phase) voltage of a three-phase mains supply.

Thus, by introducing the switching function concept, the dependent output (or input) waveforms can be analyzed and expressed easily in terms of the Fourier series by using a suitable computer-aided method. Three kinds of PWM switching functions will be described and used throughout this thesis. The conventional single-pulse switching function shown in Fig. 2.11 will also be included for comparison purposes.

## 2.2 Sinusoidal PWM (SPWM) Switching Functions: $S_i(\omega t)$

This is a PWM technique that has been widely used in static inverter applications. The associated theory and applications have already been discussed in the numerous literature [42], [43], [44],

[45], [46]. However, it is noted here that this type of switching functions can also be applied to switching mode rectifiers. Fig. 2.2 shows the derivation of an  $S_1(\omega t)$  type of switching function. An isosceles triangle wave (carrier signal) is compared to the sine wave (reference signal), crossover points determining the points of level transition, from which the two-level switching waveforms corresponding to the phases are obtained (Fig. 2.2b and 2.2c). From these two-level switching waveforms, the three-level switching waveform shown in Fig. 2.2d is derived, in the same manner as one obtains the line voltages from the phase voltages of a voltage-source inverter. Finally, by setting the magnitudes to unity and by phase shifting the three-level waveform by  $-30$  degrees with respect to the reference signal the resulting switching function  $S_1(\omega t)$  is obtained (Fig. 2.2e). In most cases the carrier is synchronized with the reference, and an odd integral (multiple of three) ratio between carrier and reference frequencies is maintained to improve harmonic content. The pulse-widths of  $S_1(\omega t)$  can be varied by variation of the modulation index  $M$  which is defined as the ratio of the amplitude of the reference signal ( $A_r$ ) and that of the carrier signal ( $A_c$ ). Consequently, the fundamental component of the switching functions can be controlled by the modulation index  $M$ , and  $M$  must be restricted less than unity for normal operation. With this restriction it can be shown that only carrier frequency harmonics with fundamental frequency related side bands appear at the frequency spectrum of an  $S_1(\omega t)$ , thus the low-order harmonic components can be moved far away from the fundamental

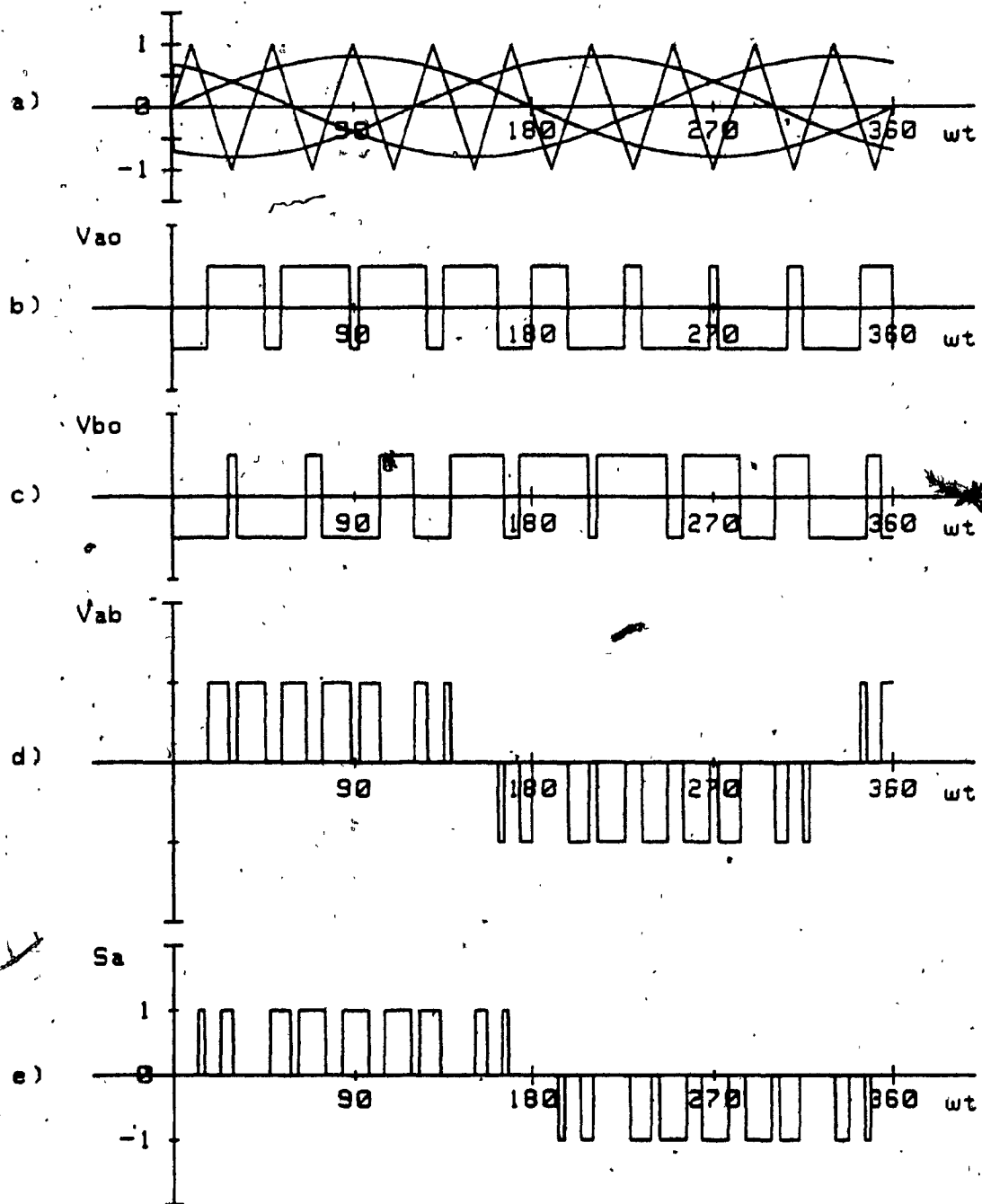


Fig. 2.2: The SPWM switching function.

- a) Definition of the SPWM scheme.
- b,c) Output phase voltages of an SPWM inverter.
- d) Output line to line voltage of the inverter.
- e) Switching function of the SPWM scheme.

component (Fig. 2.4), depending on the carrier frequency. The ratio between the carrier frequency  $f_c$  and the reference frequency  $f_r$ , or normalized carrier frequency, determines the number of pulses per half-cycle of an  $S_{nx}(wt)$  and is given by:

$$f_c / f_r = N_h \quad (2.5)$$

where

$N_h$  = number of pulses per half-cycle of an  $S_{nx}(wt)$ .

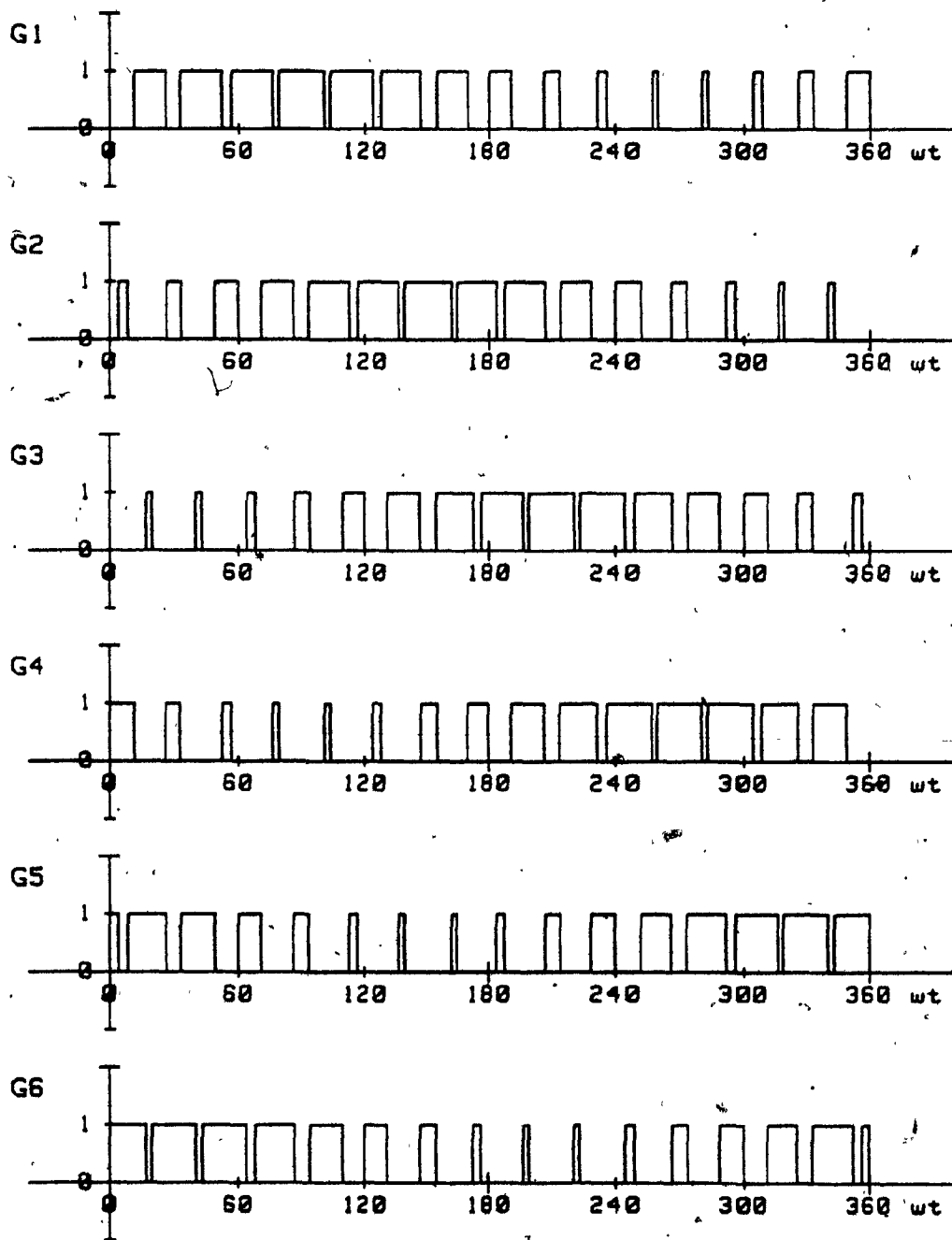
Once a switching function has been specified, the gating signals for a three-phase bridge converter (rectifier or inverter) can be easily obtained according to the operating principle of voltage-source or current-source converter; that is, at any instant the sum of line voltages or currents should be zero. This is equated as follows.

$$V_{ab}(t) + V_{bc}(t) + V_{ca}(t) = 0 \quad (2.6a)$$

or

$$I_a(t) + I_b(t) + I_c(t) = 0 \quad (2.6b)$$

Fig. 2.3 shows examples of the gating signals for voltage-source and current-source converters. From this figure it can be seen that for the same number of pulses ( $N_h$ ) the switching frequency of a voltage-source converter switch,  $f_{sv}$ , is lower than that ( $f_{sc}$ ) of a current-source converter switch. Specifically:



(a)

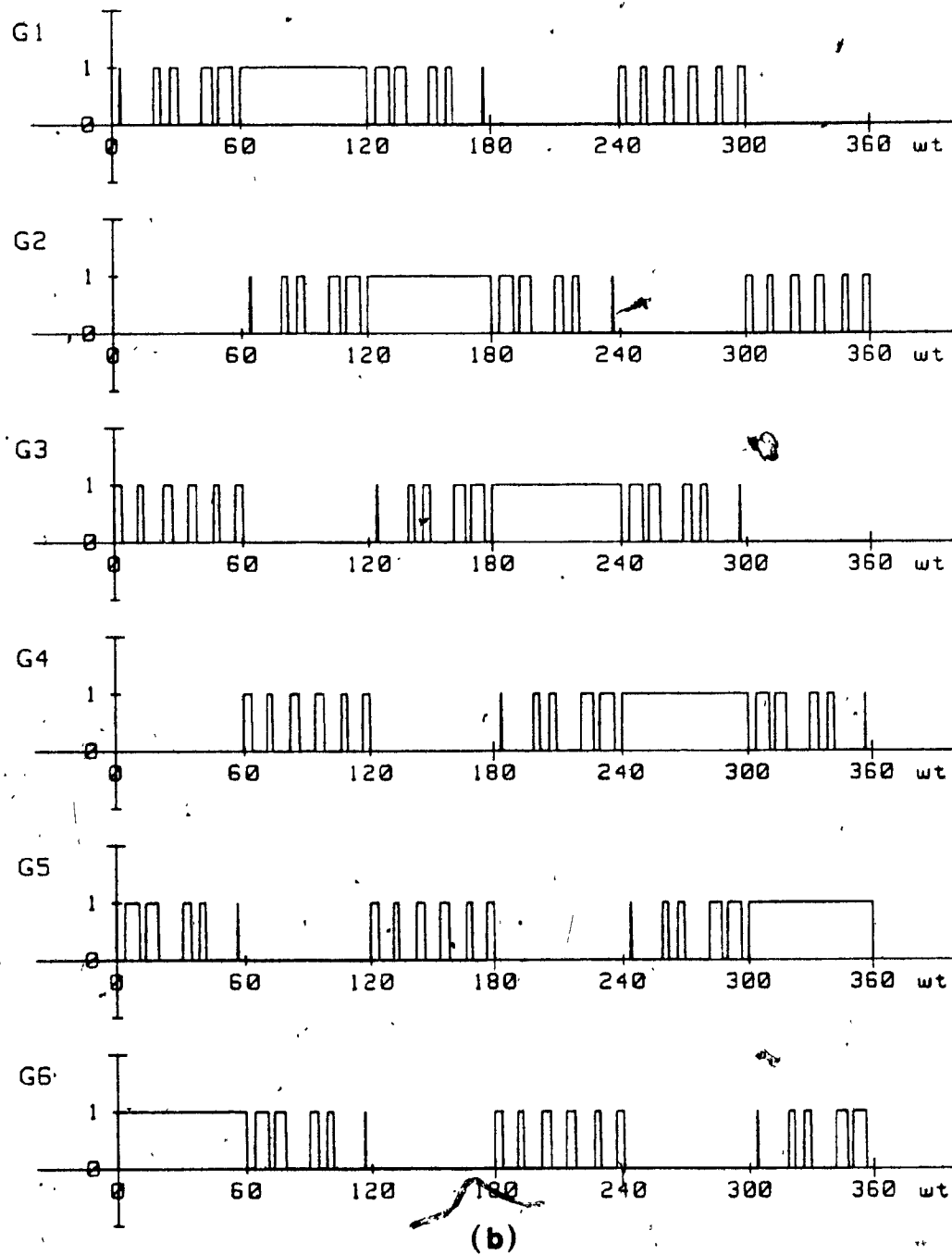


Fig. 2.3: Examples of SPWM gating signals for voltage-source and current-source converters with  $N_h = 15$  and  $M = 0.8$ .

- (a) For voltage-source converters.
- (b) For current-source converters.

$$f_{sv} = N_h \cdot f_r \quad (2.7a)$$

$$f_{sc} = (N_h + 2)f_r \quad (2.7b)$$

Fig. 2.4 shows the frequency spectra of  $S_1$  (wt) with  $N_h=15$  and 21, and the figure illustrates the fact that the order of dominant harmonic components ( $d_l$  and  $d_h$ ) of an  $S_1$  (wt) are a function of  $N_h$  given by:

$$\begin{aligned} d_l &= N_h - 2 \\ d_h &= N_h + 2 \end{aligned} \quad (2.8)$$

where

$d_l$  = order of the lower dominant harmonic frequency component,  
 $d_h$  = order of the higher dominant harmonic frequency component.

or, they can be expressed in terms of  $f_c$  and  $f_r$ ; that is,

$$\begin{aligned} d_l &= f_c - 2f_r \\ d_h &= f_c + 2f_r \end{aligned} \quad (2.9)$$

Their magnitudes are shown in Fig. 2.5 as a function of the modulation index  $M$ , and it is observed that their maximum values occur at  $M=1$ .

In order to observe the effects of the harmonic characteristics of  $S_1$  (wt) as  $N_h$  increases, a parameter  $DF_s$ , which is the distortion factor of a switching function next defined, is introduced.

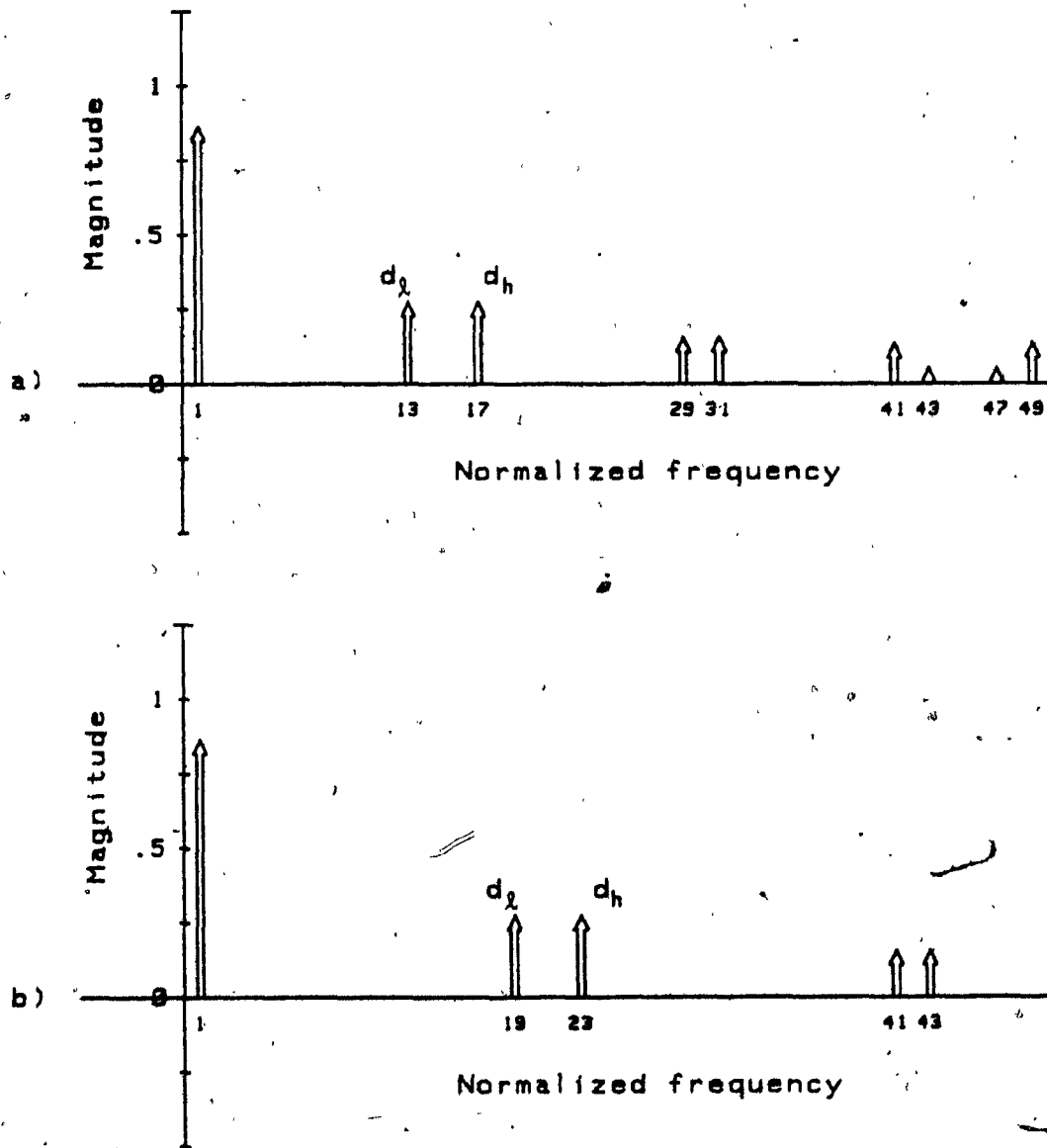


Fig. 2.4: Examples of the frequency spectra of SPWM switching functions with  $N_h = 15$  and  $21$  at  $M=1$ .

a) With  $N_h=15$ .

b) With  $N_h=21$ .

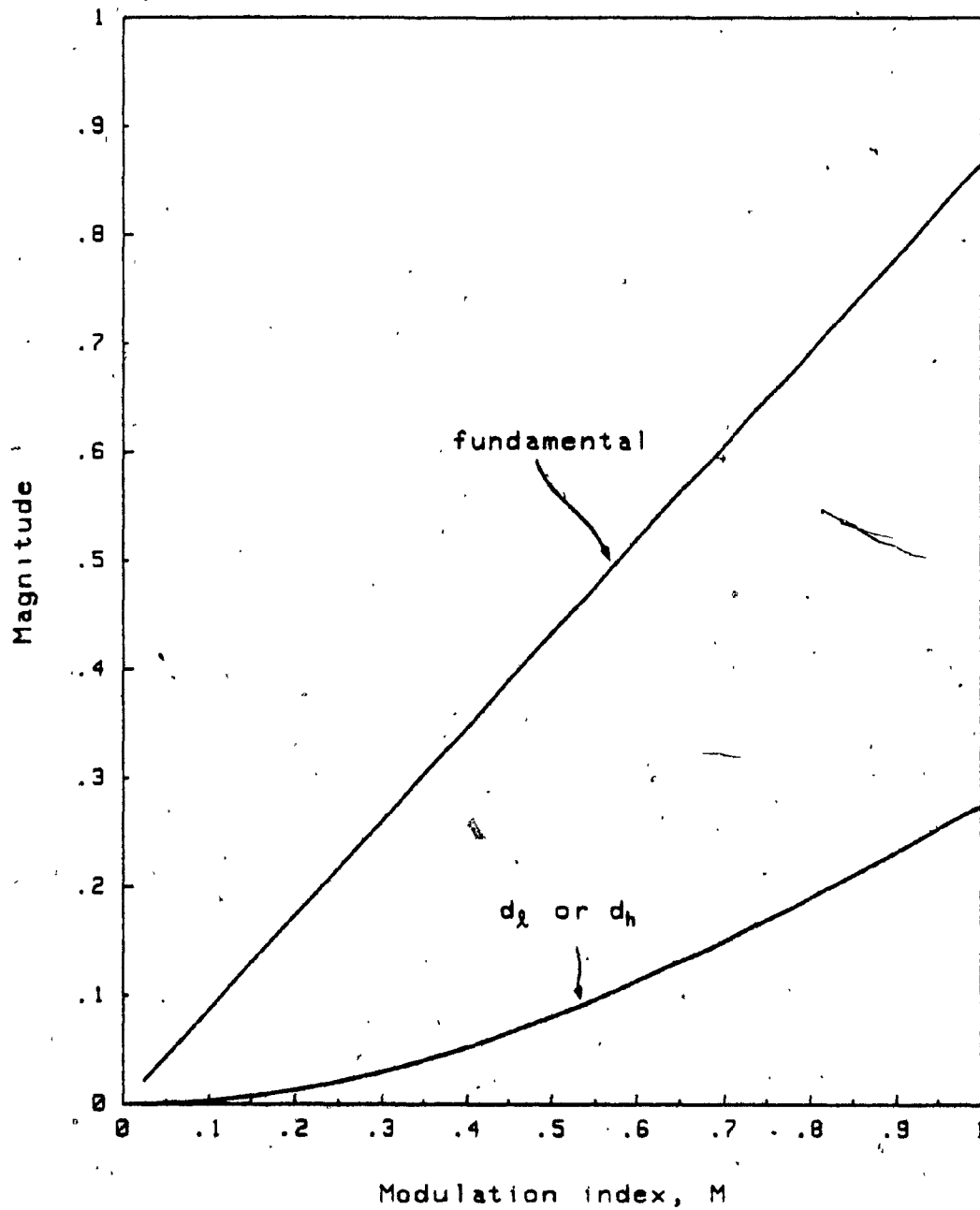


Fig. 2.5: Variation of dominant harmonic components,  $d_1$  and  $d_h$ , of a SPWM switching function as a function of the modulation index,  $M$ .

$$DF_s = \frac{100}{A_1} \left[ \sum_{k=5,7,\dots}^{\infty} \left( \frac{A_k}{k^2} \right)^2 \right]^{1/2} \quad (2.10)$$

where

$A_k$  = amplitude of the k-th harmonic component of an  $S_{nx}(wt)$   
 ( $1/k^2$  represents the gain of a general second-order filter).

The exact relation between  $DF_s$  and  $N_h$  is shown in Fig. 2.6, and from that figure it can be seen that the  $DF_s$  improvement, past the  $N_h=27$  point becomes insignificant. Therefore, 27-pulses per half-cycle may be adopted, in this case, as the optimum  $N_h$  value, since in general the switching loss of a switching device increases as  $N_h$  increases. However, it is noted that the maximum practical  $N_h$  value is also dependent on the switching capability of the particular switching device employed.

### 2.3 Modified SPWM (MSPWM) Switching Functions: $S_2(wt)$

The SPWM technique discussed in Section 2.2 can be modified so that the magnitude of the resulting fundamental component is further increased, and its harmonic characteristics improved. This Modified SPWM (MSPWM) technique has been independently proposed in [47], [48]. Fig. 2.7 illustrates the method for deriving the  $S_2(wt)$  type of switching function which results from the MSPWM. In this case, the carrier wave is applied only during the first and the last 60 degree intervals per half-cycle (i.e.  $0^\circ - 60^\circ$  and  $120^\circ - 180^\circ$ ) of  $S_2(wt)$  (Fig. 2.7a), and then, from the intersecting points between the carrier

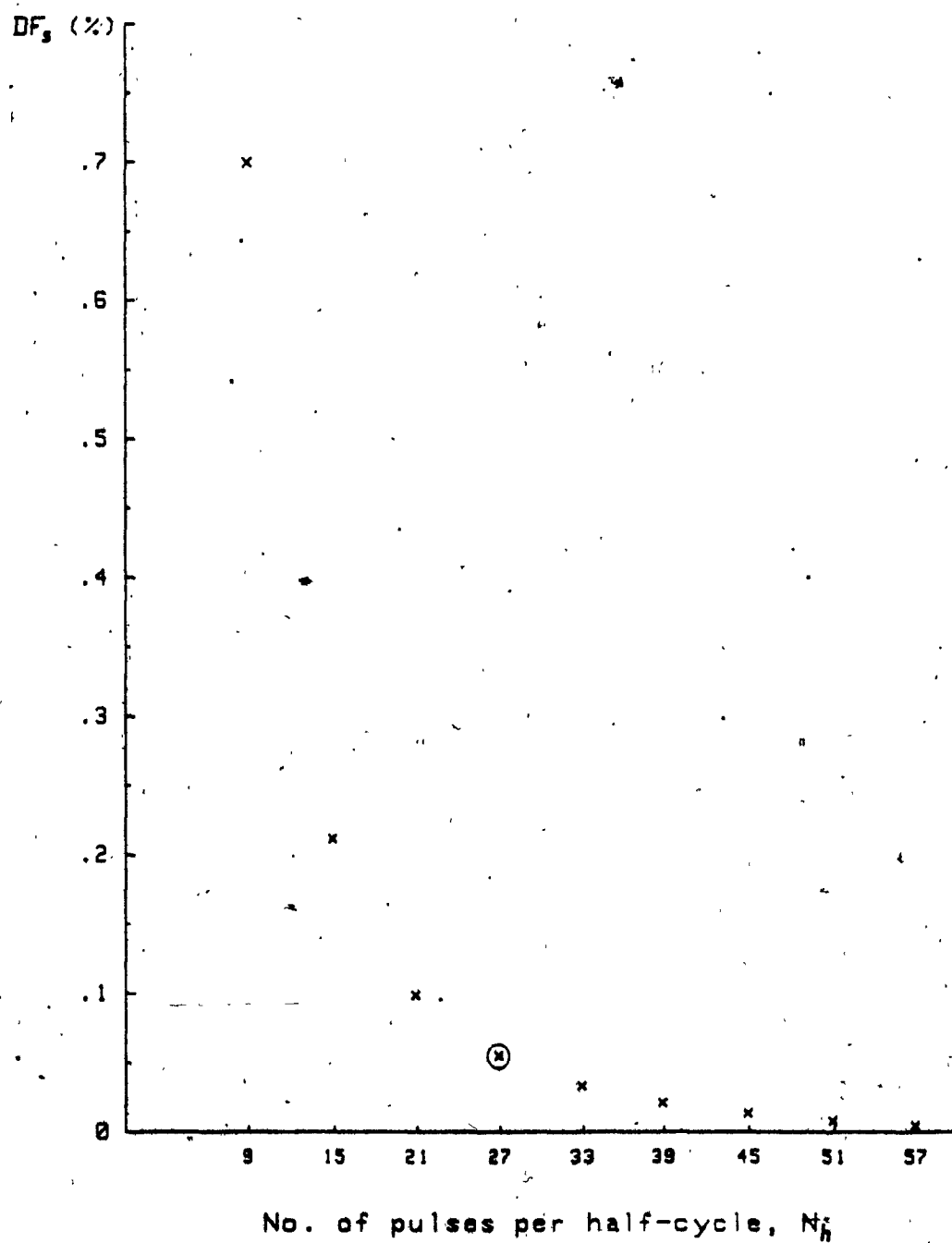


Fig. 2.6:  $DF_s$  (eqn. (2.10)) -vs-  $N_h$  plot with SPWM switching functions at  $M=1$ .

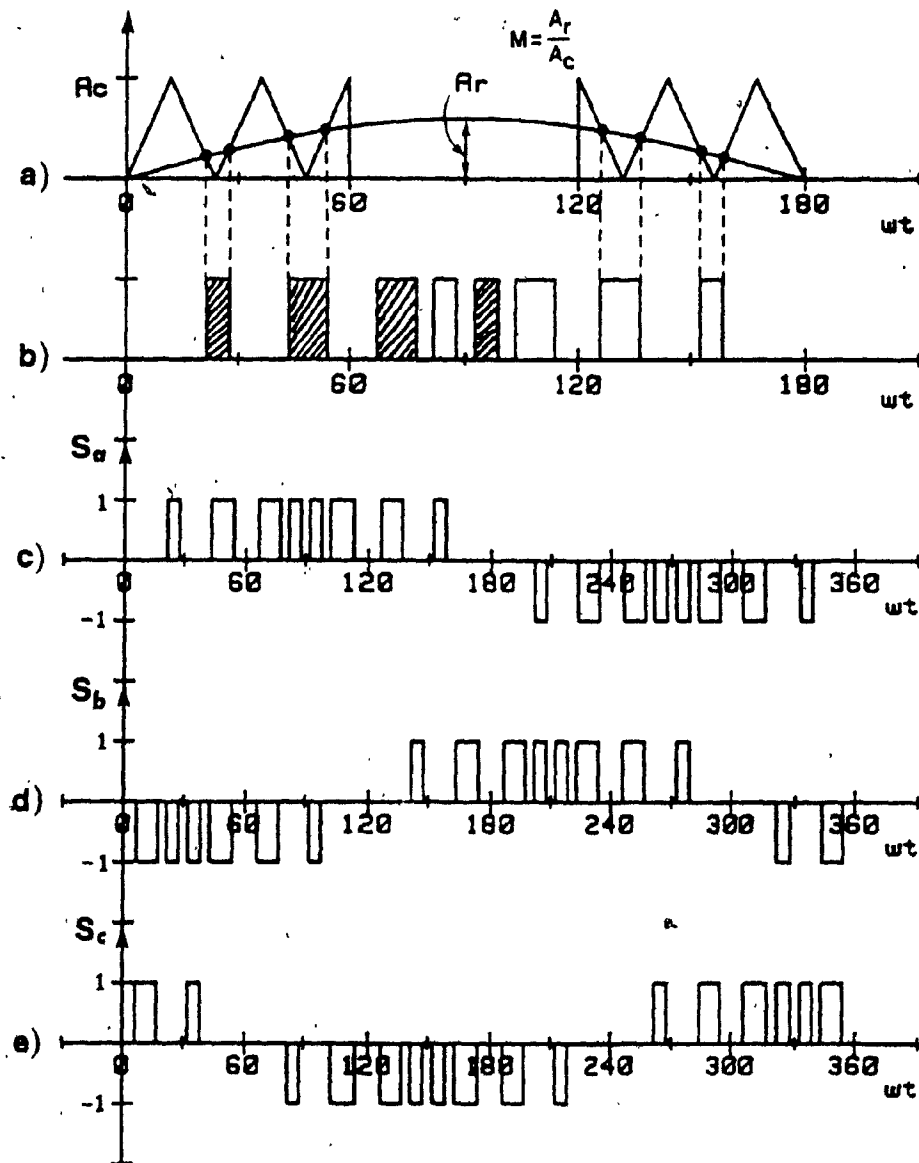


Fig. 2.7: The MSPWM switching function.

a,b) Derivation of an MSPWM switching function.

c-e) MSPWM switching function for three-phase converters.

signal and the reference signal, the switching points (hence pulses) can be determined (Fig. 2.7b). The pulses in the middle ( $60^\circ - 120^\circ$ ) of  $S_2$  (wt) are determined by considering the mirror images of the pulses in the first and last 60 degree intervals (Fig. 2.7b), while the next half-cycle of the  $S_2$  (wt) can readily be determined by considering the half-wave symmetry condition.

Furthermore, the width of the pulses as well as the amplitude of the fundamental component of  $S_2$  (wt) can be varied by varying the modulation index  $M$  in the manner described earlier when discussing the SPWM technique. Also,  $M$  must be restricted below unity to ensure normal operation. The normal operation of a balanced three-phase system requires that the following correspondence between the carrier frequency and the reference frequency be satisfied.

$$f_c / f_r = 6m + 3, \quad m=1, 2, 3, \dots \quad (2.11)$$

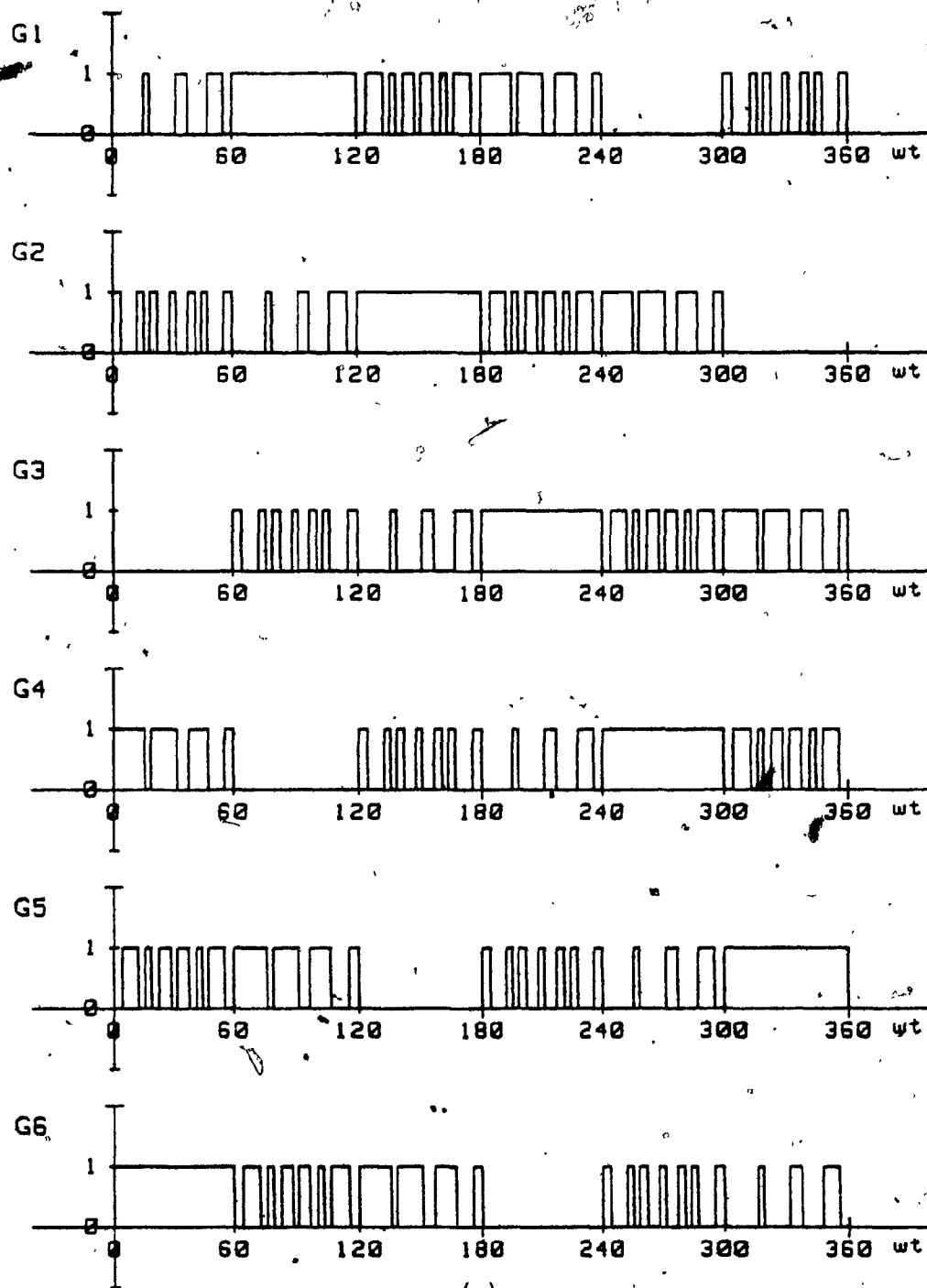
where

$m$  = number of pulses in the first 60 degree interval  
of an  $S_2$  (wt).

Therefore, the number of pulses per half-cycle  $N_h$  is given by:

$$N_h = 4m \quad (2.12)$$

Fig. 2.8 shows examples of the gating signals for voltage-source and current-source converters. From this figure it is apparent that for the same number of pulses, the switching frequency of a voltage-source



(a)

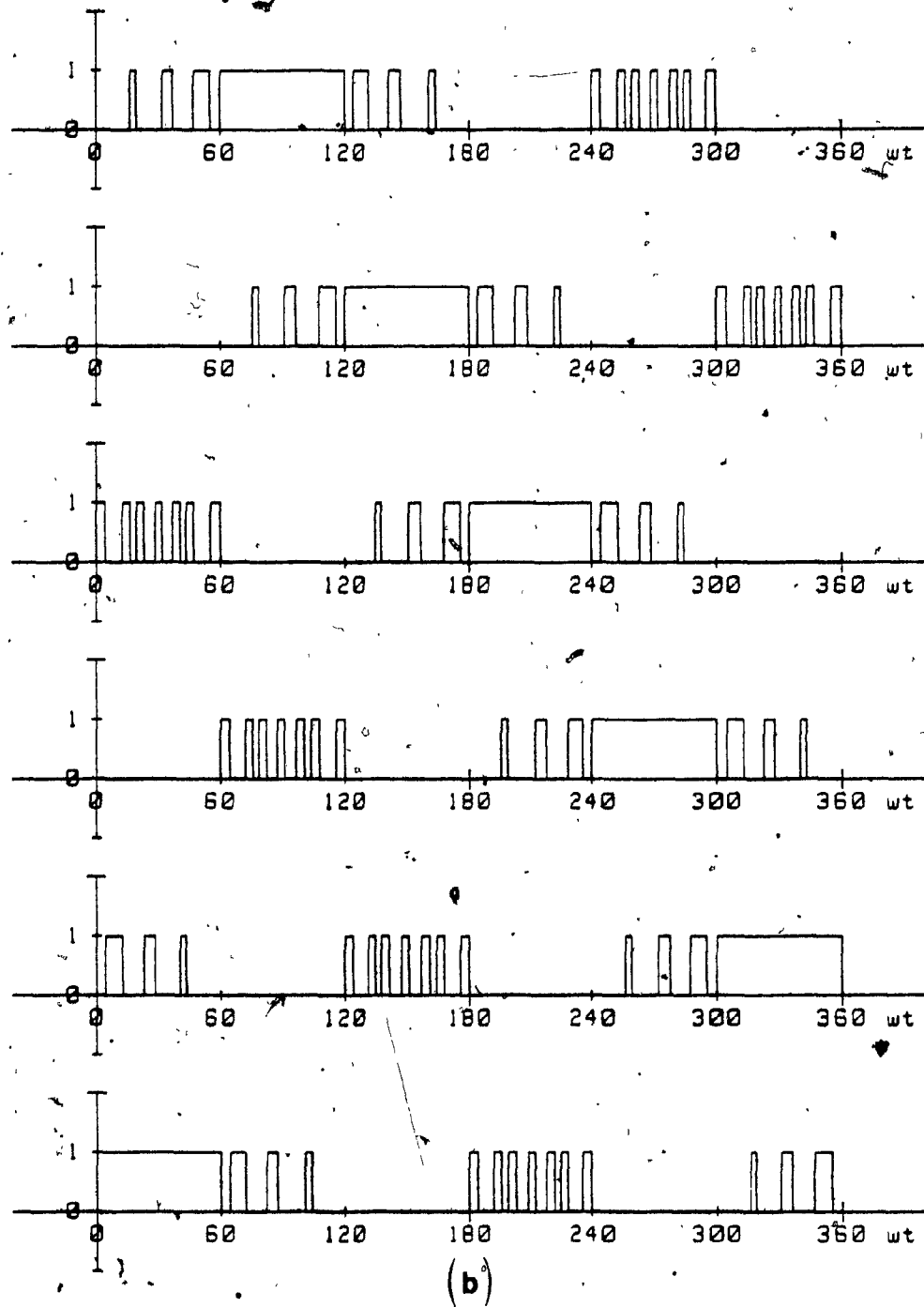


Fig. 2.8: Examples of MSPWM gating signals for voltage-source and current-source converters with  $N_p=12$  and  $M=0.6$ .

- (a) For voltage-source converters.
- (b) For current-source converters.

converter switch is higher than that of a current-source converter switch. Those switching frequencies are given by:

$$f_{sv} = \left(\frac{3}{2} N_h + 3\right) f_r \quad (2.13a)$$

$$f_{sc} = (N_h + 2) f_r \quad (2.13b)$$

Fig. 2.9 shows the frequency spectra of  $S_2$  (wt) with  $N_h=8$  and 12 at  $M=1$ , from which it is observed that the order of dominant harmonic components ( $d_l$  and  $d_h$ ) of an  $S_2$  (wt) are a function of  $N_h$ , and they are given by:

$$d_l = 1.5 N_h + 1 \quad (2.14)$$

$$d_h = 1.5 N_h + 5$$

or, they can be expressed in terms of  $f_c$  and  $f_r$ ; i.e.,

$$d_l = f_c - 2f_r \quad (2.15)$$

$$d_h = f_c + 2f_r$$

Hence, they can easily be specified when the  $N_h$  (or  $f_c$ ) is known. Moreover, Fig. 2.10 shows their magnitudes in terms of the modulation index  $M$ , and, as can be seen from this figure, their maximum values occur at  $M=0.7$ .

Finally, the corresponding  $DF_s$  values (eqn. 2.10) versus  $N_h$  are plotted in Fig. 2.11, from which it is observed that the  $DF_s$  improvement past the  $N_h=16$  point is relatively insignificant.

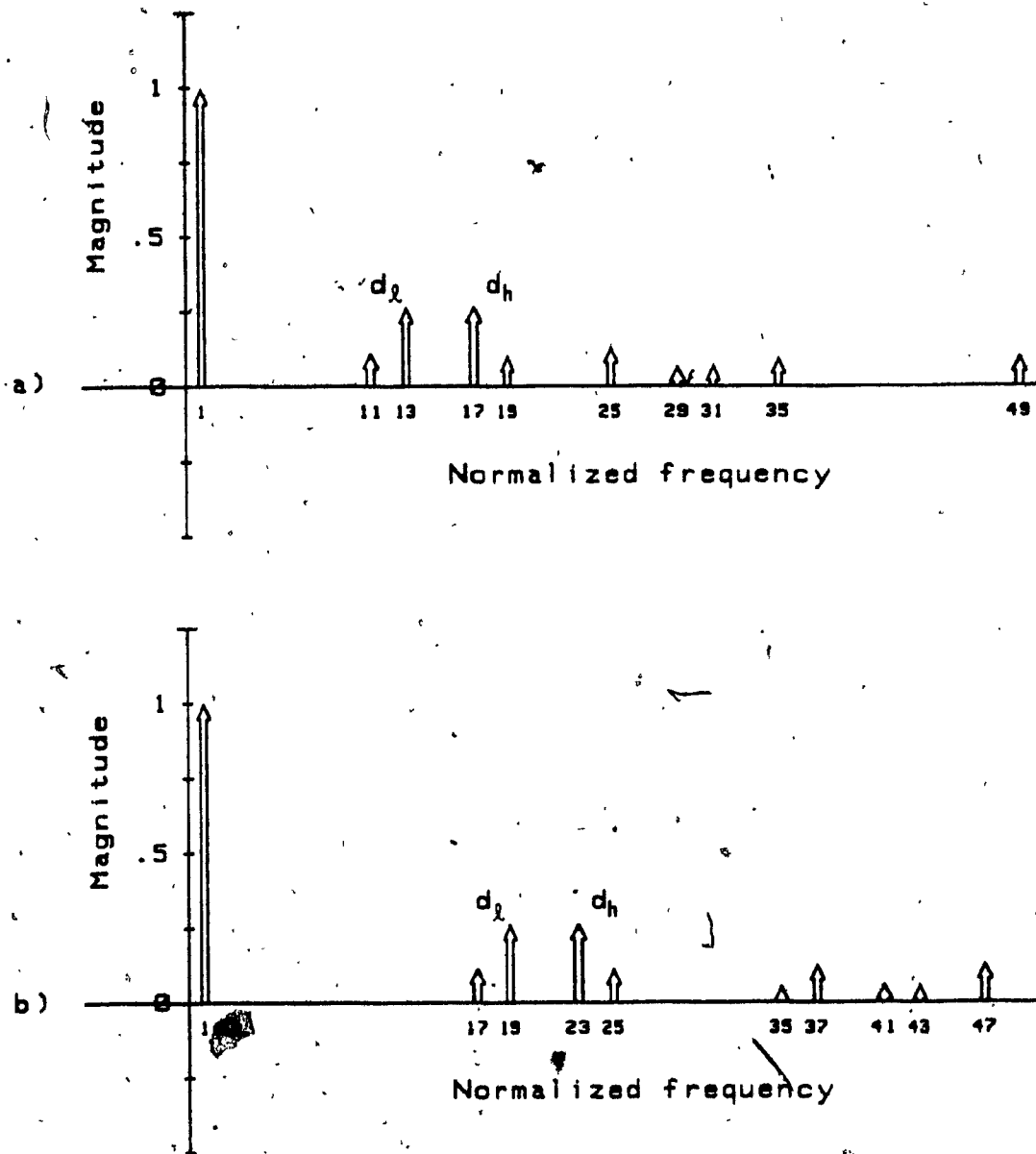


Fig. 2.9: Examples of the frequency spectra of MSPWM switching functions with  $N_h=8$  and 12 at  $M=1$ .

- a) With  $N_h=8$ .
- b) With  $N_h=12$ .

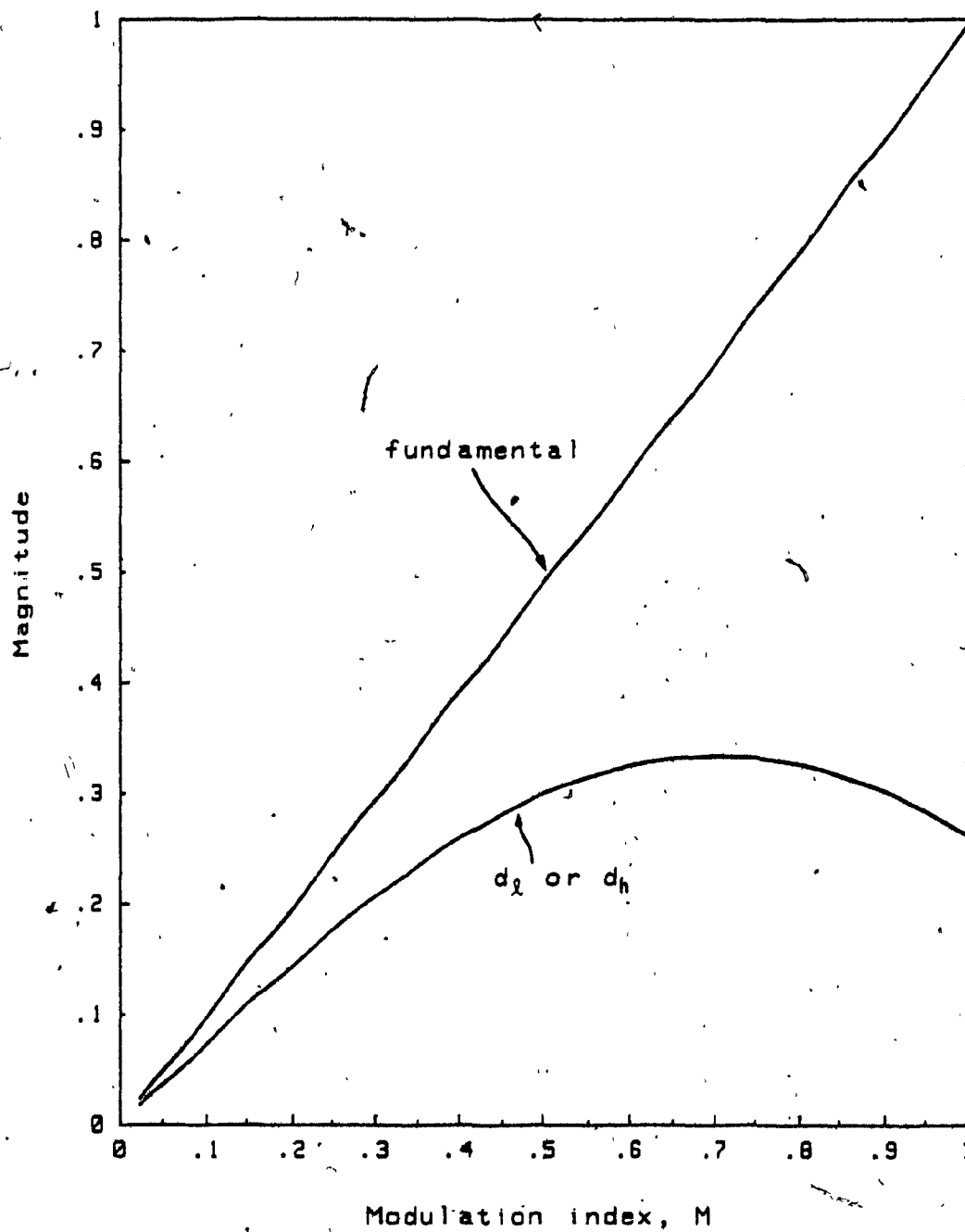


Fig. 2.10: Variation of dominant harmonic components,  $d_l$  and  $d_h$ , of an MSPWM switching function as a function of the modulation index,  $M$ .

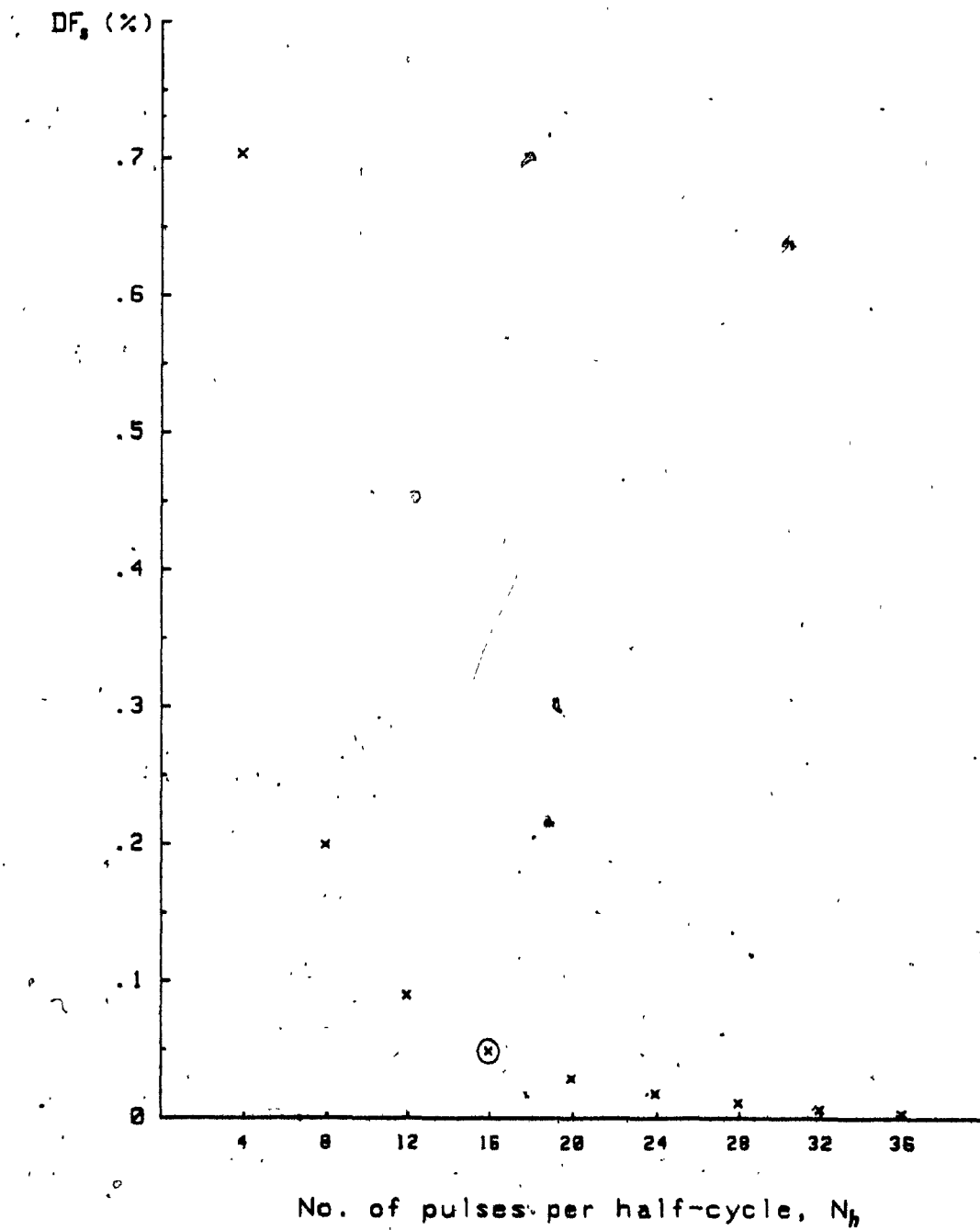


Fig. 2.11:  $DF_s$  -vs-  $N_h$  plot with MSPWM switching functions at  $M=1$ .

Therefore, 16-pulses per half-cycle can be assumed to be the optimum  $N_h$  for the  $S_2$  (wt) type of switching function, assuming that suitable switching devices are available.

#### 2.4 Optimized PWM (OPWM) Switching Functions: $S_3$ (wt)

An interesting alternative to the previously discussed PWM technique is the technique of selected harmonic elimination [49], [50] which has recently received wide attention [51]. In this case, the switching points are chosen at predetermined angles of a square wave so that a number of selected harmonic components can be eliminated. However, since elimination of selected harmonics does not necessarily yield an optimum frequency spectrum, variations of this technique that yield further improved frequency spectrum can be employed [52]. These further improvements can be obtained by optimizing specific object functions that represent system qualities such as the size of input and output filters, pulsating torques, speed ripple, motor losses. An example of such a technique and the resulting switching function is shown in Fig. 2.12. Since in this case the objective is to minimize the size of input/output filters, the object function employed to determine switching angles  $\alpha_1$  to  $\alpha_5$  of the  $S_3$  (wt) in Fig. 2.12a is  $DF_s$  of the  $S_3$  (wt). It is noted that the total pulse-width per half-cycle is 120 degrees, which is also the maximum pulse-width that can be utilized for three-phase systems.

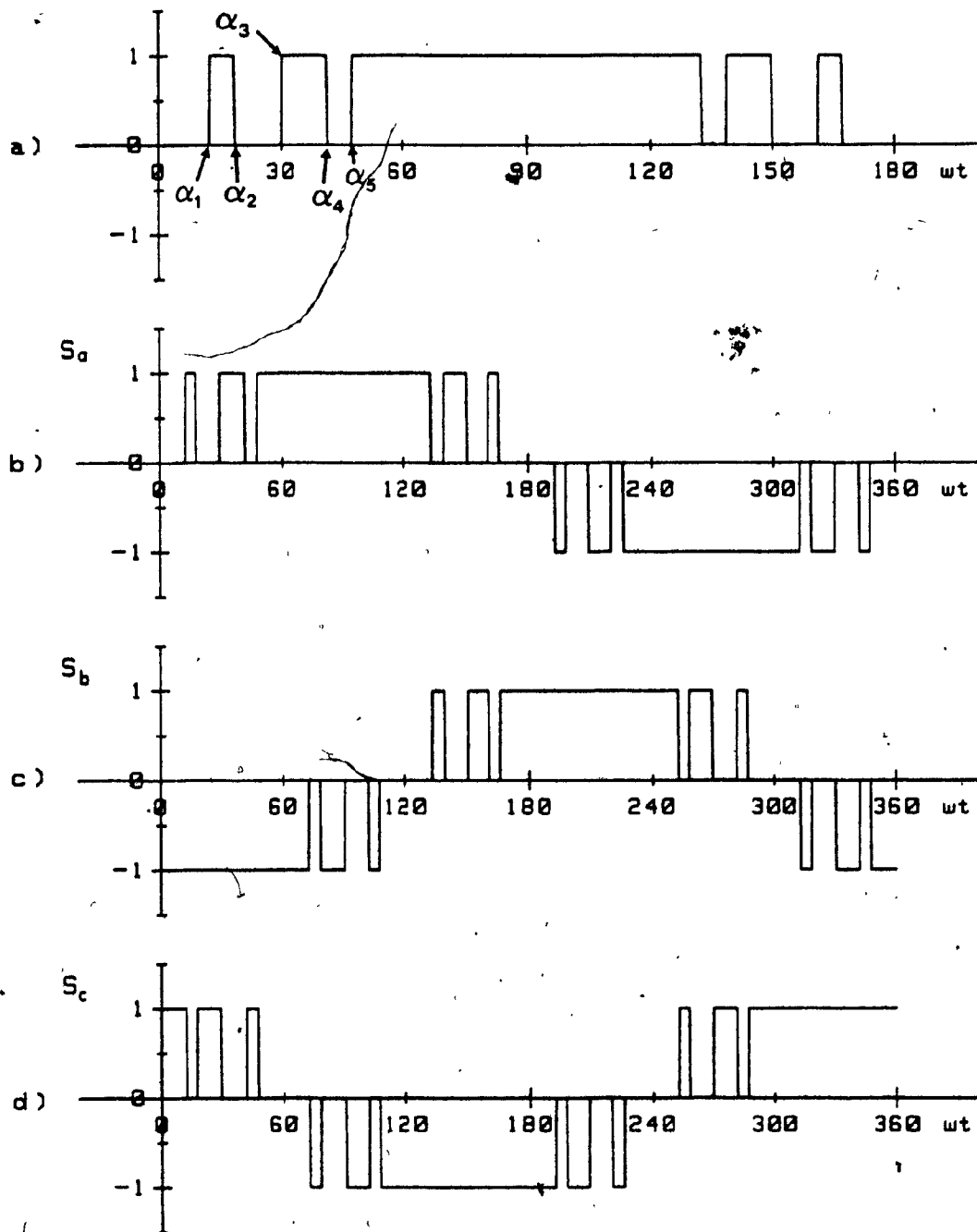


Fig. 2.12: The OPWM switching function.

The frequency spectra of  $S_3$  (wt) with  $N_h=9$  and 11 are plotted in Fig. 2.13, and it is noted that the dominant harmonic components,  $d_1$  and  $d_h$ , can not be given by general equations.

Finally, Fig. 2.14 shows the characteristic  $DF_s$  -vs-  $N_h$  curve for  $S_3$  (wt) type of switching functions, and from this figure it can be concluded that 11-pulses per half-cycle is an optimum  $N_h$  value for the OPWM switching function.

## 2.5 Conventional Single-Pulse Switching Function: $S_4$ (wt)

This is the well-known switching function which is composed of a 120 degree single pulse per half-cycle (Fig. 2.11) for three-phase controlled bridge rectifier and six-step inverter. Since this type of switching function has been widely used in industrial applications, it is included here for comparison purposes. Its frequency spectrum is shown in Fig. 2.15, from which it can be seen that there exist low-order harmonic components having the magnitude of  $100/k$  % (where  $k$  is the harmonic order) of the fundamental component.

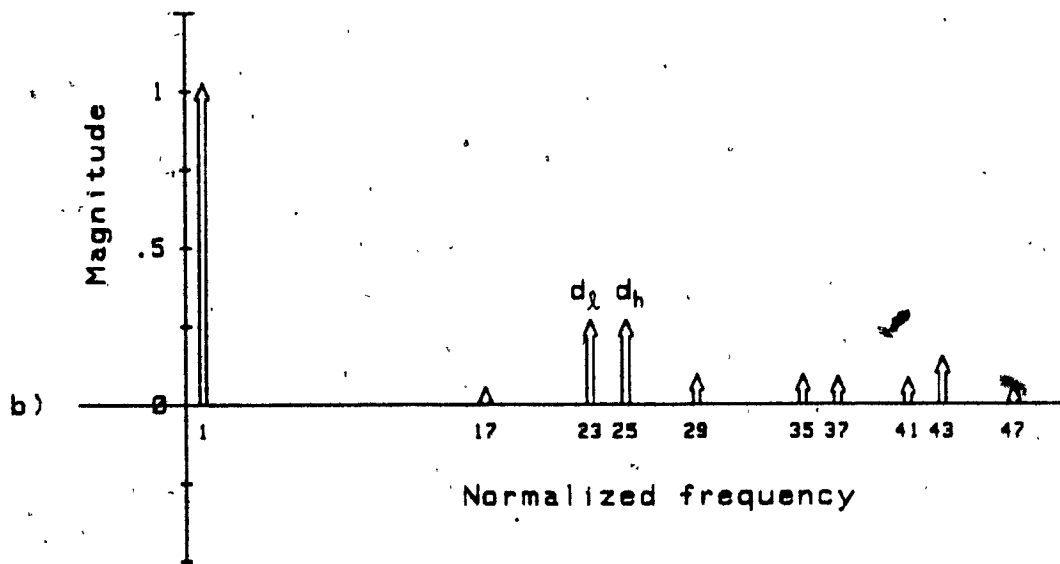
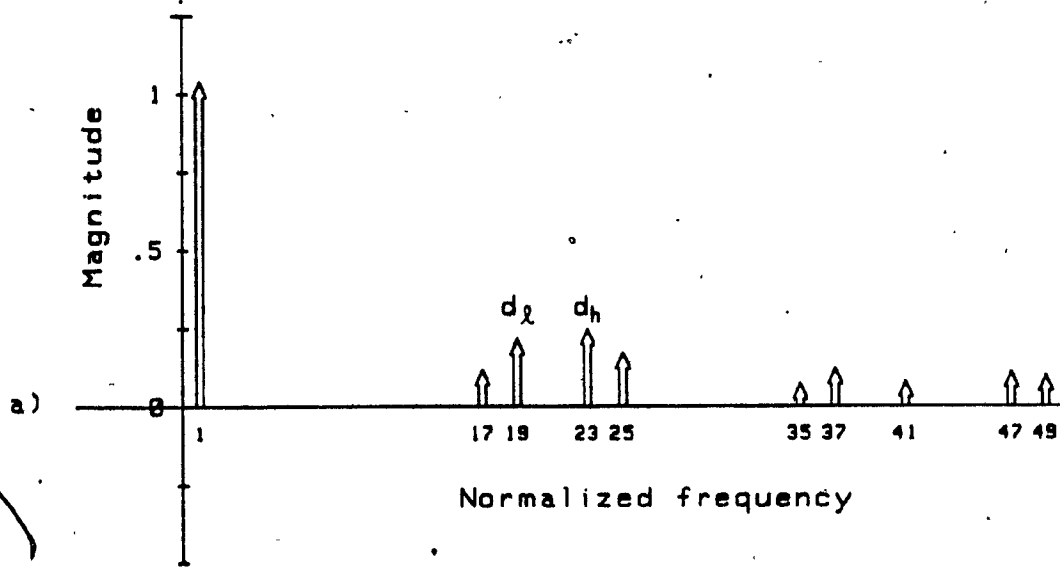


Fig. 2.13: Examples of the frequency spectra of OPWM switching function with  $N_h = 7$  and 9.

- a) With  $N_h = 7$ .  
b) With  $N_h = 9$ .

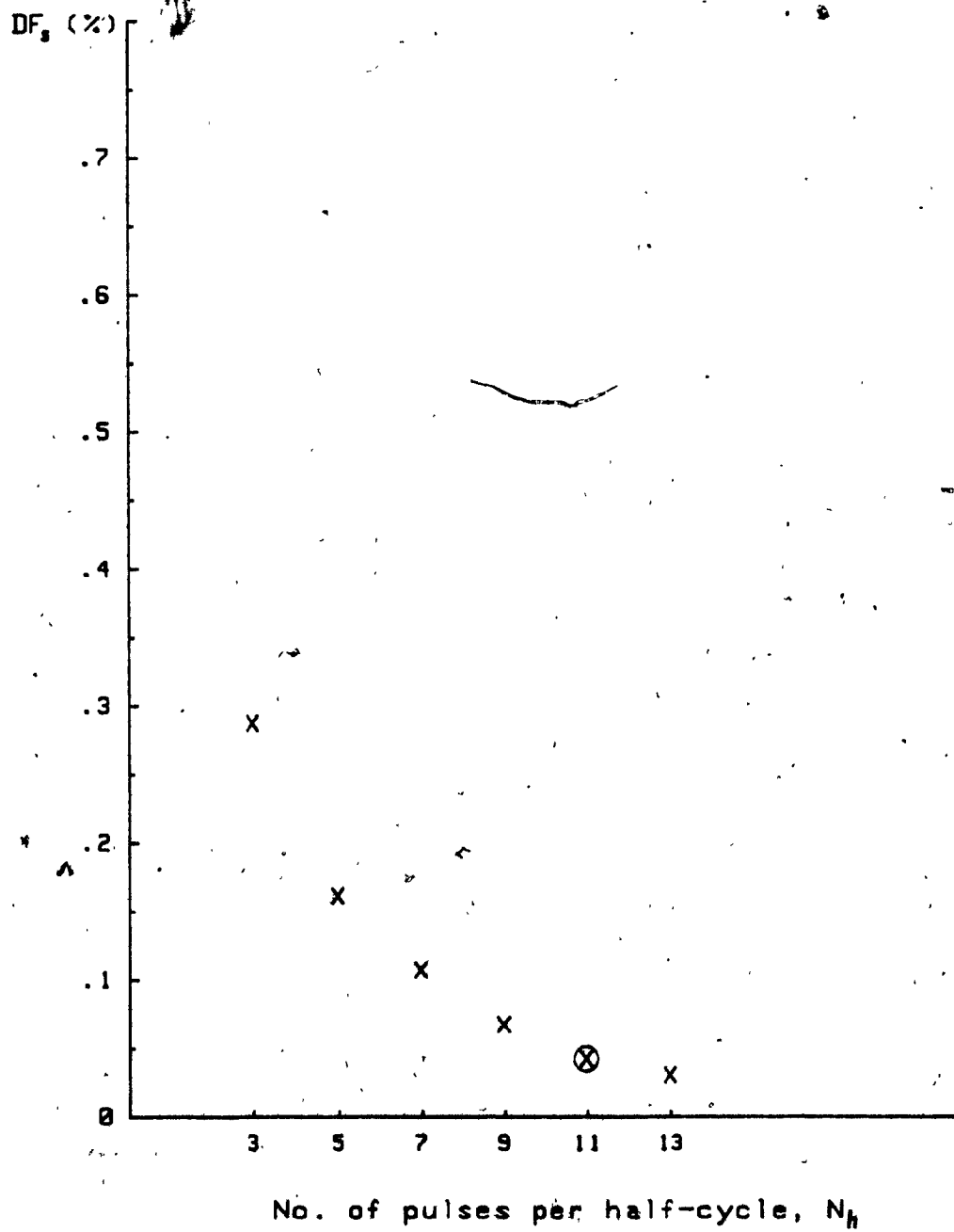


Fig. 2.14:  $DF_s$  -vs-  $N_h$  plot with OPWM switching functions.

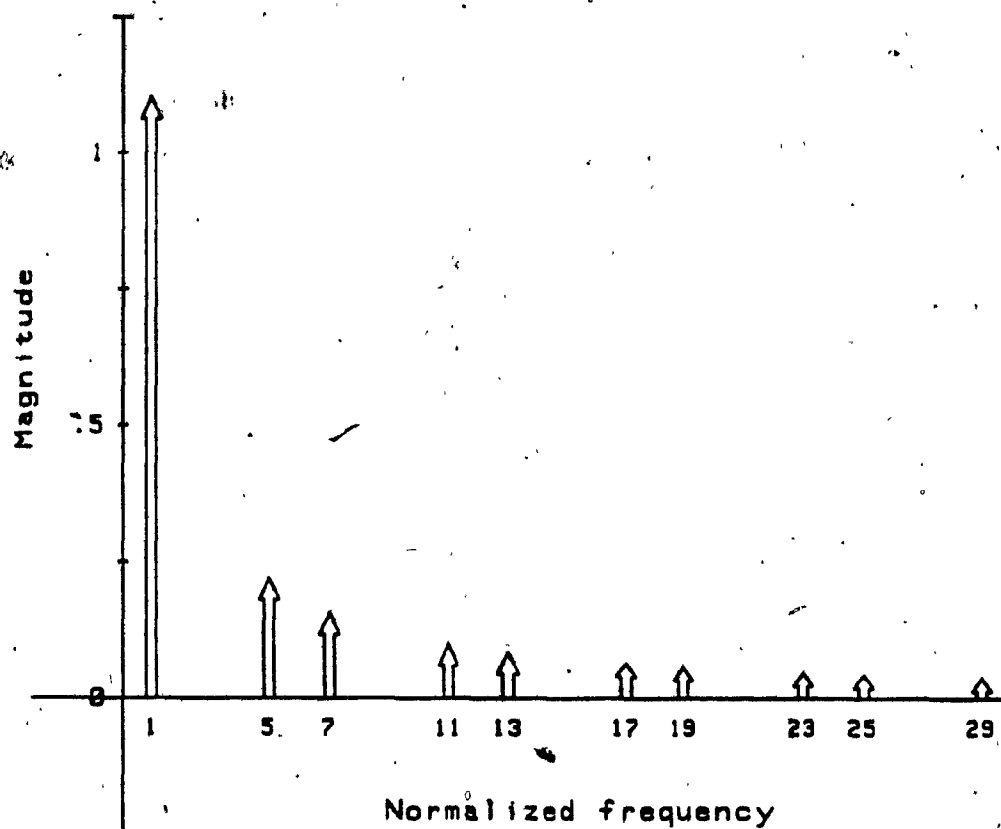


Fig. 2.15: Frequency spectrum of the conventional single-pulse switching function.

## 2.6 Discussion

Regarding the  $S_1$  (wt),  $S_2$  (wt), and  $S_3$  (wt) type of switching functions, it is noted that the associated distortion factor ( $DF_s$ ) approaches zero as the number of pulses per half-cycle  $N_h$  approaches infinity and that the optimised PWM switching functions offer the best harmonic characteristics. Moreover, the microcomputer (or digital PWM) is especially adaptable to this type of PWM where the required gating signals (or look-up table of the angles) can be stored in a ROM. However, since the switching points of  $S_3$  (wt) functions are fixed, they are suitable for uncontrolled converter applications. The maximum fundamental magnitudes for the four types of switching functions are listed in Table 2.1.

TABLE 2.1: MAXIMUM FUNDAMENTAL AMPLITUDES OF FOUR SWITCHING FUNCTIONS.

	$S_1$ (wt)	$S_2$ (wt)	$S_3$ (wt)	$S_4$ (wt)
p.u.	0.866	0.998	1.025	1.103
%	86.8	100.0	102.7	110.5

Comparing the SPWM and the MSPWM switching functions, the MSPWM switching functions yield 13 % higher amplitude compared to the fundamental component of the SPWM switching functions. To overcome this shortcoming of the SPWM switching functions, the third-harmonic-injection SPWM technique described in Appendix A can be applied to both rectifiers and inverters. However, the third-harmonic-injection SPWM switching functions are not included here because the amplitude of the fundamental component and harmonic characteristics are more or less the same as those of the MSPWM switching functions.

## 2.7 Conclusion

In order to simplify the analysis and design of static power converters, the switching function concept has been introduced and defined. Four kinds of switching functions have been described and their characteristics discussed in detail in order to make the best use of them in the following chapters.

## CHAPTER 3

### ANALYSIS AND DESIGN OF OPTIMUM THREE-PHASE PWM RECTIFIERS

#### 3.1 Introduction

As discussed in Chapter 1 the ac/dc conversion is of considerable practical importance, typically achieved by using phase-controlled rectifiers. However, the phase-controlled rectifier has some disadvantages, such as poor input power factor, and a considerable amount of low-order harmonics in the input line currents and output voltage. To overcome these shortcomings, some auxiliary reactive components which include power-factor correction capacitors and large sized input/output filters are generally required. This chapter will demonstrate that the introduction of forced commutation (hence PWM control technique) is the required step towards minimizing the input/output filters and improving the input power factor as well.

Three kinds of PWM switching functions,  $S_1(\omega t)$ ,  $S_2(\omega t)$ , and  $S_3(\omega t)$  described in Chapter 2, are considered in order to minimize the input/output filters and/or to improve the input power factor [53]. Since the conventional single-pulse switching function  $S_4(\omega t)$  shown in Fig. 2.11 has been widely used in industrial applications, it is included here for comparison purposes. The input and output stages are analyzed in detail, and the algorithms for designing input/output filters are proposed. Special emphasis is given on the 'optimum' input

filter design, since no comprehensive information on this topic is available. All the relevant data such as the optimum filter component values, the corresponding kVA ratings, and the total input power factor characteristics are presented. Finally, some predicted key results are experimentally verified on a 1 kW laboratory set-up.

### 3.2 System Description and Principles of Operation

Fig. 3.1 shows the simplified circuit diagram of a three-phase rectifier system investigated in this chapter. It consists of a three-phase mains, a set of input filter, a PWM rectifier, an output filter, and a load. The three-phase mains is assumed to be balanced and distortion-free. The input and output filters are assumed to be of second order and lossless. Switches  $SW_1$  to  $SW_6$  are assumed to be ideal and to be of gate turn-off type, such as bipolar transistors, MOSFET's, GTO's, etc.. The load can be of any type requiring a dc supply, such as dc motors, batteries, inverters, etc.. However, for the sake of simplicity, it is represented here by an equivalent resistive load. For the best use of derived results, the per unit (p.u.) system is employed, in which the rated dc output voltage and current are taken as 1 p.u. voltage and 1 p.u. current, respectively. Samples of four kinds of switching functions,  $S_1(wt)$ ,  $S_2(wt)$ ,  $S_3(wt)$ , and  $S_4(wt)$ , and their corresponding rectifier output voltage waveforms are shown in Figs. 3.2, 3.3, 3.4, and 3.5, respectively. It is noted that since for  $n=1, 2, 3, 4$ ,  $S_{nb}(wt)=S_{na}(wt-120^\circ)$  and  $S_{nc}(wt)=S_{na}(wt-240^\circ)$ , only

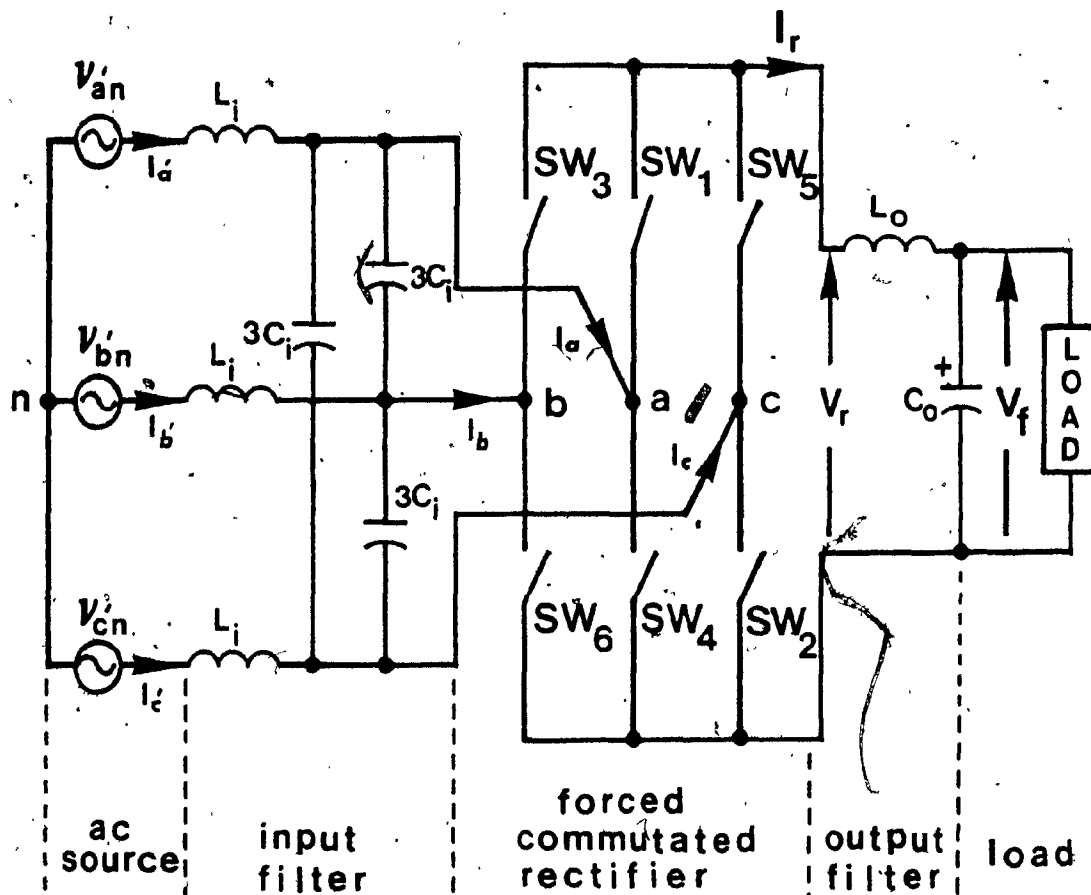


Fig. 3.1: Simplified circuit diagram of a three-phase rectifier studied.

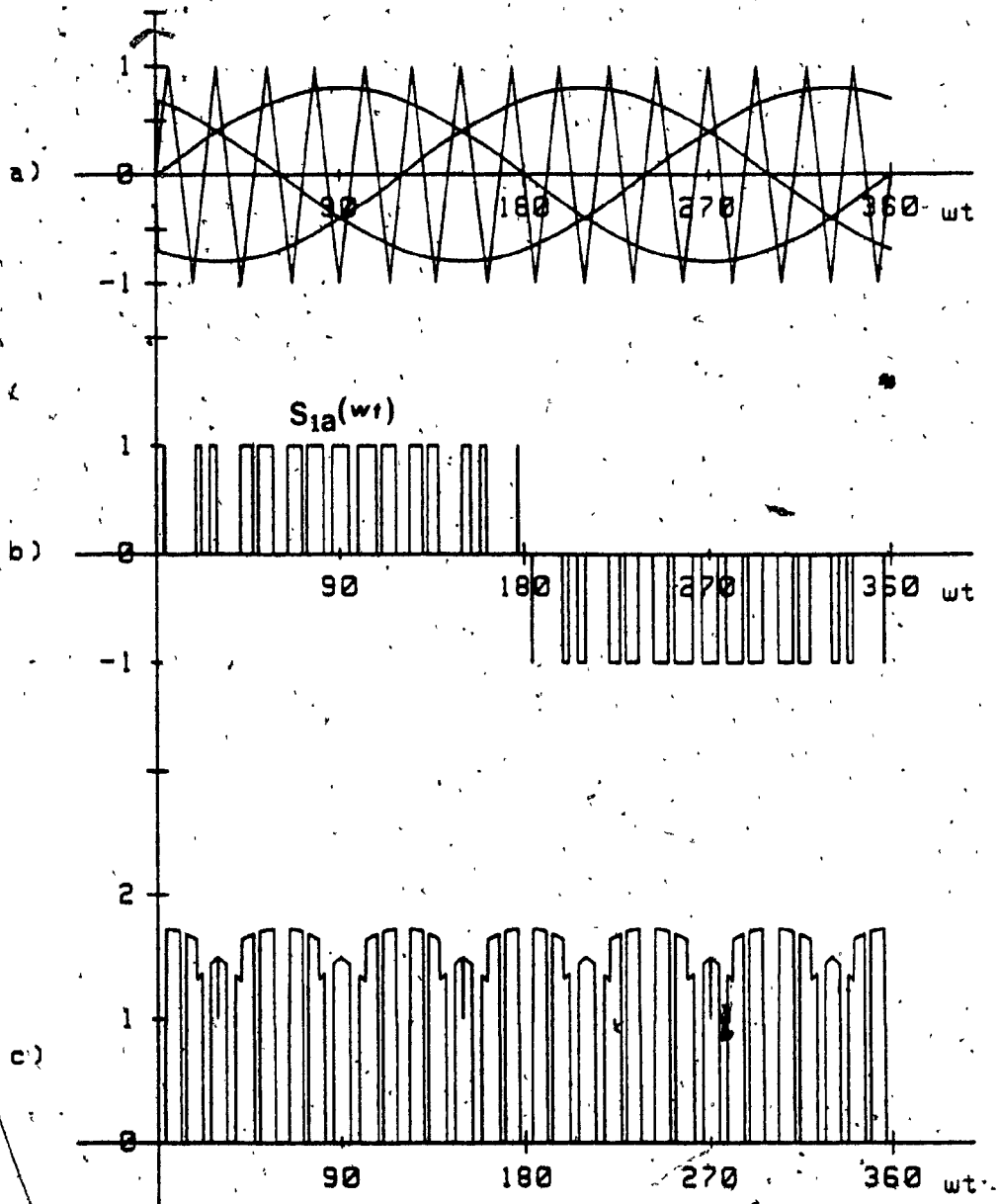


Fig. 3.2: Rectifier voltage control by means of SPWM scheme.

- a) Definition of the SPWM scheme.
- b) Sample of an  $S_1(\omega t)$  type of switching function.  
( $N_h=15$  and  $M=0.8$ )
- c) Resulting rectifier output voltage,  $V_r(\omega t)$ .

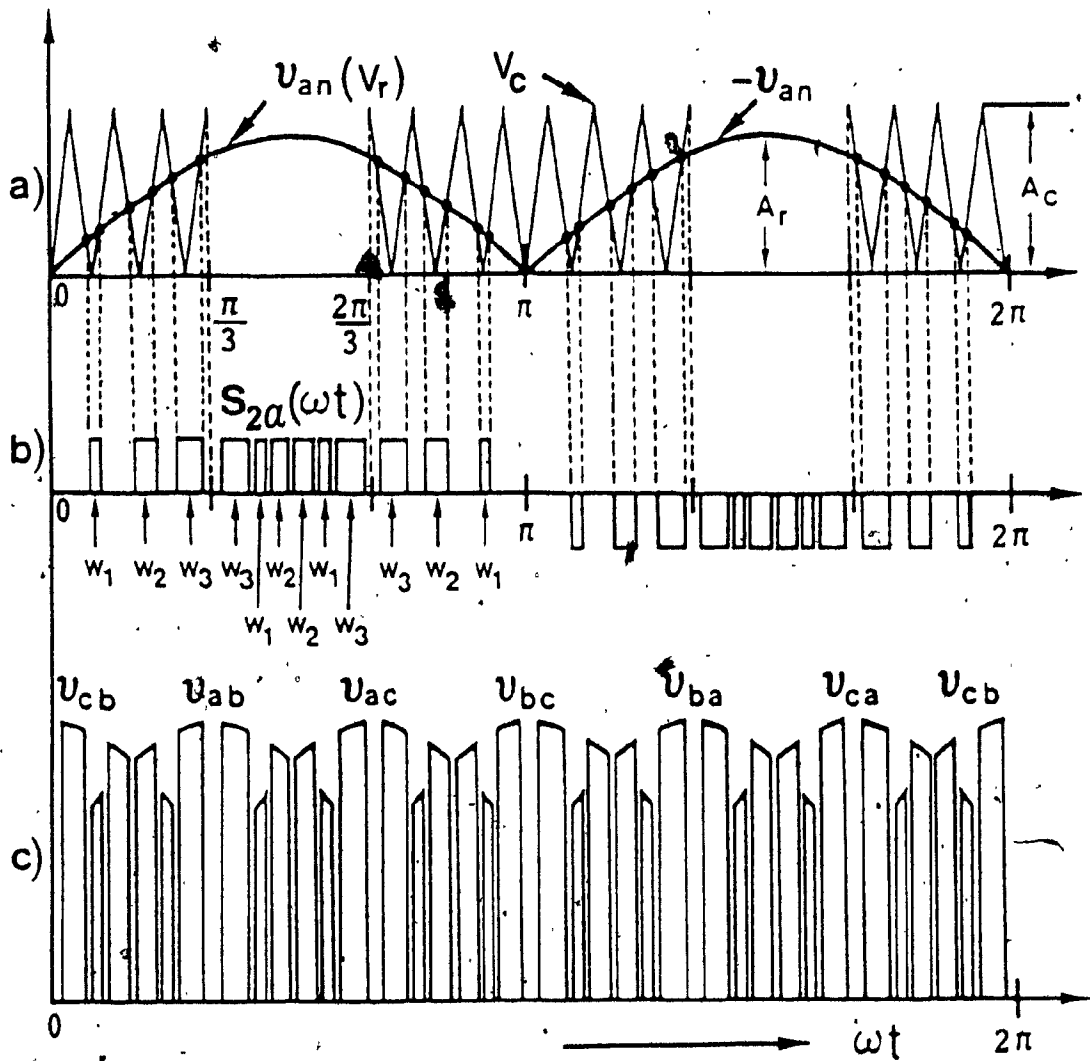


Fig. 3.3: Rectifier voltage control by means of MSPWM scheme.

- a) Method of modulation ( $M=0.8$ ).
- b) Sample of an  $S_2(\omega t)$  type of switching function ( $N_h=12$ ).
- c) Resulting rectifier output voltage.

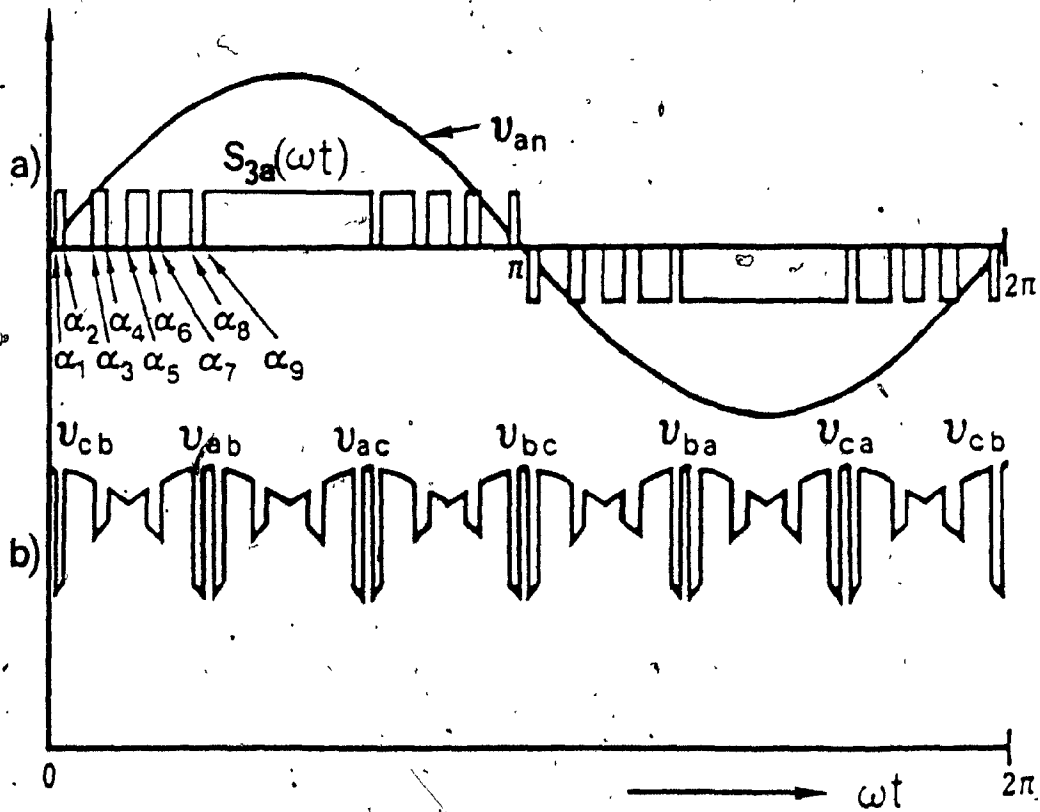


Fig. 3.4: Rectifier voltage control by means of OPWM scheme .

- a) Sample of an  $S_{3a}(\omega t)$  type of switching function.  
 ( $\alpha_1=2^\circ, \alpha_2=4.6^\circ, \alpha_3=17.4^\circ, \alpha_4=22.3^\circ, \alpha_5=30^\circ,$   
 $\alpha_6=37.7^\circ, \alpha_7=42.6^\circ, \alpha_8=55.4^\circ, \text{ and } \alpha_9=58^\circ$ )  
 b) Resulting rectifier output voltage.

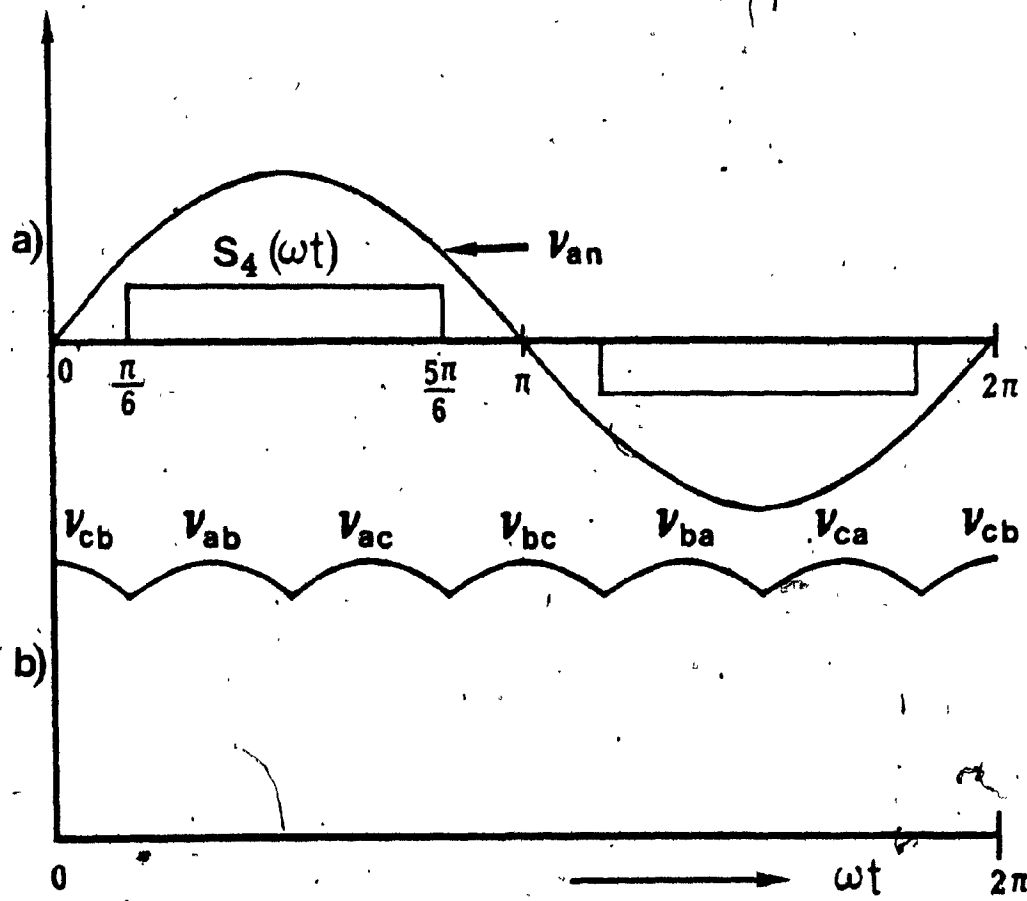


Fig. 3.5: Rectifier voltage control by means of the conventional method (with zero phase shift).

- a) Switching function and the corresponding phase voltage.
- b) Rectifier output voltage.

functions  $S_{no}(wt)$  need to be shown. Moreover, for  $n=1, 2, 3, 4$ ,  $x=a, b, c$ , and with reference to the switching functions it follows that:

- $S_{nx}(wt)=1 \Rightarrow$  switches in the positive group (i.e.  $SW_1, SW_3, SW_5$ ) are conducting,
- $S_{nx}(wt)=-1 \Rightarrow$  switches in the negative group (i.e.  $SW_4, SW_6, SW_2$ ) are conducting, and
- $S_{nx}(wt)=0 \Rightarrow$  both switches in the one of the three legs (i.e.  $SW_1$  and  $SW_4, SW_3$  and  $SW_6$ , or  $SW_5$  and  $SW_2$ ) are conducting.

and that at any instant a pair of switches (one from the positive group other from negative group) should be gated and conducting.

With  $S_1(wt)$  and  $S_2(wt)$  type of switching functions,  $N_h=15$  and 12 values are respectively chosen as examples. Thus, from (2.7b) and (2.13b) the switching frequencies per switch, are given by 1020 Hz and 840 Hz, respectively. In terms of controllability of power flow, these functions offer two 'degrees of freedom'; that is, (a) control by the modulation index  $M$  and (b) control by the phase shift (i.e.  $\alpha$  control). This implies that, for every rectifier operating point, a set of  $[M, \alpha]$  values, that yield required output power, exist. However, since the phase shifting technique inherently yields poor input power factor, only the control by the modulation index  $M$  is considered for the switching functions,  $S_1(wt)$  and  $S_2(wt)$ .

With  $S_3 (wt)$  type of switching functions, 9-pulses per half-cycle is chosen as an example; the gating signals are provided in Fig. 3.6. The switching frequency of a switch for the  $S_3 (wt)$  type of switching functions,  $f_s$ , is given by:

$$\begin{aligned} f_s &= N_h f_r \\ &= 9 \times 60 = 540 \text{ Hz} \end{aligned} \quad (3.1)$$

The control of power flow with this  $S_3 (wt)$  type of switching function can be achieved only by phase shifting  $S_3 (wt)$  with respect to its corresponding line-to-neutral voltage. Consequently, the significant improvement of the input power factor with this type of switching functions is not feasible. This problem, however, can be solved by introducing a variation of  $S_3 (wt)$  functions defined as:

$$S_{3x}(wt) = \frac{1}{2} [S_{3x}(wt+\alpha) + S_{3x}(wt-\alpha)] \quad (3.2)$$

(3.2) implies that a leading phase displacement can be obtained by phase shifting the  $S_3 (wt)$  function by  $-\alpha$  (i.e. advanced firing) with respect to the line-to-neutral voltage. Hence, it is possible to compensate any phase lag introduced by the delayed angle control (or by the supply transformer, etc.) by means of this leading phase displacement, always resulting in unity displacement power factor. The implementation of  $S_3 (wt)$  type of switching functions requires two rectifiers operating in parallel as shown in Fig. 3.7. Consequently,

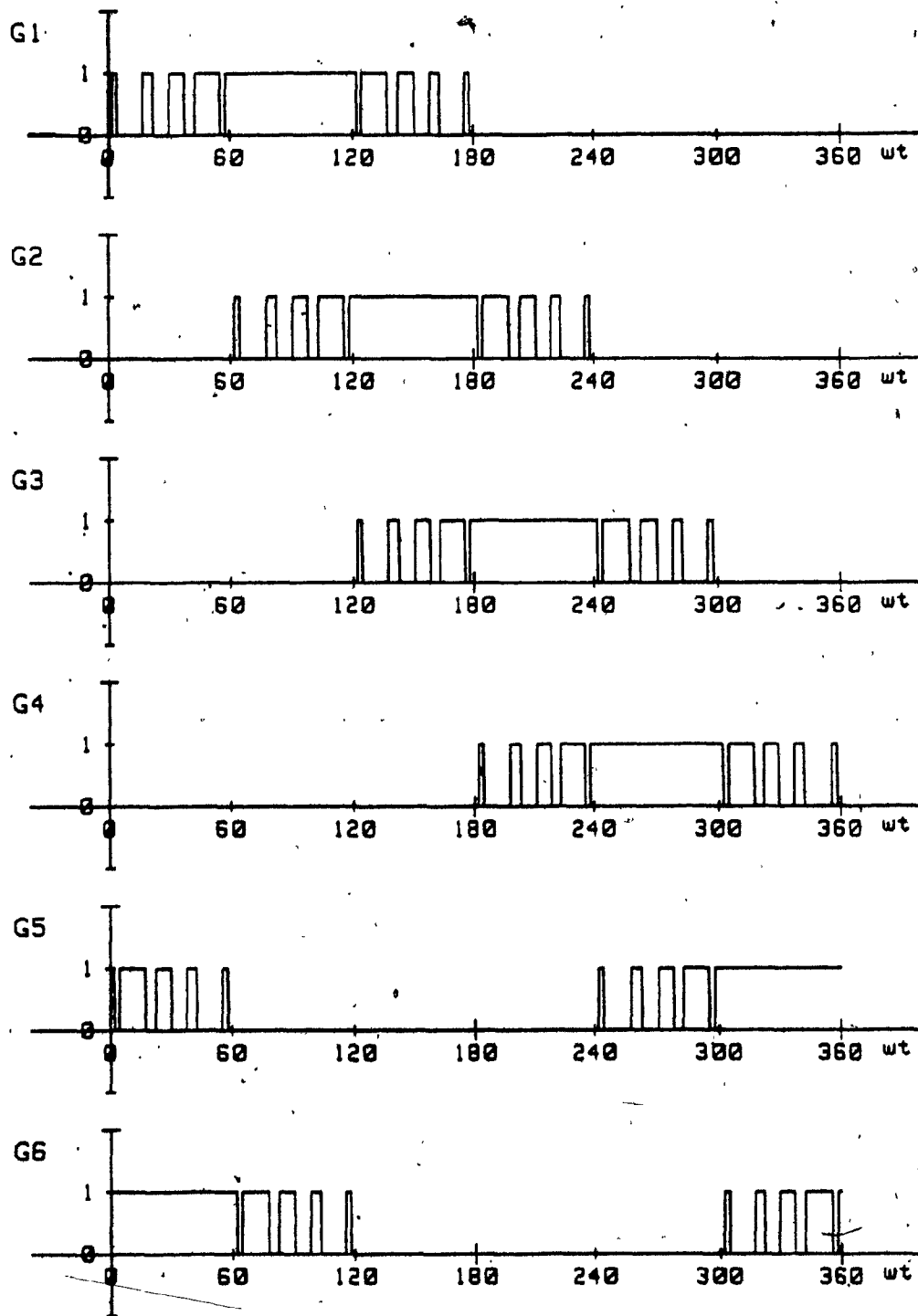


Fig. 3.6: Gating signals for the  $S_3$  (wt) type of switching function with  $N_h = 9$ .

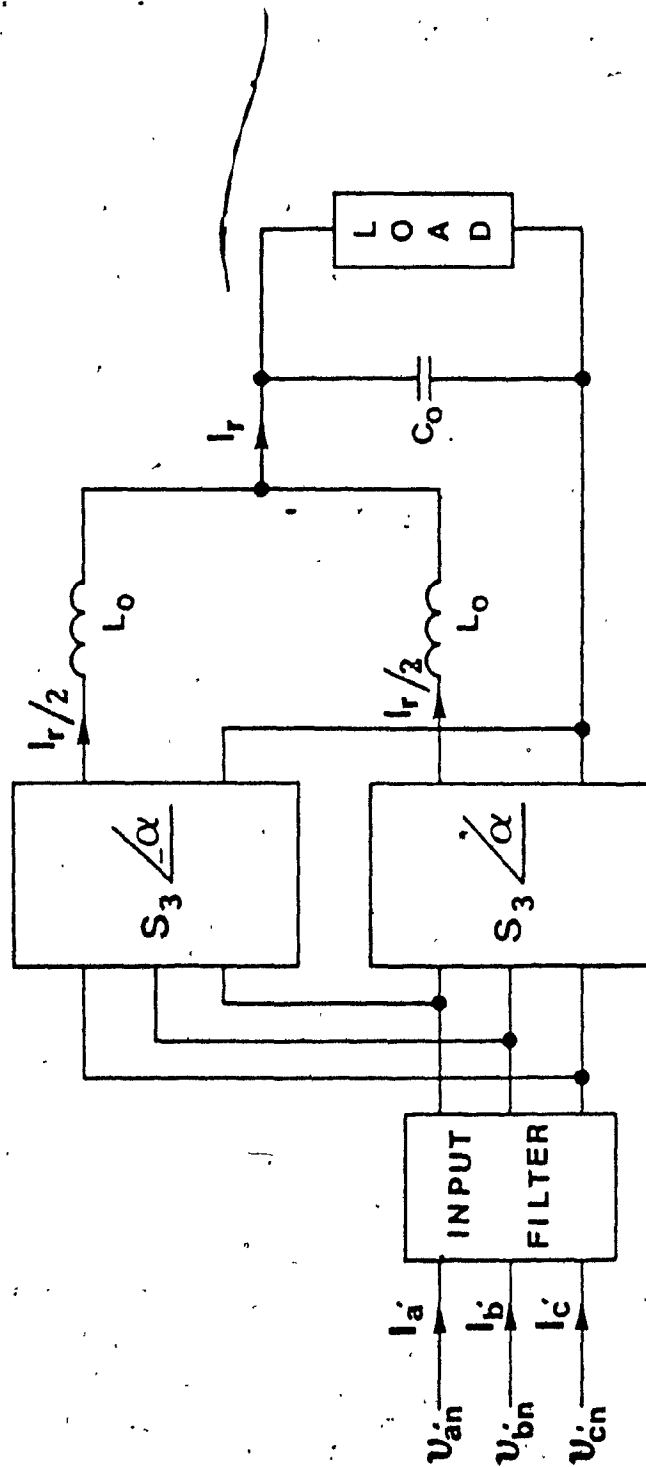


Fig. 3.7: Implementation of the  $S_3$  (wt) type of switching function.

they are suitable for higher power applications and the  $S_3$  (wt) type of switching functions are suitable for unregulated converters (i.e. constant dc bus voltage applications).

### 3.3 Input Stage Analysis and Input Filter Design

In addition to the assumptions mentioned in the previous section, the output rectifier current,  $I_r$ , is assumed to be ripple-free in this section. Moreover, in designing the input filter, four sets of design curves are proposed so that 'optimum' input filter components can be selected.

#### 3.3.1 Input stage analysis

As described in Section 2.1, (2.2), any one of the three input line currents,  $I_x(\omega t)$ , with  $S_{nx}(\omega t)$  type of switching function is given by:

$$I_x(\omega t) = I_r \cdot S_{nx}(\omega t) \quad (3.3)$$

where

$I_r$  = ripple-free dc output current.

In order to establish the harmonic characteristics of  $I_x(\omega t)$  with 1 p.u.  $I_r$  (i.e.  $S_{nx}(\omega t)$  itself), the distortion factor  $DF_n$  values defined in (2.10) are plotted in Fig. 3.8 as a function of the normalized output voltage,  $V_{dcN}$ . From this figure it can be seen that the PWM

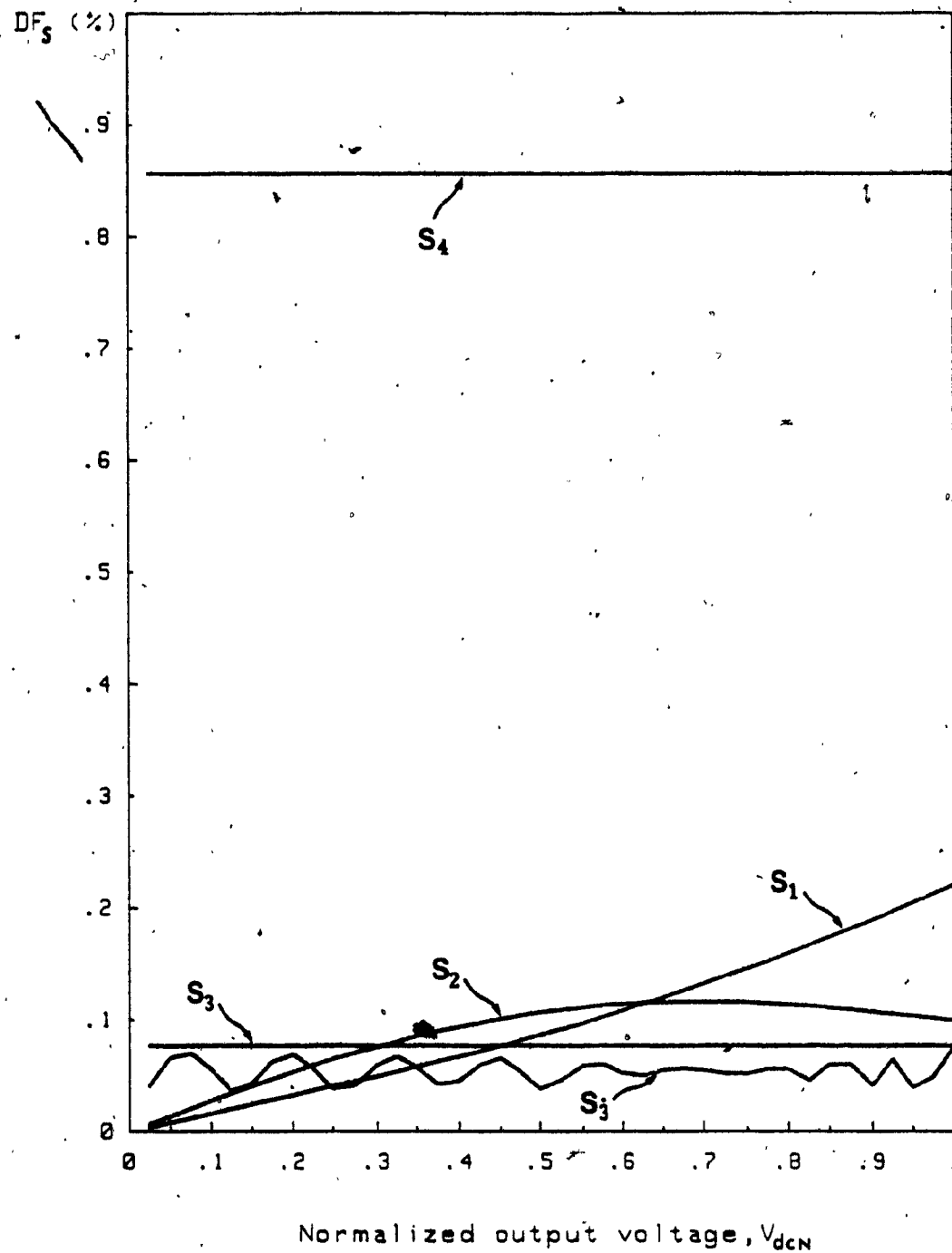


Fig. 3.8: Distortion factors of rectifier input line current versus normalized output voltage with switching functions  $S_1(wt)$  (1020 Hz),  $S_2(wt)$  (840 Hz),  $S_3(wt)$  (540 Hz),  $S_5(wt)$  (540 Hz), and  $S_4(wt)$  (60 Hz).

switching functions,  $S_1(wt)$ ,  $S_2(wt)$ , and  $S_3(wt)$  (also  $S_4(wt)$ ), yield considerably less harmonic distortion factor (DF) than that of the conventional switching function,  $S_4(wt)$ . It is therefore expected that the size of the input filter with the PWM switching function will be considerably smaller than that with the conventional switching function.

Another leading performance indicator for the PWM switching function is the resulting rectifier Total Input Power Factor (TIPF) characteristics. The TIPF is defined by:

$$\text{TIPF} = \frac{\text{Re}(\bar{I}_{x,1})}{\bar{I}_x} \quad (3.4)$$

where

$\bar{I}_x$  = rms value of the input line current,  $I_x(wt)$ , (Fig. 3.1),  
 $\text{Re}(\bar{I}_{x,1})$  = rms value of the fundamental real component  
of the  $I_x(wt)$ .

Plots of TIPF values computed without presence of the input filter are shown in Fig. 3.9, from which it is observed that the  $S_1(wt)$ ,  $S_2(wt)$ , and  $S_3(wt)$  functions provide significant overall improvements in the TIPF characteristics.

### 3.3.2 Total harmonic distortion of the input line current: THD<sub>i</sub>

Fig. 3.10 shows the analytical model of a lossless input filter. The input line current of a rectifier is considered to originate from a

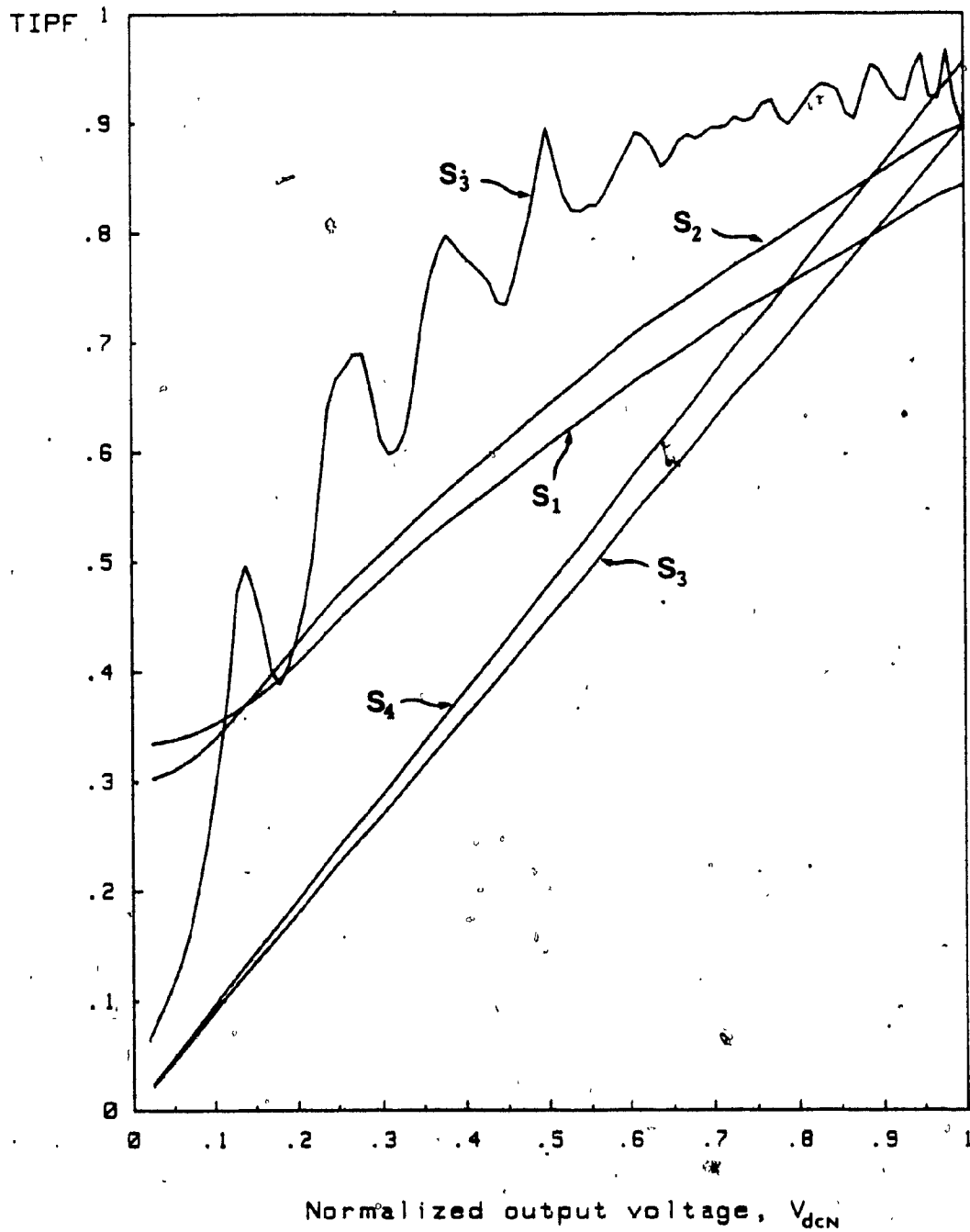


Fig. 3.9: TIPF (eqn. (3.4)) -vs-  $V_{dcN}$  plots without input filters.

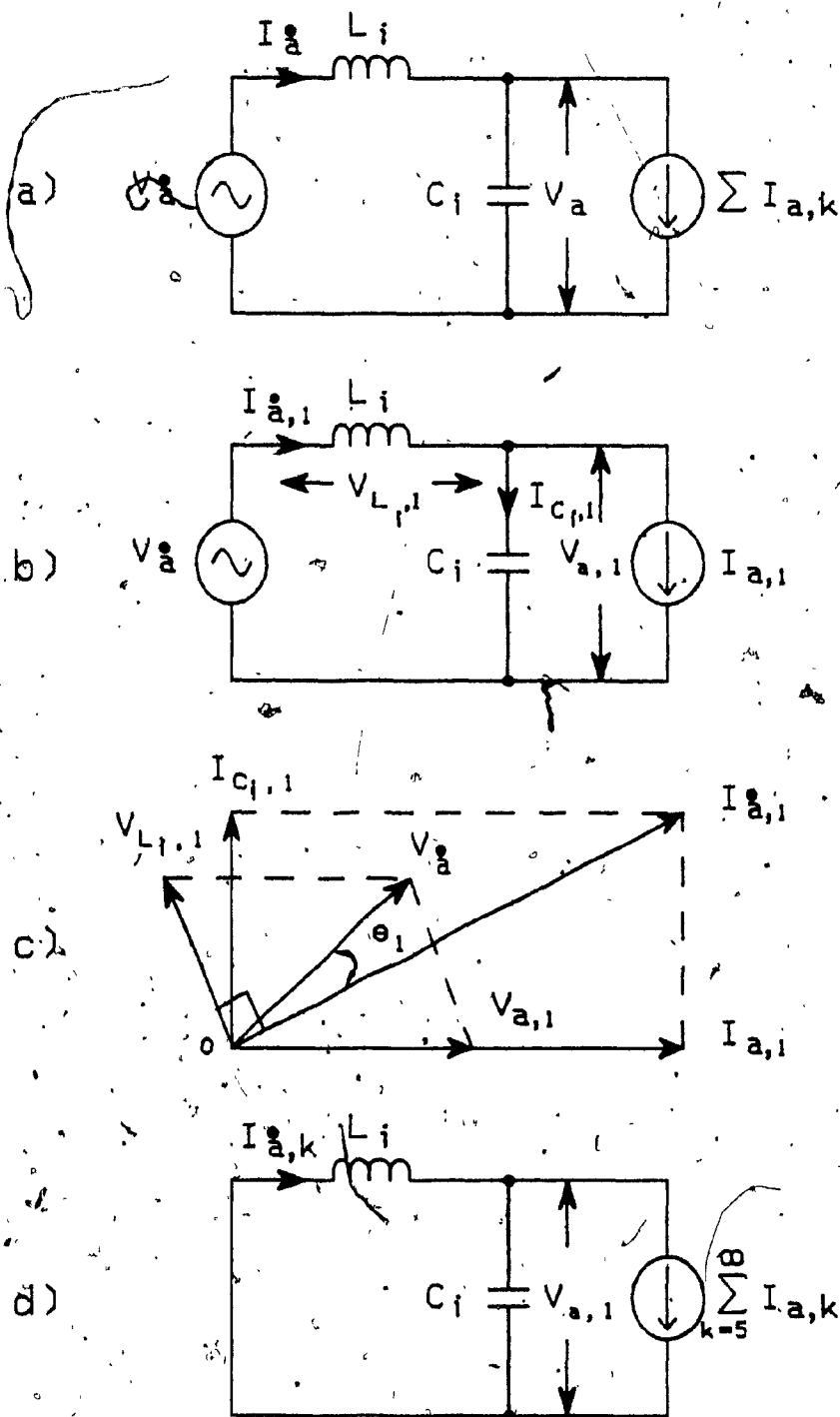


Fig. 3.10: Analytical model of a lossless input filter.

- a) Single-phase equivalent circuit.
- b) Single-phase equivalent circuit at fundamental frequency.
- c) Phasor diagram corresponding to b).
- d) Single-phase equivalent circuit at harmonic frequencies.

current source which includes all the harmonic components (Fig. 3.10a). The single-phase equivalent circuit for phase a at fundamental frequency and the corresponding phasor diagram are shown in Fig. 3.10b and 3.10c, respectively. Since the mains voltages are assumed to be purely sinusoidal, they can be regarded as short circuits for harmonic frequencies (other than the fundamental) as shown in Fig. 3.10d.

The input line current of a rectifier (for phase A) defined in (3.3) may be rewritten as:

$$I_a(\omega t) = \sum_{k=1}^{\infty} I_{a,k} \sin(k\omega t + \theta_{a,k}) \quad (3.5)$$

where

$I_{a,k}$  = amplitude of the k-th component of the rectifier input current,  $I_a(\omega t)$ ,

$\theta_{a,k}$  = phase displacement of the k-th component with respect to the reference signal (i.e. line-to-neutral voltage).

However, when a second-order input filter is introduced between the mains and the rectifier input stage, the fundamental voltage across the capacitor,  $V_{\alpha,1}$ , is adopted as the reference signal (Fig. 3.10).

The input current of the input filter,  $I_x(\omega t)$ , shown in Fig. 3.10a, can be expressed by:

$$I_x(\omega t) = \sum_{k=1}^{\infty} I_{x,k} \sin(k\omega t + \theta_{x,k}) \quad (3.6)$$

where

$I_{a,k}$  = amplitude of the k-th component of the input line current,  $I_a(wt)$ ,

$\theta_{a,k}$  = phase displacement of the k-th component of the  $I_a(wt)$  with respect to the reference voltage,  $V_{a,1}$ .

By relating the input and output current components of the input filter, the harmonic components in the  $I_x(wt)$  can be determined by:

$$I_{a,k} = - \frac{X_{C_1}}{k^2 X_{L_1} - X_{C_1}} I_{a,k}, \quad k=5,7, \dots \quad (3.7)$$

where

$X_{L_1}$  = impedance of the input filter inductor,  $L_1$ , at fundamental frequency,

$X_{C_1}$  = impedance of the input filter capacitor,  $C_1$ , at fundamental frequency.

The fundamental component of the ac source current,  $I_{a,1}$ , can be determined by the vector sum of  $I_{a,1}$  and the fundamental current through the capacitor  $C_1$ ,  $I_{c,1}$ ; that is,

$$I_{a,1} = I_{a,1} + I_{c,1} \quad (3.8)$$

where

$$I_{c,1} = - \frac{V_{a,1}}{X_{C_1}} \quad (3.9)$$

where

$V_{a,1}$  = amplitude of the fundamental component of the rectifier input voltage,  $V_a(wt)$ .

Since the harmonic content of the ac source current ( $I_a(wt)$ ) should be restricted to a certain acceptable level, the total harmonic distortion of the ac source current,  $THD_i$ , as next defined, can be used to select the  $L_i$  and  $C_i$  component values.

$$THD_i = \frac{100}{I_{a,1, \text{rated}}} (I_a^2 - I_{a,1}^2)^{1/2} \quad (3.10)$$

where

$I_a$  = amplitude of the input line current,  $I_a(wt)$ ,

$I_{a,1}$  = amplitude of the fundamental component of the  $I_a(wt)$ .

Therefore, the first set of design curves for the input filter is shown in Fig. 3.11, which illustrates a family of  $THD_i$  -vs-  $X_{C_i}$  curves for various  $X_{L_i}$  values. In this case, the  $THD_i$  values are plotted for the  $S_3(wt)$  function by assuming, for example, that the  $THD_i$  limit is 5 % of the rated rms fundamental current. They can be obtained as follows :

- (i) the frequency spectrum of  $I_a(wt)$ , obtained from (3.3) and (3.5) through Fourier series analysis,
- (ii) the frequency spectrum of  $I_a(wt)$ , computed from (3.7) and (3.8) for a given set of  $X_{L_i}$  and  $X_{C_i}$  values,

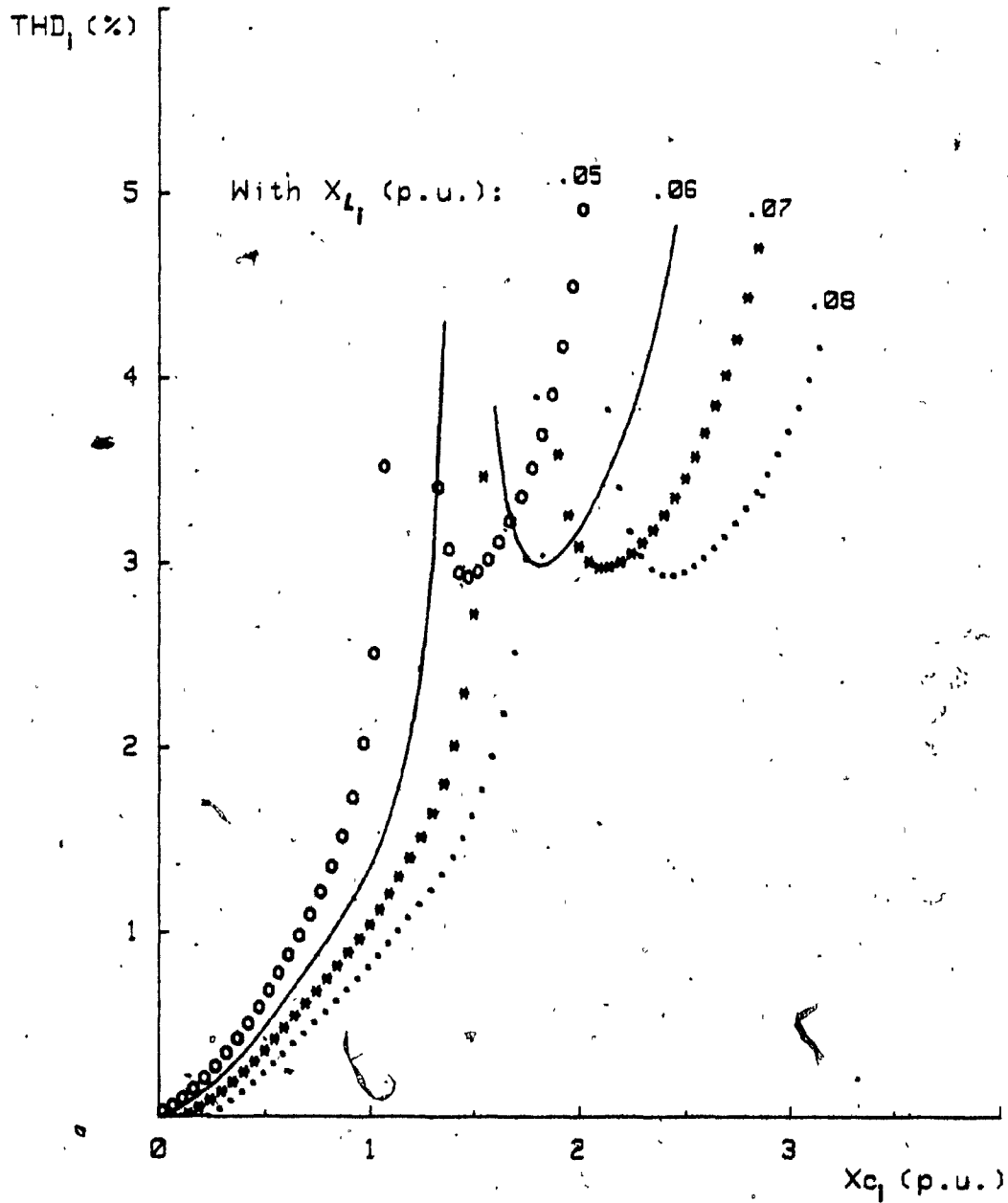


Fig. 3.11: THD<sub>1</sub> (eqn. (3.10)) vs- X<sub>c1</sub> plots for various X<sub>L1</sub> values with the OPWM switching function.

(iii) the  $\bar{I}_a$  and  $\bar{I}_{a,1}$  values, computed from (3.6), (3.7), and (3.8), and

(iv) the THD<sub>i</sub> value corresponding to the aforementioned set of  $X_{L_i}$  and  $X_{C_i}$ , computed from (3.10).

It is noted that the discontinuities observed from the curves are caused by the excitation of the input filter double pole by all the input line current components. This means that the  $X_{L_i}$  and  $X_{C_i}$  combination that causes resonant circuit should be avoided for all the input line current components: that is,

$$X_{C_i} \neq k^2 X_{L_i}, \quad k=1,5,7,\dots \quad (3.11)$$

### 3.3.3 Total harmonic distortion of the input voltage: THD<sub>v</sub>

It is noted that even though there is no restriction for the harmonic distortion of a rectifier input voltage it is good practice to limit it below a certain level, because the more the harmonic distortion in the input voltage, the more the ripple components are generated in the output voltage. Consequently, a large-sized output filter is required to provide a stiff dc bus voltage/current. Therefore, a parameter THD<sub>v</sub>, which is the total harmonic distortion of a rectifier input voltage, may be used as a guideline to select a proper set of  $L_i$  and  $C_i$  values. This parameter is defined here as:

$$THD_v = \frac{100}{\bar{V}_{a,1}} (\bar{V}_a^2 - \bar{V}_{a,1}^2)^{1/2} \quad (3.12)$$

where

$\bar{V}_a$  = rms value of the input phase voltage of a rectifier,  $V_a(wt)$ ,

$\bar{V}_{a,1}$  = rated rms value of the fundamental component of the  $V_a(wt)$ .

In addition to  $\bar{V}_{a,1}$ ,  $\bar{V}_a$  contains an infinite number of harmonic components;  $\bar{V}_{a,k}$ , generated by the flow of the current harmonics  $\bar{I}_{a,k}$  through the  $L_1$  and  $C_1$ ; that is,

$$\bar{V}_{a,k} = \frac{k X_{L_1} X_{C_1}}{k^2 X_{L_1}^2 - X_{C_1}^2} \bar{I}_{a,k}, \quad k=5,7,\dots \quad (3.13)$$

where

$\bar{V}_{a,k}$  = rms value of the k-th component of the  $V_a(wt)$ .

Therefore,

$$\bar{V}_a = (\bar{V}_{a,1}^2 + \sum_{k=5}^{\infty} \bar{V}_{a,k}^2)^{1/2} \quad (3.14)$$

The second set of design curves for the input filter is shown in Fig. 3.12 which depicts a family of  $THD_V$ -vs- $X_{C_1}$  curves for the same  $X_{L_1}$  values in  $THD_I$  curves. In this case, the maximum permissible  $THD_V$  values are assumed to be less than 10 % of the rated rms input voltage with, again, the  $S_3(wt)$  function.

At this stage, the two unknown values of  $L_1$  and  $C_1$  can be selected from the two sets of design curves. However, the selection of their

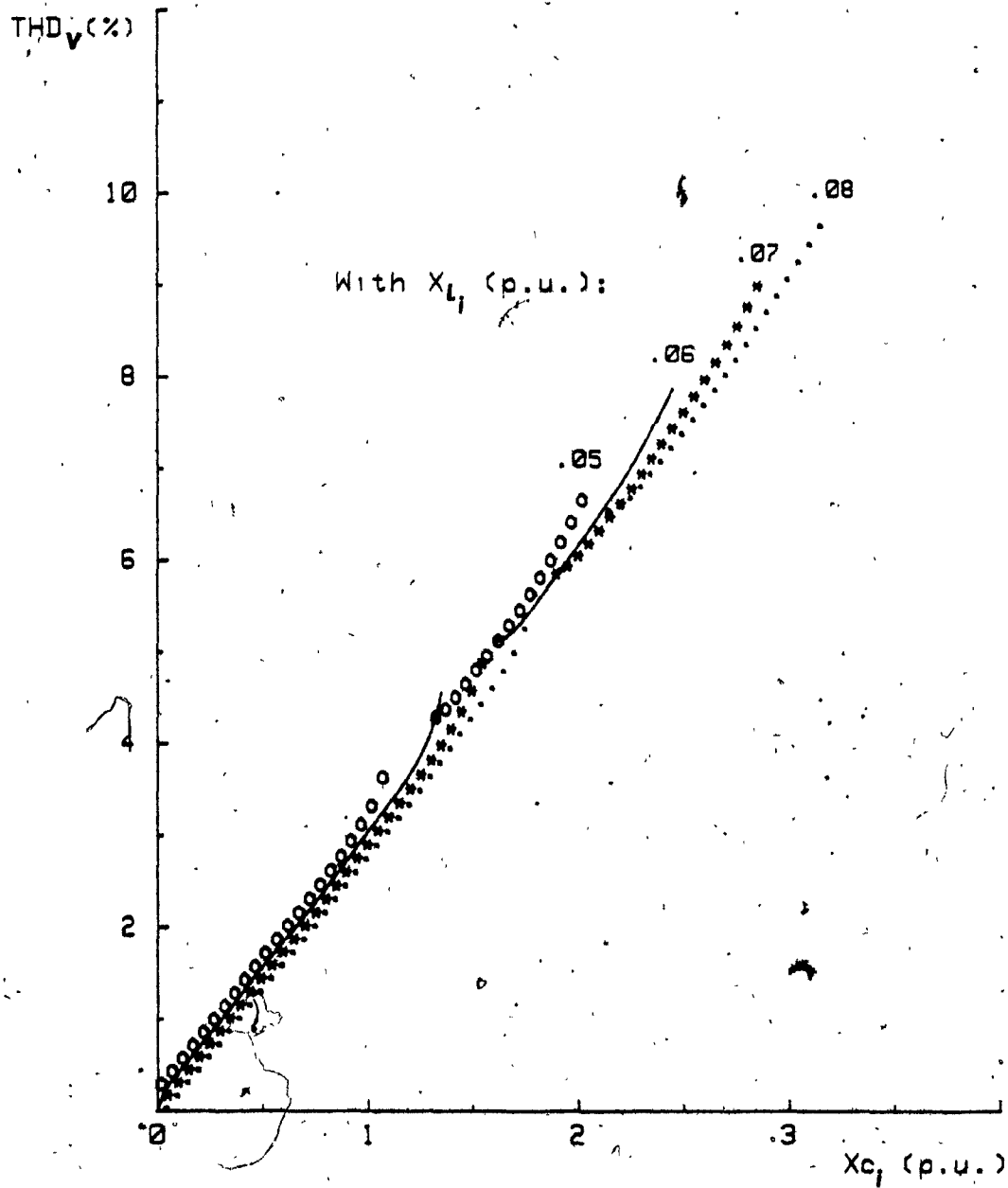


Fig. 3.12:  $THD_V$  (eqn. (3.12)) -vs-  $X_{C1}$  plots corresponding to the  $THD_I$  plots.

'optimum' values may not be possible because there are a number of combinations which satisfy the specified THD<sub>i</sub> and THD<sub>v</sub> limits. Therefore, further study is necessary to select the optimum component values of the input filter.

### 3.3.4 Total kVA rating of the input filter: TKVA

The kVA ratings of the filter components are defined here as follows:

$$LKVA = \sum_{k=1}^{\infty} k \bar{I}_{a,k}^2 X_{L_1} \quad (3.15a)$$

$$CKVA = \sum_{k=1}^{\infty} \frac{k \bar{V}_{a,k}^2}{X_{C_1}} \quad (3.15b)$$

where

LKVA = kVA rating of the inductor  $L_1$ ,

CKVA = kVA rating of the capacitor  $C_1$ .

Thus, the total kVA rating of the input filter (TKVA) can be defined by:

$$TKVA = \rho LKVA + CKVA$$

$$= \sum_{k=1}^{\infty} \left( \rho k \bar{I}_{a,k}^2 X_{L_1} + \frac{k \bar{V}_{a,k}^2}{X_{C_1}} \right) \quad (3.16)$$

where

$\rho$  = ratio between the price of the inductor and that of the capacitor for same kVA rating.

It is noted that the price of inductive kVA may not be same as that of the capacitive kVA, so a scale factor  $\rho$  may be considered to minimize the cost (or TKVA rating) of the input filter. Since the filter cost is directly related with the TKVA rating, the optimum input filter may be designed by minimizing the TKVA value with a given  $\rho$ . The third set of design curves for the input filter is shown in Fig. 3.13 depicting a family of TKVA curves corresponding to the Figs. 3.11 and 3.12, assuming  $\rho = 1$  in (3.16). It can be seen that the TKVA values decrease as  $X_{C_i}$  increases, as expected.

### 3.3.5 Displacement power factor angle: $\theta_1$

As discussed in Chapter 1, it is always desirable to improve the input power factor of a given converter. The power factor of a converter consists of the product of two components: distortion and displacement. The distortion power factor is associated with the present harmonic components, and can be improved by introducing a filter. The displacement power factor is the ratio of the active power of the fundamental wave in watts, to the apparent power of the fundamental wave in voltamperes, and can be represented by the value of  $\cos \theta_1$  where  $\theta_1$  is the phase displacement angle between the fundamental voltage and the fundamental current (Fig. 3.10c). When the input filter is introduced between the mains and the rectifier input stage to reduce the harmonic components (hence improve the distortion power factor), it may increase  $\theta_1$ , if the filter components  $L_i$  and  $C_i$  are

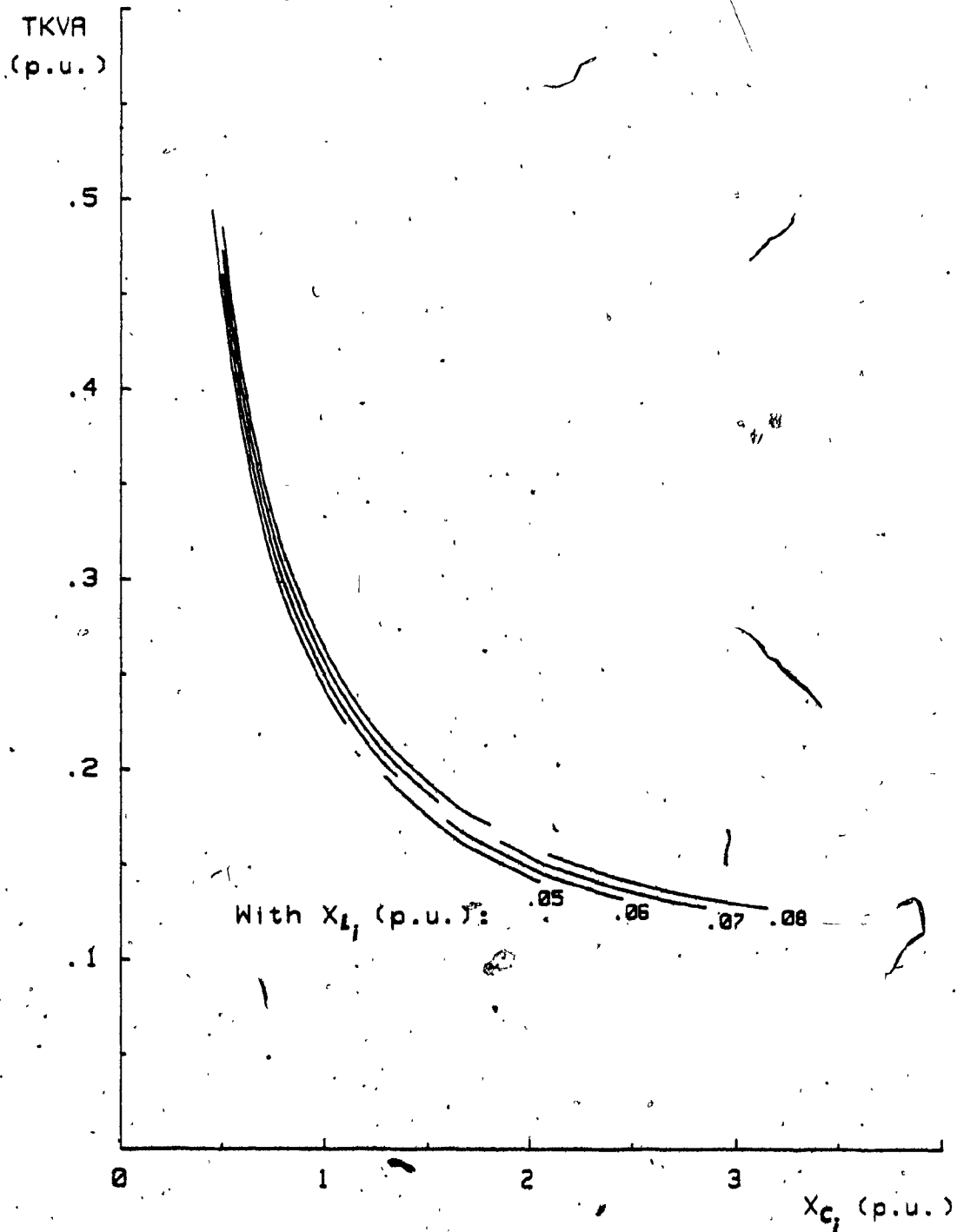


Fig. 3.13: TKVA (eqn. (3.16)) -vs-  $X_{C1}$  plots corresponding to the THD and THD plots.

not selected properly. Therefore, it is useful to plot the  $\theta_1$  curves corresponding to the Figs. 3.11 and 3.12. The  $\theta_1$  curves for this case are shown in Fig. 3.14.

### 3.3.6 Design of an optimum input filter

The previous four sets of design curves for the input filter can be utilized to select the optimum set of  $L_1$  and  $C_1$  values, according to the following:

- (i) plot the  $\text{THD}_i$  curves as a function of  $X_{C_1}$  value for various  $X_{L_1}$  values,
- (ii) plot the  $\text{THD}_v$  -vs-  $X_{C_1}$  curves for the same  $X_{L_1}$  values in (i),
- (iii) plot the  $\text{TKVA}$  -vs-  $X_{C_1}$  curves corresponding to the  $\text{THD}_i$  and  $\text{THD}_v$  curves,
- (iv) plot the  $\theta_1$  -vs-  $X_{C_1}$  curves corresponding to the  $\text{THD}_i$  and  $\text{THD}_v$  curves, and
- (v) select the set of  $X_{L_1}$  and  $X_{C_1}$  values yielding minimum  $\text{TKVA}$  value from the  $\text{TKVA}$  curves by considering the  $\text{THD}_i$ ,  $\text{THD}_v$ , and  $\theta_1$  curves.

However, the exact optimum values of  $X_{L_1}$  and  $X_{C_1}$  are found by using a suitable computer-aided design (CAD) program (Appendix B). Fig. 3.15 shows the flow chart of the CAD program, and the constants,  $K_T$  and  $K_v$ , in the figure denote the given  $\text{THD}_i$  and  $\text{THD}_v$  limits, respectively.

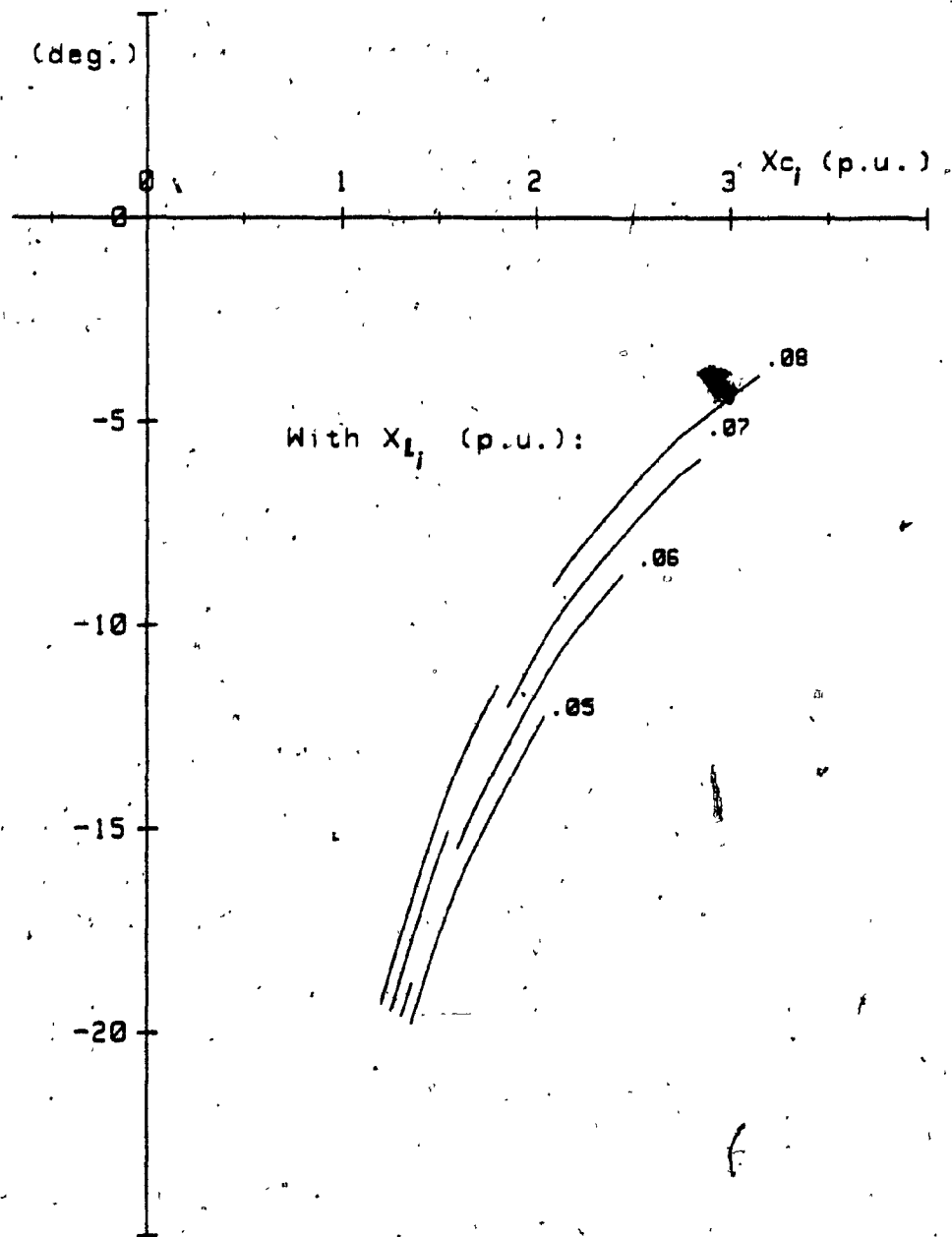


Fig. 3.14: Displacement power-factor angles corresponding to the  $THD_i$  and  $THD_v$  plots.

The optimum input filter is designed for each switching function by utilizing the proposed procedure and the CAD program. The results are presented in Table 3.1. In this case, the  $THD_i$  and  $THD_v$  limits are assumed to be 5 % and 10 % of their rated fundamental values, respectively, and the  $\rho$  is assumed to be 1. In designing the input filter the worst conditions should be considered, and the worst cases with  $S_1$  (wt) and  $S_2$  (wt) types of switching functions occur at  $M=1$  and 0.7, respectively. From Table 3.1, it can be seen that by employing the PWM control techniques the TKVA value which represents the input filter cost can be minimized significantly, as compared to that obtained with the conventional single-pulse switching function.

### 3.3.7 Evaluation of the optimum input filter

In order to examine the performance characteristics of the optimum input filters presented in Table 3.1, the  $THD_i$ ,  $THD_v$ , and TPF curves are plotted in Figs. 3.16, 3.17, and 3.18 as a function of the normalized output voltage. As expected, the  $THD_i$  and  $THD_v$  values resulting from the  $S_3$  (wt) and  $S_4$  (wt) functions are independent on the normalized output voltage. With the  $S_1$  (wt),  $S_2$  (wt), and  $S_3$  (wt) functions, however, the  $THD_i$  and  $THD_v$  values are strongly dependent on the normalized output voltage. It is noteworthy that the PWM switching functions,  $S_1$  (wt),  $S_2$  (wt), and  $S_3$  (wt) provide considerable overall improvements in the TPF characteristic (Fig. 3.18).

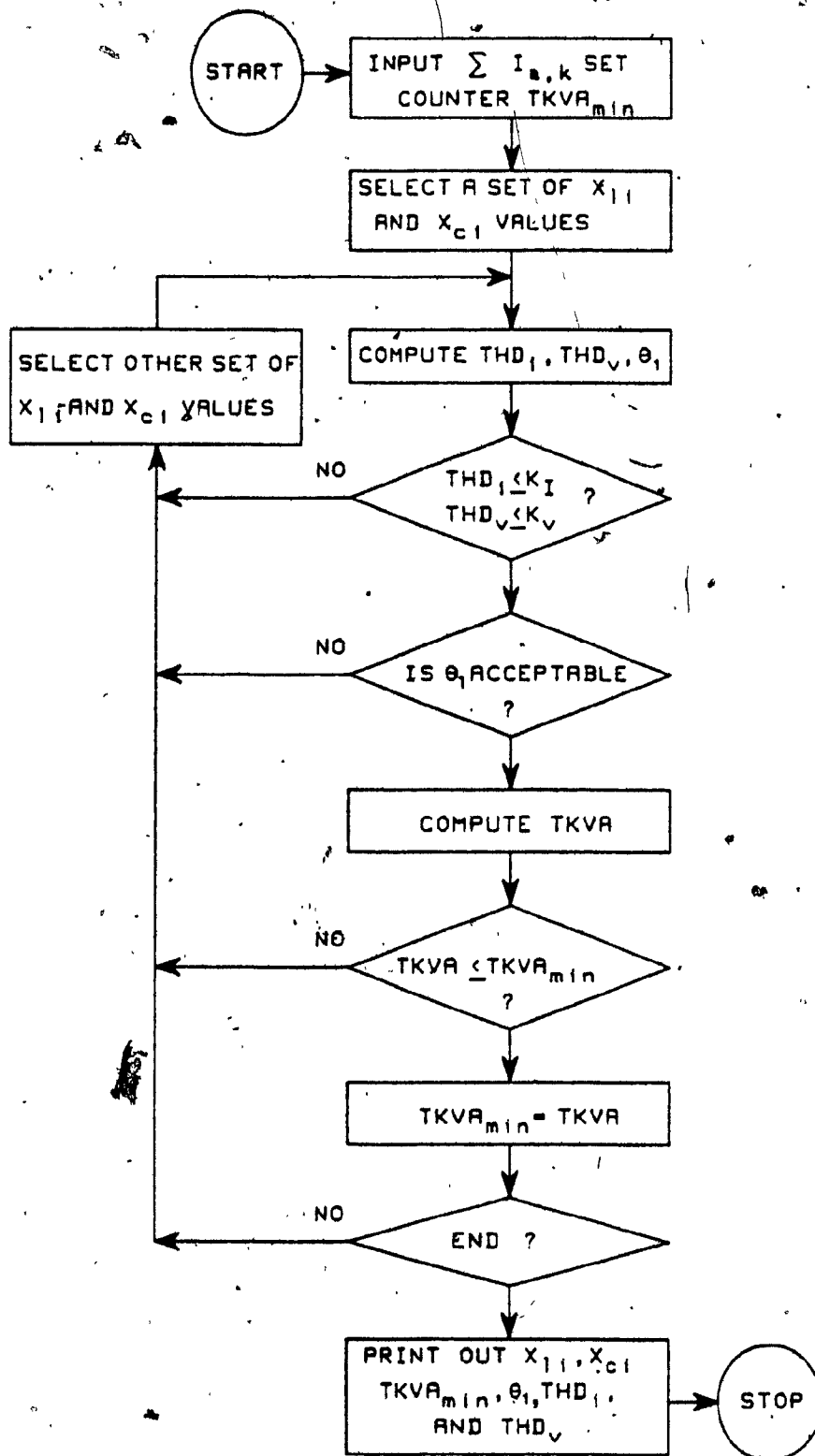


Fig. 3.15: Flow chart of the CAD program for designing optimum input filter.

TABLE 3.1: OPTIMUM RECTIFIER INPUT FILTER DATA (p.u.).

	$S_1(\text{wt})$	$S_2(\text{wt})$	$S_3(\text{wt})$	$S_4(\text{wt})$
$X_{L_i}$	0.12	0.13	0.08 <sup>†</sup>	0.18
$X_{C_i}$	2.45	2.60	2.55	0.95
TKVA	0.195	0.146	0.141	0.352
LKVA	0.053	0.044	0.046	0.148
CKVA	0.141	0.102	0.095	0.204
$\theta_1$	12 deg.	3 deg.	13 deg.	8 deg.

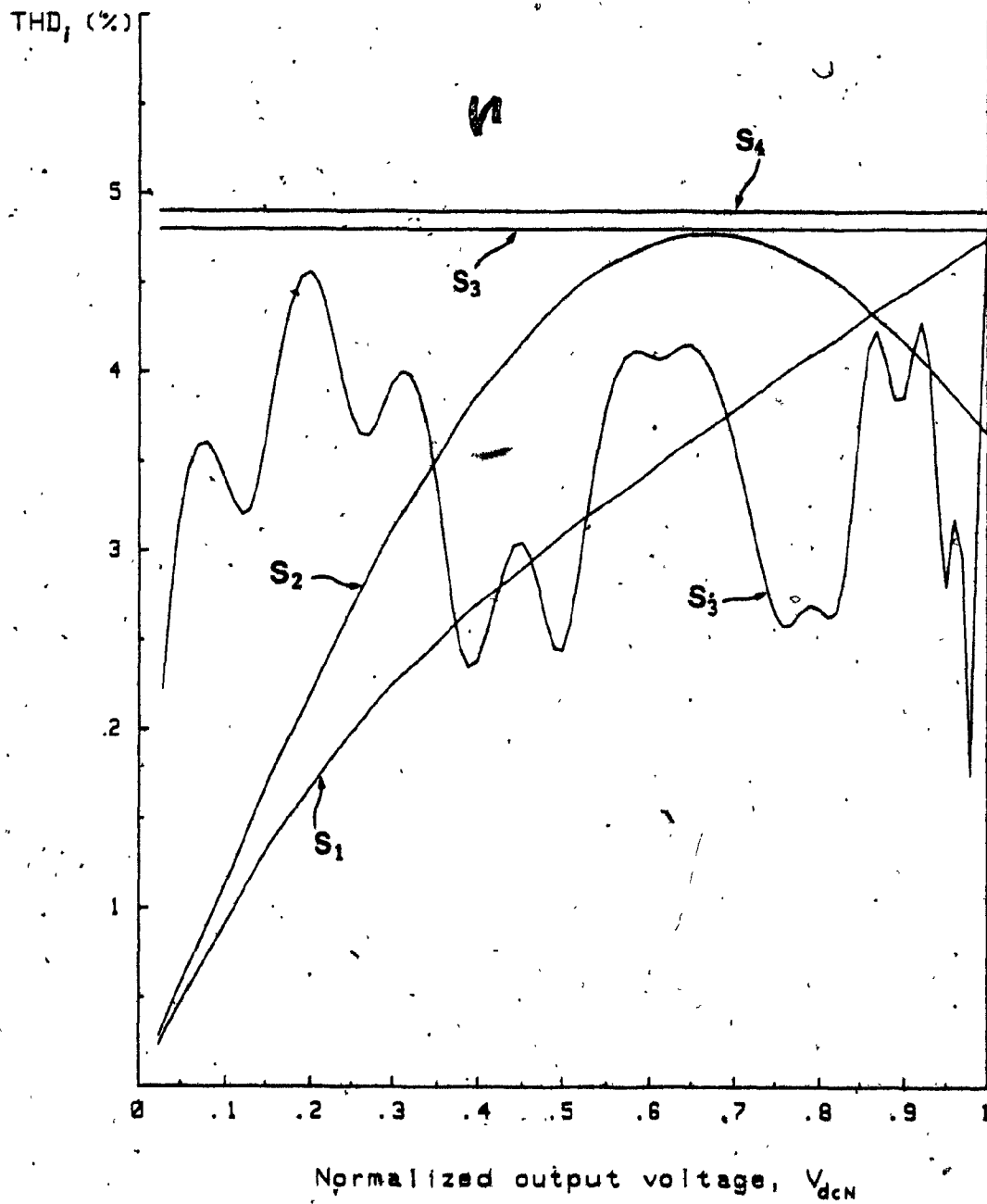


Fig. 3.16: THD<sub>1</sub> values versus  $V_{dcN}$  with the specified input filters in Table 3.1.

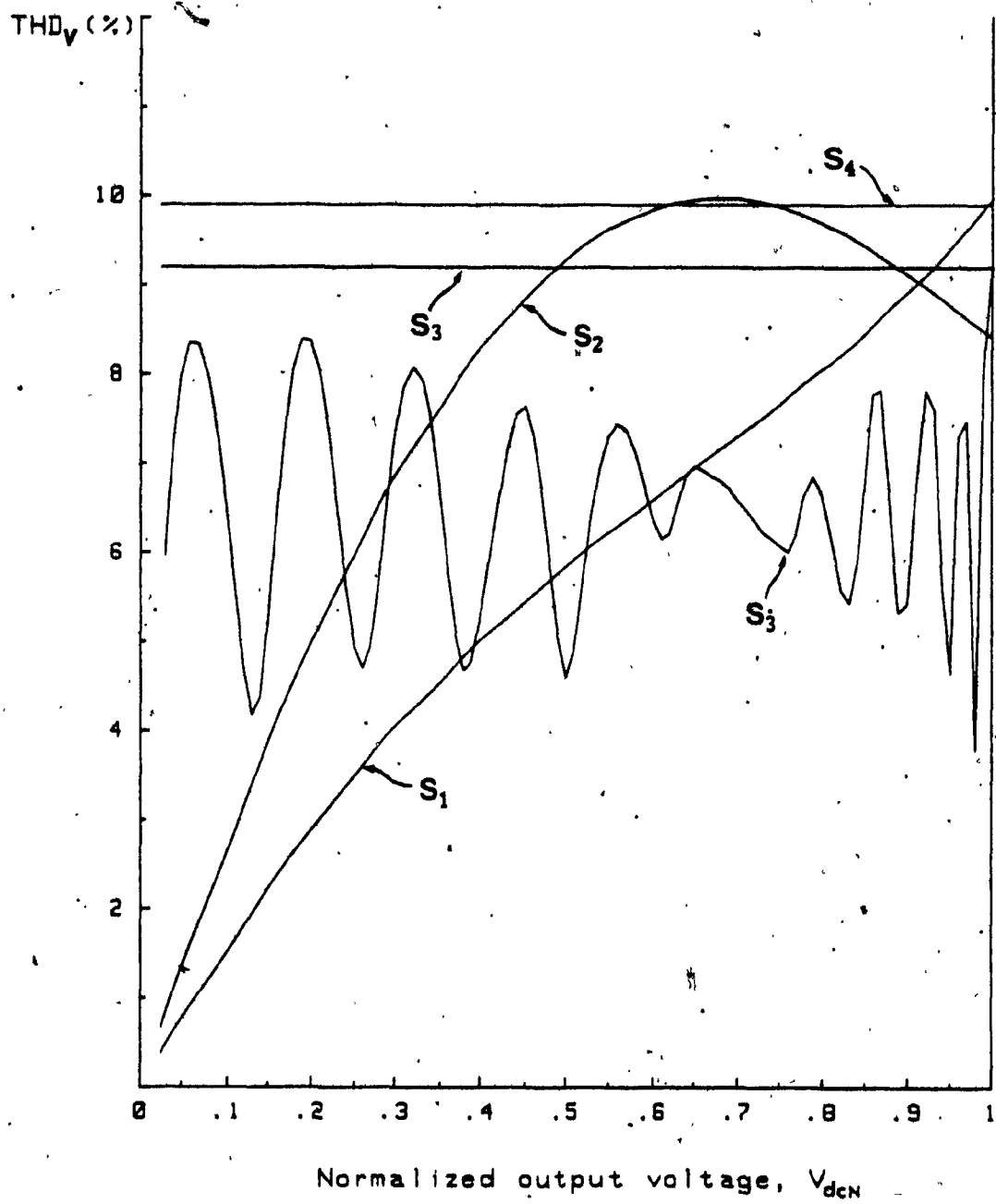


Fig. 3.17: THD<sub>V</sub> values versus  $V_{dcN}$  with the specified input filters in Table 3.1.

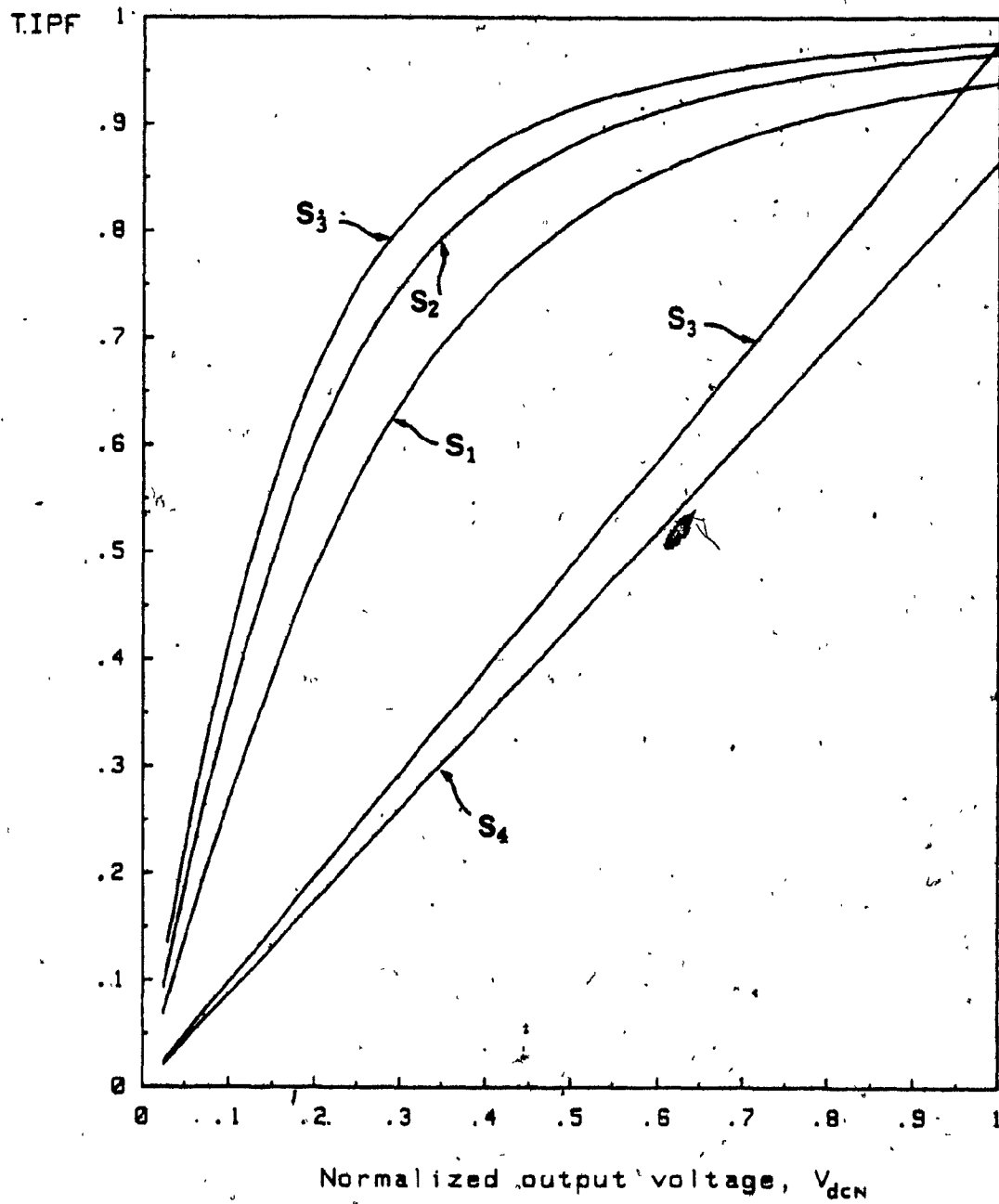


Fig. 3.18: T.I.P.F. values versus  $V_{dcN}$  with the specified input filters in Table 3.1.

### 3.4 Output Stage Analysis and Output Filter Design

The output stage analysis and output filter design are developed according to the assumptions described in Section 3.2. In addition, the output current is assumed to be continuous. Moreover, in selecting the output filter components two design curves are utilized.

#### 3.4.1 Output stage analysis

Once gating signals are specified (Figs. 2.4b, 2.7b, 3.6), the output voltage of a rectifier,  $V_r(wt)$ , is determined by the switching operations of the rectifier switches. The  $V_r(wt)$  can be represented by:

$$V_r(wt) = V_{dc} + \sum_{n=6}^{\infty} V_{r,n} \sin(nwt + \phi_{r,n}) \quad (3.17)$$

where

$V_{dc}$  = dc component of the output voltage,  $V_r(wt)$

$V_{r,n}$  = amplitude of the n-th component of the  $V_r(wt)$

$\phi_{r,n}$  = phase displacement of the n-th component of the  $V_r(wt)$ .

As with the conventional phase-controlled rectifier (Fig. 3.5b), the  $V_{dc}$  and  $V_{r,n}$  are determined as a function of the phase control angle by the definition of Fourier series; that is,

$$\begin{aligned} V_{dc} &= \frac{3}{\pi} \int_{\alpha + \frac{\pi}{3}}^{\alpha + \frac{2\pi}{3}} \sqrt{2} V_1 \sin wt \, d(wt) \\ &= \frac{3\sqrt{2}}{\pi} V_1 \cos \alpha \end{aligned} \quad (3.18a)$$

$$V_{r,n} = (a_n^2 + b_n^2)^{1/2}, \quad n=6,12, \dots \quad (3.18b)$$

and

$$\phi_{r,n} = \tan^{-1} \left( \frac{a_n}{b_n} \right) \quad (3.18c)$$

where

$V_1$  = amplitude of the fundamental input phase voltage (i.e.  $V_{a,1}$ )

$$a_n = \frac{6}{\pi} \int_{\alpha + \frac{\pi}{3}}^{\alpha + \frac{2\pi}{3}} V_r(\omega t) \cos n\omega t d(\omega t) \quad (3.19a)$$

$$b_n = \frac{6}{\pi} \int_{\alpha + \frac{\pi}{3}}^{\alpha + \frac{2\pi}{3}} V_r(\omega t) \sin n\omega t d(\omega t) \quad (3.19b)$$

However, when PWM control techniques are employed the determination of all the coefficients in (3.18) by means of the typical method may be difficult, because of the numerous points to be evaluated in the  $V_r(\omega t)$  (Figs. 3.2c, 3.3c, and 3.4c). Thus, another method, without evaluating all the points, needs to be developed. The subsequent analysis focuses on this aspect.

Let the three-phase mains  $[V_I(t)]$  and the rectifier switching function  $[S_R(t)]$  be:

$$[V_I(t)] = \begin{bmatrix} V_{an}(\omega t) \\ V_{bn}(\omega t) \\ V_{cn}(\omega t) \end{bmatrix} = \begin{bmatrix} V_1 \sin \omega t \\ V_1 \sin (\omega t - 2\pi/3) \\ V_1 \sin (\omega t + 2\pi/3) \end{bmatrix} \quad (3.20)$$

and

$$[S_R(t)] = \begin{bmatrix} S_{na}(\omega t - \alpha) \\ S_{nb}(\omega t - \alpha) \\ S_{nc}(\omega t - \alpha) \end{bmatrix} = \begin{bmatrix} \sum_{k=1}^{\infty} A_k \sin(\omega t - \alpha) \\ \sum_{k=1}^{\infty} A_k \sin k(\omega t - \alpha - 2\pi/3) \\ \sum_{k=1}^{\infty} A_k \sin k(\omega t - \alpha + 2\pi/3) \end{bmatrix} \quad (3.21)$$

where

$\alpha$  = phase delay angle in radian when the phase shifting

method is used to control the output voltage.

Then, the output voltage,  $V_r(\omega t)$ , can be determined by:

$$V_r(\omega t) = [S_R(t)] \cdot [V_I(t)] \quad (3.22)$$

By inserting (3.20) and (3.21) into (3.22), one gets

$$V_r(\omega t) = \begin{bmatrix} S_{na}(\omega t - \alpha) & S_{nb}(\omega t - \alpha) & S_{nc}(\omega t - \alpha) \end{bmatrix} \begin{bmatrix} V_{an}(\omega t) \\ V_{bn}(\omega t) \\ V_{cn}(\omega t) \end{bmatrix} \quad (3.23a)$$

or

$$\begin{aligned} V_r(\omega t) &= S_{na}(\omega t - \alpha) \cdot V_{an}(\omega t) + S_{nb}(\omega t - \alpha) \cdot V_{bn}(\omega t) + S_{nc}(\omega t - \alpha) \cdot V_{cn}(\omega t) \\ &= S_{na}(\omega t - \alpha) \cdot V_{an}(\omega t) + S_{na}(\omega t - \alpha - 2\pi/3) \cdot V_{an}(\omega t - 2\pi/3) \\ &\quad + S_{na}(\omega t - \alpha - 4\pi/3) \cdot V_{an}(\omega t - 4\pi/3) \\ &= \sum_{m=0}^2 S_{na}(\omega t - \alpha - 2m\pi/3) \cdot V_{an}(\omega t - 2m\pi/3) \end{aligned} \quad (3.23b)$$

(3.23b) represents the compact form of a rectifier output voltage,  $V_r(\omega t)$ , which can further be expanded as follows:

$$\begin{aligned}
 V_r(\omega t) &= \sum_{k=1}^{\infty} A_k \sin k(\omega t - \alpha) V_1 \sin \omega t \\
 &+ \sum_{k=1}^{\infty} A_k \sin k(\omega t - \alpha - 2\pi/3) V_1 \sin(\omega t - 2\pi/3) \\
 &+ \sum_{k=1}^{\infty} A_k \sin k(\omega t - \alpha + 2\pi/3) V_1 \sin(\omega t + 2\pi/3) \\
 &= \frac{1}{2} V_1 \sum_{k=1}^{\infty} A_k \left[ \cos((k-1)\omega t - \alpha) - \cos((k+1)\omega t - \alpha) \right. \\
 &\quad + \left[ \cos((k-1)\omega t - \alpha - 2\pi(k-1)/3) - \cos((k+1)\omega t - \alpha - 2\pi(k+1)/3) \right] \\
 &\quad \left. + \left[ \cos((k-1)\omega t - \alpha + 2\pi(k-1)/3) - \cos((k+1)\omega t - \alpha + 2\pi(k+1)/3) \right] \right]
 \end{aligned} \tag{3.24}$$

By trigonometric manipulation, this reduces to:

$$\begin{aligned}
 V_r(\omega t) &= \frac{1}{2} V_1 \sum_{k=1}^{\infty} A_k \left[ (C_{1,k}^2 + S_{1,k}^2) \sin((k-1)\omega t + \phi_{1,k}) \right. \\
 &\quad \left. + (C_{2,k}^2 + S_{2,k}^2) \sin((k+1)\omega t + \phi_{2,k}) \right]
 \end{aligned} \tag{3.25}$$

where

$$\begin{aligned}
 C_{1,k} &= [1 + 2\cos(2\pi(k-1)/3)] \cos \alpha \\
 S_{1,k} &= [1 + 2\cos(2\pi(k-1)/3)] \sin \alpha \\
 C_{2,k} &= -[1 + 2\cos(2\pi(k+1)/3)] \cos \alpha \\
 S_{2,k} &= -[1 + 2\cos(2\pi(k+1)/3)] \sin \alpha \\
 \phi_{1,k} &= \tan^{-1}(C_{1,k}/S_{1,k}), \quad \phi_{2,k} = \tan^{-1}(C_{2,k}/S_{2,k})
 \end{aligned} \tag{3.26}$$

Hence, the dc component  $V_{dc}$ , all the ripple components  $V_{r,n}$ , and  $\phi_{r,n}$  in (3.17) can be determined by evaluating (3.25) and (3.26), and they are given by:

$$\begin{aligned} V &= 1.5 A_1 V_i \sin \phi_{1,1} \\ &= \frac{3}{2} A_1 V_i \cos \alpha \end{aligned} \quad (3.27)$$

$$V_{r,n} = \frac{1}{2} V_i (C_n^2 + S_n^2)^{\frac{1}{2}} \quad \text{for } n=6, 12, \dots \quad (3.28)$$

$$\phi_{r,n} = \tan^{-1} \left( \frac{C_n}{S_n} \right)$$

where

$$C_n = A_{n+1} (C_{1,n+1}^2 + S_{1,n+1}^2)^{\frac{1}{2}} \sin \phi_{1,n+1} + A_{n-1} (C_{2,n-1}^2 + S_{2,n-1}^2)^{\frac{1}{2}} \sin \phi_{2,n-1} \quad (3.29)$$

$$S_n = A_{n+1} (C_{1,n+1}^2 + S_{1,n+1}^2)^{\frac{1}{2}} \cos \phi_{1,n+1} + A_{n-1} (C_{2,n-1}^2 + S_{2,n-1}^2)^{\frac{1}{2}} \sin \phi_{2,n-1}$$

In order to examine the content of harmonic components or 'ripple voltage' of a rectifier output voltage, a parameter  $DF_V$ , which is the distortion factor of the rectifier output voltage, may be introduced.

$$DF_V = \frac{100}{V_{dc, \text{rated}}} \left[ \sum_{n=6}^{\infty} \left( \frac{\bar{V}_{r,n}}{2} \right)^2 \right]^{\frac{1}{2}} \quad (3.30)$$

where

$\bar{V}_{r,n}$  = rms value of the n-th unwanted component of a rectifier output voltage,  $V_r(wt)$ .

This  $DF_V$  gives the information about harmonic distortion (or ripple voltage) of the rectifier output voltage, emphasizing on the effect of

low-order harmonic components. The  $DF_{V_n}$ -vs-  $V_{dcn}$  curves are plotted in Fig. 3.19, from which it is observed that the maximum  $DF_{V_n}$  value with  $S_4$  (wt) function is approximately four times larger than those values with the PWM switching functions. As a result of this, the size of the output filter using the PWM switching functions will be much smaller.

### 3.4.2 Ripple factor of the load voltage: $RF_{V_n}$

Fig. 3.20 shows the analytical model of the output filter under study. It consists of a voltage source containing all the harmonic components, a second-order filter, and a load. The nature of the load (resistive, inductive, back EMF, etc.) affects the harmonic currents that can flow. Assuming the load to be 1 p.u. resistive for simplicity, the transfer function of the output filter,  $H_n$ , is given by:

$$H_n = \frac{X_{C_o}}{(X_{C_o} - n^2 X_{L_o}) + jn X_{L_o} X_{Z_o,n}} \\ = \frac{1}{(1 - n^2 X_{L_o} / X_{C_o}) + jn X_{L_o}} \quad n=6, 12, \dots \quad (3.31)$$

where

$X_{L_o}$  = impedance of the output filter inductor  $L_o$  at the input frequency,

$X_{C_o}$  = impedance of the output filter capacitor  $C_o$  at the input frequency,

$Z_{o,n}$  = impedance of the load at the  $n$ -th harmonic frequency.

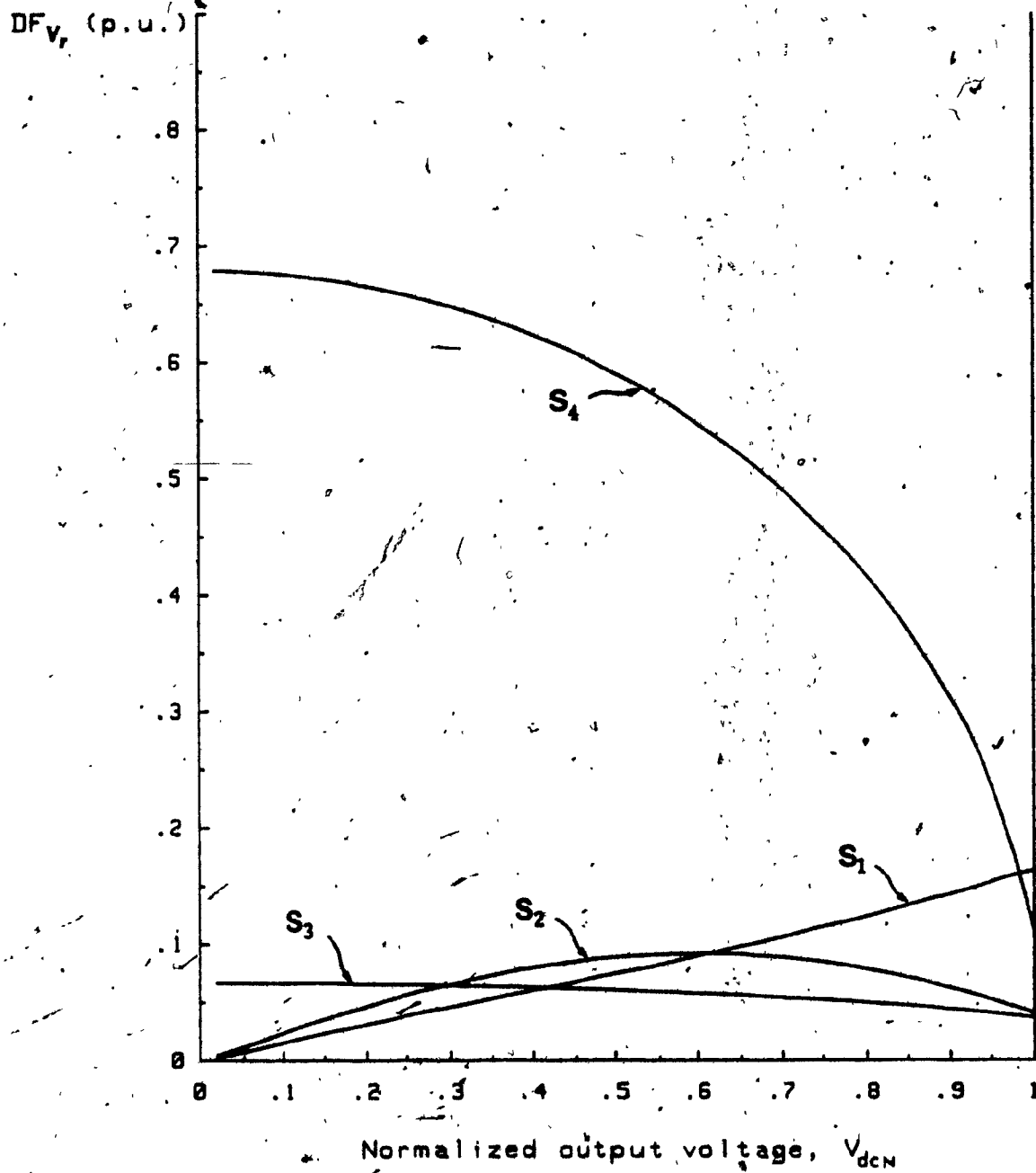


Fig. 3.19: Distortion factors of rectifier output voltages versus  $V_{dcN}$ .

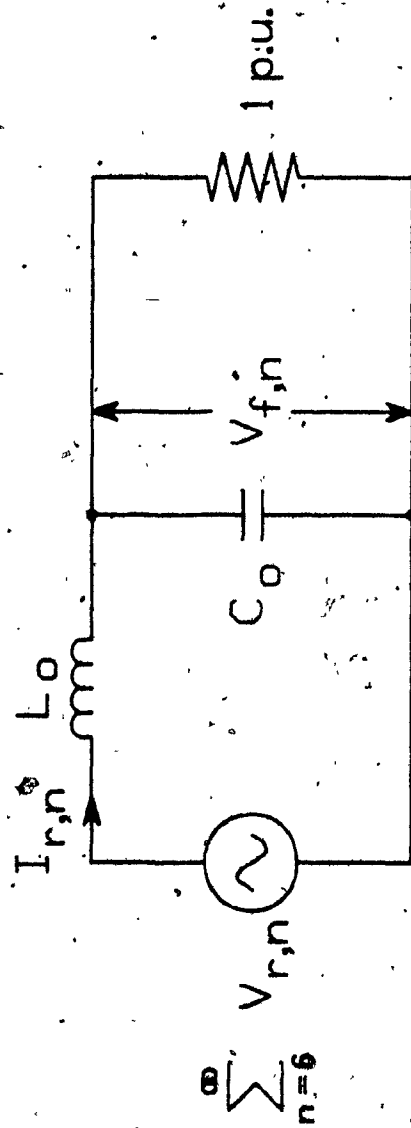


Fig. 3.20: Analytical model of a lossless output filter.

The load voltage  $V_f(\omega t)$  can be represented as a Fourier series by:

$$V_f(\omega t) = V_{dc} + \sum_{n=6}^{\infty} V_{f,n} \sin(n\omega t + \phi_{f,n}) \quad (3.32)$$

where

$V_{f,n}$  = amplitude of the  $n$ -th component of the load voltage,  $V_f(\omega t)$ ,

$\phi_{f,n}$  = phase displacement of the  $n$ -th component of the  $V_f(\omega t)$ .

Since the harmonic components in the rectifier output voltage are reduced by the filter, the harmonic components in the load voltage are determined by:

$$V_{f,n} = H_n \cdot V_{r,n}, \quad n=6,12,\dots \quad (3.33)$$

Thus the ripple factor of the load voltage,  $RF_{V_f}$ , may be defined as:

$$RF_{V_f} = \frac{100}{V_{dc}} (\bar{V}_f^2 - V_{dc}^2)^{\frac{1}{2}} \quad (3.34)$$

where

$\bar{V}_f$  = rms value of the load voltage,  $V_f(\omega t)$ .

In designing the dc filter, it is noted that there are no available rules specifying the method of selection of the  $L_o$  and  $C_o$  values. However, some guidelines are given in [54], [55], where the dc filter is designed under a no-load condition (i.e. neglecting load-current effect), followed by the selection of component values by

considering the  $RF_V$  (eqn. (3.34)) limit and the guidelines. The guidelines are as follows:

- (i) the inductor dissipates much more power than the capacitor, therefore a low L/C ratio is more efficient,
- (ii) a low L/C ratio reduces the 'overshoot' of the output voltage if the load is suddenly disconnected,
- (iii) a low L/C ratio reduces the 'dip' of the output voltage, if the load is suddenly increased,
- (iv) if L/C ratio is too low, the load essentially becomes a capacitor, causing the current to become discontinuous and the average direct voltage to approach the peak voltage,
- (v) a low L/C ratio results in larger peak output current from the rectifier, when first switched on ( $i=Cdv/dt$  and  $e=Ldi/dt$ ), and
- (vi) economic aspects; i.e., in general the price of a choke is more expensive than that of a capacitor.

Thus, the dc filter design will more or less depend on the importance of the different aspects for a particular application. However, in addition to the  $RF_V$  and the guidelines described above another parameter, the ripple factor of the output current through  $L_o$ , will be next introduced in order to select proper  $L_o$  and  $C_o$  values.

### 3.4.3 Ripple factor of the rectifier output current: $RF_{I_r}$

Since the input stage analysis and input filter design in Section 3.3 are executed under the assumption that the output current is ripple-free, the ripple components of the rectifier output current must be limited to a certain level. Referring to Fig.3.20, the rectifier output current,  $I_r(wt)$ , is given by:

$$\begin{aligned}\bar{I}_r &= \frac{V_{dc}}{R_L} + \sum_{n=6}^{\infty} \frac{\bar{V}_{r,n}}{Z_{o,n}} \\ &= I_{dc} + \sum_{n=6}^{\infty} \bar{I}_{r,n}\end{aligned}\quad (3.35)$$

where

$$\begin{aligned}Z_{o,n} &= jn X_{L_o} + \frac{-j R_L X_{C_o}/n}{R_L - j X_{C_o}/n} \\ &= \frac{n X_{L_o} X_{C_o} + j(n X_{L_o} - X_{C_o})}{n - j X_{C_o}}, \quad n=6,12,\dots\end{aligned}\quad (3.36)$$

$\bar{I}_r$  = rms value of the rectifier output current,  $I_r(wt)$ ,

$R_L$  = resistance of the load,

$I_{dc}$  = dc component of the rectifier output current,  $I_r(wt)$ ,

$\bar{I}_{r,n}$  = rms value of the n-th component of the  $I_r(wt)$ .

Then the ripple factor of the rectifier output current,  $RF_{I_r}$ , may be defined as:

$$RF_{I_r} = \frac{100}{I_{dc}} (\bar{I}_r^2 - I_{dc}^2)^{\frac{1}{2}} \quad (3.37)$$

#### 3.4.4 Selection of the output filter component values

The guidelines for selecting the output filter component values are as follows:

- (i) plot  $RF_{V_f}$  -vs-  $X_{C_o}$  curves for various  $X_{L_o}$  values (Fig. 3.21),
- (ii) plot  $RF_{I_r}$  -vs-  $X_{C_o}$  curves for same  $X_{L_o}$  values used in the  $RF_{V_f}$  plot (Fig. 3.22), and
- (iii) select the  $X_{L_o}$  and  $X_{C_o}$  values satisfying the given  $RF_{V_f}$  and  $RF_{I_r}$  limits by considering the guidelines.

However, in order to show the contrast between the PWM control techniques and the conventional method, only the  $RF_{V_f}$  and  $RF_{I_r}$  curves are utilized to select the  $L_o$  and  $C_o$  values for the four switching functions. The  $RF_{V_f}$  and  $RF_{I_r}$  limits are, in this case, assumed to be :

- (i) the ripple factor of the load voltage,  $RF_{V_f}$ , remains below 20 % of its dc component value in the range of 0.1 - 1 p.u. dc voltage, and
- (ii) the ripple factor of the output inductor current,  $RF_{I_r}$ , remains below 50 % of its dc component value in the range of 0.1 - 1 p.u. dc current.

The output filter component values designed with the above conditions are presented in Table 3.2. This table shows that the filter component values with the PWM switching functions are much lower than corresponding values obtained with the conventional switching function.

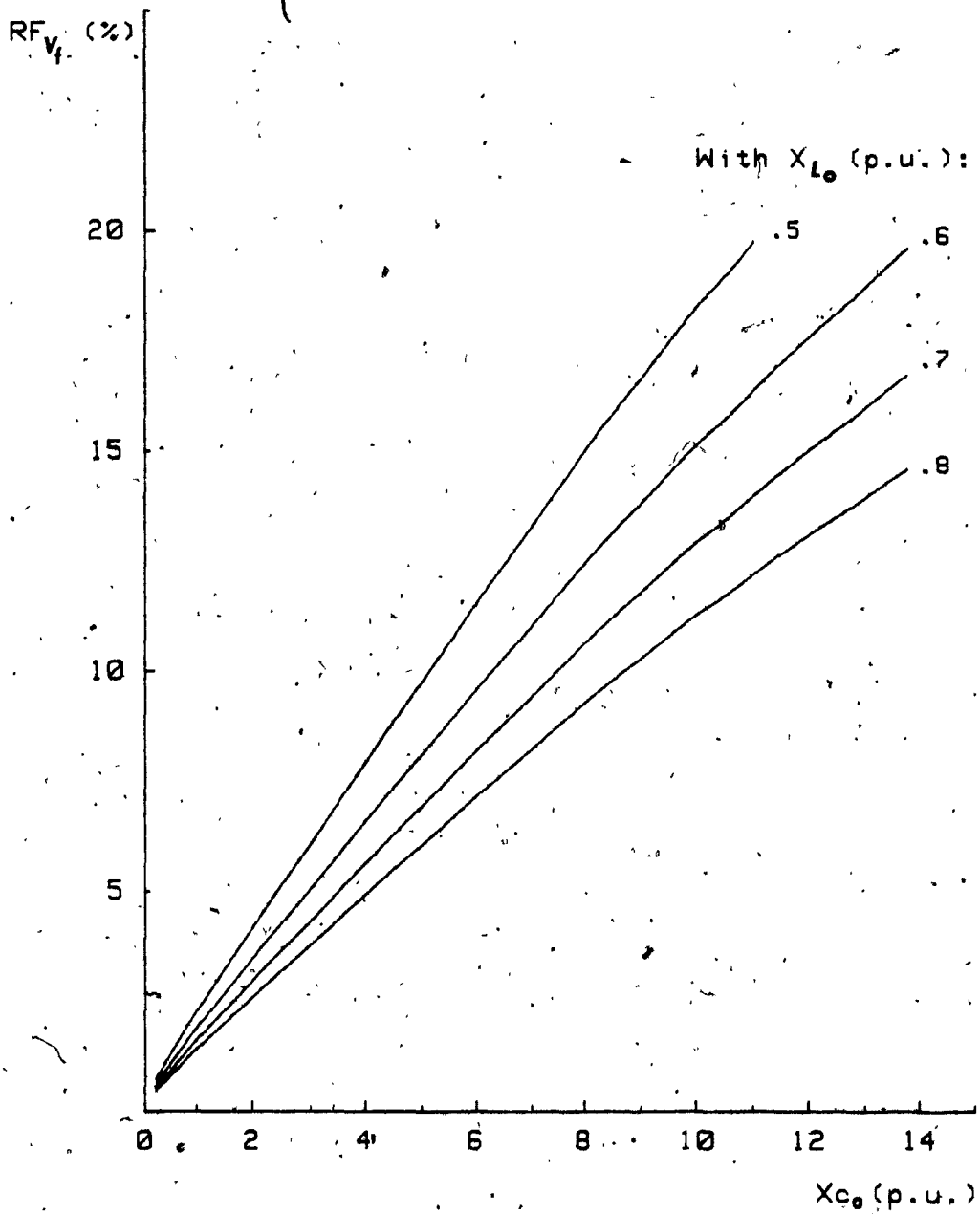


Fig. 3.21: Ripple factors of the load voltage versus  $X_{C_0}$  for various  $X_{L_0}$  values with the OPWM switching function.

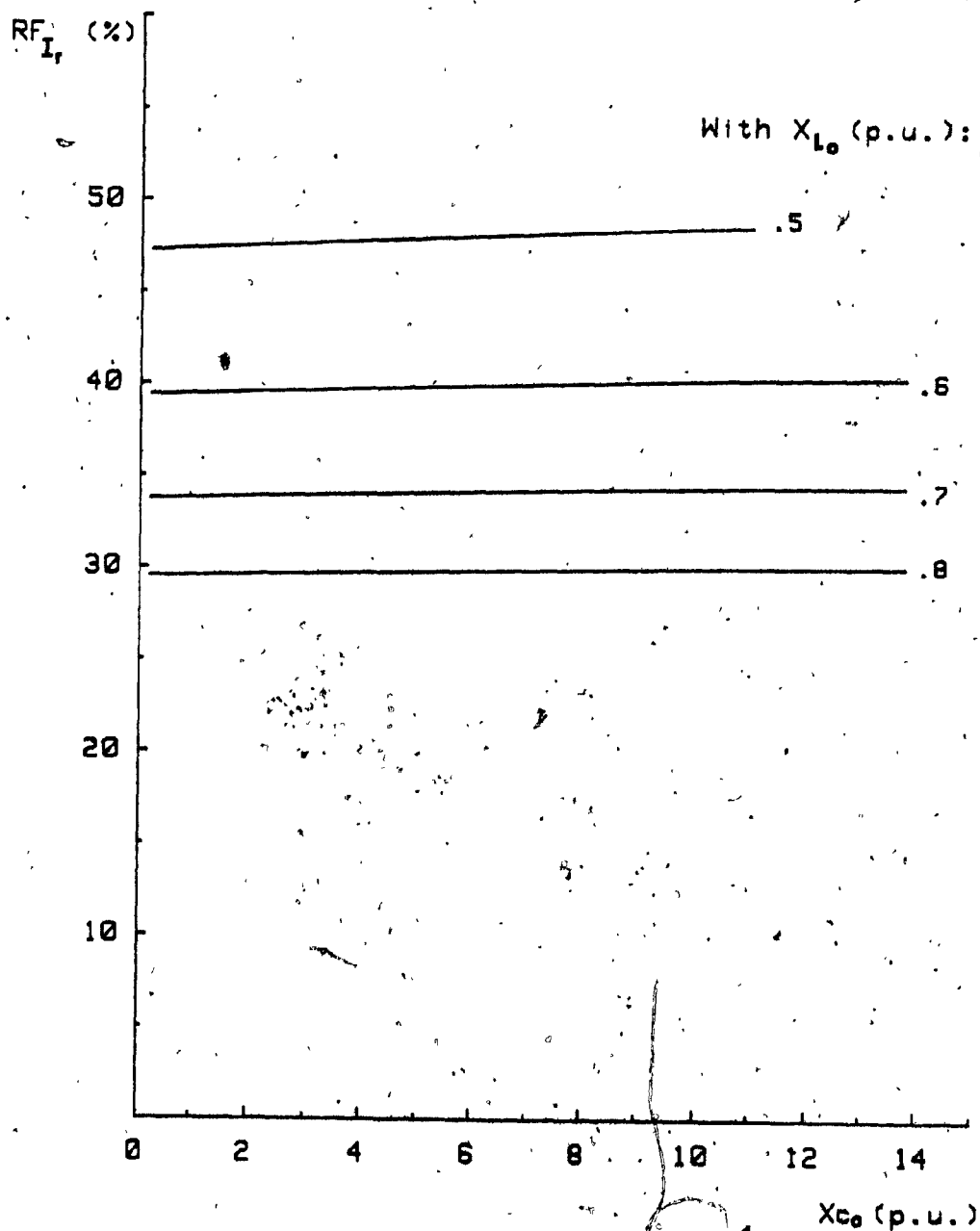


Fig. 3.22: Ripple factors of the rectifier output current corresponding to the Fig. 3.21.

TABLE 3.2: RECTIFIER OUTPUT FILTER DATA (p.u.).

	$S_1(\text{wt})$	$S_2(\text{wt})$	$S_3(\text{wt})$	$S_4(\text{wt})$
$X_{L_0}$	0.18	0.165	0.50	1.26
$X_{C_0}$	10.4	14.4	11.0	2.70
$I_{L_0, \max}$	0.122	0.129	0.035	0.036
$I_{C_0, \max}$	0.111	0.107	0.032	0.033

### 3.4.5 Evaluation of the output filter

In order to illustrate the effects of the harmonic characteristics resulting from the output filters designed in the previous subsection, the  $RF_{V_f}$  and  $RF_{I_r}$  curves are plotted in Figs. 3.23 and 3.24 respectively, as a function of the normalized output voltage/current. From these figures it can be observed that the  $S_3$  (wt) and  $S_4$  (wt) functions yield similar ripple factor (eqns. (3.34), (3.37)) characteristics, because of the common control method of power flow employed. Also, observable are the almost negligible ripple factors near the rated power operating points with  $S_3$ (wt) and  $S_4$ (wt) switching functions. The absolute ripple factor values with the same output filters,  $RF_{V_f}$  (eqn. (3.38)) and  $RF_{I_r}$  (eqn. (3.39)), are plotted in Figs. 3.25 and 3.26, respectively. This is done to provide the maximum ripple currents (included in Table 3.2),  $I_{L_o,max}$  and  $I_{C_o,max}$ , through the inductor  $L_o$  and capacitor  $C_o$ , because these maximum ripple currents are required to select the output filter components.

where

$$RF_{V_f} = \frac{100}{V_{dc, rated}} (\bar{V}_f^2 - \bar{V}_{dc}^2)^{\frac{1}{2}} \quad (3.38)$$

$$RF_{I_r} = \frac{100}{I_{dc, rated}} (\bar{I}_r^2 - \bar{I}_{dc}^2)^{\frac{1}{2}} \quad (3.39)$$

Hence, the ripple current through the capacitor  $C_o$ ,  $I_{C_o}$ , is given by:

$$I_{C_o} = \left[ \sum_{n=6}^{\infty} \left( \frac{n \bar{V}_{f,n}}{X_{C_o}} \right)^2 \right]^{\frac{1}{2}} \quad (3.40)$$

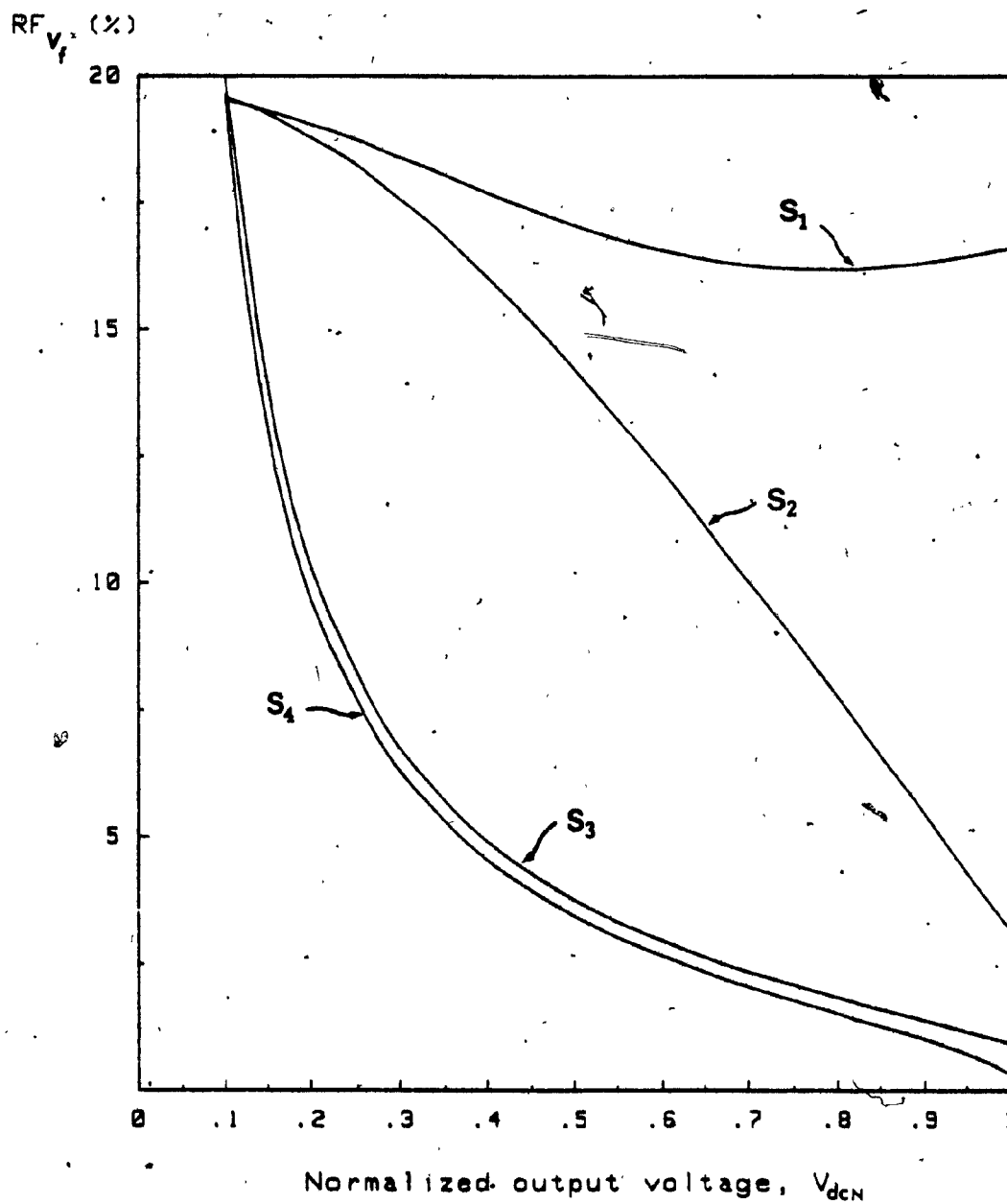


Fig. 3.23: Ripple factors of the load voltages versus  $V_{dcN}$  with the specified output filters in Table 3.3.

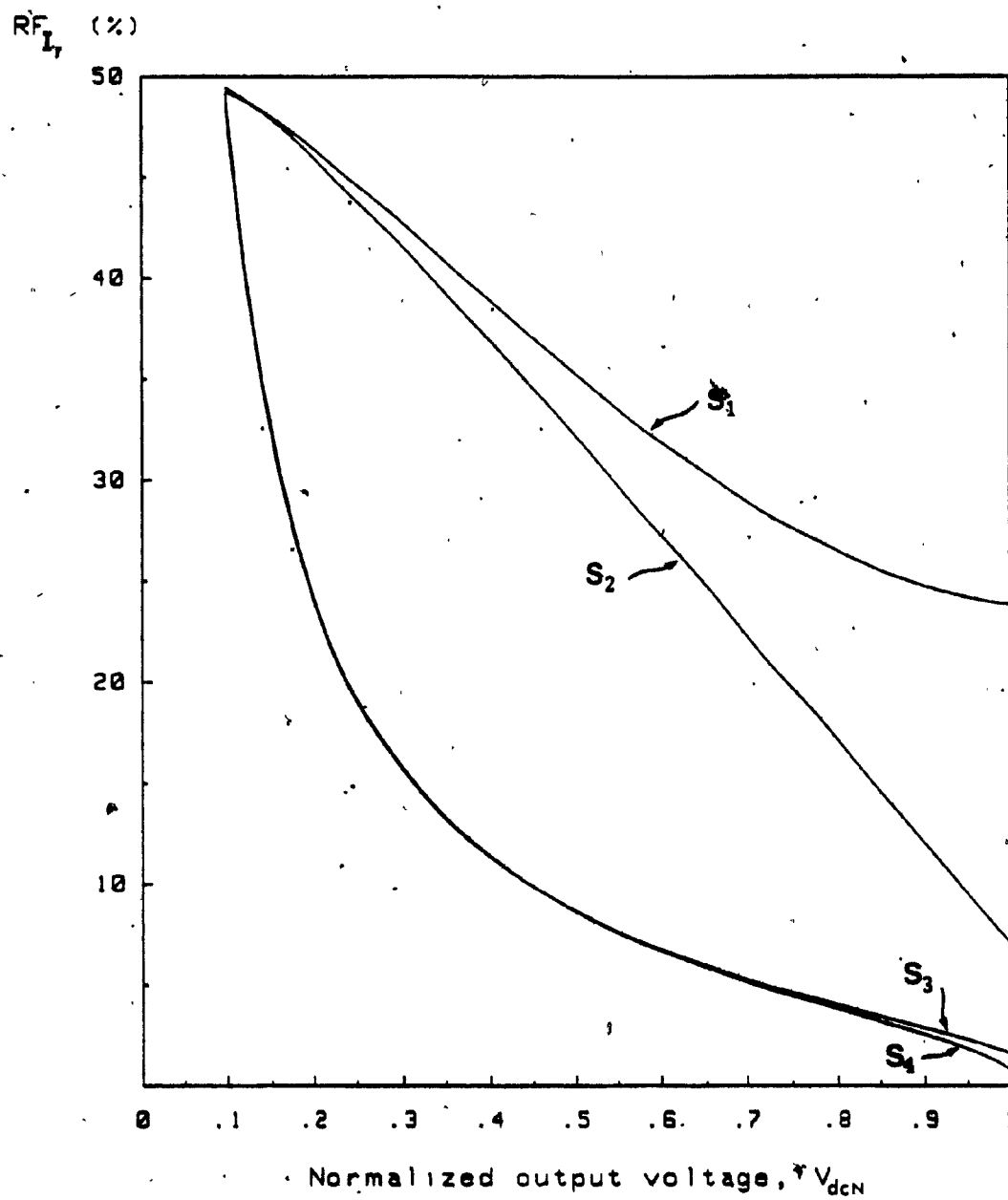


Fig. 3.24: Ripple factors of the rectifier output currents versus  $V_{dcN}$  with the specified output filters in Table 3.3.

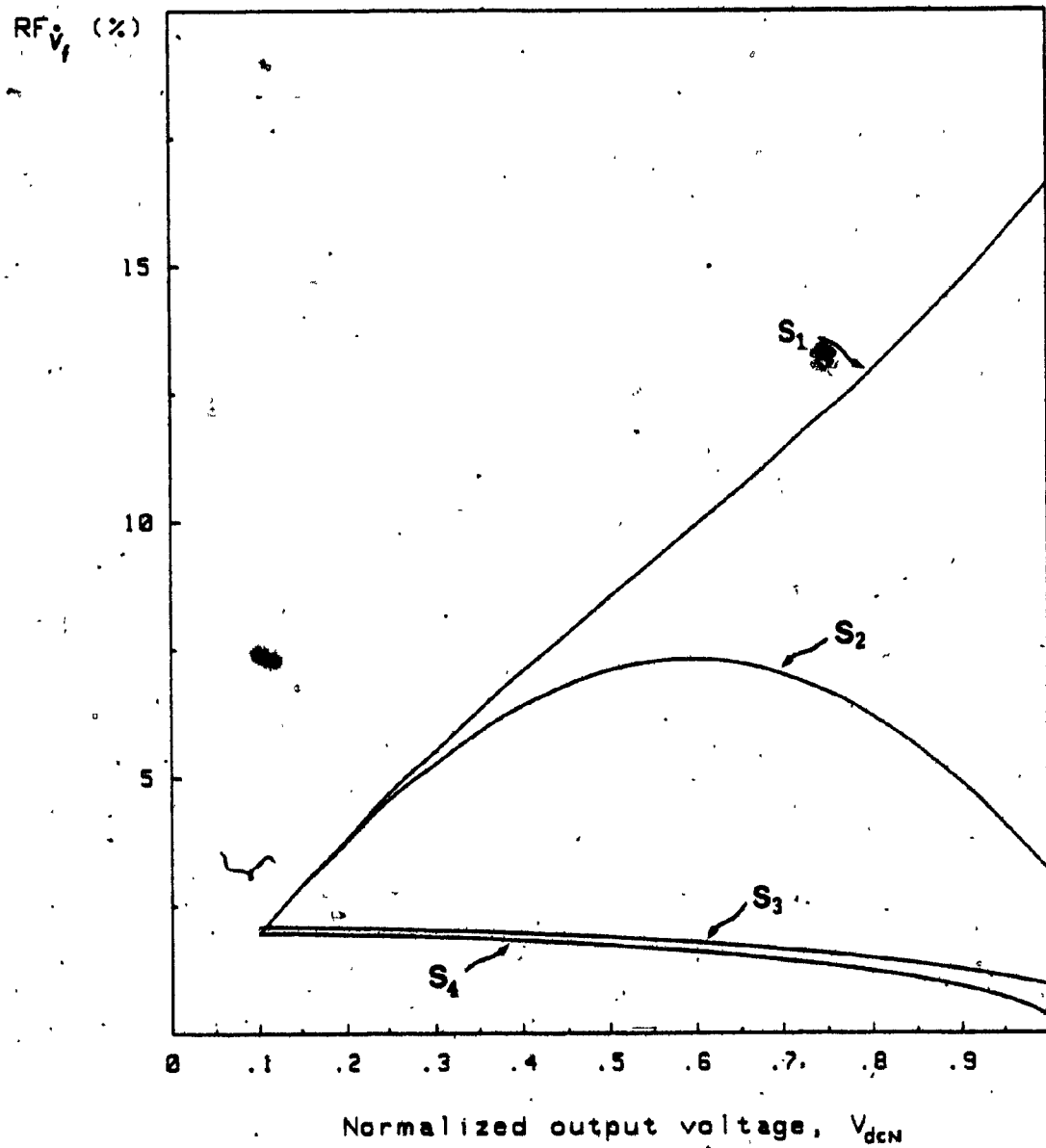


Fig. 3.25:  $RF_v$  (eqn. (3.39)) vs-  $V_{dcN}$  plots with the output filters in Table 3.3.

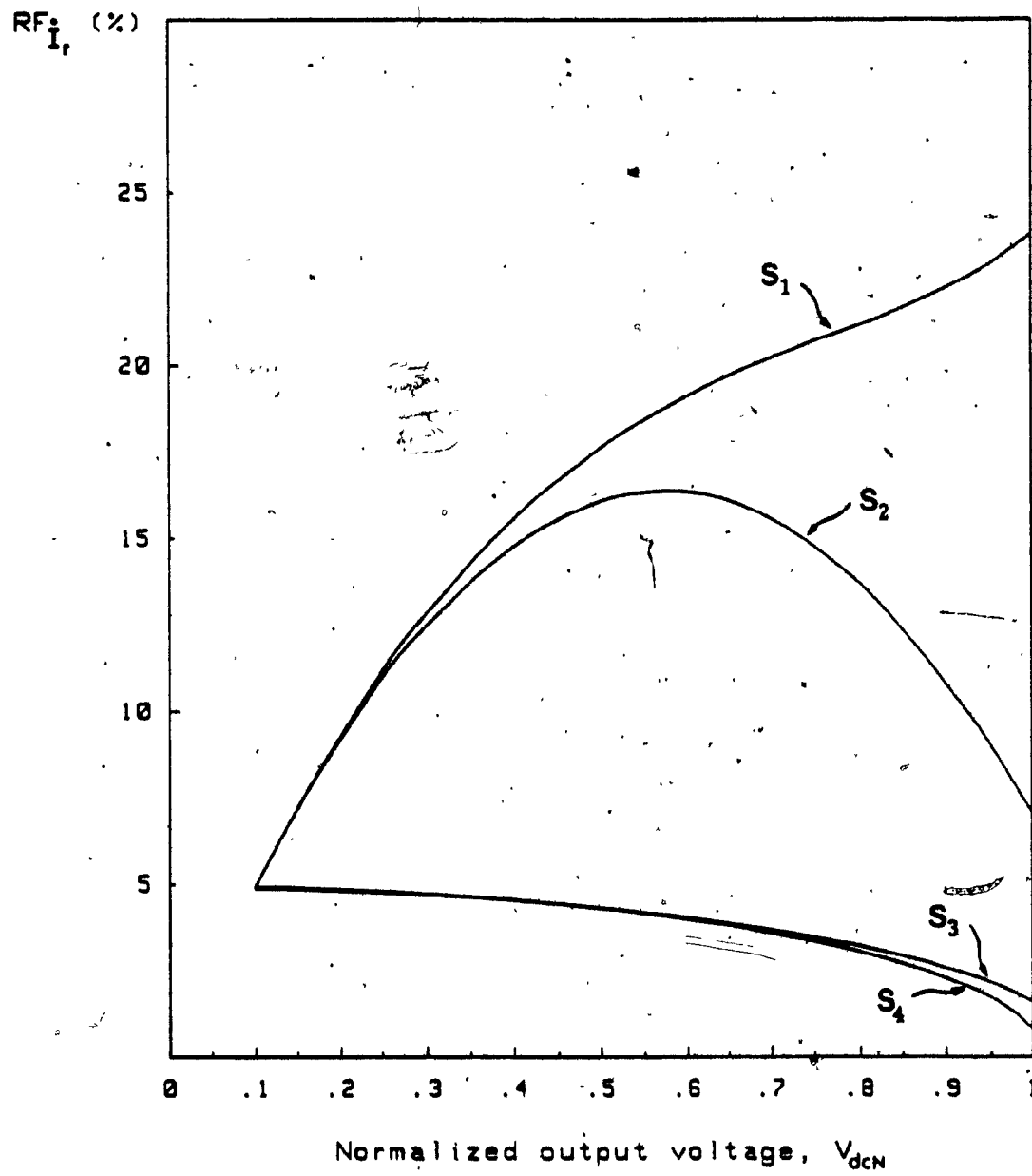


Fig. 3.26:  $RF_I$  (eqn. (3.40)) -vs-  $V_{dcN}$  plots with the output filters in Table 3.3.

where

$\bar{V}_{f,n}$  = rms value of the n-th component of the load voltage,  $V_f$  (wt), with a given output filter.

### 3.5 Discussion

It should be noted at this point that the harmonic limits employed in this chapter to design the input/output filters are oriented towards high performance applications with strict harmonic specifications. For example, the 5 % THD, limit adopted for the input line currents of a rectifier has been borrowed from the relevant military standards [56] applied to 60 Hz sources. Moreover, the reasons for selecting 20 %  $RF_{V_f}$  limit and 50 %  $RF_{I_r}$  limit are: (a) to provide a reasonably 'stiff' dc voltage to the load and (b) to ensure that the output current of a rectifier is continuous. For example, many ac motor drives with constant voltage/frequency control exhibit instability at the continuous-to-discontinuous rectifier current crossover point.

Further reductions in the input/output filter sizes (or cost) can be achieved if the switching frequency of the switches (or the number of pulses per half-cycle) with the PWM switching functions is further increased. However, this should be weighed against the switching losses as well as the snubber losses in determining the optimum switching frequency of the switches for a particular application.

### 3.6 Design Example and Experimental Results

In this section, the validity of the theoretical results obtained in the previous sections is verified experimentally on a 1 kW laboratory unit with the following example.

- Rated output voltage : 200 V dc
- Rated output current : 5 A dc
- Input frequency : 60 Hz
- Maximum THD<sub>i</sub> : 5 %
- Maximum THD<sub>v</sub> : 10 %
- Maximum RF<sub>V<sub>f</sub></sub> : 20 %
- Maximum RF<sub>I<sub>r</sub></sub> : 50 %

Thus, from the above specifications

- 1 p.u. voltage : 200 V
- 1 p.u. current : 5 A
- 1 p.u. Impedance : 40  $\Omega$

If the  $S_2$  (wt) type of switching function with 12-pulse per half-cycle is chosen, the actual values are determined as follows.

(i) Required rms input line-to-neutral voltage

$$(\sqrt{2}/3) \text{ p.u.} \times 200 \text{ V} = 94.3 \text{ V}$$

(ii) Rated rms input line current

$$(1/\sqrt{2}) \text{ p.u.} \times 5 \text{ A} = 3.54 \text{ A}$$

(iii) Optimum input filter components

$$L_O = (0.13 \text{ p.u.} \times 40) / 377 = 13.8 \text{ mH}$$

$$C_O = 1 / (2.60 \text{ p.u.} \times 40 \times 377) = 25.5 \text{ uF}$$

hence,

$$LKVA = 0.044 \text{ p.u.} \times 1 \text{ kVA} = 0.044 \text{ kVA}$$

$$CKVA = 0.102 \text{ p.u.} \times 1 \text{ kVA} = 0.102 \text{ kVA}$$

$$TKVA = \rho LKVA + CKVA = 0.146 \text{ kVA (by assuming } \rho = 1)$$

(iv) Output filter components

$$L_O = (0.165 \times 40) / 377 = 17.5 \text{ mH}$$

$$C_O = 1 / (14.4 \times 40 \times 377) = 4.6 \text{ uF}$$

hence

$$I_{L_O, \max} = 0.129 \times 5 \text{ A} = 0.645 \text{ A}$$

$$I_{C_O, \max} = 0.107 \times 5 \text{ A} = 0.535 \text{ A}$$

Experimental results obtained with the specific component values derived above are shown in Figs. 3.27, 3.28, 3.29, 3.30, 3.31, and 3.32. These results have been recorded by using a DATA6000 waveform analyzer to show their frequency spectra.

In particular, Fig. 3.27 shows the rectifier input line current (unfiltered),  $I_{L_O}$ , and its frequency spectrum at modulation index  $M=0.6$  (worst case regarding the output spectrum). It can be seen that even though the input line current is distorted (because the output current is not ripple-free in practice) its frequency spectrum is in close agreement with the theoretical spectrum. This justifies some of the

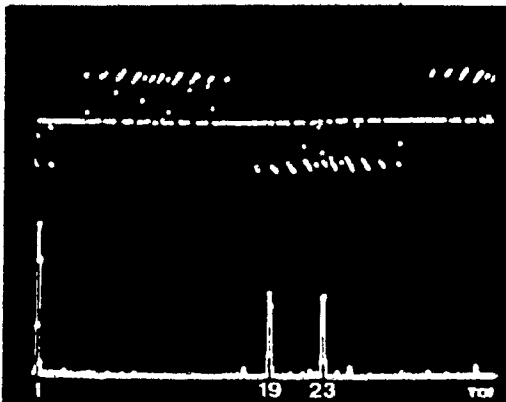


Fig. 3.27: Experimental input line current of the rectifier,  $I_a$ , and its frequency spectrum.

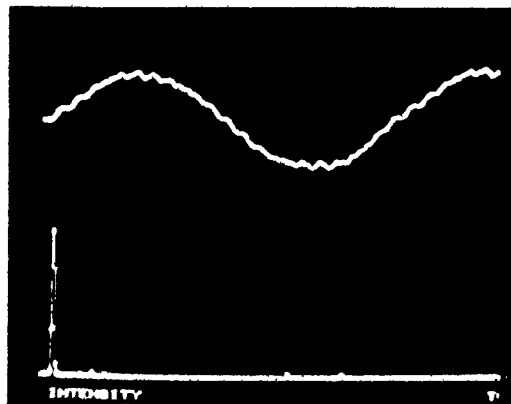


Fig. 3.28: Experimental ac source current,  $I_a$ , and its frequency spectrum.

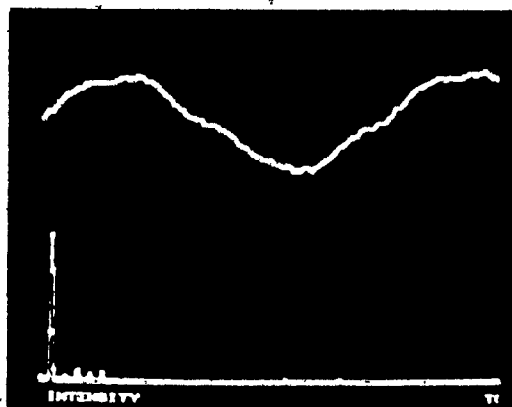


Fig. 3.29: Experimental input voltage,  $V_a$ , and its frequency spectrum.

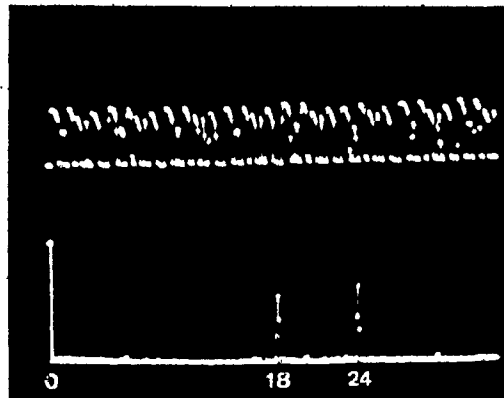


Fig. 3.30: Experimental rectifier output voltage,  $V_r$ , and its frequency spectrum.

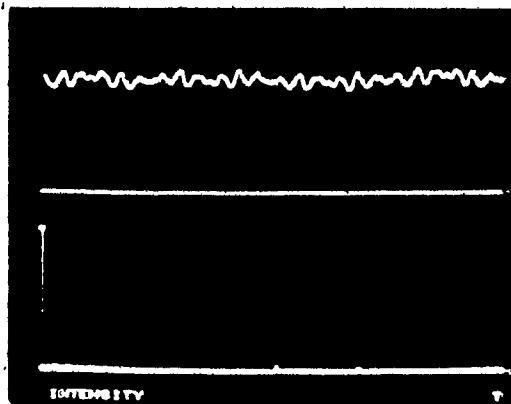


Fig. 3.31: Experimental load voltage,  $V_f$ , and its frequency spectrum.

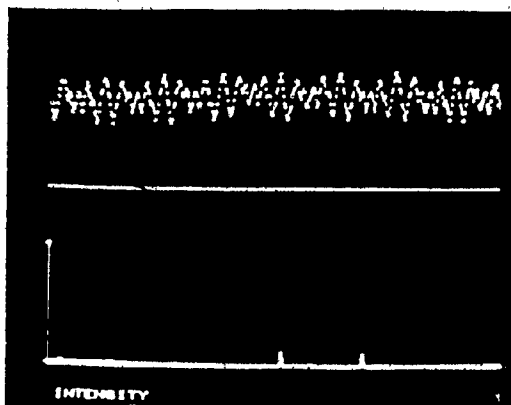


Fig. 3.32: Experimental rectifier output current,  $I_r$ , and its frequency spectrum.

design assumptions made earlier in Section 3.3. Fig. 3.28 shows the filtered source line current,  $I_o$ , and its frequency spectrum obtained with the optimum input filter. The measured  $THD_i$  value of this waveform is about 4.7 % of the rated fundamental current and is in agreement with the 5 % limit set earlier. Also, it can be observed that the maximum magnitude of any single harmonic component does not exceed more than 3 % of the rated fundamental current [56].

Fig. 3.29 shows the input voltage waveform,  $V_o$ , and its frequency spectrum, from which the  $THD_v$  value is measured to be about 9.0 % of its fundamental voltage.

Regarding the rectifier output voltage characteristics, Fig. 3.30 represents the unfiltered rectifier output voltage,  $V_r$ , and its frequency spectrum, where only dominant harmonics (high frequencies) exist. The filtered load voltage,  $V_f$ , and its frequency spectrum, obtained with the actual  $L_o - C_o$  values selected and 1 p.u. resistive load, are shown in Fig. 3.31, where it is noted that the measured  $RF_{V_f}$  value is about 13 % of its dc voltage.

Finally, the rectifier output inductor current,  $I_r$ , and its frequency spectrum are shown in Fig. 3.32. The measured  $RF_{I_r}$  value is 28 % of its dc current, which is within the upper  $RF_{I_r}$  limit.

### 3.7 Conclusion

It has been predicted and experimentally verified that by applying carefully selected PWM control techniques to three-phase rectifiers:

- (i) the size or cost of input/output filters can be reduced significantly (Tables 3.1 and 3.2),
- (ii) the total input power factor can be improved significantly (without using power-factor correction capacitors) with  $S_1$  (wt),  $S_2$  (wt), and  $S_3$  (wt) type of switching functions,
- (iii) if desired, a leading input power factor can be obtained with the  $S_3$  (wt) type of switching functions.

## CHAPTER 4

### OPTIMUM SYSTEM DESIGN OF A THREE-PHASE RECTIFIER-INVERTER FREQUENCY CHANGER

#### 4.1 Introduction

Rectifier-Inverter Frequency Changers (RIFC's) are used in a variety of applications, which include the speed control of ac machines by adjusting the frequency of the applied voltages, UPS systems for critical loads, and 60 Hz to 50 Hz frequency changers. As discussed in Chapter 1, a typical RIFC system, in addition to the rectifier-inverter pair, employs a pair of dc link components ( $L_o - C_o$  in Fig. 4.1):

- (i) to provide a dc bus capable of supplying and storing energy on a transient basis,
- (ii) to decouple the output from the input terminals,
- (iii) to reduce the voltage distortion across the inverter input terminal, and
- (iv) to reduce the ripple components in the dc link current.

In typical RIFC applications, the dc link components and the ac input filter components are relatively large, costly, and heavy. This is partially because of the lack of high frequency semiconductor switches, and partially because the analysis and design of RIFC systems

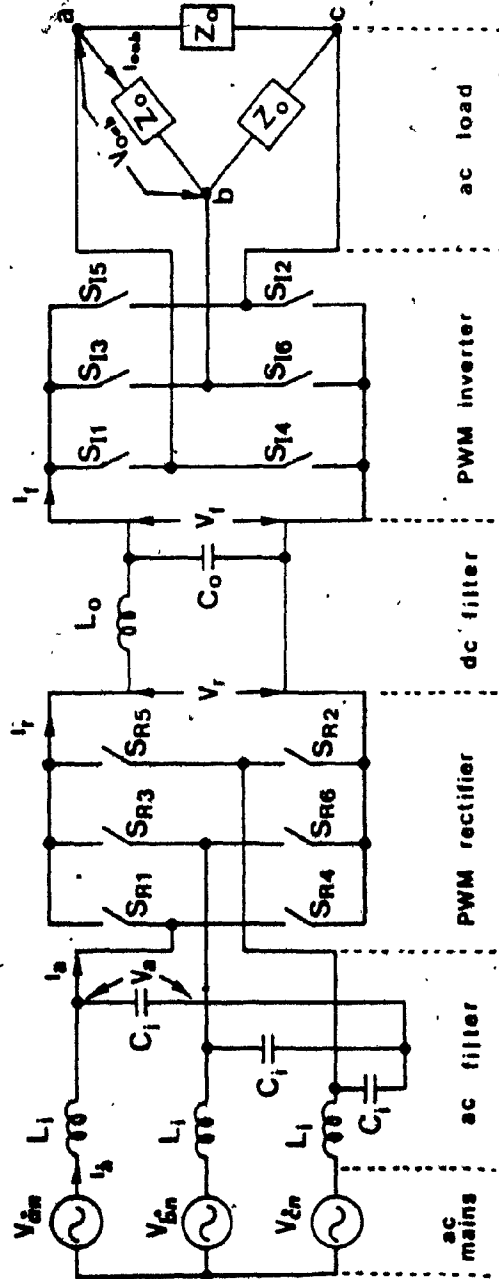


Fig. 4.1: Simplified circuit diagram of a three-phase Rectifier-Inverter Frequency Changer (RIFC).

have so far been focused on the inverting stage of RIFC systems, ignoring the effects of rectifier-inverter interaction.

In contrast, this chapter focuses on the 'optimum' design of an overall RIFC system from ac mains to ac load [57]. Moreover, the converter structures considered here are assumed to employ recently developed high frequency switches, such as bipolar or FET power transistors, asymmetrical SCR's, GTO's, etc.. This task is accomplished as follows. First, rectifier and inverter PWM control schemes which generate minimum possible harmonic distortion are discussed. By using suitable computer-aided analysis and design methods developed in Chapter 3, the optimum (minimum size/weight) ac and dc filters are designed. Additional design data for the rectifier and inverter components are also presented, along with the investigation of three kinds of RIFC structures, including the typical RIFC structure. Finally, some of the predicted key results are verified by simulation on a HP9836 - DATA6000 system.

#### 4.2 Generalized Transfer Function of a Three-Phase AC/AC Converter

Fig. 4.2 shows the black box of a generalized ideal 3-phase to 3-phase frequency changer. Suppose that the desired output currents are specified as:

$$[I_o(t)] = \begin{bmatrix} I_{oa}(\omega_o t) \\ I_{ob}(\omega_o t) \\ I_{oc}(\omega_o t) \end{bmatrix} = \begin{bmatrix} I_m \sin(\omega_o t + \theta) \\ I_m \sin(\omega_o t + \theta - 2\pi/3) \\ I_m \sin(\omega_o t + \theta + 2\pi/3) \end{bmatrix} \quad (4.1)$$

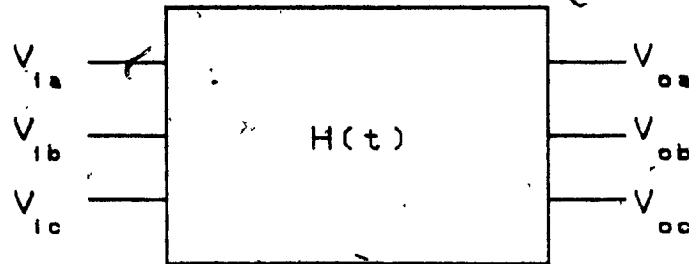


Fig. 4.2: Simplified block diagram of a generalized three-phase to three-phase frequency changer.

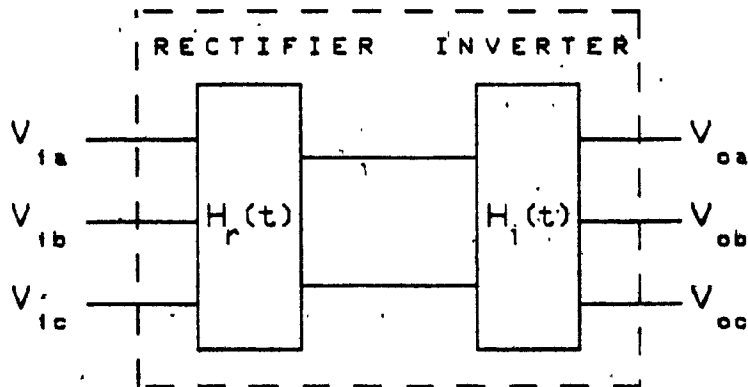


Fig. 4.3: Simplified block diagram of an indirect frequency changer.

and the three input voltages are defined as:

$$[V_I(t)] = \begin{bmatrix} V_{an}(\omega_1 t) \\ V_{bn}(\omega_1 t) \\ V_{cn}(\omega_1 t) \end{bmatrix} = \begin{bmatrix} V_1 \sin \omega_1 t \\ V_1 \sin (\omega_1 t - 2\pi/3) \\ V_1 \sin (\omega_1 t + 2\pi/3) \end{bmatrix} \quad (4.2)$$

then the input and output relationships in matrix form can be expressed as:

$$[V_o(t)] = [H(t)] \cdot [V_I(t)] \quad (4.3)$$

$$[I_I(t)] = [H(t)] \cdot [I_o(t)] \quad (4.4)$$

where

$[V_o(t)] = 3 \times 1$  matrix of the output voltages,

$[I_I(t)] = 3 \times 1$  matrix of the input currents,

$[H(t)] = 3 \times 3$  matrix of the converter transfer function,

$[V_I(t)] = 1 \times 3$  matrix of the input voltages,

$[I_o(t)] = 1 \times 3$  matrix of the output currents.

Let

$$[H(t)] = \begin{bmatrix} h_{a1}(t) & h_{a2}(t) & h_{a3}(t) \\ h_{b1}(t) & h_{b2}(t) & h_{b3}(t) \\ h_{c1}(t) & h_{c2}(t) & h_{c3}(t) \end{bmatrix} \quad (4.5)$$

then the entries of the matrix  $[H(t)]$  may be defined as:

$$h_{a1}(t) = K_a + K_{a12} \cos(A-B+\phi_{a12}) + K_{a13} \cos(A+B+\phi_{a13})$$

$$h_{a2}(t) = K_a + K_{a22} \cos(A-B+\phi_{a22}) + K_{a23} \cos(A+B+\phi_{a23})$$

$$h_{a3}(t) = K_a + K_{a32} \cos(A-B+\phi_{a32}) + K_{a33} \cos(A+B+\phi_{a33})$$

$$h_{b1}(t) = K_b + K_{b12} \cos(A-B+\phi_{b12}) + K_{b13} \cos(A+B+\phi_{b13})$$

$$h_{b2}(t) = K_b + K_{b22} \cos(A-B+\phi_{b22}) + K_{b23} \cos(A+B+\phi_{b23})$$

$$h_{b3}(t) = K_b + K_{b32} \cos(A-B+\phi_{b32}) + K_{b33} \cos(A+B+\phi_{b33})$$

$$h_{c1}(t) = K_c + K_{c12} \cos(A-B+\phi_{c12}) + K_{c13} \cos(A+B+\phi_{c13})$$

$$h_{c2}(t) = K_c + K_{c22} \cos(A-B+\phi_{c22}) + K_{c23} \cos(A+B+\phi_{c23})$$

$$h_{c3}(t) = K_c + K_{c32} \cos(A-B+\phi_{c32}) + K_{c33} \cos(A+B+\phi_{c33}) \quad (4.6)$$

where

the letter  $K$  denotes constant value,

the letter  $\phi$  denotes phase displacement,

$A = \omega t$ , and  $B = \omega_0 t$ .

Depending on how the unknown values are selected, the three-phase ac/ac conversion can be achieved by direct scheme [58], [59], [60] or by indirect scheme. For example, if the set of unknown values is chosen such that

$$K_a = K_b = K_c = \frac{1}{3}$$

$$K_{a12} = K_{a22} = K_{a32} = K_{b12} = K_{b22} = K_{b32} = K_{c12} = K_{c22} = K_{c32} = \frac{2}{3} \lambda_1$$

$$K_{a13} = K_{a23} = K_{a33} = K_{b13} = K_{b23} = K_{b33} = K_{c13} = K_{c23} = K_{c33} = \frac{2}{3} \lambda_2$$

$$\phi_{a12} = \phi_{a13} = \phi_{b22} = \phi_{b33} = \phi_{c32} = \phi_{c23} = 0$$

$$\phi_{a22} = \phi_{a23} = \phi_{b13} = \phi_{b32} = \phi_{c12} = \phi_{c33} = -\frac{2\pi}{3}$$

and  $\phi_{a32} = \phi_{a33} = \phi_{b12} = \phi_{b23} = \phi_{c22} = \phi_{c13} = \frac{2\pi}{3}$

where

$$\lambda_1 > 0,$$

$$\lambda_2 = 1 - \lambda_1, \text{ and}$$

q = ratio between the output and the input voltages.

then this can be realized through the direct conversion scheme proposed by Venturini in [59].

However, if  $K_a = K_b = K_c = 0$  and the rest values are selected so that

$$h_{a1} = M_r \cos A \times M_i \cos B$$

$$h_{a2} = M_r \cos(A-2\pi/3) \times M_i \cos B$$

$$h_{a3} = M_r \cos(A+2\pi/3) \times M_i \cos B$$

$$h_{b1} = M_r \cos A \times M_i \cos(B-2\pi/3)$$

$$h_{b2} = M_r \cos(A-2\pi/3) \times M_i \cos(B-2\pi/3)$$

$$h_{b3} = M_r \cos(A+2\pi/3) \times M_i \cos(B-2\pi/3)$$

$$h_{c1} = M_r \cos A \times M_i \cos(B+2\pi/3)$$

$$h_{c2} = M_r \cos(A-2\pi/3) \times M_i \cos(B+2\pi/3)$$

$$h_{c3} = M_r \cos(A+2\pi/3) \times M_i \cos(B+2\pi/3)$$

(4.7)

where

$M_r$  and  $M_i$  are constants.

then the entries of the transfer function can be split as:

$$[H(t)] = \begin{bmatrix} h_{ia} \cdot h_{ra} & h_{ia} \cdot h_{rb} & h_{ia} \cdot h_{rc} \\ h_{ib} \cdot h_{ra} & h_{ib} \cdot h_{rb} & h_{ib} \cdot h_{rc} \\ h_{ic} \cdot h_{ra} & h_{ic} \cdot h_{rb} & h_{ic} \cdot h_{rc} \end{bmatrix} = \begin{bmatrix} h_{ia} \\ h_{ib} \\ h_{ic} \end{bmatrix} \begin{bmatrix} h_{ra} & h_{rb} & h_{rc} \end{bmatrix} \quad (4.8)$$

where

$$[H_r(t)] = \begin{bmatrix} h_{ra} \\ h_{rb} \\ h_{rc} \end{bmatrix} = \begin{bmatrix} M_r \cos A \\ M_r \cos(A-2\pi/3) \\ M_r \cos(A+2\pi/3) \end{bmatrix} = \text{rectifier transfer function} \quad (4.9a)$$

and

$$[H_i(t)] = \begin{bmatrix} h_{ia} \\ h_{ib} \\ h_{ic} \end{bmatrix} = \begin{bmatrix} M_i \cos B \\ M_i \cos(B-2\pi/3) \\ M_i \cos(B+2\pi/3) \end{bmatrix} = \text{inverter transfer function} \quad (4.9b)$$

Thus,

$$\begin{bmatrix} v_{o,a} \\ v_{o,b} \\ v_{o,c} \end{bmatrix} = \begin{bmatrix} h_{ia} \\ h_{ib} \\ h_{ic} \end{bmatrix} \begin{bmatrix} h_{ra} & h_{rb} & h_{rc} \end{bmatrix} \begin{bmatrix} v_{an} \\ v_{bn} \\ v_{cn} \end{bmatrix} = \begin{bmatrix} h_{ra} & h_{rb} & h_{rc} \end{bmatrix} \begin{bmatrix} v_{an} \\ v_{bn} \\ v_{cn} \end{bmatrix} \begin{bmatrix} h_{ia} \\ h_{ib} \\ h_{ic} \end{bmatrix} \quad (4.10)$$

Hence, this can be realized through the indirect scheme (rectifier-inverter configuration) as shown in Fig. 4.3. This indirect scheme is investigated in this chapter and in the following chapter.

Finally, it may be stated that there may exist other sets of the unknown values so that the generalized transfer function  $[H(t)]$  can be realized, unless it is proved that no other set exists.

#### 4.3 System Description and Principles of Operation

The RIFC system topology that lends itself readily to system optimization is shown in Fig. 4.1. It consists of a three-phase mains, a second-order input filter, a PWM rectifier, a second-order dc link filter, a PWM inverter, and a three-phase balanced load. The nature of each major system component and their functions are as follows.

The ac input filter acts as an interface between the ac mains and RIFC system. As such, its function is to minimize the 'dumping' of current harmonics on utility lines (harmonic pollution) and to improve the system input power factor. The size, weight, and cost of this filter are determined mainly by the rated system power and the specified level of THD (eqn. (3.10)) of the ac input line current.

The rectifier performs the first half of the frequency changer function by converting the fixed frequency ac power into dc power. To optimize the process of rectification, the conventional six-diode

(or phase-controlled) rectifier is replaced here by one of the PWM rectifier structures investigated in Chapter 3. The optimised switching function, which is the  $S_3$  (wt) type, is chosen in order for the rectifier to provide constant unregulated dc bus voltage, acceptable here, because the control of power flow can be achieved by using the PWM inverter. Moreover, a number of inverters with independent control can be operated with a single rectifier supply, resulting in considerable savings of the rectifier cost since the dc link voltage is constant.

The function of the dc link filter is to attenuate the rectifier output voltage harmonics across the link inductor  $L_0$  and to 'sink' the inverter input current harmonics into the link capacitor  $C_0$ . To the dc link filter, the PWM rectifier appears as a source of an infinite number of voltage harmonics, while the PWM inverter as a similar source of current harmonics. However, the attenuation of the rectifier output voltage harmonics across  $L_0$  creates additional ripple current into  $C_0$ , while the sinking of the inverter input current harmonics into  $C_0$  gives rise to additional ripple voltage across  $L_0$ . Therefore, both filter components ( $L_0$  and  $C_0$ ) are affected by both harmonic sources. The size and cost of this dc filter is again determined by the rated system power, rated dc bus voltage, and the specified ripple limits of the dc link input current  $I_r$  and link output voltage  $V_f$ . It is also noted that allowing a high level of ripple current in  $I_r$  leads to rectifier input current discontinuities under light load conditions. This in turn causes the temporary loss of control of inverter input

voltage, and consequently the loss of control of the power flow to the load which can lead to system instabilities. Moreover, allowing a high ripple voltage in  $V_f$  causes voltage subharmonics in the inverter output voltages, which further degrade the overall system performance.

The inverter performs the second half of a frequency changer function by converting the unregulated dc (link) power into regulated ac power (variable voltage and variable frequency). To maximize dc voltage utilization by the inverter, the traditional SPWM scheme has been replaced by the MSPWM scheme which is a more efficient version of the SPWM scheme (i.e.  $S_2$  (wt) type of switching function). With this scheme, the inverter delivers almost sinusoidal currents to inductive types of loads.

Three kinds of RIFC structures are investigated. Structure #1, which is the traditional RIFC system, is comprised of a six-diode rectifier and a PWM inverter which employs the SPWM scheme with  $N_h=27$  for 60 Hz (1 p.u.) output frequency. This structure is included for two reasons: (a) to provide the contrast between the proposed RIFC system and the traditional one, and (b) to provide the relevant data for the design of a traditional system. Structure #2 is composed of a six-diode rectifier and a PWM inverter which employs the MSPWM scheme with  $N_h=16$  for 60 Hz output frequency. The reason for including this structure is to provide the relevant design data to users who may want to change only the inverter configuration of the traditional RIFC system. Structure #3, which is the proposed RIFC

system, consists of a PWM rectifier with  $N_h = 9, 11, 13$  (#3-1, #3-2, #3-3, respectively) and the same MSPWM inverter as in Structure #2. The reason for applying three different  $N_h$  values to the PWM rectifier is to select the optimum  $N_h$  value resulting in an optimum RIFC system.

For the best use of derived results, all the design data are expressed in per unit (p.u.), where the rated rms value of the fundamental component of the inverter output line-to-line voltage,  $V_{oab}$  (Fig. 4.1), is considered as 1 p.u. voltage, with the corresponding phase current  $I_{oab}$  as 1 p.u. current.

#### 4.4 RIFC Input Stage Analysis and Input Filter Design

The RIFC input stage analysis and optimum input filter design are carried out under the following assumptions.

- (i) The three-phase mains are balanced and distortion-free.
- (ii) The rectifier switching elements are ideal.
- (iii) The filter components are lossless.
- (iv) The dc link current is ripple-free.
- (v) The input filter delivers the rated power to the rectifier.
- (vi) The  $THD_i$  limit is 5 % of the rated fundamental component in the input line current  $I_i$  (Fig. 4.1).
- (vii) The  $THD_v$  limit is 10 % of the rated fundamental component in the input voltage of the rectifier  $V_{ar}$ .

TABLE 4.1: 'RIFC' INPUT FILTER DESIGN DATA (p.u.).

Frequency Changer Structures	System Configuration		$X_{L1}$	$X_{C1}$	KVA ( $L_1$ )	KVA ( $C_1$ )	TKVA	$\theta_1$	$I_b$	$I_{b1}$	$V_m$	$V_{a1}$	$I_a$	$I_{a1}$
	Rectifier	Inverter												
Structure #1	6-diode	SPWM ( $N_h=27$ )	0.18	0.95	0.40	0.55	0.95	-7.4°	1.56	1.49	0.77	0.70	1.69	1.29
Structure #2		HSPWM ( $N_h=16$ )	0.14	0.73	0.41	0.53	0.94	-6.1°	1.79	1.71	0.67	0.61	1.94	1.49
Structure #3	OPWM	$N_h=9$	0.06	2.4	0.13	0.22	0.35	-3.7°	1.47	1.40	0.72	0.65	2.06	1.39
		$N_h=11$	0.04	2.75	0.08	0.20	0.28	-4.9°	1.47	1.40	0.72	0.65	2.04	1.38
		$N_h=13$	0.04	3.15	0.08	0.18	0.26	-3.7°	1.47	1.40	0.72	0.65	2.03	1.38

TABLE 4.2: RECTIFIER SWITCH RATINGS OF 'RIFC' STRUCTURES (p.u.).

Frequency Changer Structures	System Configuration		Peak Current	Average Current	rms Current	$V_F/V_R^*$	$f_S^{**}$ (Hz)
	Rectifier	Inverter					
Structure #1	6-diode	SPWM	1.8	0.6	1.04	1.09	60
Structure #2	6-diode	MSPWM	2.1	0.7	1.22	0.95	60
Structure #3	OPWM	$N_h=9$	2.1	0.7	1.22	1.02	540
		$N_h=11$	2.1	0.7	1.22	1.02	660
		$N_h=13$	2.1	0.7	1.22	1.02	780

\*  $V_F/V_R$ : Peak forward and reverse blocking voltages

\*\*  $f_S$ : Switching frequency

The input stage analysis and optimum input filter design are performed in the same manner as developed in Section 3.3. The salient design data of an optimum input filter for each RIFC structure are summarized in Table 4.1, including the input filter component values and their kVA ratings, TKVA values, rated rms fundamental input voltages and currents, and rated rms input voltages and currents. In particular, the optimum input filter  $X_{L_i}$  and  $X_{C_i}$  values (Fig. 4.1) for the Structure #3-2 are found to be 0.04 p.u. and 2.75 p.u., respectively; and the TKVA value is 0.278 p.u.. For an RIFC system supplied from 60 Hz three-phase mains and rated for 30 kVA and 208 volts, the aforementioned  $X_{L_i}$ ,  $X_{C_i}$ , and TKVA (p.u.) values are equal to 460  $\mu$ H, 233  $\mu$ F, and 2.78 kVA respectively.

It is also noted from Table 4.1 that, as expected, the proposed RIFC structures (i.e. #3-1, #3-2, and #3-3) yield significant reductions (approx. 70 %) in the input filter component values and their kVA ratings and hence in the filter costs.

Moreover, as a result of the input stage analysis, the analysis and design data of the corresponding rectifier are provided in Table 4.2, including the worst case of rms, average, and peak current ratings for each rectifier switch, as well as the peak forward and reverse blocking voltages and switching frequencies. The types of gate turn-off switching devices, such as bipolar transistors, MOSFET's, GTO's etc., are not specified, because the choice of switches depends on the associated switching frequency, voltage, and current levels. Moreover, the technology of power switching devices is still in a state of flux.

#### 4.5 DC Link Analysis and DC Link Filter Design

The dc link analysis and dc link filter design are carried out under the following assumptions.

- (i) The rectifier input voltages and inverter output (line) currents are balanced and distortion-free.
- (ii) The switching devices of the rectifier and inverter are ideal.
- (iii) The dc link filter components are lossless.
- (iv) The inverter delivers the rated current to an inductive load with the worst case of operating conditions.
- (v) The switching frequency (or carrier frequency) of the inverter is fixed as the output frequency varies.
- (vi) The maximum load power factor (p.f.) is 0.9 inductive.
- (vii) The ripple factor of the inverter input voltage,  $RF_{V_f}$ , defined in (3.38), remains below 10 % of the rated dc voltage.
- (viii) The ripple factor of the link current,  $RF_{I_f}$ , defined in (3.39), remains below 10 % of the rated dc current.

Fig. 4.4a represents the equivalent circuit of a dc link, which consists of a voltage source containing all the unwanted (or ripple) components, a second-order dc filter, and a current source containing all the unwanted components. From (3.17), the rectifier output voltage  $V_r(\omega t)$  is given by:

$$V_r(\omega_1 t) = V_{dc} + \sum_{n=6}^{\infty} V_{r,n} \sin(n\omega_1 t + \theta_{r,n}) \quad (4.11)$$

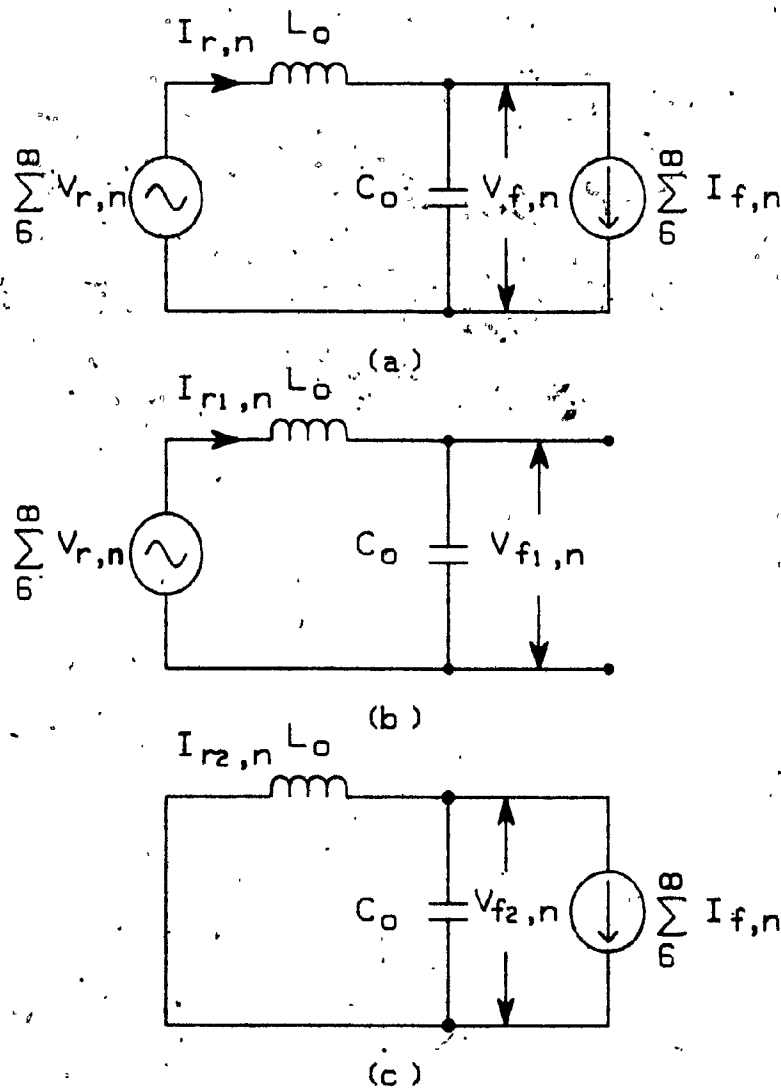


Fig. 4.4: Analytical model of an RIFC dc link.

- a) Equivalent circuit of the dc link.
- b) Harmonic equivalent circuit for the rectifier output voltage.
- c) Harmonic equivalent circuit for the inverter input current.

where

$\omega_i$  = angular frequency of the three-phase mains.

The input current of the inverter,  $I_f$  (Fig. 4.1), is given by:

$$I_f(\omega_o t) = [I_o(\omega_o t)][S_I(\omega_o t)] \quad (4.12)$$

where

$[I_o(\omega_o t)]$  = 1 x 3 matrix of the inverter output phase currents

$[S_I(\omega_o t)]$  = 3 x 1 matrix of the inverter switching functions

$\omega_o$  = angular frequency of the inverter output frequency:

After trigonometric manipulations, (4.12) may be written as :

$$I_f(\omega_o t) = I_{dc} + \sum_{n=6}^{\infty} I_{f,n} \sin(n\omega_o t + \phi_{f,n}) \quad (4.13)$$

where

$I_{dc}$  = dc component of the inverter input current,  $I_f(\omega_o t)$

$I_{f,n}$  = amplitude of the n-th component of the  $I_f(\omega_o t)$

$\phi_{f,n}$  = phase displacement of the n-th component of the  $I_f(\omega_o t)$ .

Moreover, in designing the dc link filter, the inverter input current  $I_f(\omega_o t)$  must be determined under the worst operating conditions. Fig. 4.5 shows the rms ripple current of the MSPWM inverter input current  $\bar{I}_{fR}$ , as a function of the modulation index M for various load power factors. From the figure, it can be seen that the

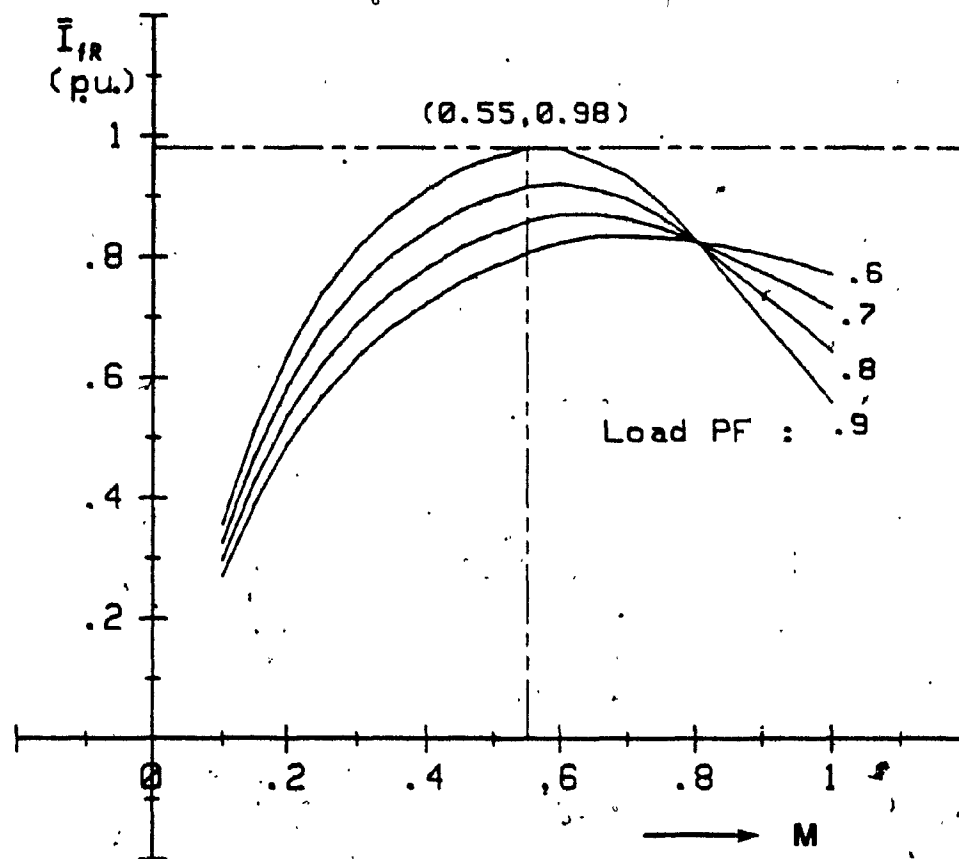


Fig. 4.5: RMS ripple current of the MSPWM inverter input current versus the modulation index,  $M$ , for various load power factors.

maximum  $\bar{I}_{fR}$  value occurs at  $M=0.55$  with load p.f.=0.9, which is the maximum load power factor in this case. In other words, this pair of values is considered to be the worst operating condition. The worst operating condition is found to be  $M=0.6$  and load power factor =0.9, as shown by the  $\bar{I}_{fR}$  -vs-  $M$  plots for the SPWM inverter in Fig. 4.6. By applying the superposition theorem to Fig. 4.4a the equivalent circuits for the unwanted components can be represented as shown in Figs. 4.4b and 4.4c. Hence, the rectifier output current,  $I_r$ , (Fig. 4.1) and the inverter input voltage,  $V_f$ , are given by:

$$\bar{I}_r = [I_{dc}^2 + \sum_{n=6}^{\infty} (\bar{I}_{r1,n}^2 + \bar{I}_{r2,n}^2)]^{1/2} \quad (4.14)$$

$$\bar{V}_f = [V_{dc}^2 + \sum_{n=6}^{\infty} (\bar{V}_{f1,n}^2 + \bar{V}_{f2,n}^2)]^{1/2} \quad (4.15)$$

where

$\bar{I}_r$  = rms value of the rectifier output current,

$\bar{V}_f$  = rms value of the inverter input voltage.

$$\bar{I}_{r1,n} = \frac{n}{n^2 X_{L_o} - X_{C_o}} \bar{V}_{r,n} \quad (4.16a)$$

$$\bar{I}_{r2,n} = - \frac{X_{C_o}}{n^2 X_{L_o} - X_{C_o}} \bar{I}_{f,n} \quad (4.16b)$$

where

$\bar{V}_{r,n}$  = rms value of the n-th harmonic component  
of the rectifier output voltage,  $V_r$

$\bar{I}_{f,n}$  = rms value of the n-th harmonic component  
of the inverter input current,  $I_f$ .

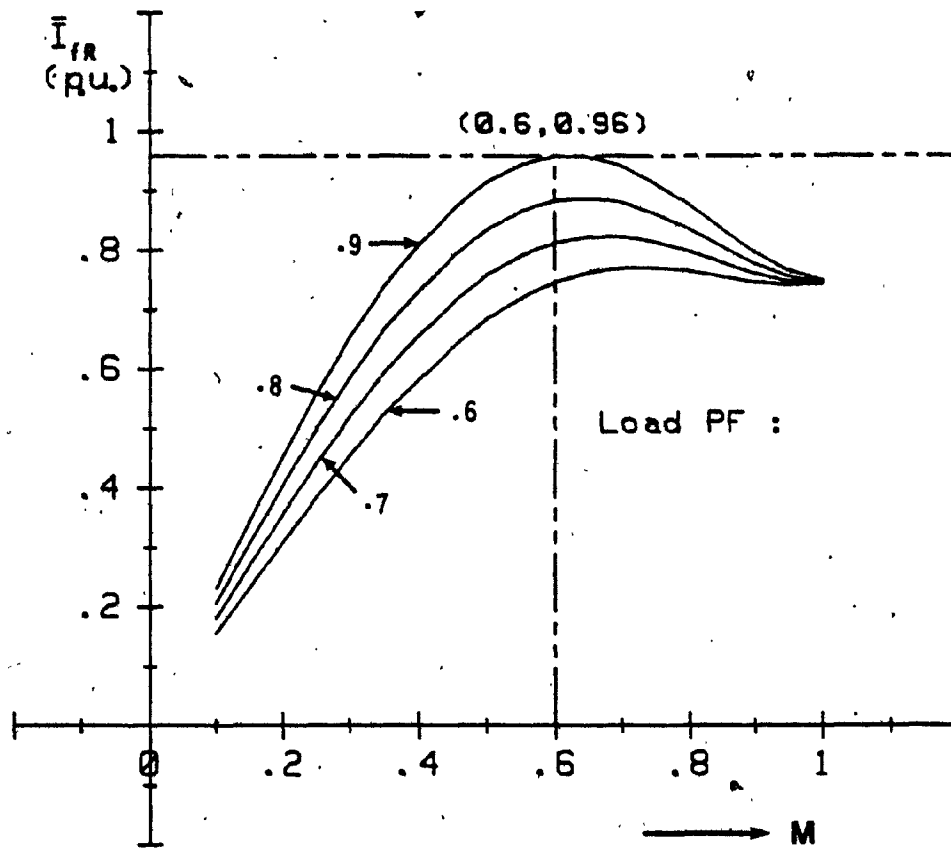


Fig. 4.6: RMS ripple current of the SPWM inverter input current versus the modulation index,  $M$ , for various load power factors.

$$\bar{V}_{f1,n} = - \frac{n \bar{I}_{r1,n}}{X_{C_o}} \quad (4.17a)$$

$$\bar{V}_{f2,n} = - \frac{n X_{L_o} X_{C_o}}{n^2 X_{L_o}^2 - X_{C_o}} \bar{I}_{f,n} \quad (4.17b)$$

The dc link components  $L_o$  and  $C_o$  are selected in exactly the same manner as developed in Section 3.4, and the salient design data for all the subject structures are summarized in Table 4.3. In particular, the  $L_o$  and  $C_o$  values for the proposed Structure #3-2 are found to be:  $X_{L_o} = 0.09$  p.u. and  $X_{C_o} = 2.8$  p.u.. Again, for an RIFC system supplied from 60 Hz mains and rated at 30 kVA and 208 volts (60 Hz), the aforementioned  $X_{L_o}$  and  $X_{C_o}$  values can be translated into:  $L_o = 1.033$  mH and  $C_o = 220$  uF. Comparison of the corresponding design data of Table 4.3 shows that the proposed RIFC structure #3's offer significant reductions in dc filter inductor values, but that they require larger dc filter capacitor values.

Finally, as a result of the analysis of inverter input current, the inverter switch ratings are shown in Table 4.4, which includes the worst rms, average, and peak current ratings per switch for each structure, as well as the peak forward and reverse-blocking voltages and switching frequencies.

#### 4.6 Evaluation of the RIFC Structures

To facilitate the evaluation of the RIFC structures, their main

TABLE 4.3: 'RIFC' DC LINK FILTER DESIGN DATA (p.u.)

Frequency Changer Structures	System Configuration		$X_{L_0}$	$X_{C_0}$	$I_{L_0}$	$I_{C_0}^{**}$	$V_{r,peak}$	$V_{dc}$	$I_{r,peak}$	$I_{dc}$	$V_{f,peak}$	$I_{f,peak}$
	Rectifier	Inverter										
Structure #1	6-diode	SPWM ( $N_n=27$ )	0.22	4.3	0.11	0.97	1.73	1.63	1.8	1.66	1.80	3.1
Structure #2	6-diode	MSPWM ( $N_n=16$ )	0.15	2.7	0.13	1.01	1.50	1.42	2.1	1.91	1.56	3.4
Structure #3	OPWM	$N_n=9$	0.10	2.9	0.13	1.02	1.69	1.42	2.1	1.91	1.56	3.4
		$N_n=11$	0.09	2.8	0.13	1.07	1.71	1.42	2.1	1.91	1.56	3.4
		$N_n=13$	0.09	2.7	0.13	1.07	1.70	1.42	2.1	1.91	1.56	3.4

\*  $I_{L_0}$ : RMS ripple current through  $L_0$

\*\*  $I_{C_0}$ : RMS ripple current through  $C_0$

TABLE 4.4: INVERTER SWITCH RATINGS OF 'RIFC' STRUCTURES (p.u.).

Frequency changer Structures	System Configuration		Peak Current	Average Current	rms Current	$V_F/V_R$	$f_s$ (Hz)
	Rectifier	Inverter					
Structure #1	6-diode	SPWM	$\sqrt{6}$	$\sqrt{6}/\pi$	$\sqrt{1.5}$	1.80	1,620
Structure #2	6-diode	MSPWM	$\sqrt{6}$	$\sqrt{6}/\pi$	$\sqrt{1.5}$	1.56	1,620
Structure #3	OPWM	$N_h=9$	$\sqrt{6}$	$\sqrt{6}/\pi$	$\sqrt{1.5}$	1.56	1,620
		$N_h=11$	$\sqrt{6}$	$\sqrt{6}/\pi$	$\sqrt{1.5}$	1.56	1,620
		$N_h=13$	$\sqrt{6}$	$\sqrt{6}/\pi$	$\sqrt{1.5}$	1.56	1,620

features are summarized in Table 4.5, which includes the values of ac and dc filter components, TKVA ratings of ac filter, switching frequencies, overall voltage utilizations, and overall system complexities. It is noted that each structure has its own advantages and disadvantages. However, if the main design objective is to minimize the size of the associated reactive components (as it is in this case), then the Structure #3s are by far the best alternative. Among the Structures #3-1, #3-2, #3-3, the Structure #3-2 is found to represent the 'optimum' RIFC system, because although the Structure #3-3 employs a larger  $N_h$  value (to the rectifier) than that of Structure #3-2, there are no significant reductions in the reactive component values of the ac/dc filters and the TKVA value.

Furthermore, some selected design data, such as input voltage, rated fundamental input line current, and rated dc link voltage and current for each structure, are shown in Table 4.6. They are expressed in p.u. and have been obtained under the worst load condition (i.e. p.f.=0.9 and  $M=1$ ). These values provide a quick estimate of component ratings and a frame work for comparing the structures. For this purpose, Table 4.6 also includes the values of three Voltage Utilization Factors (VUF's) for each structure. These factors are: the rectifier VUF,  $\eta_R$ , the inverter VUF,  $\eta_I$ , and the overall RIFC VUF,  $\eta_T$  which represents the product of the previous two. From Table 4.6 it can be seen that the best and worst overall RIFC VUF values are obtained with the Structure #2 and Structure #1, respectively. Consequently, the circuit components comprising RIFC Structure #2 have the highest

TABLE 4.5: PERFORMANCE CHARACTERISTICS OF 'RIFC' STRUCTURES.

CHARACTERISTICS	STRUCTURE #1	STRUCTURE #2	STRUCTURE #3
Values of ac input filter components	Large	Large	Small
Total input filter reactive KVA	Large	Large	Small
Rectifier switching frequency	Low	Low	Medium
Values of dc link filter reactor	Large	Medium	Small
Values of dc link filter capacitor	Small	Medium	Medium
Inverter switching frequency	High	High	High
Overall voltage utilization	Low	High	Medium
Level of (system) complexity	Low	Medium	High

TABLE 4.6: SELECTED DESIGN DATA FOR 'RIFC' STRUCTURES OBTAINED  
WITH  $M=1$  AND LOAD POWER FACTOR=0.9 (p.u.).

Frequency changer Structures	System Configuration		$V_1$	$I_{a,1}$	$V_{dc}$	$I_{dc}$	$\eta_R^*$ (%)	$\eta_I^{**}$ (%)	$\eta_T^{***}$ (%)
	Rectifier	Inverter							
Structure #1	6-diode	SPWM	0.62	1.49	1.63	1.66	95.5	86.6	82.7 (100)
Structure #2	6-diode	MSPWM	0.54	1.71	1.42	1.91	95.5	99.8	95.3 (115.2)
Structure #3	OPWM	$N_h=9$	0.64	1.40	1.42	1.91	88.7	99.8	88.5 (107)
		$N_h=11$	0.65	1.40	1.42	1.91	88.4	99.8	88.2 (106.7)
		$N_h=13$	0.65	1.40	1.42	1.91	88.6	99.8	88.4 (106.9)

\*  $\eta_R$  = rectifier output dc voltage / rectifier input peak line voltage, \*\*  $\eta_I$  = inverter output peak line voltage / inverter output dc voltage

\*\*\*  $\eta_T = \eta_R \cdot \eta_I$

current and the lowest voltage ratings. The opposite is true for the circuit components comprising Structure #1.

#### 4.7 Simulated Results

To verify the analytical key results, the aforementioned 'optimum' RIFC Structure #3-2, as specified in the fourth row of Tables 4.1 to 4.6, was tested by simulation on a HP9836-DATA6000 system. A dedicated computer program for HP9836 computer was employed to generate the voltage and current waveforms, which were further processed on the DATA6000 waveform analyzer. These simulated waveforms and their corresponding frequency spectra are shown in Figs. 4.7 to 12.

In particular, Figs. 4.8 and 4.9 show the ac source current,  $I_a$ , and the input voltage of rectifier  $V_a$  waveforms, with the optimum input filter and the corresponding frequency spectra. From these figures it is apparent that they have very low total harmonic distortions (THD<sub>i</sub> and THD<sub>v</sub>). These results are in close agreement with the specified THD limits (i.e. 5 % and 10 %, respectively). Figs. 4.11 and 4.12 show the dc link current  $I_l$  and inverter input voltage  $V_f$  waveforms and their frequency spectra, which also reveal that they contain very low ripple components. Again, these results are in close agreement with the specified ripple factor limits (i.e. 10 % and 10 %). Moreover, Figs. 4.7 and 4.10 verify that the selected PWM control technique (i.e. optimized PWM) of the rectifier attenuates the low-order harmonics of the rectifier input line current and output voltage very effectively.

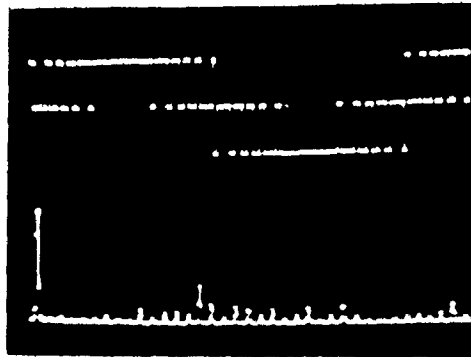


Fig. 4.7: Simulated input line current waveform of the 'RIFC' Structure #3-2 with ripple-free dc link current, and its frequency spectrum.

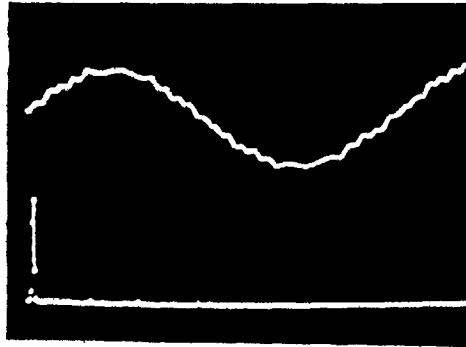


Fig. 4.8: Simulated filtered ac mains side current waveform of the RIFC Structure #3-2, and its frequency spectrum.

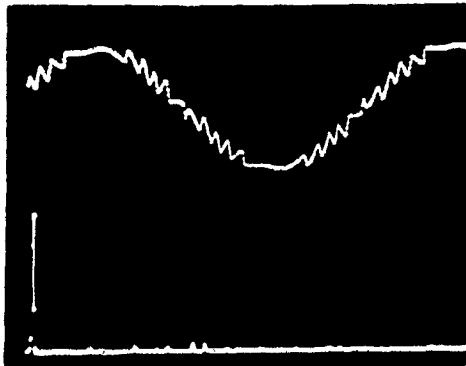


Fig. 4.9: Simulated input line-to-neutral voltage waveform of the 'RIFC' Structure #3-2, and its frequency waveform.

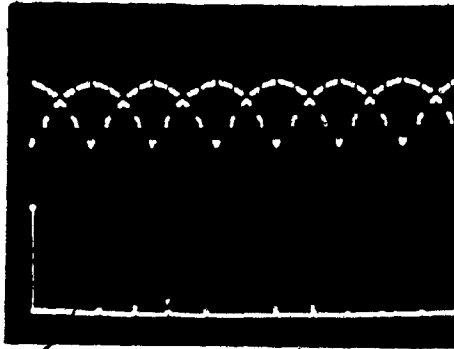


Fig. 4.10: Simulated rectifier output voltage waveform of the 'RIFC' Structure #3-2, and its frequency spectrum.

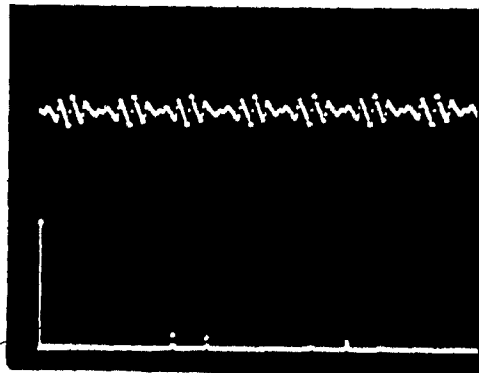


Fig. 4.11: Simulated dc link current waveform of the 'RIFC' Structure #3-2, and its frequency spectrum.

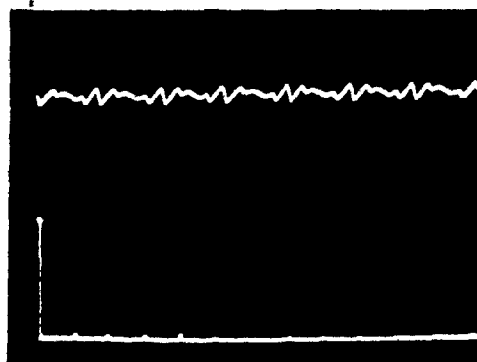


Fig. 4.12: Simulated inverter input voltage waveform of the 'RIFC' Structure #3-2, and its frequency spectrum.

#### 4.8 Conclusion

This chapter has dealt with the 'optimum' system design of a three-phase rectifier-inverter frequency changer by means of the minimization of the associated reactive components, as well as the improvement of the overall RIFC system performance. To achieve this task, the advanced PWM control techniques discussed in Chapter 2 have been applied to the rectifier and the inverter. Three RIFC structures have been investigated to make a comparison and to provide system design data. The ac/dc filter design methods developed in Chapter 3 were utilized to select proper filter component values, and some other useful system design data were also provided. The analytical and simulated results have shown that the RIFC systems employing the advanced PWM control technique to the rectifier (i.e. Structure #3's) require considerably smaller sized ac/dc filters. Moreover, the 'optimum' RIFC system has been found to be the system which consists of a PWM rectifier employing the optimized PWM switching function with  $N_h = 11$  and a PWM inverter employing the MSPWM switching function.

On the other hand, the proposed Structure #3's are more complex and expensive than their six-diode rectifier counterparts. However, with the semiconductor prices falling, the prices of inductors and capacitors remaining stable, floor space for static power converters becoming more expensive, and the harmonic standards becoming stricter, the PWM rectifier has already begun to attract considerable attention.

## CHAPTER 5

### RECTIFIER-INVERTER FREQUENCY CHANGERS WITH SUPPRESSED DC LINK COMPONENTS

#### 5.1 Introduction

In response to expectations towards motor frame mounted converters the RIFC systems studied in Chapter 4 are reconsidered here to study the feasibility of further reductions in converter volume, cost, and weight through the suppression (or complete elimination) of the dc link components  $L_o$  and  $C_o$  (Fig. 4.1). The dc link components in general:

- (i) are bulky and heavy,
- (ii) require a good portion of overall cabinet space,
- (iii) slow down system response, and
- (iv) complicate power regeneration to the ac source.

These disadvantages have motivated the investigation of RIFC topologies with suppressed dc link components (referred to as 'SRIFC'). In this case, the rectifier must have the capability of regeneration, because of the elimination of the energy storage of dc link capacitor. Two such structures are introduced and thoroughly discussed in this chapter [61]. The discussion includes:

- (i) changes in rectifier structures required to create a stable dc bus without using the passive components  $L_o$ ,  $C_o$  (Fig. 4.1),
- (ii) quantization of the distortion of dc bus voltage and

- methods of distortion control,
- (iii) effects of dc bus distortion on the load voltages and methods of improving the corresponding frequency spectra,
  - (iv) quantization of the distortion of input currents (ac mains side) and input filter design, and
  - (v) analysis method and design data for the two SRIFC structures and their system performances.

Finally, some of the key results are experimentally verified on a 1 kVA laboratory set-up.

## 5.2 System Description and Principles of Operation

Fig. 5.1 shows the circuit diagram of the SRIFC system studied. It consists of a three-phase mains, an input filter, a regenerative rectifier, an inverter, and a three-phase load. Depending on the rectifier configuration, two kinds of SRIFC structures are considered.

Structure #1, having the harmonic control capability of the output voltage and input current, is shown in Fig. 5.2. It consists of a PWM regenerative rectifier (comprised of bidirectional switches) which employs the optimised PWM scheme with  $N_h = 11$ , and a PWM inverter which employs the MSPWM scheme at switching frequencies of about 6 kHz. For ac/dc conversion the PWM regenerative rectifier operates in the rectification mode to provide the dc bus for the PWM inverter, while for dc/ac conversion it operates in inversion mode, producing a three-phase PWM waveform at the ac terminals so as to send the regenerated

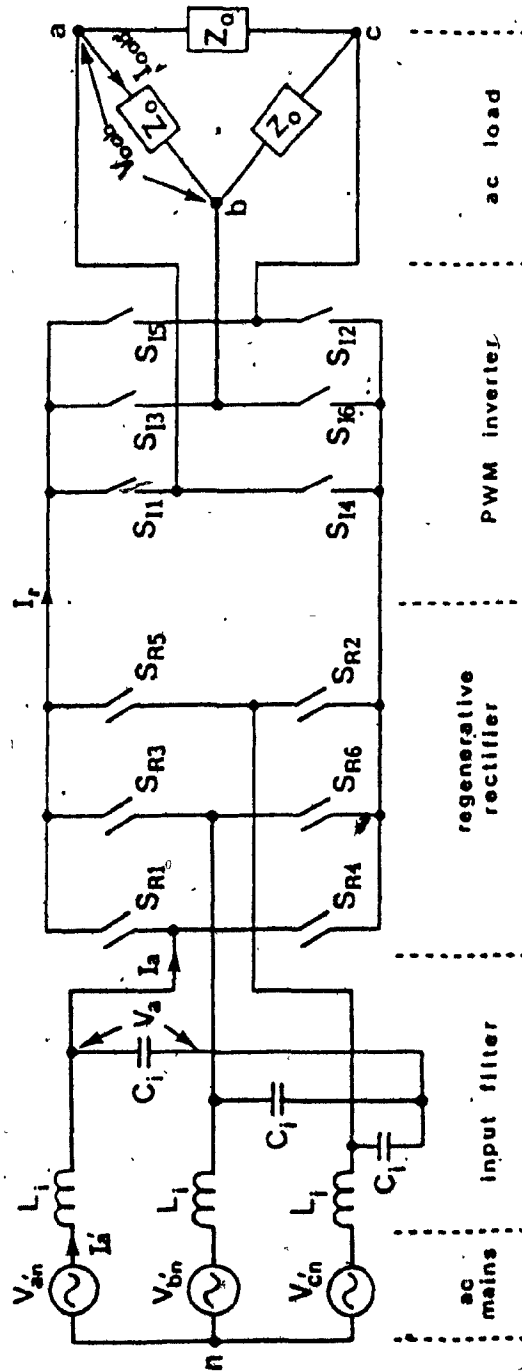
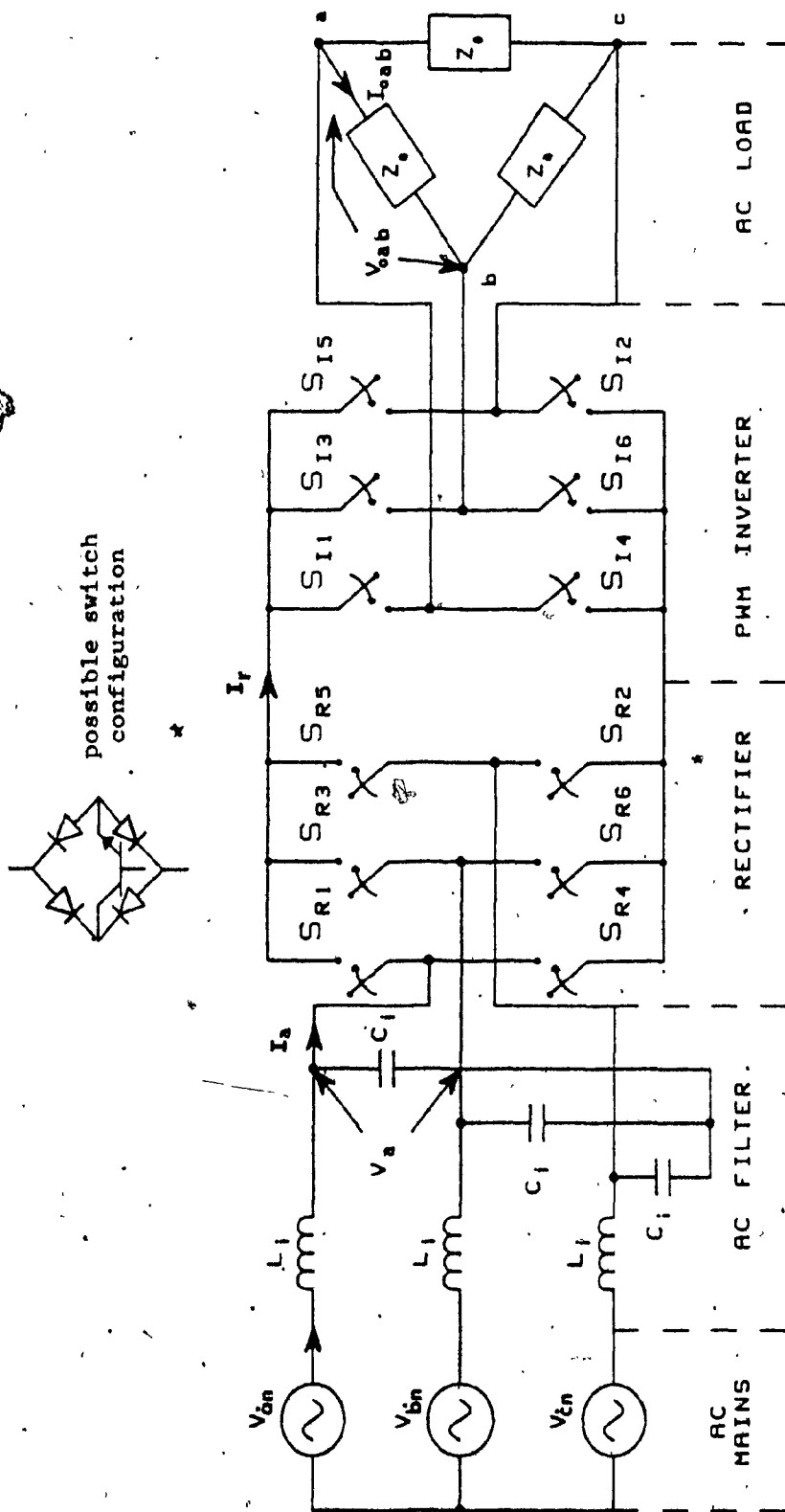


Fig. 5.1: Simplified circuit diagram of the SRIFC system studied.



energy back to the source.

Structure #2, having only the harmonic control capability of the output voltage, is shown in Fig. 5.3. From this figure it can be seen that the configuration of the regenerative rectifier is exactly the same as that of a typical PWM inverter. Therefore, Structure #2 has the advantage of employing interchangeable rectifier and inverter modules. This regenerative rectifier operates as follows [62]. For ac/dc conversion, the six switches are gated only during the normal conduction interval (120 degrees) of their corresponding antiparallel diodes. Continuous gating on each switch only during the time, when the antiparallel diode conducts, will not interfere with the rectification action of the circuit provided that each switch is turned off when the antiparallel diode ceases conduction. During inverting mode operation, by gating on the switches for 120 degrees as described previously, a three-phase voltage waveform of the six-step type is produced at the ac terminals. Therefore, provided the switches are turned on and off synchronously in relation to the ac supply voltage, the regenerative rectifier will deliver or accept dc current.

The power flow of both structures is controlled by varying the modulation index  $M$  of the inverters so that an optimized PWM switching function can be applied to the rectifier (Structure #1). Since dc link components are not employed, all the harmonic components of the rectifier output voltage have a direct effect on the inverter output voltages. Similarly, all the components of the inverter input current

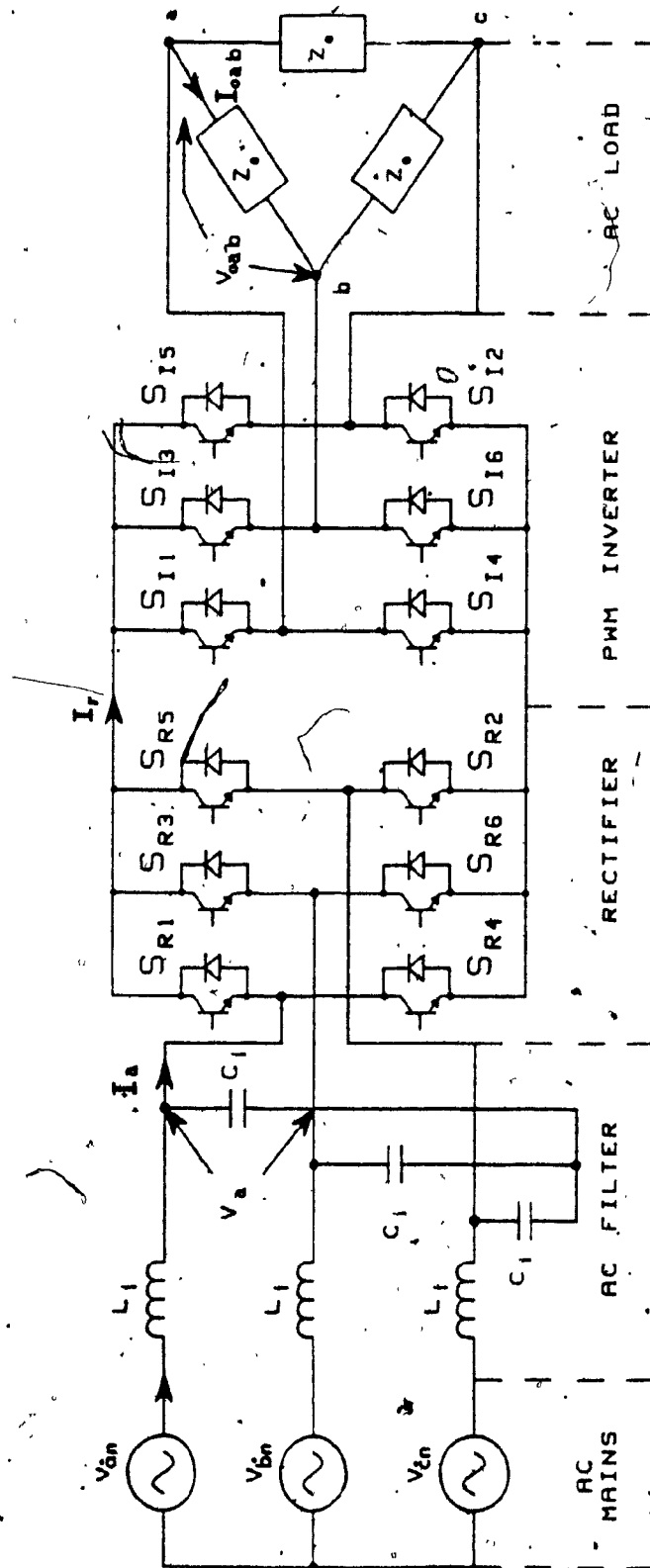


Fig. 5.3: Simplified circuit diagram of the proposed SRIFC Structure #2.

have a direct effect on the input line currents of the rectifier. Hence, the frequency spectra and the magnitudes of both rectifier and inverter switching functions are of significant practical importance, and both switching functions must be chosen carefully.

The three-phase load is assumed to be a balanced delta connection with 1 p.u. impedance, and the range of the load power factor is assumed to be 0.4 to 0.9 inductive. The rated rms output voltage of the inverter is defined as 1 p.u. voltage. Output frequencies up to 100 Hz are commonplace, with 250 Hz or 400 Hz available in special cases [25]. In fact, the maximum output frequency depends on the applications and switching devices. However, in this case, the maximum and base frequencies are assumed to be 150 Hz and 60 Hz (1 p.u. frequency), respectively.

### 5.3 Output Stage Analysis

From (3.17) the output voltage of a rectifier is given by:

$$V_r(\omega_1 t) = V_{dc} + \sum_{k=6}^{\infty} V_{r,k} \sin(k\omega_1 t + \theta_{r,k}) \quad (5.1)$$

where

$V_{dc}$  = dc component of a rectifier output voltage,

$V_{r,k}$  = amplitude of the k-th unwanted component,

$\theta_{r,k}$  = phase displacement of the k-th unwanted component,

$\omega_1$  = angular frequency of a three-phase mains.

Assuming the switching function of an inverter to be:

$$[S_I(t)] = \begin{bmatrix} S_{na}(\omega_o t) \\ S_{nb}(\omega_o t) \\ S_{nc}(\omega_o t) \end{bmatrix} = \begin{bmatrix} \sum_{m=1}^{\infty} B_m \sin m \omega_o t \\ \sum_{m=1}^{\infty} B_m \sin m(\omega_o t - 2\pi/3) \\ \sum_{m=1}^{\infty} B_m \sin m(\omega_o t + 2\pi/3) \end{bmatrix} \quad (5.2)$$

then the output voltage of the inverter,  $[V_o(t)]$ , can be expressed by:

$$[V_o(t)] = V_r(t) \cdot [S_I(t)] \quad (5.3)$$

By inserting (5.1) and (5.2) into (5.3),

$$\begin{bmatrix} V_{ab}(t) \\ V_{bc}(t) \\ V_{ca}(t) \end{bmatrix} = \left[ V_{dc} + \sum_{k=6}^{\infty} V_{r,k} \sin(k\omega_o t + \theta_{r,k}) \right] \begin{bmatrix} \sum_{m=1}^{\infty} B_m \sin m \omega_o t \\ \sum_{m=1}^{\infty} B_m \sin m(\omega_o t - 2\pi/3) \\ \sum_{m=1}^{\infty} B_m \sin m(\omega_o t + 2\pi/3) \end{bmatrix}$$

$$= V_{dc} B_1 \begin{bmatrix} \sin \omega_o t \\ \sin(\omega_o t - 2\pi/3) \\ \sin(\omega_o t + 2\pi/3) \end{bmatrix} + [V_{oh}(t)] \quad (5.4)$$

where

$[V_{oh}(t)]$  = unwanted components of the output voltages

of the inverter, and is given by:

$$[V_{oh}(t)] = V_{dc} \begin{bmatrix} \sum_{m=5,7}^{\infty} B_m \sin m \omega_o t \\ \sum_{m=5,7}^{\infty} B_m \sin m(\omega_o t - 2\pi/3) \\ \sum_{m=5,7}^{\infty} B_m \sin m(\omega_o t + 2\pi/3) \end{bmatrix}$$

$$\begin{aligned}
 & \left[ \sum_{k=6,12}^{\infty} \sum_{m=1}^{\infty} V_{r,k} B_m \sin(k\omega_1 t + \theta_{r,k}) \sin m\omega_0 t \right. \\
 & + \sum_{k=6,12}^{\infty} \sum_{m=1}^{\infty} V_{r,k} B_m \sin(k\omega_1 t + \theta_{r,k}) \sin m(\omega_0 t - 2\pi/3) \\
 & \left. + \sum_{k=6,12}^{\infty} \sum_{m=1}^{\infty} V_{r,k} B_m \sin(k\omega_1 t + \theta_{r,k}) \sin m(\omega_0 t + 2\pi/3) \right] \quad (5.5)
 \end{aligned}$$

Consider the unwanted components for phase A,  $V_{oh,a}(t)$ , only. By using the trigonometric identity; i.e.

$$\sin A \sin B = 0.5 [\cos(A-B) - \cos(A+B)] \quad (5.6)$$

$$\begin{aligned}
 V_{oh,a}(t) = & \sum_{m=5,7,\dots}^{\infty} B_m \sin \omega_0 t \\
 & + \sum_{k=6,12,\dots}^{\infty} \sum_{m=1}^{\infty} \frac{1}{2} B_m V_{r,k} \cos[(k\omega_1 - m\omega_0)t + \theta_{r,k}] \\
 & - \sum_{k=6,12,\dots}^{\infty} \sum_{m=1}^{\infty} \frac{1}{2} B_m V_{r,k} \cos[(k\omega_1 + m\omega_0)t + \theta_{r,k}] \quad (5.7)
 \end{aligned}$$

(5.7) implies that the output voltage of the inverter contains spectral components at frequencies

$$f_{oh,1} = m f_0, \quad m=5,7,\dots \quad (5.8a)$$

$$f_{oh,2} = |k f_1 - m f_0| \quad k=6,12,\dots \quad (5.8b)$$

$$f_{oh,3} = k f_1 + m f_0 \quad m=1,5,7,\dots \quad (5.8c)$$

where

$f_1$  and  $f_0$  are the input and output frequencies of an SRIFC.

In general, the output waveform of an SRIFC can contain frequency components lower than the fundamental output frequency. These

components are called subharmonics. In ac motor-drive applications, such voltage subharmonics in the output of an inverter can have a serious effect on the machine performance, because the amplitude of the flux wave produced in the ac machine by a particular voltage component is, to a first approximation, inversely proportional to its frequency. Thus, subharmonics of even a small amplitude can give rise to large components of flux if the frequency of these components is low enough. Since subharmonics can also create a number of related problems such as magnetic saturations, torque pulsations, energy losses, light flickerings, etc., they should be minimized whenever possible.

Among the three sets of harmonic frequencies in (5.8) the middle set may contain subharmonic components when  $f_{oh,2} = |kf_i - mf_o| < f_o$ . Thus, these components can be avoided if always

$$f_{oh,2} = |kf_i - mf_o| > f_o \quad (5.9)$$

that is

$$\frac{k}{m-1} < \frac{f_o}{f_i} \quad (m \neq 1) \quad (5.10a)$$

or

$$\frac{k}{m+1} > \frac{f_o}{f_i} \quad (5.10b)$$

It is noted that in principle the inequalities (5.10a) and (5.10b) cannot be satisfied for all  $k$  and  $m$  values simultaneously, since  $k = 6, 12, \dots, \infty$  and  $m = 1, 5, 7, \dots, \infty$ . However in practice, these

inequalities can be satisfied to yield subharmonics of negligible amplitudes, if the  $kf_i$  and  $(m + 1)f_o$  are assumed to represent only the frequencies of dominant components in the rectifier output voltage and inverter switching function, respectively. Techniques which can be used to satisfy (5.9) and (5.10) (and therefore avoid subharmonics) are described in Subsections 5.3.1 and 5.3.2. These techniques exploit the fact that the dominant frequency components can be controlled (as  $f_o$  is varied) by controlling the rectifier and/or inverter switching frequencies.

In variable-frequency variable-voltage applications (such as ac variable-speed drives), the required frequency range is commonly at least 10:1, and often greater. It is not usually practical to allow the carrier frequency to vary so widely, because, if it is too low, the motor time constant is insufficient or inadequate for smoothing of the current drawn by the motor; and if it is too high, the commutation losses in the power circuit will be unacceptably large. Clearly, for a synchronous PWM system to be capable of operation over a wide frequency range, it is necessary to change the ratio of carrier to modulating frequency whenever the carrier frequency becomes too high or too low for the satisfactory operation of the system. This ratio-changing method was proposed by Houldsworth and Burgum in [63] and by Grant in [64], and it now offers an economic solution to the problem of generating high quality PWM waveforms over a wide frequency range, particularly in digital PWM systems.

### 5.3.1 Output stage analysis with Structure #1

The waveform of the inverter output voltage can, in general, be obtained by multiplying the waveform of the rectifier output voltage with the waveform of the inverter switching functions. Similarly, the spectrum of the inverter output voltage can be obtained by multiplying the spectrum of the rectifier output voltage with the spectra of the inverter switching functions. The product of the two frequency components yields corresponding components with frequencies equal to the sum and difference of the multiplied components. Therefore, in order to avoid the generation of low-order frequency components in the inverter output voltage, the dominant harmonic components of the inverter switching functions should be 'placed' as far as possible from the corresponding components of the rectifier output voltage.

The output frequency spectrum of a rectifier with Structure #1 is presented in Table 5.1, and the unwanted components are plotted in Fig. 5.4a. Also, the dominant harmonic components ( $d_l, d_h$ ) of an inverter switching function (MSPWM) are shown in Fig. 5.4b. Since the dc component as well as subharmonic components of the output voltage of an SRIFC should be avoided (or minimized), the switching frequencies of the inverter have to be chosen properly so that the resulting dominant components of the inverter switching functions are located in a 'safe operating area' (for example: band A) in Fig. 5.4a.

As stated in Chapter 2, the dominant harmonic components,  $d_l$  and  $d_h$ , of the inverter switching functions (MSPWM) are dependent on the

TABLE 5.1: FREQUENCY SPECTRA OF 'SRIFC' RECTIFIER OUTPUT VOLTAGES.

Harmonic  Order	Output Voltages			
	Structure No. 1 ( $N_h = 11$ )		Structure No. 2 ( $N_h = 1$ )	
	(p.u.)	(%)	(p.u.)	(%)
0	1.417	100.00	1.417	100.00
6	.086	.40	.081	5.71
12	.048	3.39	.020	1.40
18	.097	6.87	.009	.62
24	.191	13.47	.005	.35
30	.063	4.43	.003	.22
36	.002	.16	.002	.15
42	.109	7.68	.002	.11
48	.107	7.54	.001	.09
54	.034	2.43	.001	.07
60	.008	.53	.001	.06
66	.058	4.12	.001	.05
72	.045	3.16	.001	.04
78	.004	.31	0.000	.03
84	.005	.33	0.000	.03
90	.005	.32	0.000	.02
96	.001	.06	0.000	.02
102	.013	.88	0.000	.02
108	.017	1.21	0.000	.02
114	.034	2.37	0.000	.02
120	.027	1.91	0.000	.01
126	.001	.07	0.000	.01
132	.024	1.72	0.000	.01
138	.038	2.65	0.000	.01
144	.017	1.23	0.000	.01
150	0.000	0.00	0.000	0.00

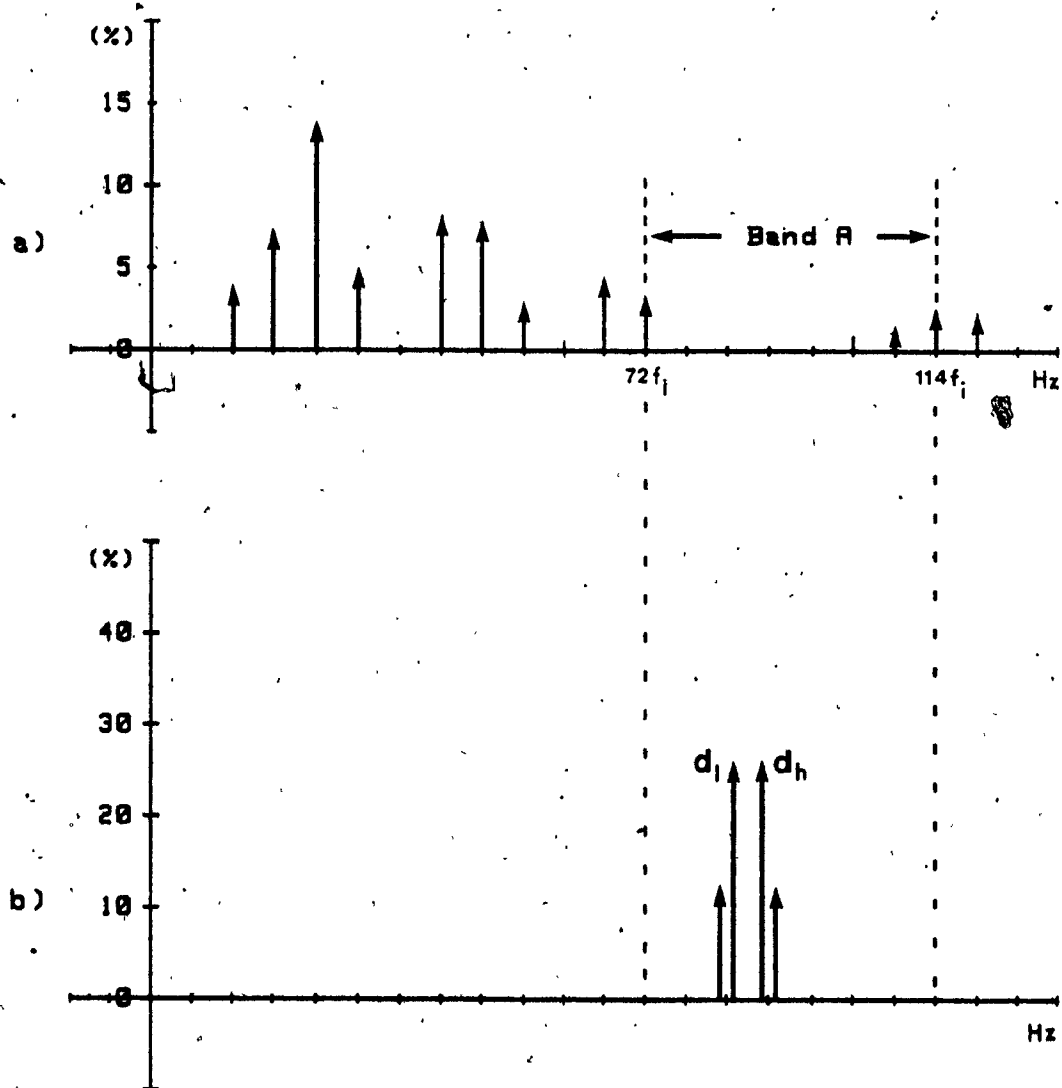


Fig. 5.4: Frequency spectra of the unwanted components in the rectifier output voltage and the inverter switching function, with SRIFC Structure #1.

- a) In the rectifier output voltage.
- b) In the inverter switching function.

number of pulses per half-cycle,  $N_h$ , (or switching frequency:  $f_s$ ) of the inverter and are given by (eqn.(2.14)):

$$d_l = \left(\frac{3}{2} N_h + 1\right) f_o \quad (5.11)$$

$$d_h = \left(\frac{3}{2} N_h + 5\right) f_o$$

and the maximum amplitudes (i.e. the worst case) occur at modulation index  $M = 0.7$  and their values are 35 % of the rated fundamental amplitude (Fig. 2.10). Thus, in order to be able to operate within band A in Fig. 5.4a, the  $d_l$  and  $d_h$  should be located between  $72f_i$  (4.32 kHz) and  $114f_i$  (6.84 kHz) when a ratio-changing method is applied. Fig. 5.5 shows the variation of the inverter switching frequency for the ratio-changing method shown in Table 5.2. As apparent in Fig. 5.5 and Table 5.2, the  $N_h$  values for  $f_o = 60$  Hz (1 p.u.) and  $f_o = 42$  Hz (0.7 p.u.) are 56 and 88, respectively. Since the  $d_l$  and  $d_h$  are the only components of interest here, the minimum  $d_l$  and maximum  $d_h$  are kept to be 4.6 kHz and 6.6 kHz, respectively. From (2.13a) the switching frequency of an inverter switch,  $f_{si}$ , is given by:

$$f_{si} = \left(\frac{3}{2} N_h + 3\right) f_o \quad (5.12)$$

Thus, the maximum  $f_{si}$  is about 6.6 kHz and minimum  $f_{si}$  is about 4.6 kHz. However, the maximum  $f_{si}$  (or  $d_h$ ) for below 10 Hz may be increased further (for example, up to about 10 kHz), because the gradual changes are very small. While considering the worst conditions, the maximum dc or subharmonic value that can be produced with this particular technique is about 0.15 % of the rated output voltage of the SRIFC, and it may be ignored.

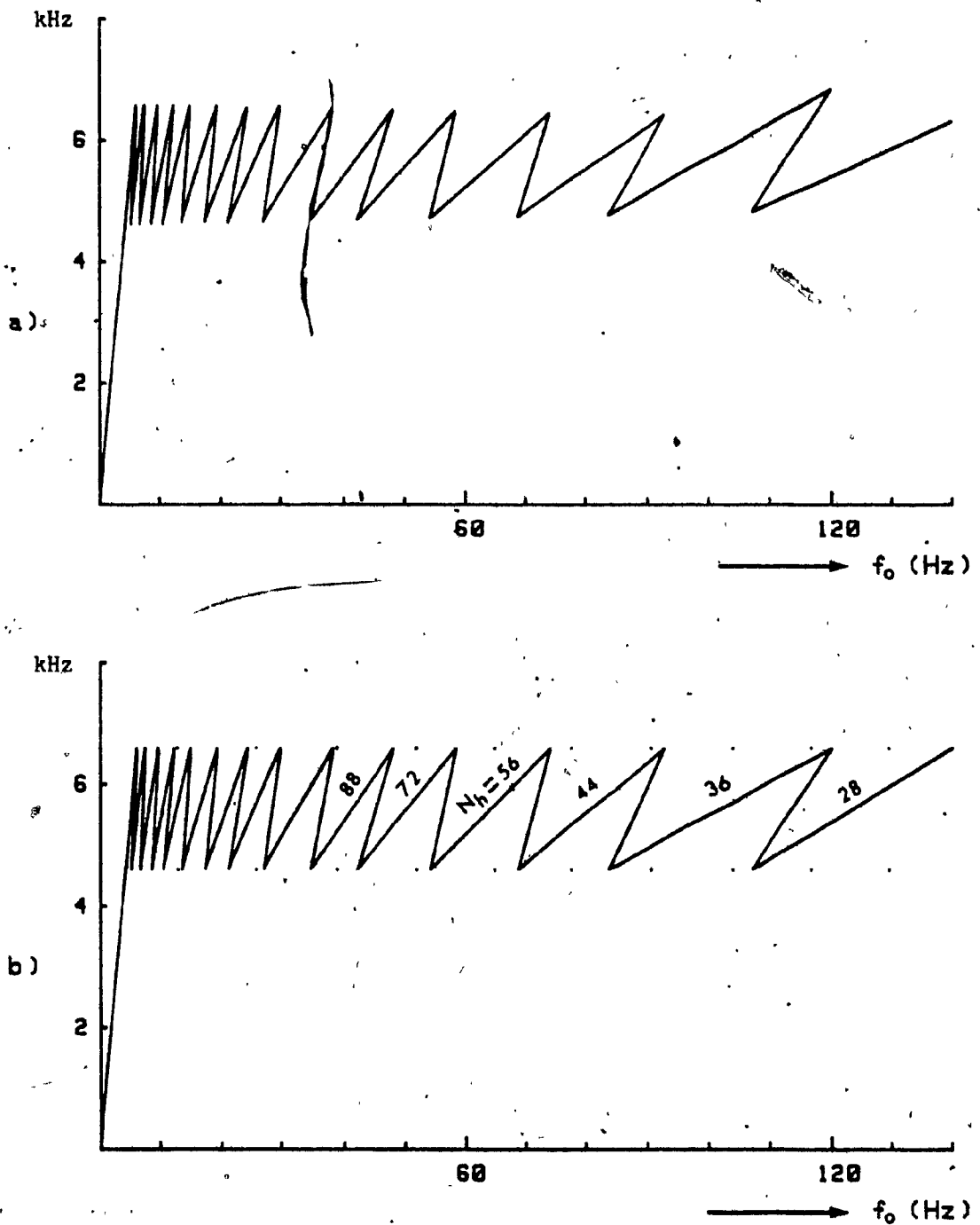


Fig. 5.5: Characteristics of the ratio-changing method applicable to the inverter of the SRIFC Structure #1.

- a) Switching frequencies of the inverter.
- b) Range of the dominant harmonic frequencies in the inverter switching function.

TABLE 5.2: RATIO-CHANGING METHOD APPLICABLE TO THE INVERTER OF 'SRIFC' STRUCTURE #1.

$N_h$	Output Frequency ( Hz )	Switching Frequency ( Hz )	Range <sup>a</sup> of $d_l$ and $d_h$ (Hz)
28	107.0 --- 140.0	4815 --- 6300	4600 --- 6600
36	83.6 --- 120.0	4765 --- 6840	4600 --- 6600
44	68.7 --- 93.0	4740 --- 6417	4600 --- 6600
56	54.1 --- 74.2	4707 --- 6455	4600 --- 6600
72	42.2 --- 58.4	4685 --- 6482	4600 --- 6600
88	34.6 --- 48.2	4671 --- 6507	4600 --- 6600
112	27.2 --- 38.2	4651 --- 6532	4600 --- 6600
144	21.2 --- 30.0	4643 --- 6570	4600 --- 6600
176	17.4 --- 24.5	4646 --- 6542	4600 --- 6600
224	13.7 --- 19.4	4644 --- 6577	4600 --- 6600
288	10.6 --- 15.1	4610 --- 6570	4600 --- 6600
352	8.7 --- 12.4	4620 --- 6585	4600 --- 6600
448	6.8 --- 9.8	4614 --- 6580	4600 --- 6600
576	5.3 --- 7.6	4611 --- 6585	4600 --- 6600
704	4.4 --- 6.2	4609 --- 6588	4600 --- 6600
704	0.0 --- 4.4	0 --- 4609	0 --- 4669

Fig. 5.6 shows the simulated voltage and current waveforms with Structure #1 for  $f_o = 100$  Hz,  $N_h = 36$ ,  $M = 1$ , and 0.78 (lag) load power factor. The frequency spectra of the output voltage and current for  $k=6, 12, \dots, 150$  and  $m=1, 5, \dots, 150$  in (5.4) and (5.5) are presented in Table 5.3. As it can be seen from the Fig. 5.6e and Table 5.3, the output current is almost sinusoidal. Also, the frequency spectra of the output voltage and current with Structure #1 for  $f_o = 42$  Hz,  $N_h = 88$  and  $M = 0.7$  are provided in Table 5.4, showing that although there exist some subharmonics, their amplitudes are very small, and hence they can be ignored.

### 5.3.2 Output stage analysis with Structure #2

The output frequency spectrum of a rectifier with Structure #2 is presented in Table 5.1, while the unwanted components are plotted in Fig. 5.7a. Since their amplitudes decrease exponentially as harmonic frequency increases, the safe operating area can be chosen anywhere after the 12-th frequency component. Thus, the subharmonics of the output voltage can be made negligible, if  $f_o \leq 180$  Hz. However, the subharmonics having the amplitude of 2.85 % occur when  $f_o > 180$  Hz because of the 6-th harmonic component of 5.71 % in the rectifier output voltage. In this case, band B in Fig. 5.7a is chosen as a safe operating area as an example. A ratio-changing method is proposed in Fig. 5.8 and Table 5.5. The minimum  $d_{\lambda}$  and maximum  $d_h$  are kept at 1.2 kHz and 2 kHz, respectively, for up to about 1 p.u. output frequency and the same  $N_h$  value (i.e. 16) is used for greater than 1 p.u. output frequencies.

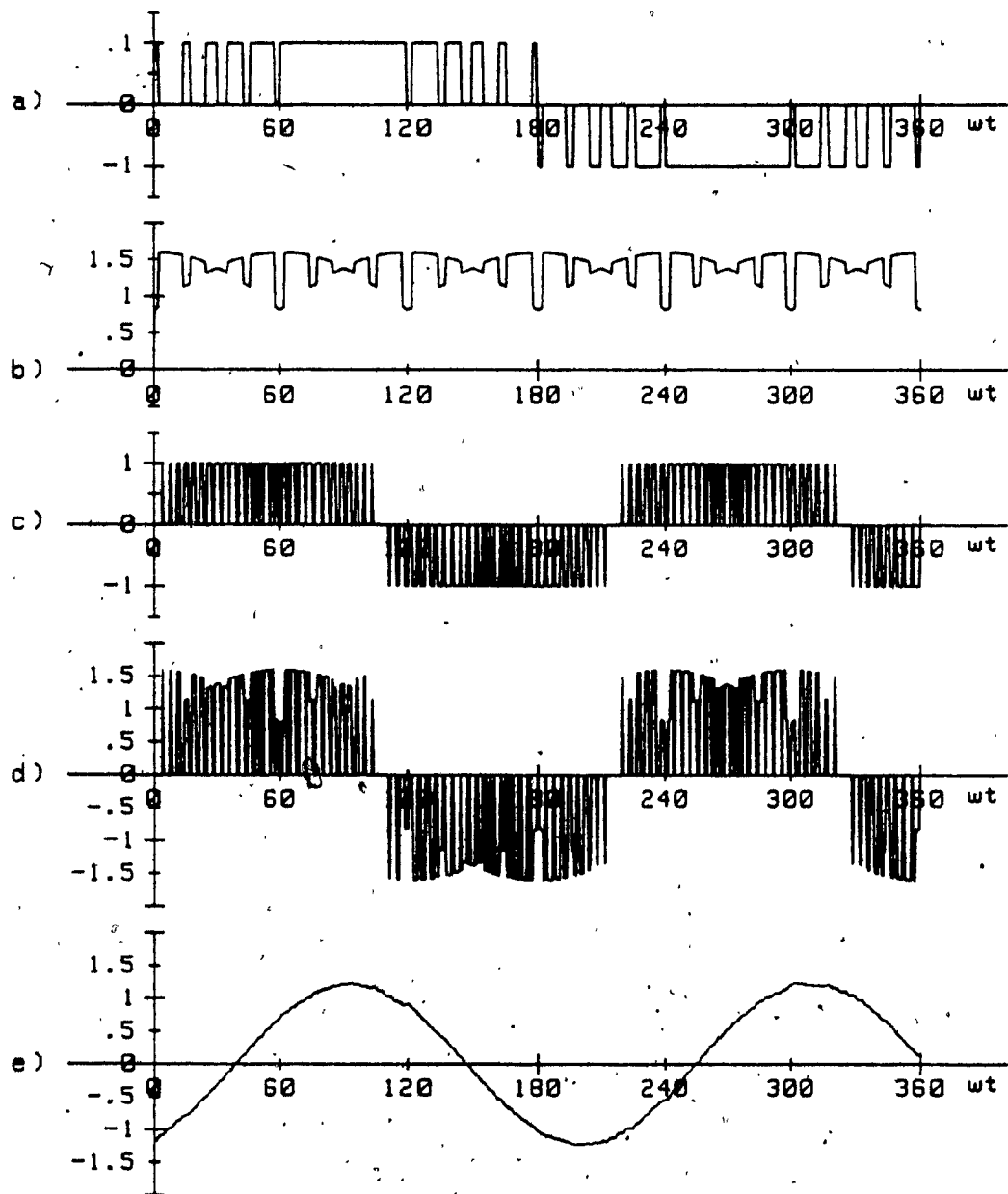


Fig. 5.6: Simulated waveforms related to the outputs of the SRIFC-Structure #1 ( $f_o=100$  Hz,  $N_h=36$ ,  $M=1$ ).

- a) Rectifier switching function.
- b) Rectifier output voltage.
- c) Inverter switching function.
- d) Inverter output voltage,  $V_{oab}$ .
- e) Inverter output phase current,  $I_{oab}$  (load p.f.=0.78).

TABLE 5.3: FREQUENCY SPECTRA OF INVERTER OUTPUT VOLTAGE AND CURRENT WITH 'SRIFC' STRUCTURE #1.

$f_o=100$ Hz, $N_h=36$ , $M=1$ , and load power factor=0.78 (lag)				
*				
Harmonic	Output Voltage		Output Current	
Order	(p.u.)	(%)	(p.u.)	(%)
.20	0.0000	.001	0.0000	.002
1.00	1.0000	100.000	1.0000	100.000
6.20	.0172	1.716	.0043	.434
8.20	.0166	1.658	.0032	.320
9.80	.0326	3.255	.0053	.527
11.80	.0384	3.842	.0052	.517
13.40	.0650	6.500	.0077	.772
15.40	.0726	7.265	.0075	.751
17.00	.0225	2.249	.0021	.211
19.00	.0215	2.150	.0018	.180
24.20	.0341	3.409	.0022	.225
26.20	.0481	4.807	.0029	.293
27.80	.0333	3.329	.0019	.191
29.80	.0475	4.754	.0025	.255
31.40	.0121	1.207	.0006	.061
33.40	.0124	1.237	.0006	.059
38.60	.0129	1.289	.0005	.053
40.60	.0379	3.789	.0015	.149
42.20	.0119	1.188	.0004	.045
44.20	.0246	2.462	.0009	.089
44.60	.0173	1.725	.0006	.062
53.00	.1149	11.494	.0035	.346
55.00	.2561	25.606	.0074	.744
59.00	.2561	25.608	.0069	.693
61.00	.1149	11.490	.0030	.301
69.40	.0148	1.478	.0003	.034
73.40	.0162	1.616	.0004	.035

\* Voltage harmonics less than 1 % and the corresponding current harmonics are omitted.

TABLE 5.4: FREQUENCY SPECTRA OF INVERTER OUTPUT VOLTAGE AND CURRENT WITH 'SRIFC' STRUCTURE #1.

f <sub>o</sub> =42 Hz, N <sub>h</sub> =88, M=0.7, and load power factor=0.9 (lag)				
Harmonic Order	Output Voltage		Output Current	
	(p.u.)	(%)	(p.u.)	(%)
.14	0.0000	.001	0.0000	.001
.71	0.0000	.002	0.0000	.002
1.00	.7000	100.000	.7000	100.000
16.14	.0119	1.702	.0017	.240
18.14	.0119	1.704	.0015	.214
24.71	.0241	3.444	.0022	.319
26.71	.0241	3.445	.0021	.295
33.29	.0472	6.737	.0032	.463
35.29	.0472	6.737	.0031	.437
41.86	.0155	2.220	.0009	.122
43.86	.0155	2.221	.0008	.116
59.00	.0270	3.854	.0010	.150
61.00	.0270	3.857	.0010	.145
64.43	.0123	1.750	.0004	.062
67.57	.0264	3.770	.0009	.128
68.43	.0123	1.750	.0004	.059
69.57	.0264	3.770	.0009	.124
73.00	.0125	1.783	.0004	.056
77.00	.0125	1.783	.0004	.053
93.29	.0145	2.071	.0004	.051
95.29	.0145	2.074	.0003	.050
98.71	.0219	3.127	.0005	.073
101.86	.0111	1.586	.0002	.036
102.71	.0219	3.127	.0005	.070
103.86	.0111	1.587	.0002	.035
107.29	.0111	1.592	.0002	.034
111.29	.0111	1.592	.0002	.033
133.00	.3250	46.431	.0056	.801
137.00	.3250	46.432	.0054	.777

\* Voltage harmonics less than 1.5% and the corresponding current harmonics are omitted.

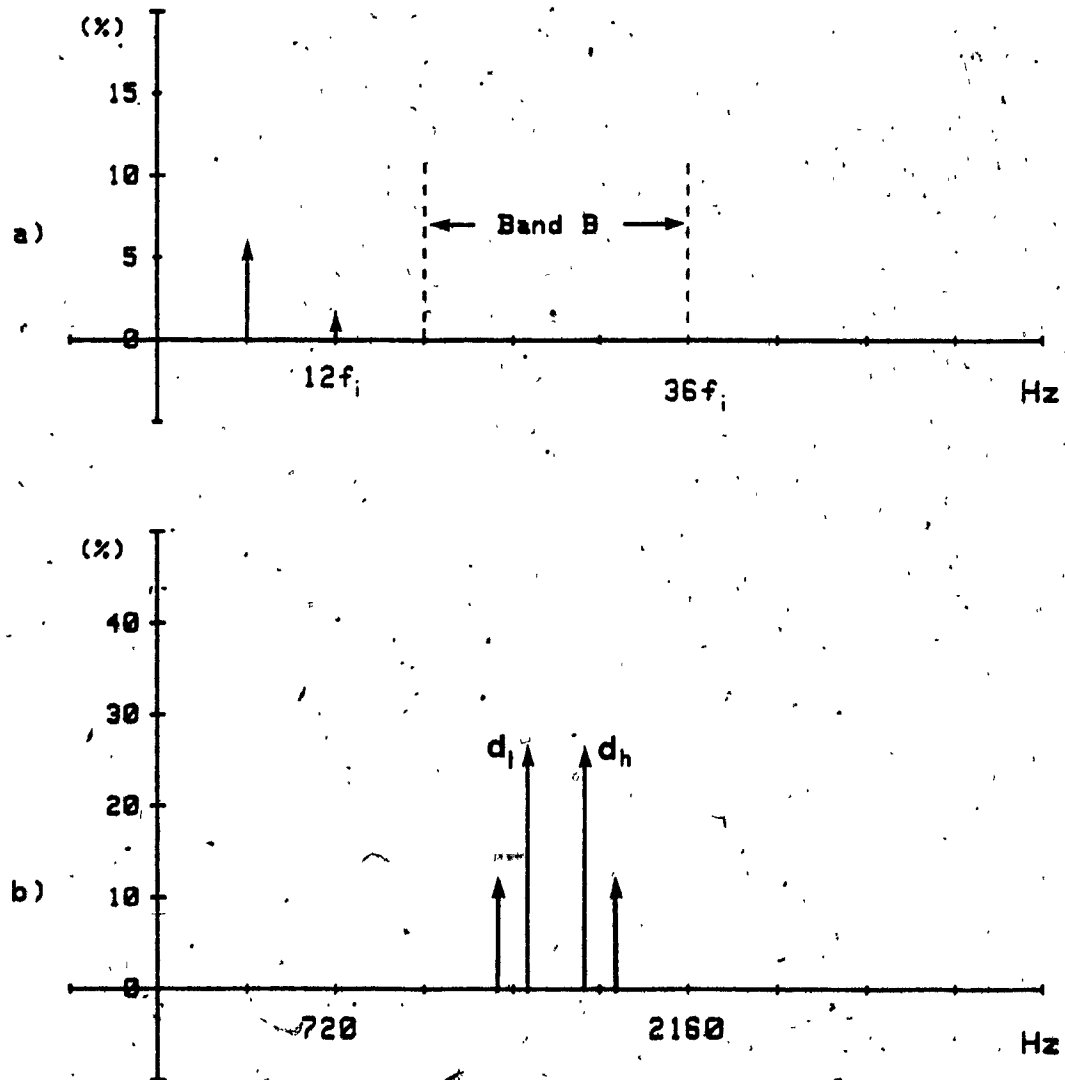


Fig. 5.7: Frequency spectra of the unwanted components in the rectifier output voltage and the inverter switching function, with the SRIFC Structure #2.

- a) In the rectifier output voltage.
- b) In the inverter switching function.

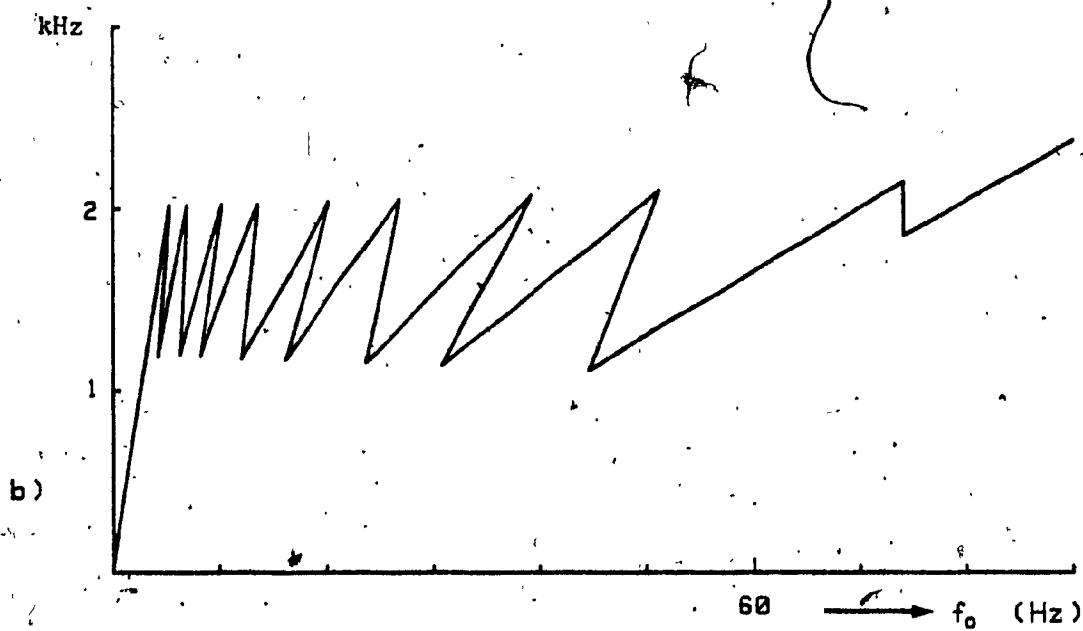
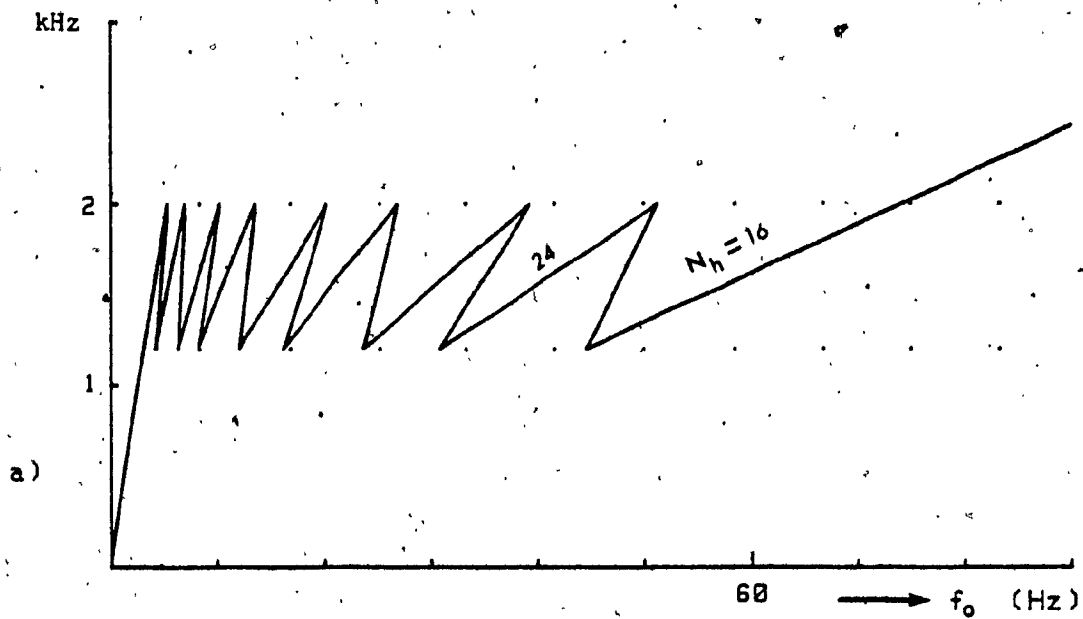


Fig. 5.8: Characteristics of the ratio-changing method applicable to the inverter of the SRIFC Structure #2.

- a) Switching frequencies of the inverter.
- b) Range of the dominant harmonic frequencies in the inverter switching function.

TABLE 5.5: RATIO-CHANGING METHOD APPLICABLE TO THE INVERTER OF 'SRIFC' STRUCTURE #2.

$N_h$	Output Frequency ( Hz )	Switching Frequency ( Hz )	Range of $d_i$ and $d_h$ (Hz)
16	74.1 --- 150.0	2000 --- 4050	1853 --- 4350
16	44.4 --- 74.1	1200 --- 2000	1110 --- 2149
24	30.8 --- 51.3	1200 --- 2000	1140 --- 2103
32	23.5 --- 39.2	1200 --- 2000	1152 --- 2078
48	16.0 --- 26.7	1200 --- 2000	1168 --- 2056
64	12.1 --- 20.2	1200 --- 2000	1174 --- 2040
96	8.2 --- 13.6	1200 --- 2000	1189 --- 2026
128	6.2 --- 10.3	1200 --- 2000	1197 --- 2029
192	4.1 --- 6.9	1200 --- 2000	1185 --- 2022
256	3.1 --- 5.2	1200 --- 2000	1194 --- 2023
256	0.0 --- 3.1	0 --- 1200	0 --- 1200

Fig. 5.9 shows some simulated voltage and current waveforms of the SRIFC Structure #2 for  $f_o = 60$  Hz,  $M = 1$  and 0.9 (lag) load power factor. The frequency spectra of the output voltage and current of the SRIFC for  $k=6,12,\dots,150$  and  $m=1,5,\dots,150$  in (5.4) and (5.5) are presented in Table 5.6. The frequency spectra of the output voltage and current for  $f_o=42$  Hz,  $N_h=24$ , and  $M=0.7$  are shown in Table 5.7. From these tables it is noted that even though there are, as expected, low-order unwanted components the output currents are almost sinusoidal and the subharmonmics, negligible.

#### 5.4 Input Stage Analysis and Input Filter Design

As defined in Chapter 4, the input current of an inverter (also, in this case, the output current of a rectifier),  $I_f(t)$ , is given by (eqn. (4.4)):

$$I_f(\omega_o t) = I_{dc} + \sum_{m=6,12,\dots}^{\infty} I_{f,m} \sin(m\omega_o t + \phi_{f,m}) \quad (5.13)$$

where

$I_{dc}$  = dc component of the inverter input current,  $I_f(\omega_o t)$ ,

$I_{f,m}$  = amplitude of m-th unwanted component of the  $I_f(\omega_o t)$ .

Then, the input current of an SRIFC,  $[I_I(t)]$ , is defined by :

$$[I_I(t)] = [S_R(t)] \cdot I_f(t) \quad (5.14)$$

By substituting (5.13) into (5.14), one gets

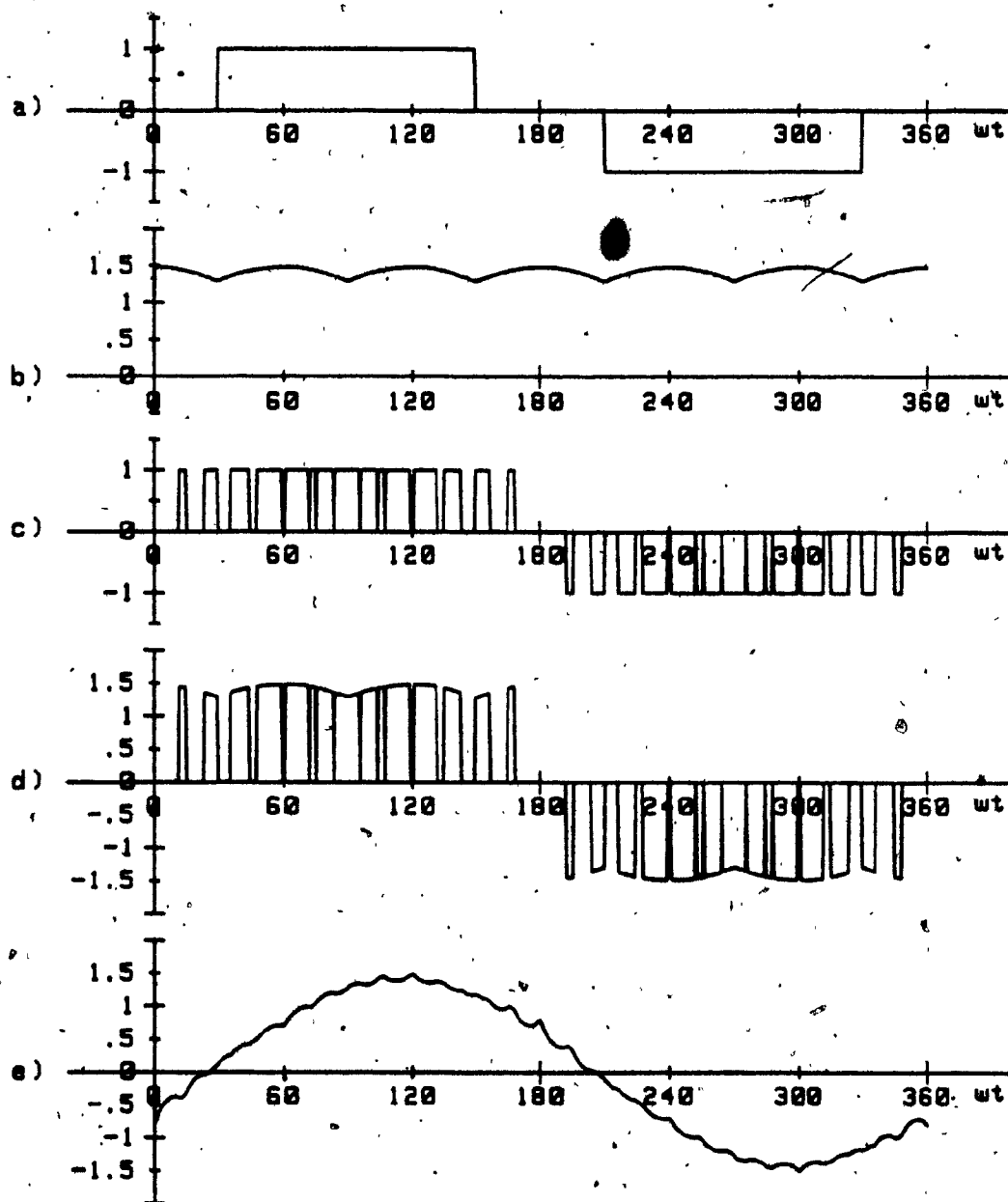


Fig. 5.9: Simulated waveforms related to the outputs of the SRIFC Structure #2 ( $f_o=60$  Hz,  $N_h=16$ ,  $M=1$ ).

- a) Rectifier switching function.
- b) Rectifier output voltage.
- c) Inverter switching function.
- d) Inverter output voltage.
- e) Inverter output phase current (load p.f.=0.9).

TABLE 5.6: FREQUENCY SPECTRA OF INVERTER OUTPUT VOLTAGE AND CURRENT WITH 'SRIFC' STRUCTURE #2.

$f_o=60$ Hz, $N_h=16$ , $M=1$ , and load power factor=0.9 (lag)				
Harmonic Order	Output Voltage		Output Current	
	(p.u.)	(%)	(p.u.)	(%)
1.00	1.0000	100.000	1.0000	100.000
5.00	.0286	2.859	.0121	1.212
7.00	.0293	2.935	.0092	.923
19.00	.0121	1.210	.0015	.145
23.00	.1139	11.392	.0113	1.132
25.00	.2581	25.808	.0236	2.360
29.00	.2584	25.836	.0204	2.039
31.00	.1132	11.319	.0084	.836
35.00	.0101	1.006	.0007	.066
43.00	.0121	1.209	.0006	.064
47.00	.0540	5.402	.0026	.263
49.00	.1224	12.242	.0057	.573
53.00	.0560	5.599	.0024	.242
55.00	.0562	5.616	.0023	.234
59.00	.1237	12.371	.0048	.481
61.00	.0520	5.198	.0020	.195
65.00	.0163	1.634	.0006	.058
67.00	.0170	1.698	.0006	.058
71.00	.0302	3.015	.0010	.097
73.00	.0847	8.471	.0027	.266
77.00	.0304	3.038	.0009	.090
79.00	.0176	1.756	.0005	.051
83.00	.0183	1.832	.0005	.051
85.00	.0319	3.191	.0009	.086
89.00	.0887	8.872	.0023	.229
91.00	.0203	2.030	.0005	.051
95.00	.0101	1.014	.0002	.024
97.00	.0693	6.928	.0016	.164

\* Voltage harmonics less than 1 % and the corresponding current harmonics are omitted.

TABLE 5.7: FREQUENCY SPECTRA OF INVERTER OUTPUT VOLTAGE AND CURRENT WITH 'SRIFC' STRUCTURE #2.

$f_o=42$ Hz, $N_h=24$ , $M=0.7$ , and load power factor=0.9 (lag)				
Harmonic Order	Output Voltage		Output Current	
	(p.u.)	(%)	(p.u.)	(%)
.14	0.0000	.003	0.0000	.003
.71	0.0000	.003	0.0000	.004
1.00	.7000	100.000	.7000	100.000
7.57	.0200	2.855	.0058	.835
9.57	.0200	2.855	.0047	.669
28.43	.0093	1.332	.0008	.107
31.00	.0097	1.393	.0007	.103
32.43	.0094	1.339	.0007	.095
37.00	.3271	46.732	.0203	2.893
41.00	.3273	46.760	.0183	2.613
45.57	.0093	1.334	.0005	.067
47.00	.0106	1.516	.0005	.074
49.00	.0077	1.097	.0004	.051
49.57	.0093	1.335	.0004	.062
65.00	.0105	1.498	.0004	.053
67.00	.0144	2.053	.0005	.070
71.00	.0267	3.813	.0009	.123
73.00	.1443	20.615	.0045	.648
77.00	.1042	14.891	.0031	.444
79.00	.1042	14.881	.0030	.432
83.00	.1447	20.666	.0040	.571
85.00	.0272	3.886	.0007	.105
89.00	.0153	2.182	.0004	.056
91.00	.0116	1.664	.0003	.042
95.00	.0088	1.260	.0002	.030
97.00	.0085	1.219	.0002	.029

\* Voltage harmonics less than 1 % and the corresponding current harmonics are omitted.

$$\begin{bmatrix} I_a(t) \\ I_b(t) \\ I_c(t) \end{bmatrix} = \begin{bmatrix} \sum_{k=1}^{\infty} A_k \sin k\omega_1 t \\ \sum_{k=1}^{\infty} A_k \sin k(\omega_1 t - 2\pi/3) \\ \sum_{k=1}^{\infty} A_k \sin k(\omega_1 t + 2\pi/3) \end{bmatrix} \left[ I_{dc} + \sum_{m=6,12,\dots}^{\infty} I_{f,m} \sin(m\omega_0 t + \phi_{f,m}) \right]$$

$$= A_1 \cdot I_{dc} \begin{bmatrix} \sin \omega_1 t \\ \sin(\omega_1 t - 2\pi/3) \\ \sin(\omega_1 t + 2\pi/3) \end{bmatrix} + [I_{ih}(t)] \quad (5.15)$$

where

$[I_{ih}(t)] = 3 \times 1$  matrix of the unwanted components in the input line currents of an SRIFC, and is given by:

$$[I_{ih}(t)] = I_{dc} \begin{bmatrix} \sum_{k=5,7,\dots}^{\infty} A_k \sin k\omega_1 t \\ \sum_{k=5,7,\dots}^{\infty} A_k \sin k(\omega_1 t - 2\pi/3) \\ \sum_{k=5,7,\dots}^{\infty} A_k \sin k(\omega_1 t + 2\pi/3) \end{bmatrix}$$

$$+ \begin{bmatrix} \sum_{k=1}^{\infty} \sum_{m=6,12,\dots}^{\infty} A_k I_{f,m} \sin(k\omega_1 t) \sin(m\omega_0 t + \phi_{f,m}) \\ \sum_{k=1}^{\infty} \sum_{m=6,12,\dots}^{\infty} A_k I_{f,m} \sin k(\omega_1 t - 2\pi/3) \sin(m\omega_0 t + \phi_{f,m}) \\ \sum_{k=1}^{\infty} \sum_{m=6,12,\dots}^{\infty} A_k I_{f,m} \sin k(\omega_1 t + 2\pi/3) \sin(m\omega_0 t + \phi_{f,m}) \end{bmatrix} \quad (5.16)$$

Consider only the unwanted components for phase A,  $I_{ih,a}(t)$ . By using the trigonometric identity (eqn. (5.6)), (5.16) can be rewritten as:

$$I_{ih,a}(t) = \sum_{k=5,7,\dots}^{\infty} A_k \sin k\omega_1 t$$

$$+ \sum_{k=1}^{\infty} \sum_{m=6,12,\dots}^{\infty} \frac{1}{2} A_k I_{f,m} \cos[(m\omega_0 - k\omega_1)t + \phi_{f,m}]$$

$$+ \sum_{k=1}^{\infty} \sum_{m=6,12,\dots}^{\infty} \frac{1}{2} A_k I_{f,m} \cos[(m\omega_0 + k\omega_1)t + \phi_{f,m}] \quad (5.17)$$

(5.17) implies that the input line current of an SRIFC contains spectral components at frequencies

$$f_{ih,1} = kf_1, \quad k=5,7,\dots \quad (5.18a)$$

$$f_{ih,2} = |mf_0 - kf_1| \quad k=1,5,7,\dots \quad (5.18b)$$

$$f_{ih,3} = mf_0 + kf_0 \quad m=6,12,\dots \quad (5.18c)$$

As discussed in Section 5.3, the  $f_{ih,2}$  set may contain subharmonic components when  $f_{ih,2} = |mf_0 - kf_1| < f_1$ . Thus, the following conditions should be satisfied in order to avoid the subharmonic components in the the input line currents of an SRIFC.

$$f_{ih,2} = |mf_0 - kf_1| > f_1 \quad (5.19)$$

that is

$$\frac{m}{k+1} > \frac{f_1}{f_0} \quad \text{for} \quad \begin{matrix} k=1,5,7,\dots,\infty \\ m=6,12,\dots,\infty \end{matrix} \quad (5.20a)$$

or

$$\frac{m}{k-1} < \frac{f_1}{f_0} \quad (k \neq 1) \quad \text{for} \quad \begin{matrix} k=5,7,\dots,\infty \\ m=6,12,\dots,\infty \end{matrix} \quad (5.20b)$$

The input stage analyses are performed under the same operating conditions discussed in Subsections 5.3.1 and 5.3.2.

#### 5.4.1 Input stage analysis and input filter design with Structure #1

The dominant frequency components ( $d_1, d_h$ ) of the inverter input current with Structure #1 is shown in Fig. 5.10a, and the frequency spectrum of corresponding rectifier switching function (see Table 5.8) is plotted in Fig. 5.10b. These  $d_1$  and  $d_h$  are dependent on the  $N_h$  values of the inverter, and their amplitudes are plotted as a function of  $M$  with different load power factors in Fig. 5.11. From this figure, it is noted that the worst amplitudes of the dominant components occurs at  $M=1.0$  with load p.f.=0.4 (lag), and their values are 0.52 p.u.. Moreover, the extremely worst case that generates a dc component by the multiplication of the dominant components of the inverter input current by those of the rectifier switching function does not occur, because the dominant components of the rectifier switching function are  $29f_i$  and  $31f_i$  and those of the inverter input current are located within a predetermined area (band A).

Fig. 5.12 shows some of the simulated waveforms which are related to the input current of the SRIFC Structure #1 for  $f_o=100$  Hz,  $M=1$  and 0.78 (lag) load power factor; and the exact frequency spectrum of the input line current,  $I_a(\omega t)$ , for  $k=1,5,\dots,150$  and  $m=6,12,\dots,150$  in (5.15) and (5.16) is shown in Table 5.9.

In designing the input filter the same technique developed as in Section 3.3 is applied. Assuming that the THD<sub>i</sub> value of the input line

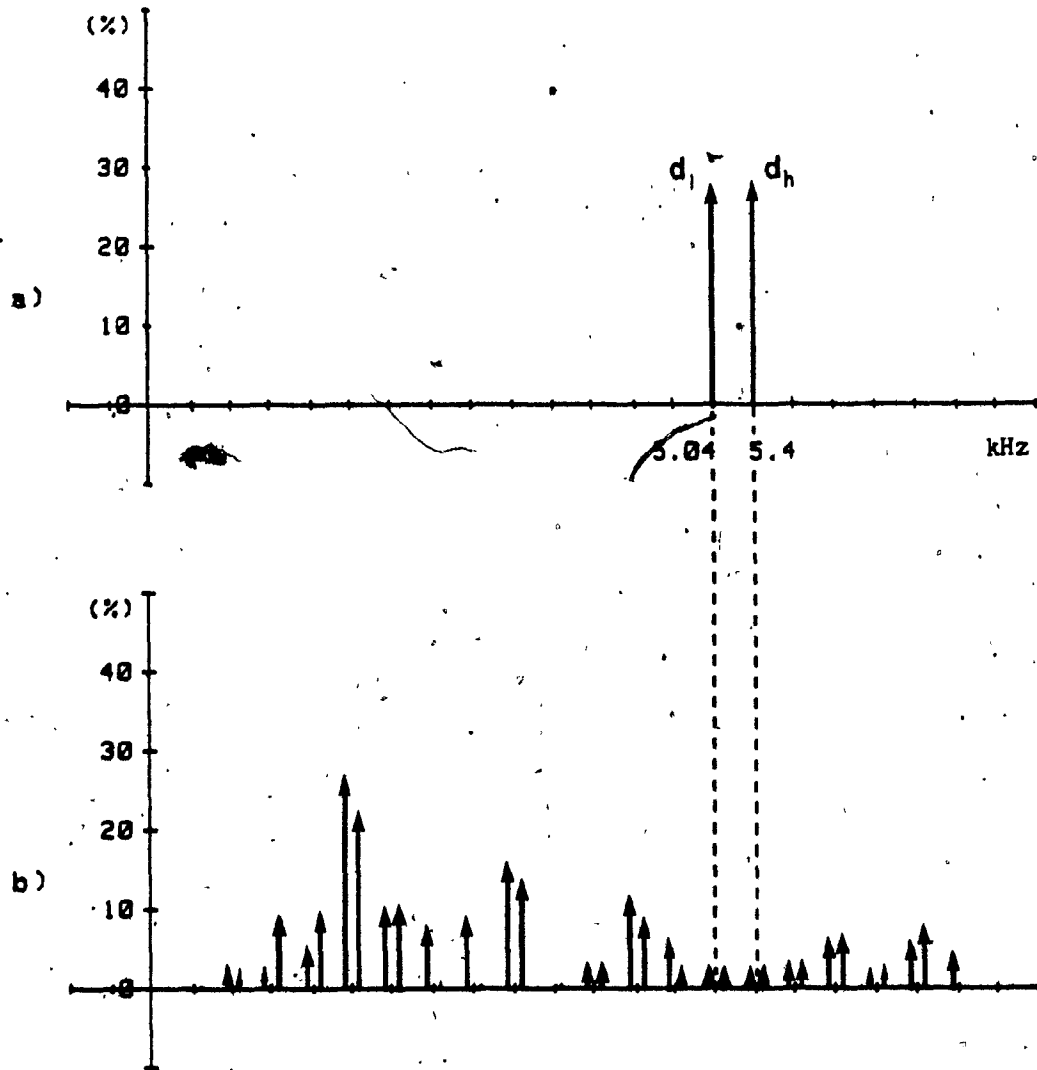


Fig. 5.10: Frequency spectra of the unwanted components in the inverter input current and the rectifier switching function, with the SRIFC Structure #1.

- a) In the inverter input current ( $f_0=60$  Hz,  $N_h=56$ ,  $M=1$ ).
- b) In the rectifier switching function.

TABLE 5.8: FREQUENCY SPECTRA OF 'SRIFC' RECTIFIER SWITCHING FUNCTIONS.

Harmonic  Order	Switching Functions			
	Structure No. 1 ( $N_h = 11$ )		Structure No. 2 ( $N_h = 1$ )	
	(p.u.)	(%)	(p.u.)	(%)
1	1.021	100.00	1.103	100.00
5	-.001	.11	-.221	20.00
7	.003	.29	-.158	14.29
11	.022	2.12	.100	9.09
13	-.013	1.27	.085	7.69
17	-.017	1.64	-.065	5.88
19	-.087	8.51	-.058	5.26
23	.047	4.60	.048	4.35
25	-.091	8.87	.044	4.00
29	.264	25.91	-.038	3.45
31	.219	21.47	-.036	3.23
35	-.094	9.18	.032	2.86
37	-.095	9.34	.030	2.70
41	.071	6.93	-.027	2.44
43	-.008	.76	-.026	2.33
47	.081	7.90	.023	2.13
49	.004	.36	.023	2.04
53	.154	15.10	-.021	1.89
55	.129	12.66	-.020	1.82
59	-.001	.09	.019	1.69
61	.005	.45	.018	1.64
65	.025	2.44	-.017	1.54
67	-.017	1.68	-.016	1.49
71	.113	11.03	.016	1.41
73	.080	7.87	.015	1.37
77	.054	5.26	-.014	1.30
79	.057	5.57	-.014	1.27
83	.033	3.20	.013	1.20
85	.036	3.53	.013	1.18
89	.040	3.94	-.012	1.12
91	.043	4.26	-.012	1.10
95	.024	2.40	.012	1.05
97	.025	2.46	.011	1.03

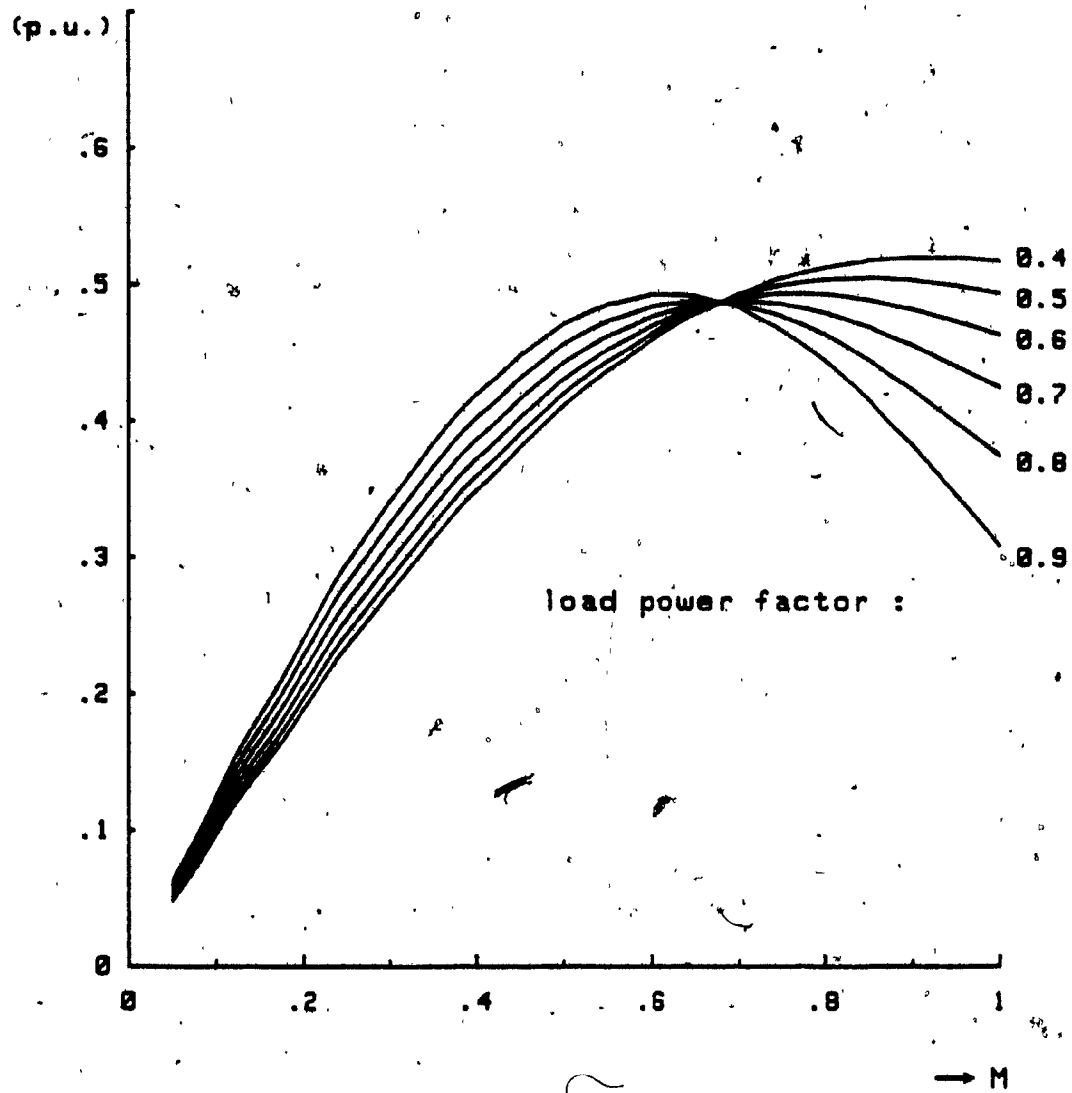


Fig. 5.11: RMS value of the dominant harmonic component,  $d_1$  and  $d_5$ , of the inverter input current versus the modulation index,  $M$ , for various load power factors (lagging).

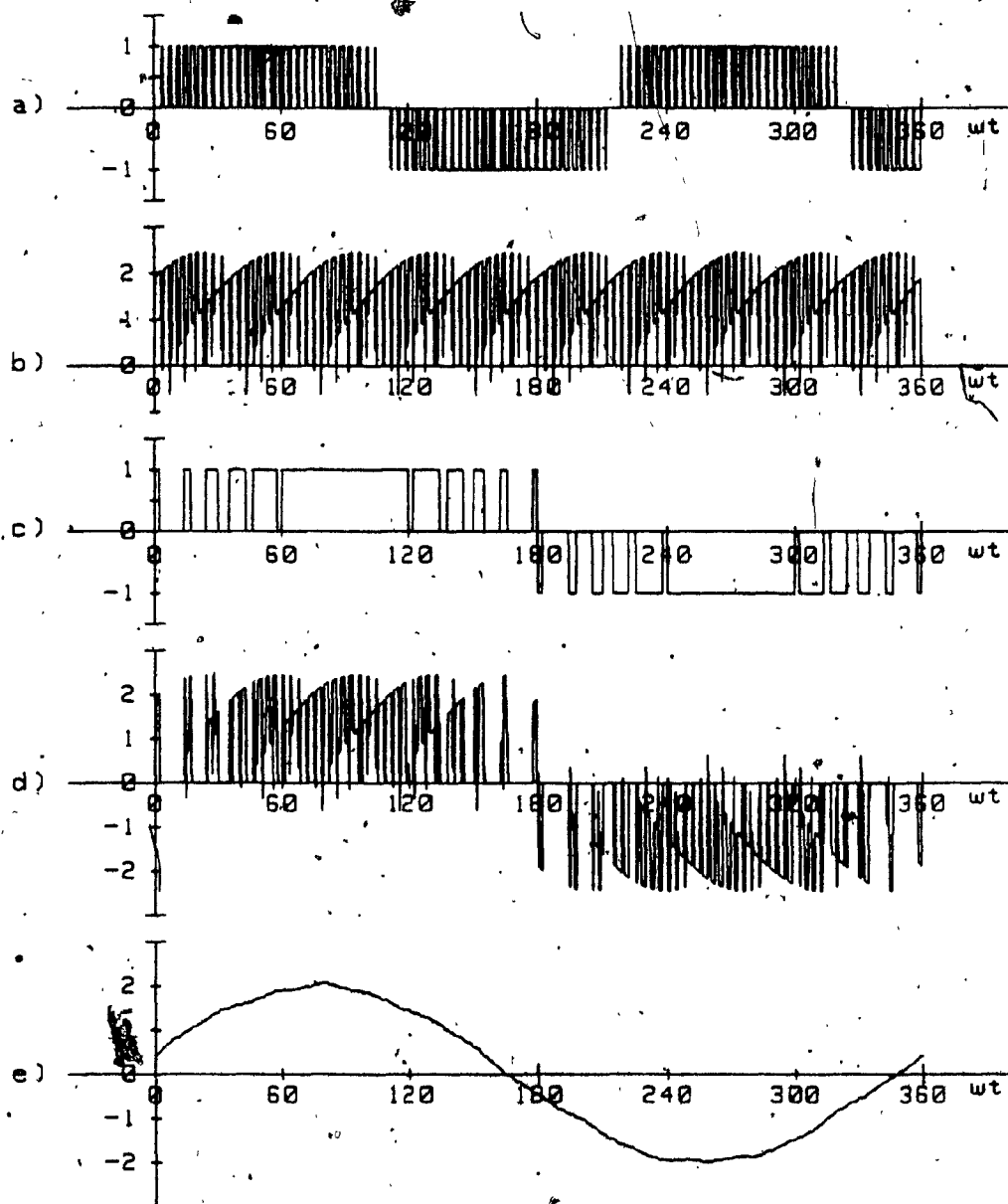


Fig. 5.12: Simulated waveforms related to the input line current, with the SRIFC Structure #1 ( $f_o=100$  Hz).

- a) Inverter switching function.
- b) Inverter input current ( $N_h=36, M=1$ ; load p.f.=0.78).
- c) Rectifier switching function.
- d) Rectifier input line current.
- e) AC source current with the input filter specified in Table 5.10.

TABLE 5.9: INPUT LINE CURRENT FREQUENCY SPECTRA WITH 'SRIFC'  
STRUCTURE #1.

$f_o=100$ Hz, $M=1.0$ , $N_h=36$ , and load power factor=0.78 (lag)				
Harmonic Order	Without Input Filter		With Input Filter	
	(p.u.)	(%)	(p.u.)	(%)
1.00	1.9416	100.000	1.9968	100.000
3.00	.0187	.962	.0370	1.852
5.00	.0180	.514	.0266	1.333
7.00	.0073	.376	.0043	.216
9.00	.0143	.736	.0041	.207
11.00	.0315	1.621	.0056	.279
13.00	.0377	1.940	.0045	.227
15.00	.0233	1.199	.0020	.103
17.00	.0421	2.167	.0028	.141
19.00	.1973	10.161	.0105	.524
21.00	.0085	.436	.0004	.018
23.00	.0935	4.816	.0033	.167
25.00	.1847	9.512	.0055	.277
27.00	.0243	1.250	.0006	.031
29.00	.5289	27.239	.0117	.585
31.00	.4256	21.921	.0082	.411
33.00	.0062	.318	.0001	.005
35.00	.2023	10.417	.0030	.153
37.00	.2164	11.146	.0029	.146
39.00	.0047	.242	.0001	.003
41.00	.1309	6.742	.0014	.072
43.00	.0451	2.323	.0004	.022
45.00	.0251	1.292	.0002	.011
47.00	.1843	9.494	.0015	.077
49.00	.0138	.710	.0001	.005

current is less than 5 % of the rated fundamental current, and that of the input voltage is less than 10 %, the optimum input filter component values can be determined. The results obtained are provided in Table 5.10.

#### 5.4.2 Input stage analysis and input filter design with Structure #2

The frequency spectrum of the unwanted components of the inverter input current with Structure #2 is shown in Fig. 5.13a, and that of the rectifier switching function is shown in Fig. 5.13b. Fig. 5.14 shows some of the simulated waveforms related to the input line current of the SRIFC Structure #2 for  $f_o=60$  Hz,  $N_h=16$ ,  $M=1$ , and 0.9 (lag) load power factor; and the exact frequency spectrum of the input line current for  $k=1,5,7,\dots,150$  and  $m=6,12,\dots,150$  in (5.15) and (5.16) is provided in Table 5.11. From this table it can be seen that there are low-order harmonic components, as expected, because of the low-order harmonic frequency components in the rectifier switching function (Table 5.8). However, the distortion factor of this spectrum is a little better than that of the six-diode rectifier input current.

The input filter is designed in the same manner in Section 5.4.1, and the results presented in Table 5.10.

TABLE 5.10: 'SRIFC' INPUT FILTER DATA.

	Structure #1	Structure #2
$X_{L_i}$	0.11 p.u.	0.14 p.u.
$X_{C_i}$	2.0 p.u.	0.75 p.u.
TKVA	0.461 p.u.	0.896 p.u.
LKVA	0.220 p.u.	0.378 p.u.
CKVA	0.241 p.u.	0.518 p.u.
$\theta_i$	0.4 deg.	6.9 deg.

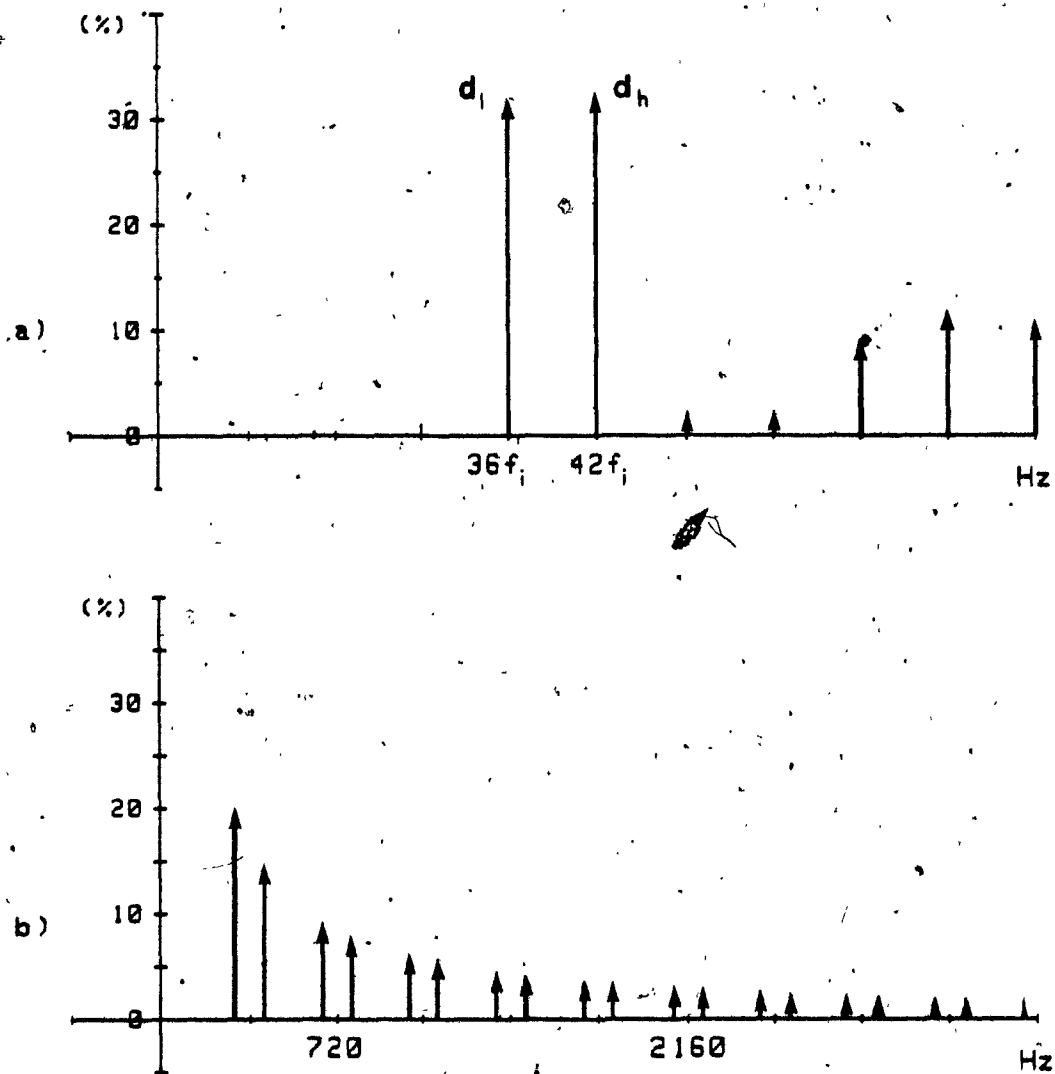


Fig. 5.13: Frequency spectra of the unwanted components in the inverter input current and the rectifier switching function, with the SRIFC Structure #2.

- a) In the inverter input current ( $f_o=60$  Hz,  $N_h=16$ ,  $M=1$ ).
- b) In the rectifier switching function.

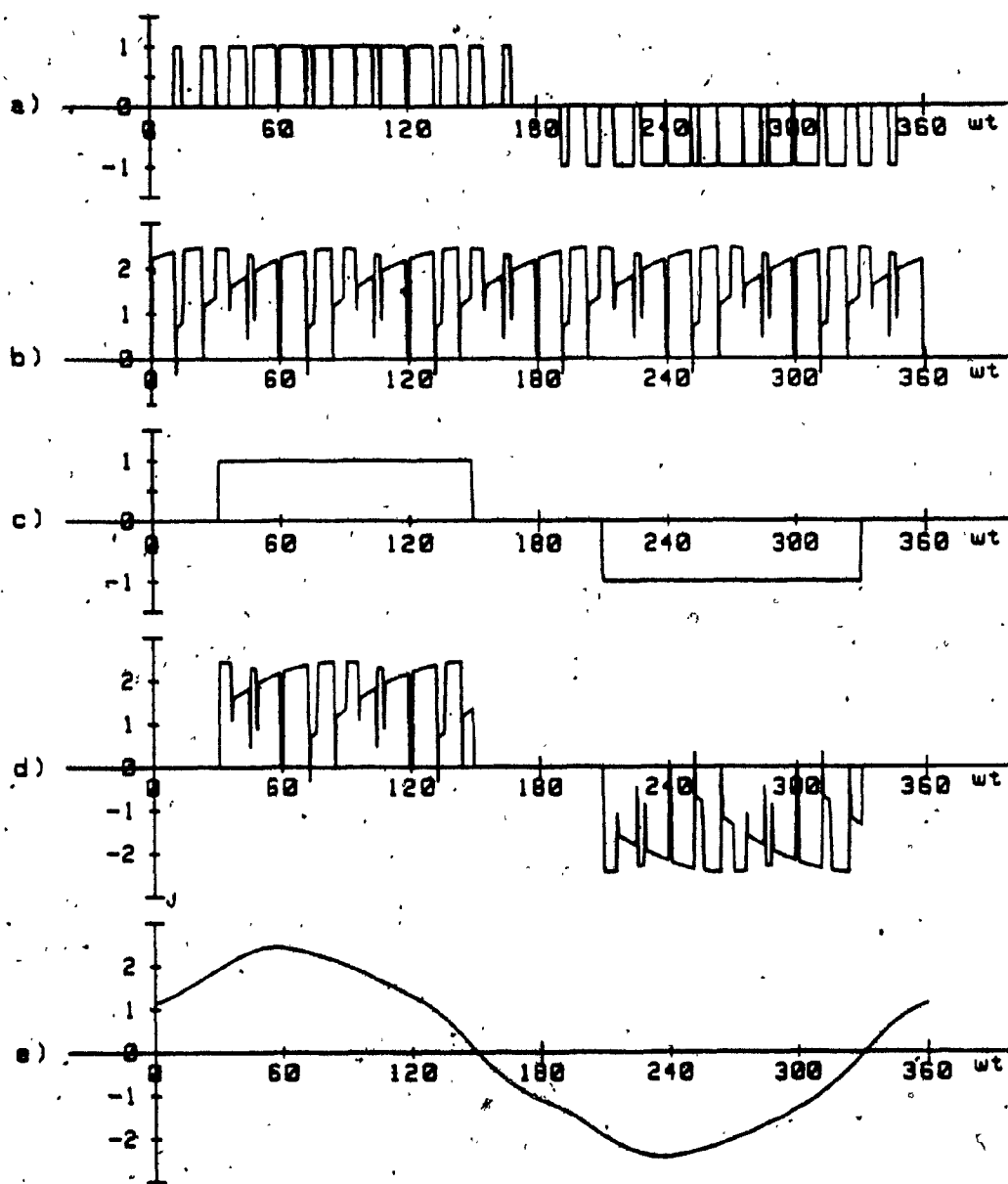


Fig. 5.14: Simulated waveforms related to the input line current, with the SRIFC Structure #2 ( $f_0=60$  Hz).

- a) Inverter switching function.
- b) Inverter input current ( $N_p=16$ ,  $M=1$ , load p.f.=0.9).
- c) Rectifier switching function.
- d) Rectifier input line current.
- e) AC source current with the input filter specified in Table 5.10.

TABLE 5.11: INPUT LINE CURRENT FREQUENCY SPECTRA WITH 'SRIFC' STRUCTURE #2.

$f_o=60$ Hz, $N_h=16$ , $M=1$ , and load power factor=0.9 (lag)				
Harmonic	Without Input Filter		With Input Filter	
Order	(p.u.)	(%)	(p.u.)	(%)
1.00	2.0661	100.000	2.3513	100.000
5.00	.3819	18.483	.1091	4.640
7.00	.2677	12.957	.0342	1.456
11.00	.1491	7.214	.0072	.305
13.00	.1265	6.124	.0043	.183
17.00	.0730	3.533	.0014	.061
19.00	.0589	2.851	.0009	.039
23.00	.1725	8.350	.0018	.078
25.00	.3177	15.375	.0028	.121
29.00	.2863	13.855	.0019	.081
31.00	.2289	11.079	.0013	.057
35.00	.0429	2.074	.0002	.008
37.00	.0576	2.787	.0002	.010
41.00	.0229	1.109	.0001	.003
43.00	.0287	1.387	.0001	.004
47.00	.0880	4.259	.0002	.009
49.00	.1342	6.495	.0003	.013
53.00	.0998	4.832	.0002	.008
55.00	.1323	6.402	.0002	.010
59.00	.0622	3.008	.0001	.004
61.00	.1607	7.778	.0002	.010
65.00	.0290	1.402	0.0000	.002
67.00	.0834	4.036	.0001	.004
71.00	.0592	2.864	.0001	.003
73.00	.1231	5.957	.0001	.005

### 5.5. Discussion

In designing an SRIFC system, it is noted that the selection of the rectifier switching function is very important in order to avoid a dc component as well as subharmonics in the input and output waveforms, since no dc link components are employed.

Regarding the inverter operation to vary the output frequency of an SRIFC system, it is worthwhile mentioning that for an asynchronous PWM operation of an inverter the third-harmonic-injection SPWM scheme shown in Appendix A can be applied in such a way that no ratio-changing method need be used. In this case, the carrier frequency can be set as constant, 5 kHz for Structure #1 for example, and let the inverter be free-running, so that the switching points can be derived from the intersections between the carrier signal and the modulating signal in the same manner as the typical SPWM operation. However, when the asynchronous PWM scheme is applied, some subharmonic components may be generated. Thus, depending on the applications of either the ratio-changing method with MSPWM scheme for synchronous PWM operation or of the third-harmonic-injection SPWM scheme for asynchronous PWM operation can be applied.

Comparing the Structures #1 and #2 by considering all the results obtained in Sections 5.3 and 5.4, the rectifier switching function for Structure #1 has to be chosen carefully to ensure the proper 'safe operating area' for the inverter operation. The switching frequencies, in this particular case, of the rectifier and inverter are higher than those values derived from Structure #2, but the size of the input

filter required is quite small. On the other hand, with Structure #2, the frequency spectrum of the rectifier output voltage is fixed and is quite ideal for the inverter operation; so that the 'safe operating area' can be chosen easily anywhere after the 12-th frequency component, depending on the applications and switching devices. However, a large-sized input filter is required. As a result, if the size of the input filter is not the prime concern, the SRIFC Structure #2 is the proper choice.

Regarding the filter components obtained with SRIFC systems, it is noted that even though the value obtained with SRIFC Structure #1 is somewhat greater than that value obtained with the corresponding RIFC Structure (i.e. #3-2 in Table 4.1) the total filter cost may be more or less the same as each other because of the dc link filter in the RIFC system. In effect, it may be stated that the input filter and the dc link filter in RIFC systems are integrated into the input filter in SRIFC systems. However, in system point of view the SRIFC systems are very attractive to build compact static power converter systems, because the input filter in SRIFC systems can, for example, be moved away from the converter close to the ac mains.

## 5.6 Experimental Results

In order to establish the feasibility of the proposed two new topologies and to evaluate the effectiveness of the theoretical results obtained in previous sections, both SRIFC systems were built and tested

on a laboratory set-up using MOSFET's. In this case, 110 volts and 3 amperes were, for an example, considered as 1 p.u. voltage and 1 p.u. current, respectively. Some of the experimental key results obtained with Structure #1 for  $f_o=100$  Hz,  $N_h=36$ ,  $M=1$ , and 0.78 lagging load power factor are shown in Fig. 5.15. The experimental results obtained with Structure #2 for  $f_o=60$  Hz,  $N_h=16$ ,  $M=1$ , and 0.9 lagging load power factor are shown in Fig. 5.16. From these figures, it is noted that all the experimental results are in close agreement with the corresponding predicted results.

## 5.7 Conclusion

In this chapter, it has been shown that the cumbersome dc link filter components encountered in typical rectifier-inverter frequency changers can be eliminated with only the modest power circuit changes. The resulting SRIFC Structures #1 and #2 have the advantages of:

- (i) not requiring dc link inductors and capacitors,
- (ii) readily allowing bilateral power flow,
- (iii) negligible input and output current/voltage distortions, and
- (iv) higher voltage gain.

However, they also:

- (i) require more complex rectifier circuits,
- (ii) are more susceptible to ac mains transients, and
- (iii) require higher switching frequencies which, for the time being, limit their applications from low to medium power levels.

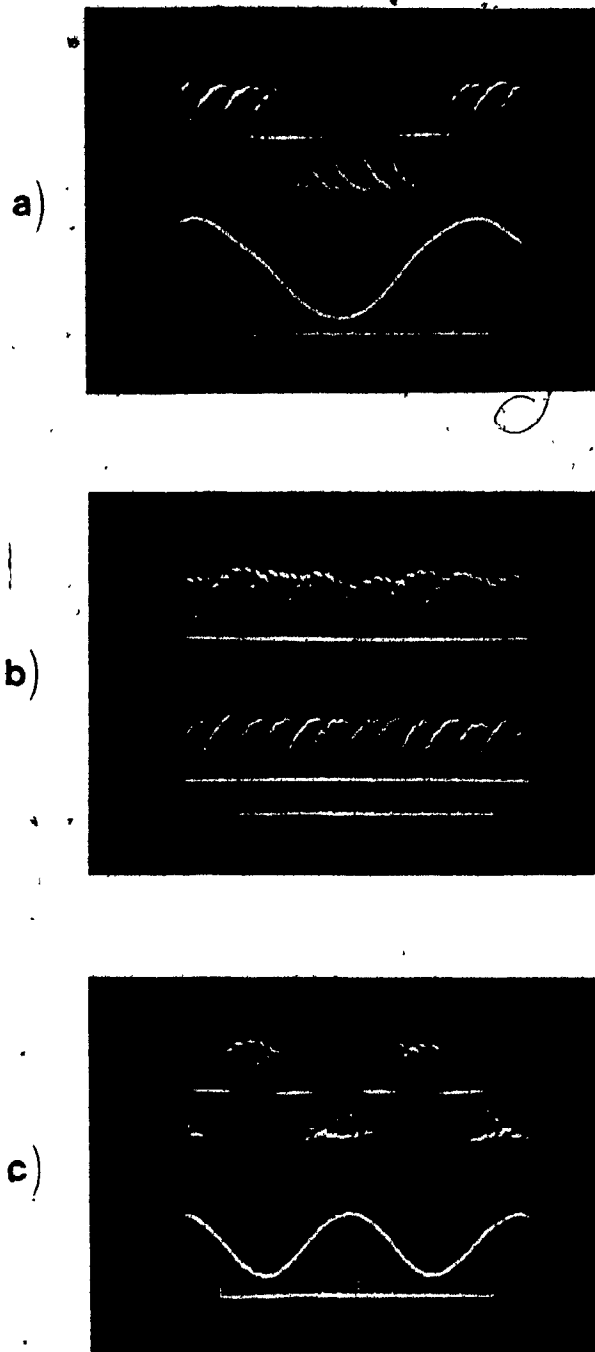
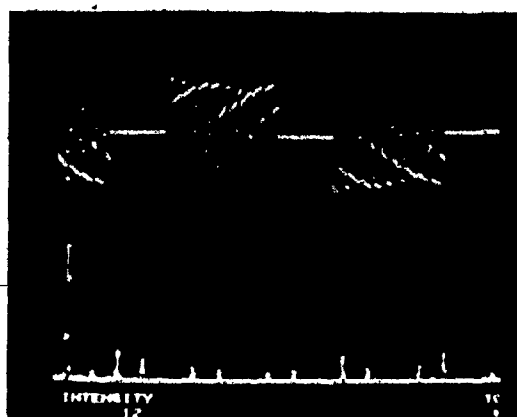
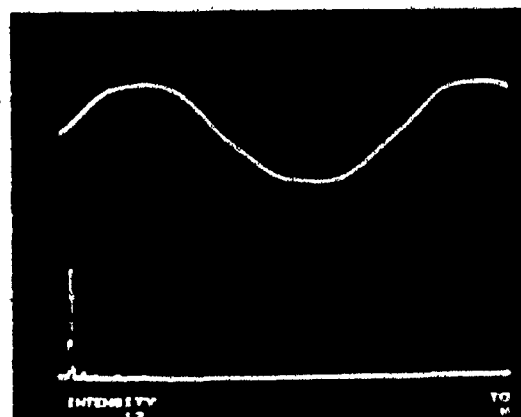


Fig. 5.15: Experimental waveforms with the 'SRIFC' Structure #1  
( $f_o=100$  Hz,  $N_h=36$ ,  $M=1$ , load p.f.=0.78).

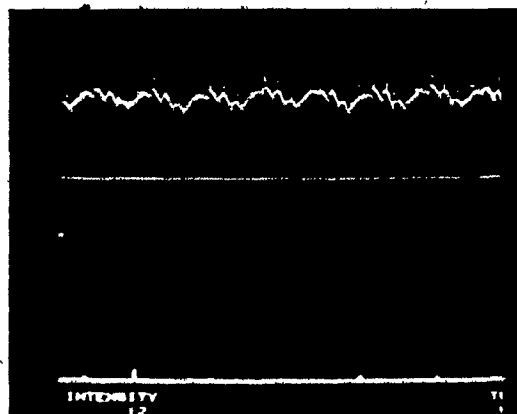
- a) Unfiltered input line current (top) and filtered ac source current (bottom) with the input filter in Table 5.10.
- b) Rectifier output voltage (top) and inverter input current (bottom).
- c) Load voltage (top) and load current (bottom).



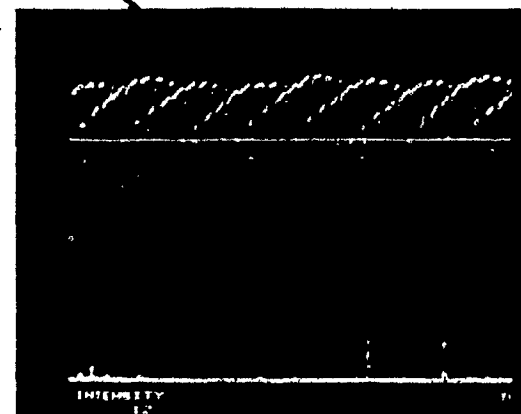
(a)



(b)



(c)



(d)

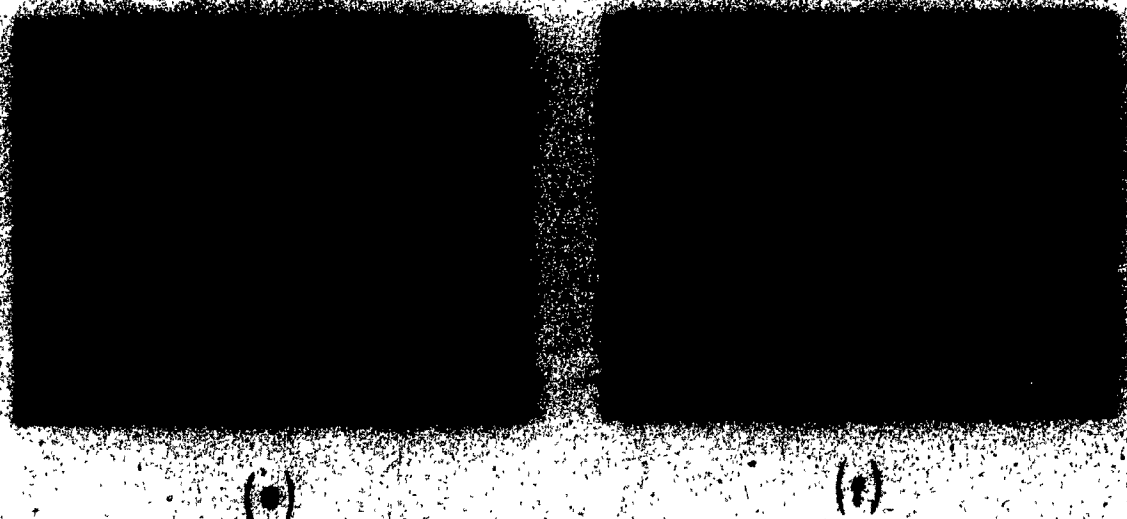


Fig. 1.18: Differential waveform with the "SRIF" Structure #2  
( $\epsilon_{\text{eff}} = 0.5$ ,  $\epsilon_{\text{eff}} = 0.1$ , and load power factor 0.9).

- (a) Waveform of the voltage and the frequency spectrum
- (b) Waveform of the current and the frequency spectrum with  
the load power factor 0.9
- (c) Waveform of the voltage and the frequency spectrum  
with the load power factor 0.1
- (d) Waveform of the current and the frequency spectrum  
with the load power factor 0.1

Also, it can be concluded that Structure #2 is 'optimum' for low to medium power applications where the THD requirement of the input current are rather loose. For applications with strict THD requirement of the input current, Structure #1 clearly offers the best choice.

## CHAPTER 6

### CONCLUSION

#### 6.1 Conclusions

Three-phase PWM rectifier systems and rectifier-inverter frequency changer systems with and without dc link components have been investigated in order to design optimum converter systems by means of the minimization of the reactive components, such as ac/dc filters, power-factor correction capacitors, etc., while improving the system's performance.

In order to achieve this task, some advanced PWM control techniques, which yielded minimum possible harmonic distortion of the input and output waveforms along with maximum possible voltage utilization, have been employed to the associated rectifiers and inverters.

Three kinds of PWM switching functions have been employed to the three-phase ac/dc converter system. By using a suitable computer-aided analysis method, the input and output waveforms have been analyzed in detail. In conjunction with the above analyses, the techniques to design the associated optimum ac/dc filters have been developed and utilized by using proper computer-aided design methods.

The main results of the study of PWM rectifier systems can be summarized as follows:

- (i) in Sections 3.3 and 3.4, it was shown that the size (or cost) of ac and dc filters can be reduced significantly,
- (ii) in Section 3.2, it has been demonstrated that the leading input power factor can be obtained with the optimized PWM switching functions, and finally
- (iii) in Section 3.3, it was shown that the total input power factor can be improved considerably without using power-factor correction capacitors.

Three kinds of three-phase RIFC structures with dc link components have also been investigated in order to design an optimum RIFC system. It is apparent that the optimum RIFC system, which consists of a PWM rectifier and a PWM inverter employing the advanced PWM control techniques, requires considerably smaller sized reactive components.

In response to expectations regarding the frame (motor) mounted converters, the above RIFC topologies have further been investigated in order to suppress their corresponding dc link components. Two such topologies have been thoroughly studied and discussed. It was shown that the proposed new RIFC structures have the following characteristics:

- (i) they do not require any dc link component,
- (ii) they readily allow bilateral power flow,
- (iii) the harmonic distortions of the input/output waveforms are negligible,

(iv) they yield good voltage gain, and

(v) they require more complex rectifier circuits.

As a general conclusion, it has been shown that the reactive components of static power converters can be reduced significantly by employing advanced PWM control techniques and new converter system structures. These structures also exhibit improved performance characteristics. However, these converter systems require more complex circuits and higher switching frequencies which limit their applications to between low and medium power levels for the time being. However, with the improving semiconductor technologies, the prices of inductors and capacitors remaining stable, the industrial (or office) floor space becoming more expensive, and the harmonic standards becoming stricter, the minimization of the associated reactive components of static power converters, by employing the converter structures investigated in this thesis, has already begun to attract considerable attention.

Moreover, some of the theoretical key results obtained have been verified experimentally or by computer simulation in time domain, and have shown that the experimental results are in close agreement with the corresponding theoretical results.

## 6.2 Suggestions for Future Work

The analysis and design of static power converter topologies discussed in this thesis have been based on the assumption that the ac mains feeding the front end rectifiers is distortion-free. This is, to a large extent, true with the power generated by large utility companies. However, in cases where power generated on site by small sized diesels or thermal generating plants, this basic assumption is not always true. In such cases, the use of a second-order input L-C filter may lead to system instabilities, especially when a number of such systems are supplied from the same ac bus. Consequently, further investigation is required to determine whether system topologies other than the ones presented in this thesis are more suitable to 'weak' bus ac mains. A good starting point could be the topologies that utilize synchronous type of rectifiers [65], [66]. These rectifiers use only a single reactor input filter which makes them more immune to system resonant frequencies. They have, however, their own intrinsic complexities, because their operation is based on the direct power (instead of voltage or current) control.

REFERENCES

- [1] Schaefer, J., Rectifier Circuits : Theory and Design, John Wiley & Sons, Inc., 1965.
- [2] Pelly, B. R., Thyristor Phase-Controlled Converters and Cycloconverters, Wiley-Interscience, 1971.
- [3] Dewan, S.B. and Straughen, A., Power Semiconductor Circuits, John Wiley & Sons, Inc., 1975.
- [4] Sen, P.C., Thyristor DC Drives, John Wiley & Sons, Inc., 1981.
- [5] Miller, D. F., " Application guide for shunt capacitors on industrial distribution systems at medium voltage levels," IEEE Trans. Ind. Appl., Vol. IA-12, No. 3, May/June 1976, pp. 444-459.
- [6] Steeper, D.E. and Stratford, R.P., "Reactive compensation and harmonic suppression for industrial power systems using thyristor converters," IEEE Trans. Ind. Appl., Vol. IA-12, No. 3, May/June 1976, pp. 232-254.
- [7] Moore, A.H., "Application of power capacitors to electrochemical rectifier systems," IEEE Trans. Ind. Appl., Vol. IA-13, No. 5, Sept./Oct. 1977, pp. 399-406.
- [8] Schieman, R. G., " Power factor correction of static drives with capacitors," in Conf. Rec., IEEE IAS Annu. Meet., 1979, pp. 749-756.

- [9] Schwartz, T. F., "Capacitor control of the power factor of thyristor drives," in Conf. Rec., IEEE IAS Annu. Meet., 1979, pp. 770-773.
- [10] Stratford, R. P. et al., "IEEE guide for harmonic control and reactive compensation of static power converters," IEEE Standard 519, 1979.
- [11] Stefanovic, V. R., "Power factor improvement with a modified phase-controlled converter," IEEE Trans. Ind. Appl., Vol. IA-15, No. 2, March/April 1979, pp. 193-201.
- [12] Dewan, S.B. and Dunford, W.G., "Improved power factor operation of a three-phase rectifier bridge through modified gating," in Conf. Rec., IEEE PESC 1980, pp. 830-837.
- [13] Ohnishi, T. and Okitsu, H., "Power-factor improvement of single-phase converter by means of bias voltage control," IEEE Trans. Ind. Appl., Vol. IA-17, No.2, March/April 1981, pp. 190-198.
- [14] Olivier, G. and Stefanovic, V.R., "Thyristor current source with an improved power factor," IEEE Trans. Ind. Electr., Vol. IE-29, No. 4, Nov. 1982, pp. 299-307.
- [15] Edelman, L., "Prediction of power supply generated interference," IEEE Trans. Electro. Compat., Vol. EMC-11, No. 3, Aug. 1969, pp. 117-122.
- [16] Galloway, J.H., "Harmonic line currents in large thyristor six-pulse converters," IEEE Trans. Ind. Appl., Vol. IA-11, No. 3, May/June 1975, pp. 256-262.

- [17] Shipp, D.D., "Harmonic analysis and suppression for electrical systems supplying static power converters and other nonlinear loads," IEEE Trans. Ind. Appl., Vol. IA-15, No. 5, Sept./Oct. 1979, pp. 453-458.
- [18] Linders, J.R., "Electric wave distortions : Their hidden costs and containment," IEEE Trans. Ind. Appl., Vol. IA-15, No. 5, Sept./Oct. 1979, pp. 458-471.
- [19] Stratford, R.P., "Rectifier harmonics in power systems," IEEE Trans. Ind. Appl., Vol. IA-16, No. 2, March/April 1980, pp. 271-276.
- [20] Stratford, R.P., "Harmonic pollution on power systems - A change in philosophy," IEEE Trans. Ind. Appl., Vol. IA-16, No. 5, Sept./Oct. 1980, pp. 617-623.
- [21] Stratford, R.P., "Analysis and control of harmonic current in systems with static power converters," IEEE Trans. Ind. Appl., Vol. IA-17, No. 1, Jan./Feb. 1981, pp. 71-81.
- [22] Bose, B.K., "Adjustable speed AC drives - A technology status review," IEEE Proc., Vol. 70, No. 2, Feb. 1982, pp. 116-135.
- [23] Chauprade, R. and Abbondanti, A., "Variable speed drives - modern concepts and approaches," in Conf. Rec., IEEE PESC 1982, pp. 20-37.
- [24] Stefanovic, V.R., "Present trends in variable speed AC drives," in Conf. Rec., IPEC-Tokyo 1983, pp. 438-449.

- [25] Jones, B.L. and Brown, J.E., "Electrical variable-speed drives," IEE Proc., Vol. 131, Pt. A, No. 7, Sept. 1984, pp. 516-558.
- [26] Gyugyi, L. and Pelly, B., Static Power Frequency Changers: Theory, Performance and Application, Wiley-Interscience, New York, 1976.
- [27] Pelly, B.R., "Power semiconductor devices - A status review," in Conf. Rec., IEEE PESC 1982, pp. 1-19.
- [28] Freundel, P., "Power MOSFETs, or bipolar power transistors for converter circuits ?," in Conf. Rec., IEEE PESC 1982, pp. 38-44.
- [29] Divan, D.M. and Barton, T.H., "Considerations on the application of improved power factor converter structures," in Conf. Rec., IEEE IAS Annu. Meet., 1983, pp. 941-948.
- [30] Lienau, W., Muller-Hellmann, A., and Skudelny, H.-C., "Self-commutated converters for ac or dc traction applications," in Conf. Rec., IEEE IAS Annu. Meet., 1978, pp. 789-797.
- [31] Kataoka, T., Mizumachi, K., and Miyairi, S., "A pulsewidth controlled ac-to-dc converter to improve power factor and waveform of ac line current," IEEE Trans. Ind. Appl., vol. IA-15, No. 6, Nov./Dec. 1979, pp. 670-675.
- [32] Jayne, M.G., Bowes, S.R., and Bird, B.M., "Developments in sinusoidal PWM inverters," in Rec., IFAC 2nd Symposium, 1977, pp. 145-153.

- [33] Marino, P., Picardi, C., and Russo, A., "AC characteristics in ac/dc/dc/ conversion," IEE Proc., Vol. 130, Pt. B, No. 3, May 1983, pp. 201-206.
- [34] Zach, F.C., "Minimization of influences on the mains for line commutated converters by pulse-time-control," in Conf. Rec., 7th IPEC-Genf, Sept. 1983.
- [35] Busse, A. and Holtz, J., "Multiloop control of a unity power factor fast switching ac to dc converter," in Conf. Rec., PESC 1982, pp. 171-179.
- [36] Doradla, S.R., Nagamani, C., and Sanyal, S., "A sinusoidal PWM three-phase ac to dc converter-fed dc motor drive," in Conf. Rec., IEEE IAS Annu. Meet., 1984, pp. 668-679.
- [37] Krause, P.C. and Woloszyk, L.T., "Comparison of computer and test results of a static AC drive system," IEEE Trans. Ind. Gen. Appl., Vol. IGA-4, No. 6, Nov./Dec. 1968, pp. 583-588.
- [38] Lipo, T.A. and Krause, P.C., "Stability analysis of a rectifier-inverter induction motor drive," IEEE Trans. Power Appar. & Sys., Vol. PAS-88, No. 1, Jan. 1969, pp. 55-66.
- [39] Lipo, T. A. and Krause, P. C., "Analysis and simplified representations of a rectifier-inverter induction motor drive," IEEE Trans. Power Appar. & Sys., Vol. PAS-88, No. 5, May 1969, pp. 588-596.

- [40] Lipo, T.A., Krause, P.C., and Jordan, H.E., "Harmonic torque and speed pulsations in a rectifier-inverter induction motor drive," IEEE Trans. Power Appar. & Sys., Vol. PAS-88, No. 5, May 1969, pp. 579-587.
- [41] Wood, P., Switching Power Converters, Van Nostrand Reinhold Co., 1981.
- [42] Schonung, A. and Stemmler, H., "Static frequency changers with subharmonic control in conjunction with reversible variable speed ac drives," Brown-Boveri Review, pp. 555-577, Aug./Sept. 1964.
- [43] Zubek, J., Abbondanti, A., and Norby, C.J., "Pulse-width modulated inverter motor drives with improved modulation," IEEE Trans. Ind. Appl., Vol. IA-11, Nov./Dec. 1975, pp. 695-703.
- [44] Bowes, S. R., "New sinusoidal pulsewidth-modulated inverter," IEE Proc., Vol. 122, Pt. B, No. 11, 1975, pp. 1279-1285.
- [45] Wilson, J. W.A. and Yeaman, J. A., "Intrinsic harmonics of idealized inverter PWM systems," in Conf. Rec., IEEE IAS Annu. Meet., 1976, pp. 967-973.
- [46] Jayne, M.G., Bowes, S.R., and Bird, B.M., "Developments in SPWM inverters," IFAC Symposium, Oct. 1977, pp. 145-153.
- [47] Boost, M. and Marinos, N., "Rectifier optimization," Technical Report, Dept. of Elec. Eng., Concordia University, Dec. 1982.

[48] Ohnishi, T. and Okitsu, H., "A novel PWM technique for three-phase inverter/converter," in Conf. Rec. IPEC-Tokyo 1983, pp. 384-395.

[49] Turnbull, F.G., "Selected harmonic reduction in static dc-ac inverters," IEEE Trans. Commun. Electron., Vol. 83, July 1964, pp. 374-378.

[50] Buja, G.S. and Indri, G.B., "Optimal pulsewidth modulation for feeding ac motors," IEEE Trans. Ind. Appl., Vol. IA-13, 1977, pp. 38-44.

[51] Patel, H. and Hoft, G., "Generalized technique of harmonic elimination and voltage control in thyristor inverters: Part I - Harmonic elimination," IEEE Trans. Ind. Appl., Vol. IA-9, 1973, pp. 310-317.

[52] Bowes, S.R. and Bullough, R., "PWM switching strategies for current-fed inverter drives," IEE Proc., Vol. 131, Pt. B, No. 5, Sept. 1984, pp. 195-202.

[53] Ziogas, P.D., Kang, Y., and Stefanovic, V.R., "PWM control for rectifier filter minimization," in Conf. Rec., IEEE PESC 1984, pp. 353-362.

[54] Bedford, B.D. and Hoft, R.G., Principles of Inverter Circuits, John Wiley & Sons Inc., New York, 1964.

[55] Canadian General Electric, Power Converter Handbook: Theory, Design and Application, 1976.

[56] Kamm, E., "Design guide for electromagnetic interference (EMI) reduction in power supplies," MIL-HDBK-241B, USA Naval Electronic Systems Command.

[57] Ziogas, P.D., Kang, Y., and Stefanovic, V.R., "Optimum system design of a three-phase rectifier-inverter frequency changer," in Conf. Rec., IEEE IAS Annu. Meet., 1984, pp. 908-919.

[58] Daniels, A.R. and Slattery, D.T., "New power converter technique employing power transistors," IEE Proc., 1978, Pt. B, Vol. 125, No. 2, pp. 146-150.

[59] Venturini, M., "A new sine wave in, sine wave out conversion technique eliminates reactive elements," Proc. of Powercon 7, 1980, pp. E3-1 - E3-15.

[60] Ziogas, P.D., Khan, S.I., and Rashid, M.H., "Some improved forced commutated cycloconverter structures," in Conf. Rec., IEEE IAS Annu. Meet., 1984, pp. 739-748.

[61] Ziogas, P.D., Kang, Y., and Stefanovic, V.R., "Rectifier-inverter frequency changers with suppressed dc link components," in Conf. Rec., IEEE IAS Annu. Meet., 1985.

[62] Wilson, J.W.A., "The forced-commutated inverter as a regenerative rectifier," IEEE Trans. Ind. Appl., Vol. IA-14, No. 4, July/Aug. 1978, pp. 335-340.

- [63] Houldsworth, J.A. and Burgum, F.J., "Induction motor drive using new digital sine-wave PWM system," IEE Conf. Publ. 179, 1979, pp. 11-14.
- [64] Grant, D.A. and Seidner, R., "Ratio changing in PWM inverters," IEE Proc., Vol. 128, Pt. B, No. 5, Sept. 1981, pp. 243-248.
- [65] Smollinger, G.J. and Raddi, W.J., "Reverse Energy through an ac line synchronized pulse width modulated sine-wave inverter," INTELEC 1981, pp.126-131.
- [66] Schlecht, M.F., "Novel topological alternatives to the design of a harmonic-free, utility/DC interface," in Conf. Rec., IEEE PESC 1983, pp. 206-216.
- [67] Houldsworth, J.A. and Grant, D.A., "The use of harmonic distortion to increase the output voltage of a three-phase PWM inverter," IEEE Trans. Ind. Appl., Vol. IA-20, No. 5, 1984, pp. 1224-1228.

## APPENDIX A

### Third-Harmonic-Injection SPWM Switching Function

Typical SPWM switching function described in Section 2.2 yields lower fundamental amplitude than that of other PWM switching functions (Table 2.1). To achieve a higher fundamental amplitude overmodulation is often used. This reduces the switching points and therefore lower harmonics occur. Furthermore the control characteristic changes, as the amplitude of fundamental component is no longer linearly dependent on the modulation index  $M$ . To avoid the reduction of switching points, but still get a high fundamental amplitude, waveforms other than a sine wave can be used. One solution is a trapezoidal wave. This wave is easy to generate and the fundamental amplitude is improved, but several lower harmonics are introduced.

Another solution is to add some triplen harmonics, because all triplen harmonics in a three-phase supply are cophasal and are eliminated from the line-to-line waveforms. Therefore, by adding some amount of third harmonic can increase the fundamental amplitude without deteriorating the harmonic characteristic of typical SPWM scheme [67].

Fig. A.1 shows the derivation of Third-Harmonic-Injection SPWM (THI-SPWM) switching function with  $N_h=15$  and  $M=1.15$ . Fig. A.2 shows the frequency spectra of SPWM and THI-SPWM switching functions with  $N_h=15$  and at  $M=1$  and  $1.15$  respectively. From this figure it is

apparent that with the THI-SPWM switching function the fundamental amplitude is increased by about 13 % as compared to that of SPWM switching function, along with improving the harmonic characteristic. Moreover, the fundamental amplitude as well as the harmonic characteristic with THI-SPWM switching function are similar to those with MSPWM switching function described in Section 2.3.

Finally, it is noted that triplen harmonics other than the third harmonic component may be added to increase the fundamental amplitude and to improve the harmonic characteristic..

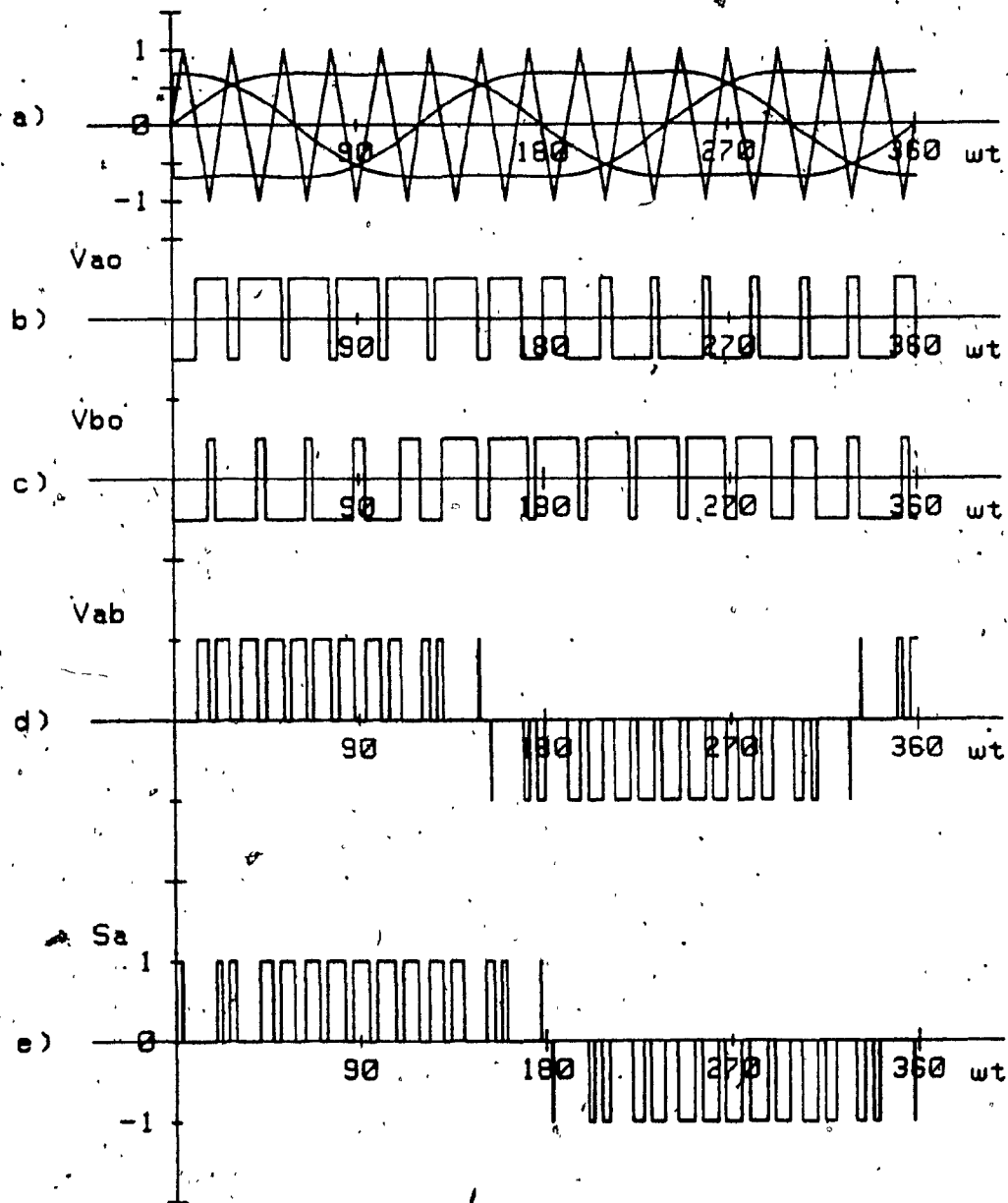


Fig. A.1: The third-harmonic-injection SPWM (THI-SPWM) scheme.

- a) Derivation of the switching points.
- b,c) Phase voltages of an inverter with the THI-SPWM scheme.
- d) Line to line voltage of the inverter.
- e) The switching function ( $N_h=15$ ,  $M=0.8$ ).

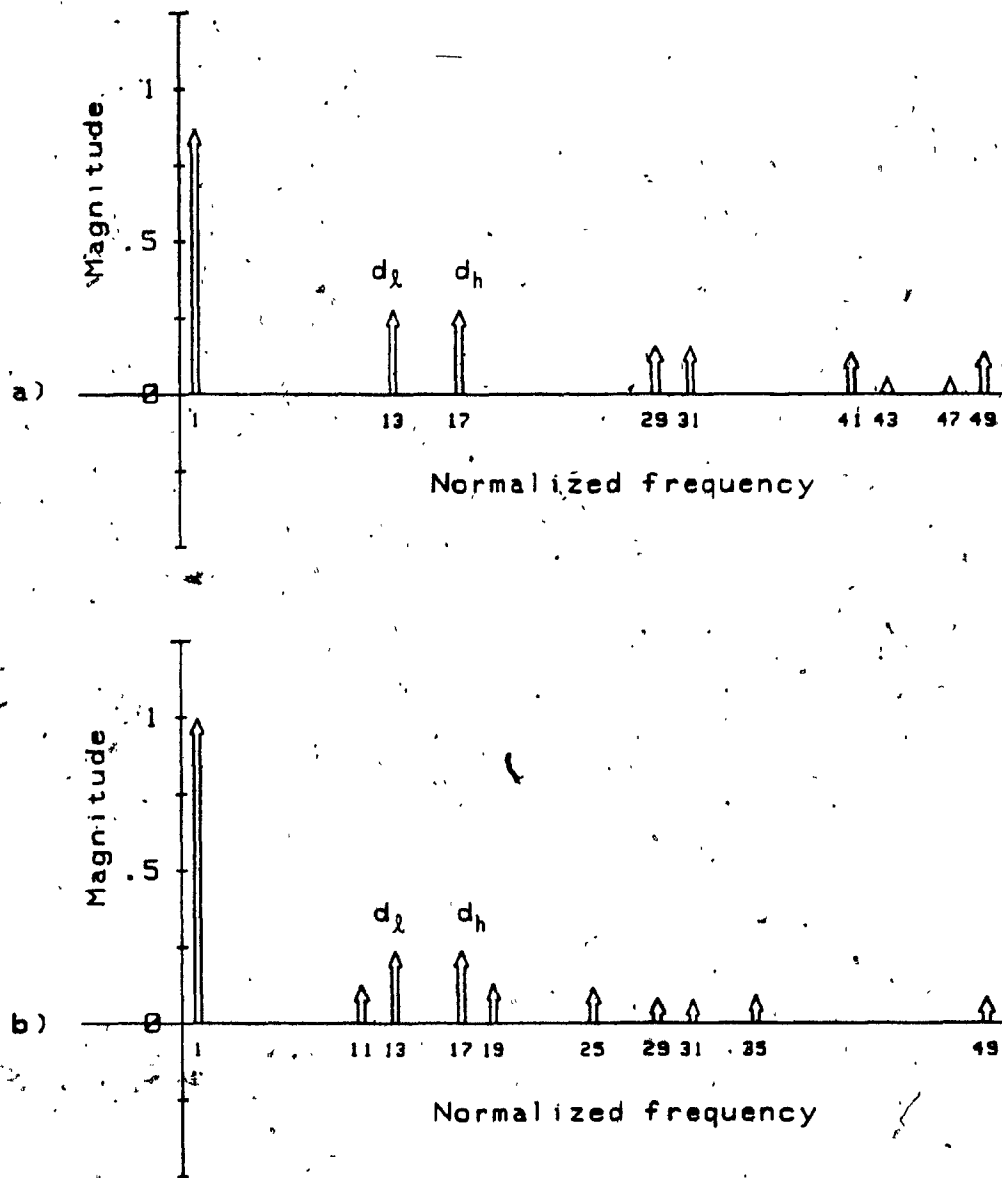


Fig. A.2: Frequency spectra of the typical SPWM and the THI-SPWM switching function with  $N_h=15$  and  $M=1$ .

- a) With the SPWM switching function.
- b) With the THI-SPWM switching function.

# APPENDIX B

In this Appendix B, some of the useful computer-aided analysis and design programs used in this thesis are listed.

## A.B.1:

```

10  SUB Mspwm(M,Nh,Sw(*),Phsw(*),Ang(*))
20
30  This subprogram computes the commutation points and the frequency
40  spectrum of an MSPWM switching function.
50
60  REAL Ti(300),Psw(150)
70  Tol=.001
80  Mul=180/PI
90  Z=PI/3
100 Np=Nh/4
110 Nd=2*Np
120 PRINT USING "****"      " ",2D," " PULSES PER HALF-CYCLE "****",Nh
130 PRINT USING "****"      MODULATION INDEX = " ",D.2D," ";M
140 RAD
150 Ti(1)=0
160 K=1
170 ***** COMPUTE THE INTERSECTING POINTS *****
180 Sf=Mul*(Np+.5)/30
190 FOR I=1 TO Np
200   Xo=Ti(K)
210   K=K+1
220 Newton:
230     F=M*SIN(Xo)+(Sf*Xo-2*I)
240     G=M*COS(Xo)+Sf
250     Xn=Xo-F/G
260     Delta=ABS((Xn-Xo)/Xn)
270     IF Delta =Tol THEN GOTO Out1
280     Xo=Xn
290     GOTO Newton
300 Out1: Ti(K)=Xn
310     Xo=Ti(K)
320     K=K+1
330 Raphson: F=M*SIN(Xo)-Sf*Xo+2*I
340     G=M*COS(Xo)-Sf
350     Xn=Xo-F/G

```

```

360      Delta=ABS((Xn-Xo)/Xn)
370      IF Delta =Tol THEN GOTO Out2
380      Xo=Xn
390      GOTO Raphson
400 Out2: Ti(K)=Xn
410      NEXT I
420      No=2*(Np+1)
430      FOR I=1 TO Np
440          N1=No+4*(I-1)
450          N2=No-1-2*(I-1)
460          N3=No-No+2*(I-1)
470          Ti(N1)=2*Z-Ti(N2)
480          Ti(N1+1)=2*Z-Ti(N2-1)
490          Ti(N1+2)=Z+Ti(N3)
500          Ti(N1+3)=Z+Ti(N3+1)
510      NEXT I
520      N5=13+6*(Np-2)
530      FOR I=1 TO Nd
540          Ti(N5+I)=Pi-Ti(No-I)
550      NEXT I
560      *****COMPUTE THE FREQUENCY SPECTRUM OF THE SWITCHING FUNCTION*****
570      Nhalf=8*Np+1
580      PRINT
590      PRINT "      COMMUTATION      POINTS"
600      PRINT
610      FOR J=1 TO Nhalf
620          PRINT USING "      "      TI(" ",2D," ")=" ",4D.2D," ";J,Ti(J)*Mul
630      NEXT J
640      PRINT/
650      PRINT "THE SPECTRUM OF THE SWITCHING FUNCTION"
660      PRINT
670      FOR N=1 TO 150 STEP 2
680          IF N MOD 3=0 THEN GOTO Nextn
690          B=0
700          Nn=Nhalf-1
710          FOR I=2 TO Nn STEP 2
720              P=N*Ti(I+1)
730              Q=N*Ti(I)
740              Dummy=(1/N)*(COS(P)-COS(Q))
750              B=B-Dummy
760          NEXT I
770          Sw(N)=2*B/PI
780          Phsw(N)=0
790          Psw(N)=100*ABS(Sw(N)/Sw(1))
800          PRINT USING "      SW(" ",3D," ")=" ",3D.4D,8D.3D," "Z" ";N,Sw(N),Psw(N)
810 Nextn:NEXT N
820      SUBEND

```

A.B.2:

```

10  SUB Rect_out(V1,Sw(*),Phsw(*),Vo(*),Phvo(*),Vdc)
20
30  This subprogram computes the output voltage of a rectifier.
40
50  REAL Ph(2,150),U(2,150),Pvo(150)
60  RAD
70  Mul=180./PI
80  Zz=2*PI/3
90  FOR I=1 TO 150 STEP 2
100     R1=Zz*(I-1)
110     R2=Zz*(I+1)
120     Fr=Phswr(I)
130     Cv1=V1*(COS(Fr)+COS(Fr-R1)+COS(Fr+R1))
140     Cv2=-V1*(SIN(Fr)+SIN(Fr-R1)+SIN(Fr+R1))
150     Cv3=-V1*(COS(Fr)+COS(Fr-R2)+COS(Fr+R2))
160     Cv4=V1*(SIN(Fr)+SIN(Fr-R2)+SIN(Fr+R2))
170     U(1,I)=SQR(Cv12+Cv22)
180     U(2,I)=SQR(Cv32+Cv42)
190     Atan2(Cv1,Cv2,Seta1)
200     Atan2(Cv3,Cv4,Seta2)
210     Ph(1,I)=Seta1
220     Ph(2,I)=Seta2
230  NEXT I
240  Vdc=1.5*V1*Sw(1)
250  FOR I=3 TO 150 STEP 2
260     K1=Sw(I-2)*U(2,I-2)
270     K2=Sw(I)*U(1,I)
280     V1=K1*SIN(Ph(2,I-2))+K2*SIN(Ph(1,I))
290     V2=K1*COS(Ph(2,I-2))+K2*COS(Ph(1,I))
300     Vo(I-1)=.5*SQR(V12+V22)
310     Pvo(I-1)=100*ABS(Vo(I-1)/Vdc)
320     Atan2(V1,V2,Seta)
330     Phvo(I-1)=Seta
340  NEXT I
350  SUBEND
360  *****
370  SUB Atan2(Im,Re,Seta)
380
390  This subprogram computes the phase angle by considering 'QUADRANT'.
400
410  RAD
420  Mul=180/PI
430  IF Re=0 THEN GOTO Zero
440  Seta=ATN(Im/Re)
450  IF Re 0 AND Im 0 THEN Seta=PI+Seta
460  IF Re 0 AND Im 0 THEN Seta=PI+Seta
470  GOTO Subend
480 Zero:
490  IF Im 0 THEN Seta=PI/2
500  IF Im 0 THEN Seta=-PI/2
510 Subend:
520  SUBEND

```

A.B.3:

```
10  SUB Srifc_out(Vdc,Vr(*),Phvr(*),Swi(*),Phswi(*))
20
30  This subprogram computes the frequency components of an 'SRIFC' output
40  voltage by the frequency multiplication between the frequency components
50  of the rectifier output voltage and the frequency components of the
60  inverter switching function.
70
80  REAL V1(15),Phv1(15),V2(50),Phv2(50),Frq(50),Voab(1500),Pvoab(1500)
90  REAL Phvrab(1500),Fvect(1500),Cvoab(1500),Svoab(1500),Ioab(1500)
100 REAL Pioab(1500),Phioab(1500)
110
120  REARRANGE the HARMONIC COMPONENTS of the RECTIFIER OUTPUT VOLTAGE
55  and INVERTER SWITCHING FUNCTION to do FREQUENCY MULTIPLICATION
130
140  RAD
150  Mul=180./PI
160  FOR I=2 TO 15
170    V1(I)=Vr(6*(I-1))
180    Phv1(I)=Phvr(6*(I-1))
190  NEXT I
200  V1(1)=Vdc
210  Phv1(1)=0.
220  FOR J=1 TO 25
230    J1=2*J-1
240    J2=2*J
250    J3=6*J-5
260    J4=6*J-1
270    Frq(J1)=J3
280    Frq(J2)=J4
290    V2(J1)=Sw1(J3)
300    V2(J2)=Sw1(J4)
310    Phv2(J1)=Phsw1(J3)
320    Phv2(J2)=Phsw1(J4)
330  NEXT J
340
350  CONSTRUCT MATRICES and VECTORS to do FREQUENCY MULTIPLICATION
360  according to the GIVEN OUTPUT FREQUENCY
370
380  W1=60.
390  Wo=60.
400  Wn=W1/Wo
410  FOR N1=1 TO 50
420    Fvect(N1)=Frq(N1)
430    Voab(N1)=Vdc*V2(N1)
440    Phvrab(N1)=Phv2(N1)
450  NEXT N1
```

```

460   FOR M=2 TO 15
470     FOR N=1 TO 50
480       Ms=100*(M-1)+N-50
490       Ma=Ms+50
500       Frq1=6.*Wn*(M-1)
510       Frq2=Frq(N)
520       Fvect(Ms)=ABS(Frq1-Frq2)
530       Fvect(Ma)=Frq1+Frq2
540       Voab(Ms)=V1(M)*V2(N)/2.
550       Voab(Ma)=-Voab(Ms)
560       Phvrab(Ms)=Phv1(M)-Phv2(N)
570       Phvrab(Ma)=Phv1(M)+Phv2(N)
580     NEXT N
590   NEXT M

600   SEPARATE the COSINE and SINE COMPONENTS
610
620   FOR I=1 TO 1450
630     Cvoab(I)=Voab(I)*SIN(Phvrab(I))
640     Svoab(I)=Voab(I)*COS(Phvrab(I))
650   NEXT I
660   SORTING
670
680   FOR M=1 TO 1449
690     M1=M+1
700     FOR N=M1 TO 1450
710       IF Fvect(M) =Fvect(N) THEN GOTO Nextn
720       Fdummy=Fvect(M)
730       Cvdummy=Cvoab(M)
740       Svdummy=Svoab(M)
750       Fvect(M)=Fvect(N)
760       Cvoab(M)=Cvoab(N)
770       Svoab(M)=Svoab(N)
780       Fvect(N)=Fdummy
790       Cvoab(N)=Cvdummy
800       Svoab(N)=Svdummy
810     Nextn:NEXT N
820   Nextm:NEXT M
830
840   COMBINE the SAME FREQUENCIES
850
860   Ftol=.0001
870   Fcheck=10000.
880   FOR L=1 TO 1449
890     IF Fvect(L)=Fcheck THEN GOTO Next1
900     L1=L+1
910     FOR N=L1 TO 1450
920       IF Fvect(N)=Fcheck THEN GOTO Next1
930       Fdelta=ABS(Fvect(L)-Fvect(N))
940     NEXT N
950   NEXT L

```

```
960      IF Fdelta Ftol THEN GOTO Nextl
970      Cvoab(L)=Cvoab(L)+Cvoab(N)
980      Svoab(L)=Svoab(L)+Svoab(N)
990      Fvect(N)=Fcheck
1000     Fdelta2=ABS(Fvect(L)-1.)
1010     IF Fdelta2 =Ftol THEN Voabl=SQR(Cvoab(L)2+Svoab(L)2)
1020     NEXT N
1030 Nextl:NEXT L
1040     Mi=1.0
1050     Wo=60.
1060     Sf=Mi*SQR(2.)/Voabl
1070     FOR M2=1 TO 1450.
1080       IF Fvect(M2)=Fcheck THEN GOTO Nextm2
1090       IF Fvect(M2) 150. THEN GOTO Nextm2
1100       Voab(M2)=SQR(Cvoab(M2)2+Svoab(M2)2)/SQR(2.)*Sf
1110       Atan2(Cvoab(M2),Svoab(M2),Seta)      ATAN2(COS COMP./SIN COMP.)
1120       Phvrb(M2)=Seta
1130       Pvoab(M2)=100.*Voab(M2)/Mi
1140
1150     OUTPUT CURRENT SPECTRA
1160
1170     Wn=60./Wo
1180     Pf=.9
1190     R1=Pf
1200     X1=SQR(1.-R12)
1210     Z1=SQR(R12+(X1*Fvect(M2)/Wn)2)
1220     Ioabl=Voabl/SQR(R12+(X1/Wn)2)
1230     Ioab(M2)=Voab(M2)/Z1
1240     Atan2((X1*Fvect(M2)),R1,Seta1)
1250     Pioab(M2)=100.*Ioab(M2)/Ioabl
1260     Pioa=Pioab(M2)
1270     NEXT M2
1280 Subend: SUBEND.
```

A.B.4:

```

10  SUB Input_filter(Idcm,Vi,Swr(*),Phswr(*),Thdiao,Xlio,Xcio,Tkvamin)
20
30  This subprogram is used for designing the OPTIMUM INPUT FILTER.
40
50  REAL Ia(150),Ixli(150),Ixc(150),Ili(150),Ici(150),Vci(150)
60  REAL Pili(150),Xli(10),Thdvc(7,51),Thdili(7,51),Pvci(150)
70  REAL Tkva(7,51),Tkval(7,51),Tkva2(7,51)
80  Tkvamin=100.
90  FOR I=1 TO 150 STEP 2
100  Ia(I)=Idcm*Swr(I)
110  NEXT I
120  Tkvamin=100
130  FOR I=1 TO 7
140  Xli(I)=(I-1)*Dxl+Xlf
150  FOR J=1 TO 51
160  Xci=(J-1)*Dxc+Xcf
170  FOR K=1 TO 150 STEP 2
180  Ixli(K)=K*Xli(I)
190  Ixc(K)=-Xci/K
200  Zi=Ixli(K)+Ixc(K)
210  IF Zi=0 THEN
220  GOTO Nextj
230  ELSE
240  IF K=1 THEN
250  Vci(1)=Vi
260  Ici(1)=-Vi/Xci
270  Ili(1)=SQR(Ia(1)2+Ici(1)2)
280  Atan2(Ici(1),Ia(1),Seta)
290  Philil=Seta
300  Vxli1=Ixli(1)*Ili(1)
310  Vanp=SQR(Vxli12+Vi2)
320  Atan2(Vi,Vxli1,Seta)
330  Phvanp=Seta
340  ELSE
350  Ili(K)=Ia(K)*Ixc(K)/Zi
360  Ici(K)=Ia(K)*Ixli(K)/Zi
370  Pili(K)=100*ABS(Ili(K)/Idcm)
380  Vci(K)=Ici(K)*Ixc(K)
390  Pvci(K)=100*ABS(Vci(K)/Vi)
400  END IF
410  END IF
420  NEXT K
430  Smi=0
440  Smv=0
450  FOR N=5 TO 150 STEP 2

```

Xlf=initial value of Xli

Xcf=initial value of Xci

```
460      Smi=Sm1+P11(N)2
470      Smv=Smv+Pvci(N)2
480      NEXT N
490      Thd11(I,J)=SQR(Smi)
500      Thdvci(I,J)=SQR(Smv)
510      PRINT
520      IF Thd11(I,J) 5 THEN
530      GOTO Nextj
540      ELSE
550      IF Thdvci(I,J) 15 THEN
560      GOTO Nextj
570      ELSE
580      END IF
590      Smli=0
600      Smci=0
610      FOR M=1 TO 150 STEP 2
620      Smli=Smli+.5*I11(M)2*ABS(Ix11(M))
630      Smci=Smci+.5*Vci(M)2/ABS(Ixci(M))
640      NEXT M
650      IF L=1 THEN
660      Tkva(I,J)=Smli+Smci
670      ELSE
680      Tkva(I,J)=2*Smli+Smci
690      END IF
700      IF Tkva(I,J) Tkvamin THEN
710      GOTO Nextj
720      ELSE
730      Tkvamin=Tkva(I,J)
740      Xli=Xli(I)
750      Xcio=Xci
760      Thdiao=Thd11(I,J)
770      END IF
780      END IF
790      GOTO Nextj
800 Nextj:NEXT J
810      NEXT I
820      Oxli=Xli
830      Oxci=Xcio
840      Otkva=Tkvamin
850 Subend:
860      SUBEND
```